STRUCTURAL STUDIES OF SOME FLUOROPHOSPHINE COMPOUNDS

by

Graham Stewart Laurenson

A thesis presented for the degree of
Doctor of Philosophy in the Faculty of Science
of the University of Edinburgh, 1983

PAGE

NUMBERING

AS ORIGINAL

D E D I C A T I O N

to the wimmin

CONTENTS

This thesis is the original composition of the author's work, unless stated otherwise,and has not been submitted previously for any other degree.

ACKNOWLEDGEMENTS

To Dr David Rankin I owe my utmost thanks for his patience and help in accumulating the material for this thesis. The work proved stimulating, a reflection on his foresight in designing the outline of my research. I am indebted to Professor Evelyn Ebsworth, Dr Stephen Cradock and Alan Boyd, without whose collaboration this work would be incomplete. Thanks also to other friends and colleagues who helped in various ways, especially Steve Henderson for daring to proof-read, and Jean Kerr for being courageous enough to type, the script.

I am grateful to the Science Research Council for their financial support.

Finally a massive vote of thanks to all who have suffered with me.

SUMMARY

This thesis describes gas phase electron diffraction determinations of the molecular structures of some difluorophosphine compounds, in some cases utilising extra information gleaned from a relatively new technique called Liquid Crystal NMR Spectroscopy. An introduction to the methods and theory behind electron diffraction and nmr spectroscopy of solutes dissolved in orienting media is included herein. The structure determinations of difluorophosphine selenide and aminodifluorophosphine illustrated the compatibility and complementary nature of ed and lcnmr data.

The structure of difluoro(isoselenocyanato)phosphine was examined by electron diffraction. Vibrational corrections were applied to this determination, which then yielded a linear N=C=Se moiety and the widest angle at a two-coordinate nitrogen site yet reported.

Other compounds studied were all fluorophosphine amines. Conformational analyses showed that both steric crowding and attractive hydrogen to fluorine interactions determined difluorophosphine moiety torsion angles. The bond orders from nitrogen to silicon, phosphorus, and to a lesser extent, germanium,were found to be greater than 1, expected since compounds of this type have a planar configuration in which the lone pair on nitrogen, lying in a p orbital, donor bonds to vacant d orbitals on the ligands.

Compounds in this group whose structures were determined by electron diffraction include methylamino-difluorophosphine, bis(difluorophosphino)amine, difluorophosphino(disilyl)amine, bis(difluorophosphino)-silylamine, and bis(difluorophosphino)germylamine.

CHAPTER 1

PRINCIPLES OF ELECTRON DIFFRACTION AND GENERAL OUTLINE OF SAMPLE PREPARATION

1.1 Fluid-Phase Structural Techniques

Methods of examining the geometries of molecules in fluid phases include electron diffraction, microwave spectroscopy, analysis of rotational fine structure in vibrational spectra, and nmr measurements on solutes dissolved in liquid crystal phases. Microwave spectroscopy can give very accurate gas phase structures of certain small molecules having a permanent dipole, preferably along more than one cartesian direction. Since a maximum of three angular momenta may be measured, isotopic substitution is normally necessary to obtain enough information to determine all structural parameters. Obviously this is not possible for elements having only one isotope. Of the gas phase structural determination techniques, electron diffraction has proved to be the most versatile.

Theories were developed to explain the scattering of electrons between 1911 and 1915 by Rutherford[1], Debye[2], and Ehrenfest[3], but it was not until the experiments of Germer[4] and Thomson[5] that these were put to the test, the results verifying the De Broglie hypothesis of wave particle duality for the electron. Mark and Weirl[6,7] first studied the effects of scattering electrons by gases, and although numerous modifications and improvements have been made in the construction of electron diffraction apparatus and in data analysis, the experiment remains essentially unchanged today.

1.2 Theory of Molecular Scattering of Electrons

The pattern made by the scattering of electrons by a molecular gas sample is circular in form with alternate maxima and minima, corresponding to constructive and destructive interference, appearing as concentric rings of shade and light respectively. The total scattering intensity (I) may be given by the expression:

(1) $I_{(total)}=I_{(incoherent)}+I_{(inelastic)}+I_{(atomic)}+I_{(molecular)}$

which may be written

(2) $I_{(total)}=I_{(background)}+I_{(molecular)}$

Inelastic scattering implies a change of momentum for the scattered electron and incoherent scattering may correspond to double-collision or extraneous scattering. Atomic scattering, which constitutes the bulk of the total, yields a smooth function falling off rapidly and asymtopically with scattering angle θ, which equals twice the angle between the diffracted and undiffracted beam. The contributions $I_{(inelastic)}$ and $I_{(incoherent)}$ may be subtracted by fitting a smooth quadratic function through the mid points of the molecular starting pattern, leaving the latter intact.

It is useful to define the quantity s having units of reciprocal length, as

$$(3) \quad s = \frac{4\pi\sin(\theta/2)}{\lambda}$$

where λ is the wavelength of electrons used. Since this parameter is independent of the dimensions of the experiment such as nozzle-to-plate distance, it is most useful when comparing data from diverse sources. The intensity of the scattering pattern varies according to the following relationship:

$$(4) \quad I \propto \frac{4\pi m^2 e^2}{h^4 \varepsilon_o s^4} \equiv A$$

and the molecular intensity contribution to the total scattering given by Equation 5.

$$(5) \quad I_{(mol)} = A \sum_{\substack{ij \\ i \neq j}} (Z_i - f_i)(Z_j - f_j)\cos(\eta_i - \eta_j) \cdot \frac{\sin s(r_{ij} - \chi_{ij}s^2)}{r_{ij}s} \cdot \frac{\exp(-u_{ij}s^2}{2}$$

m and e are the mass and charge of the electron, h is Planck's constant, ε_o the permitivity of free space, r_{ij} the distance between atoms i and j in the molecule, z_i and f_i the atomic number and scattering factor of element i, and u_{ij} the mean amplitude of vibration of the atom pair i and j. The term $\cos(\eta_i - \eta_j)$ represents the phase shift between the scattering of the atom pair i and j, which is most severe in the case where i is a light and j a heavy atom, calculated from the formula,

$$(6) \quad \eta_i - \eta_j = a_i - a_j + (b_i - b_j)s + (c_i - c_j)s^2 + (d_i - d_j)s^3$$

and using values of the constants a, b, c and d tabulated

for each element. The term χ_{ij} has been shown[8] to be related to the anharmonicity term, a, in the Morse oscillator, by the expression

$$(7) \quad \chi_{ij} = a_{ij} u_{ij}^{4}/6$$

Here, a takes the value of 200 pm^{-1} for many bonded distances. This term is zero for all non-bonded distances. Complex scattering factors and phase shifts have been tabulated by Schafer et al[9].

1.3 The Experiment

The technique of electron diffraction by gas phase molecules requires an apparatus capable of producing a monochromatic parallel beam of electrons with minimal cross-sectional area and maximum beam current, and a detection system capable of recording the scattering resultant from the intersection of this beam with a gas stream orthogonal to it. In practice the beam is usually generated by means of a hot, sharply bent tungsten filament situated in the proximity of an accelerating anode, held at a relative potential of ca. 50 kV. Those electrons accelerated along the axis of the instrument, having acquired kinetic energy according to Equation 8

$$(8) \quad \lambda = \frac{h}{(2meV)^{\frac{1}{2}}}$$

(V = accelerating potential)

which is a form of the De Broglie relationship $\lambda = h/p$, where p is the momentum of the electron passing through a narrow opening in the anode, and subsequent to passing through electrostatic or magnetic focussing lenses and various collimators, emerge as a monochromatic parallel beam of electrons with a wavelength of ca. 6 pm. The distance between the gas injection system and the intensity pattern recording system defines the minimum and maximum observable scattering angle θ. Normally two or more such distances are used to extend the range of s units over which data can be collected. In most cases the detection system will be a photographic plate. Since intensity falls off as the fourth power of scattering angle it is necessary to apply counter attenuation to the intensity pattern before recording it, because of the limited dynamic range over which the photographic emulsion's sensitivity to incident radiation is linear. This is best achieved by utilising a spinning sector[10] which opens out as a function of $s^3 \sim s^4$. Other functions may be used: for example, the reciprocal atomic scattering for a rare gas in the same row of the periodic table as the heaviest atom in the molecule to be studied. Often a compromise sector, such as one calculated to correspond to the inverse of the scattering of atomic carbon, is used.

If the intensity data are subjected to a sine Fourier transform then an intensity probability with respect to distance is obtained, since the intensity data comprises an aggregate of damped sine waves, each corresponding to a

unique interatomic distance within the molecule. For a homonuclear rigid diatomic the scattering is given by Equation 9.

$$(9) \quad I(s) = \text{Constant} \int_0^\infty P(r) \frac{\text{Sin}(r.s)}{r} dr.$$

By applying a Fourier transform to (9) we obtain Equation 10.

$$(10) \quad \frac{P(r)}{r} = \text{const.} \int_0^\infty I(s) \sin (r.s) ds$$

The procedure may be developed to enable it to be applied to only vibrating polyatomic molecules. The locus of the resulting function is called the radial distribution curve, in which peak positions correspond to interatomic distances, areas depend on the scattering powers of the two atoms involved, and peak widths at half-height are related to the vibrational amplitude of the atom pair involved. The radial distribution function for SPF_2Br with distances shown is given in Figure 1'.1. Radial distribution curves are useful in that they give a visual display of the distribution of interatomic distances, but solving the structure for a molecule depends on best-fitting calculated intensity data with experimental data. The procedures for data acquisition and handling and molecular structure determination as used at Edinburgh are given in Chapter 2.

Figure 1.1: Radial distribution curve for SPF_2Br

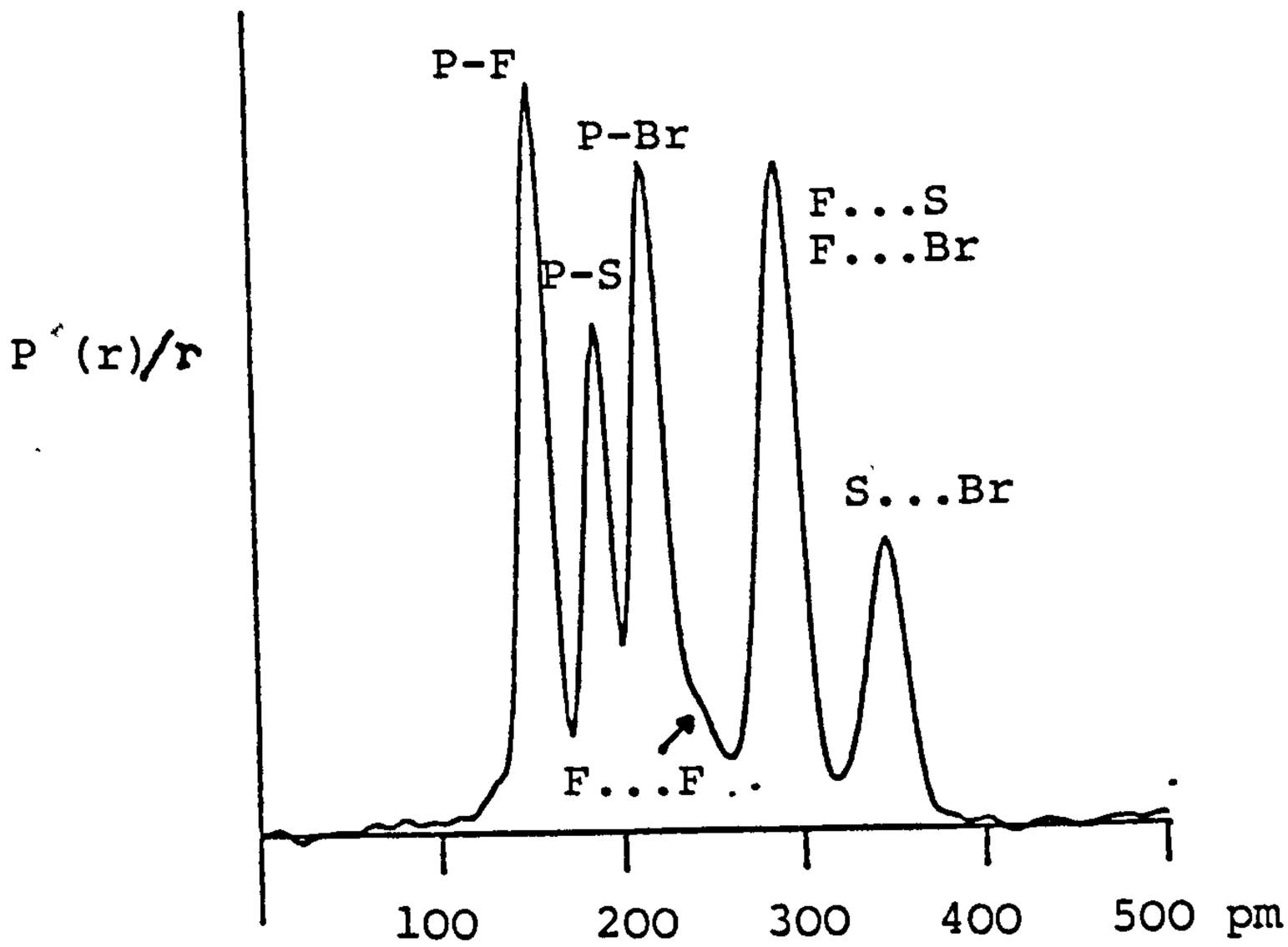

1.4 Limitations

The main prerequisite for a sample studied in the gas-phase by electron diffraction is that it shares a vapour pressure of at least ca. 5 mm of mercury at a temperature where decomposition of the sample does not take place within the timescale of the experiment. Since electron scattering power varies with atomic weight (Equation 2) molecules with only light atoms present need a proportionately higher vapour pressure than those containing heavier elements. For a similar reason it is often difficult to locate hydrogens in the presence of third row or heavier atoms, a problem echoed in X-ray structure determinations. A further limitation on the suitability of compounds for a study arises from the one-dimensional nature of the data acquired. If the separation between a pair of interatomic distances is less than ca. 5-10 pm it may prove impossible to determine these two parameters independently. This can result in an underdetermination of the structure in question. In such cases certain assumptions must be made about the geometry, or data must be included from other sources, as will be discussed in Chapters 2 and 7.

Lastly, care must be taken in interpreting data, due to the nature of the experiment, in which r_a values are observed. These constitute time average rather than mean values corresponding to the observational conditions of $\langle r^{-1} \rangle^{-1}$. Consequently when large-amplitude low-frequency bonding or torsional modes are present distortion from

Figure 1.2: Shrinkage effect in planar NR_3 group

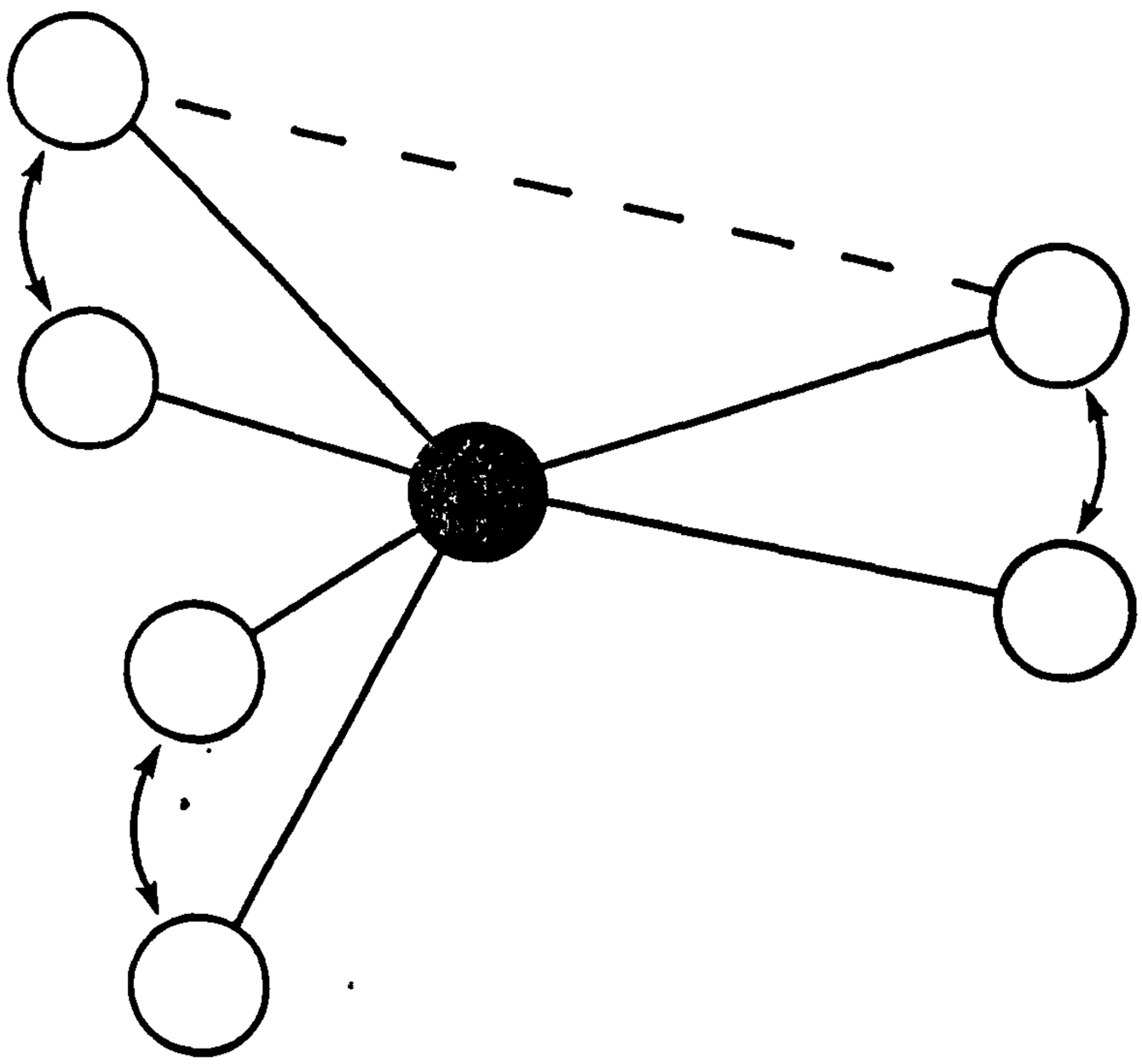

Note: broken line indicates observed average value for R-R' distance

higher local symmetries in arrangements of atoms may be seen[11]. This effect, called shrinkage[12], is responsible for some discrepancies between structures derived from microwave and electron diffraction data[13]. To allow for this certain corrections must be applied to r_a, yielding a new interatomic distance r_α. r_α is related to r_a by the expression

$$(11)\quad r_\alpha = r_a + \frac{u^2}{r_e} - K$$

Here, K represents a perpendicular amplitude correction for harmonic atomic displacements orthogonal to the vector $\underline{r}$, and, since the $\frac{u^2}{r_e}$ term is small r_e can be replaced with r_a. K values must be derived from a normal coordinate analysis of the species studied, which also gives value for the amplitudes of vibration corresponding to those obtained from the electron diffraction experiment. In simple systems, with the corrections necessary to relate structures determined by gas-phase electron diffraction and microwave spectroscopy applied, good agreement is possible[14].

1.5 The Structures of Difluorophosphine and Silyl Amines

Twenty-five years ago Hedberg[15] published the result of an electron diffraction structure investigation on the molecule trisilylamine in the gas phase. This caused considerable interest since it showed a planar coordination

of ligands about nitrogen rather than the usual pyramidal one, a result endorsed by a more recent study on the same molecule[16]. A reasonable explanation for this result would have been the possible existence of steric crowding, since the silicon-silicon distance is close to that calculated from twice the Van der Waals radius for silicon, were it not for the fact that the silicon-nitrogen bond length is some 6 pm shorter than that for a single bond calculated by the Shomaker-Stevenson method[17]. This led Hedberg to suggest that the bond order was greater than 1, and that this was due to the lone pair on nitrogen forming a p→d donor bonding π-system with vacant d orbitals on silicon. Once the phenomenon had been identified interest developed to see whether other second or higher row elements would bond to nitrogen in this way. Phosphorus, being next to silicon in the periodic table, was considered. Since compounds with phosphino groups directly bound to nitrogen are not known, presumably due to the ease of formation of ammonia in any synthetic attempt, amines containing difluorophosphino groups were next considered.

The first compound of this type to be studied in the gas phase was tris(difluorophosphino)amine[18], the results from which determination yielded a planar skeletal arrangement of ligands about nitrogen, and short P-N bonds, an arrangement similar to that for the equatorial moiety in some P^V nitrogen compounds[19]. Before the present study began the following amines had been studied: $NMe_2(SiH_3)$[20]; $NMe(SiH_3)_2$[21]; $NH(SiH_3)_2$[21]; $NH_2(PF_2)$[13];

$NMe_2(PF_2)$[13]; $P(NMe_2)_3$[22]; $NMe(PF_2)_2$[23]; and $NH(PF_2)(SiH_3)$[24]. Gas phase structures undertaken in the present study complement those listed above and include: $NHMe(PF_2)$[25]; $NH(PF_2)_2$[26]; $N(PF_2)_2(SiH_3)$ and $N(PF_2(SiH_3)_2$[27]. Only in the cases of $NMe_2(SiH_3)$, $NH_2(PF_2)$ and $NMe_2(PF_2)$, which are all mono substituted difluorophosphino or silyl amines, is the planarity of the ligands around nitrogen in question, although a microwave study on $PF_2(NH_2)$[28] does show a planar PNH_2 skeleton, suggesting that the distortion from local planarity for this group in the electron diffraction structure may be a large shrinkage effect due to a low frequency out-of-phase deformation. The time-average structure would then appear non-planar, as illustrated in Figure 2. Otherwise the results obtained in all cases support the arguments used to account for the structures of the two tertiary amines, with short M-N bonds (M = P or Si) and planar coordination of ligands around nitrogen (or wide RNR angles where there is a poorly determined imino proton). The observed M-N bond length decreases with a decreasing number of M-groups around nitrogen,as the lone pair on nitrogen is being dedicated to fewer atoms. This appears to be more pronounced for diluorophosphino than for silyl amines, suggesting that the PF_2 group is a more powerful π-acceptor than the silyl ligand. This is borne out in the case where silyl and difluorophosphino groups are bound to a common nitrogen, where the Si-N bond is weakened at the expense of the P-N bond. It is worth noting that since the Ge-N bond in $N(GeH_3)(PF_2)_2$[29] is

considerably longer than that found for trigermylamine, the germyl ligand must also be a relatively weak π-acceptor.

In all difluorophosphino amines torsion angles of PF_2 groups about P-N bonds correspond to minimum energy geometries. Three major factors have been suggested as being responsible for influencing PF_2 group conformation; these being steric crowding, lone pair/lone pair repulsions, and attractive intramolecular H...F interactions. In the tertiary case, steric factors force the phosphorus lone pairs to lie in the skeletal plane cis to fluorines on a neighbouring difluorophosphino group, giving C_3h symmetry for the molecule. However, in cases of the various secondary and primary amines, steric crowding is not so severe. All bis(difluorophosphino)amines, including $N(GeH_3)(PF_2)_2$, exhibit arrangements where the lone pairs on phosphorus and nitrogen are orthogonal, but those on adjacent phosphorus atoms lie cis to each other. This can in some cases be attributed to H...F attractive interactions, although in the case of $N(GeH_3)(PF_2)_2$ the H...F distance is such that no such interaction seems feasible. For the various mono difluorophosphino amines, however, conformations do seem to depend primarily on attractive H...F interactions.

1.6 Preparation

The various amines studied here were prepared employing

Figure 1.3: Syntheses of PF_2-amines

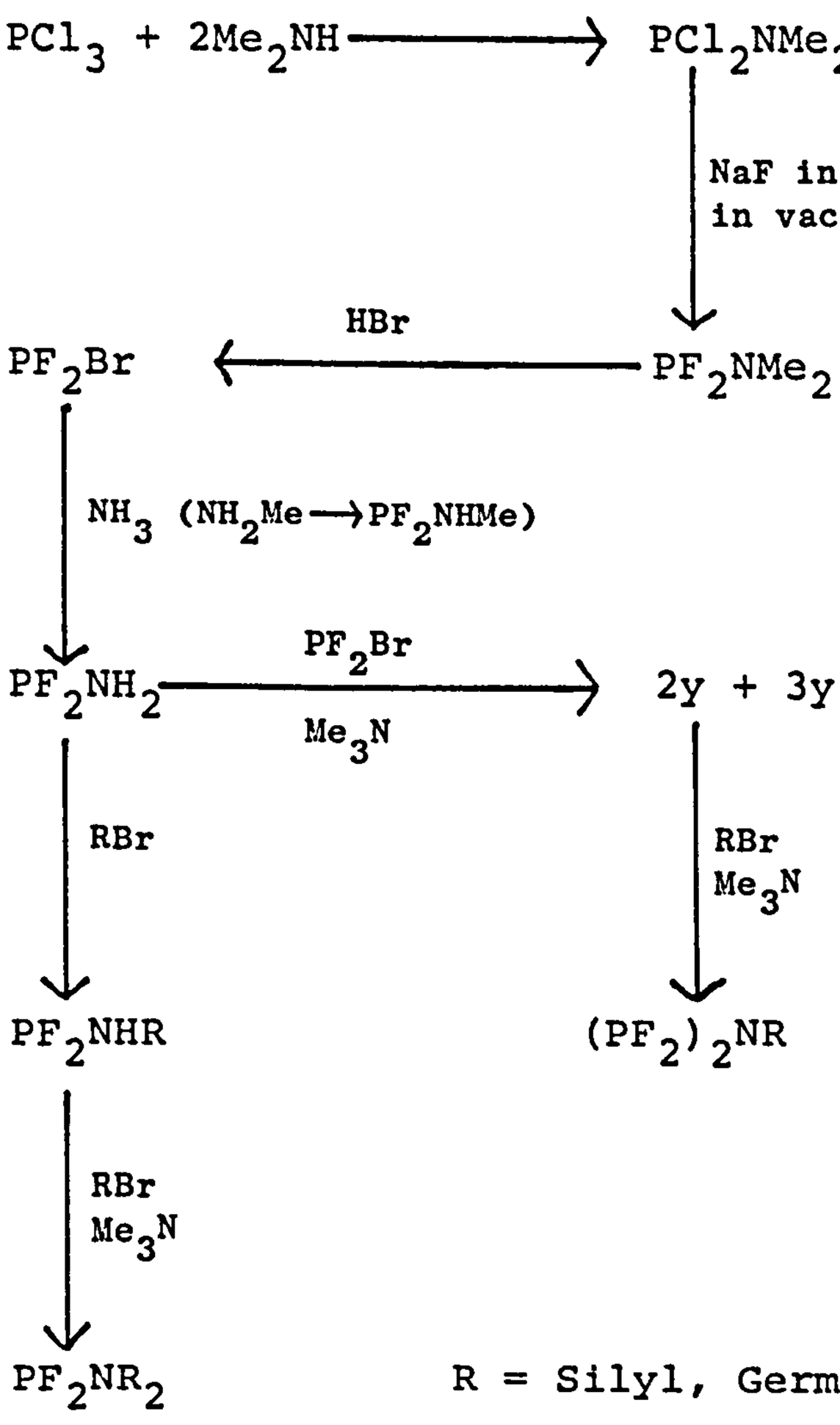

standard vacuum-line techniques and a series of condensation reactions designed to make use of the stability of quaternary ammonium salts. Specific preparations are described for each compound studied in the relevant chapter, but a general outline of the chemistry is given by Figure 1.3

As with all volatile and non air-stable compounds, care had to be taken to ensure that all glassware used was scrupulously clean and dry. When handling valuable electron diffraction samples, glassware to be used was first flushed with silyl bromide in order to remove any reactive contaminants. Purification of each sample was undertaken by ensuring that any impurities or unreacted starting materials were separable and then applying repeated fractional condensations in vacuo. Purities were checked by infrared or nmr spectroscopy, immediately prior to collecting electron diffraction data, and where possible immediately afterwards on the residual sample. With such precautions taken good data were obtained for all compounds studied.

CHAPTER 2

ELECTRON DIFFRACTION DATA COLLECTION AND HANDLING

2.1 Apparatus

The equipment now installed at Edinburgh was obtained from Cornell University in 1977 and was subsequently operational in its new location by 1978. Originally designed by Bauer and Kimura[30] and constructed by Robert Jenkins, the instrument has had various modifications and improvements effected on it since crossing the Atlantic. These mainly constitute upgrading ancilliary monitoring devices.

The instrument comprises a large chamber constructed mainly of non-magnetic stainless steel and brass, with lead glass viewing windows in strategic locations. The chamber is evacuated by means of two 10 cm Consolidated Vacuum oil diffusion pumps surrounded by Freon-cooled baffles, backed by nitrogen-cooled condensation traps and an Edwards rotary pump. Pressure is monitored using VEECO equipment in two ways; the backing pressure by means of switchable DVIM thermocouple heads wired to a TG 70 control unit, and the pressure of high vacuum under diffusion pumping by an RG 75P ion gauge head coupled to an RG 1002 gauge. Backing and chamber pressures thus monitored are $<10^{-4}$ torr and ca. 3×10^{-7} torr respectively during standby operating conditions.

Since the apparatus was constructed in a horizontal format, the Canal Industrial Corporation electron gun sits at one end of the chamber. This is serviced by its own 5 cm Consolidated Vacuum oil diffusion pump with Freon

cooled baffle, linked to the main backing pressure by a valve. The gun utilises a V shaped tungsten wire filament on a mica support washer in a cathode assembly which is given a negative in potential of ca. 40-55 kV during typical operating conditions. This is located ca. 10 mm from the anode which is held at ground potential. The cathode has a polished stainless steel grid cap and the anode is of similar material; the former is insulated from the chassis, which is held at ground potential, by a ceramic washer while the latter is earthed. A small current of <50 μA may be passed through the filament so causing electrons to boil off towards the anode. For the tungsten filament it has been found that 10 or 12.5 micron wire is most suitable, the former giving the higher resolution and lower beam current, corresponding to saturating at a lower filament current, whereas the latter is more suitable for low volatility compounds, since it gives a higher beam current and therefore more scattering intensity for a given exposure time.

All constituent parts of the electron gun must be kept scrupulously clean, since foreign matter will induce discharging at high potential, and procedures for cleaning are described in the service manual.

Focusing of the emergent beam is accomplished by two magnetic lenses designed to carry up to 100 ma DC current, each with mechanical adjustment which moves the orientation of the lenses and gun with respect to the target. This is the centre of a fluorescent screen at the

far end of the chamber. The image of the electron beam on the screen may be viewed via a mirror set at 45° to the beam through a telescope. The conditions of focusing and alignment which must be met before attempting to acquire any data is that the spot viewed on the screen be as small and intense as possible, typically 0.3 mm diameter and positioned in the centre of the beam stop. This is a narrow aluminium tube, designed to avoid back-reflection of undiffracted beam, positioned in the centre of the rotating sector which is situated immediately before the target screen. A centrifugal shutter closes the beam stop aperture when the sector is spinning. In addition to the focusing lenses, the beam passes through various clean-up apertures, the two most critical being 0.8 mm in diameter, positioned immediately after each lens,and also through a compensator, which applies a three-fold symmetrical field to help reduce any superposition of triangular cross section on the beam by the filament shape.

The sample injection system comprises an aluminium nozzle, ca. 0.3 mm internal diameter at the tip, mounted on a hollow stainless steel boom arm which emerges from beneath the chamber via an 'o' ring seal and terminates in a throttle valve and glass Quickfit B14 socket. This is a convenient method of accepting a glass tap ampoule, the preferred format for storing volatile compounds. The nozzle arm may be rotated and raised or lowered such that two nozzle-to-plate distances are

possible with the nozzle aligned so that influxing sample intersects the electron beam. A shadow image of the cone-shaped nozzle may be viewed on the fluorescent screen if the beam is defocussed to a diameter in excess of the width of the nozzle tip. The nozzle is then positioned so that its centre is aligned vertically with, and is about one spot-diameter away from, the focused beam position. At the short, wide angle distance, an extra clean up screen is inserted between the nozzle and target, to help reduce extraneous scattering in this configuration. A cryogenic pump, cooled by a reservoir of self-circulating nitrogen and coated with activated carbon for optimum adsorption, is located immediately above the nozzle. This fast condenses inflowing vapour and maintains a pressure of ca. 10^{-6}-10^{-5} torr for the chamber during sample injection. This is important in minimising extraneous scattering.

The detection system for recording diffraction patterns is photographic. The fluorescent screen is part of a camera, the mechanism of which is capable of reliably positioning, in sequence, up to 10 Kodak Electron Image plates, at a reproducible distance from the nozzle. With the facility to expose 10 plates at two discrete nozzle-to-plate distances without evacuating the chamber it is possible to collect sufficient data for a complete structure in a single run. Compared with some other machines this represents rapid and efficient data collection. A block diagram of the apparatus is

Figure 2.1: Schematic diagram of Cornell/Edinburgh ed apparatus;
(a) main chamber, (b) electron gun

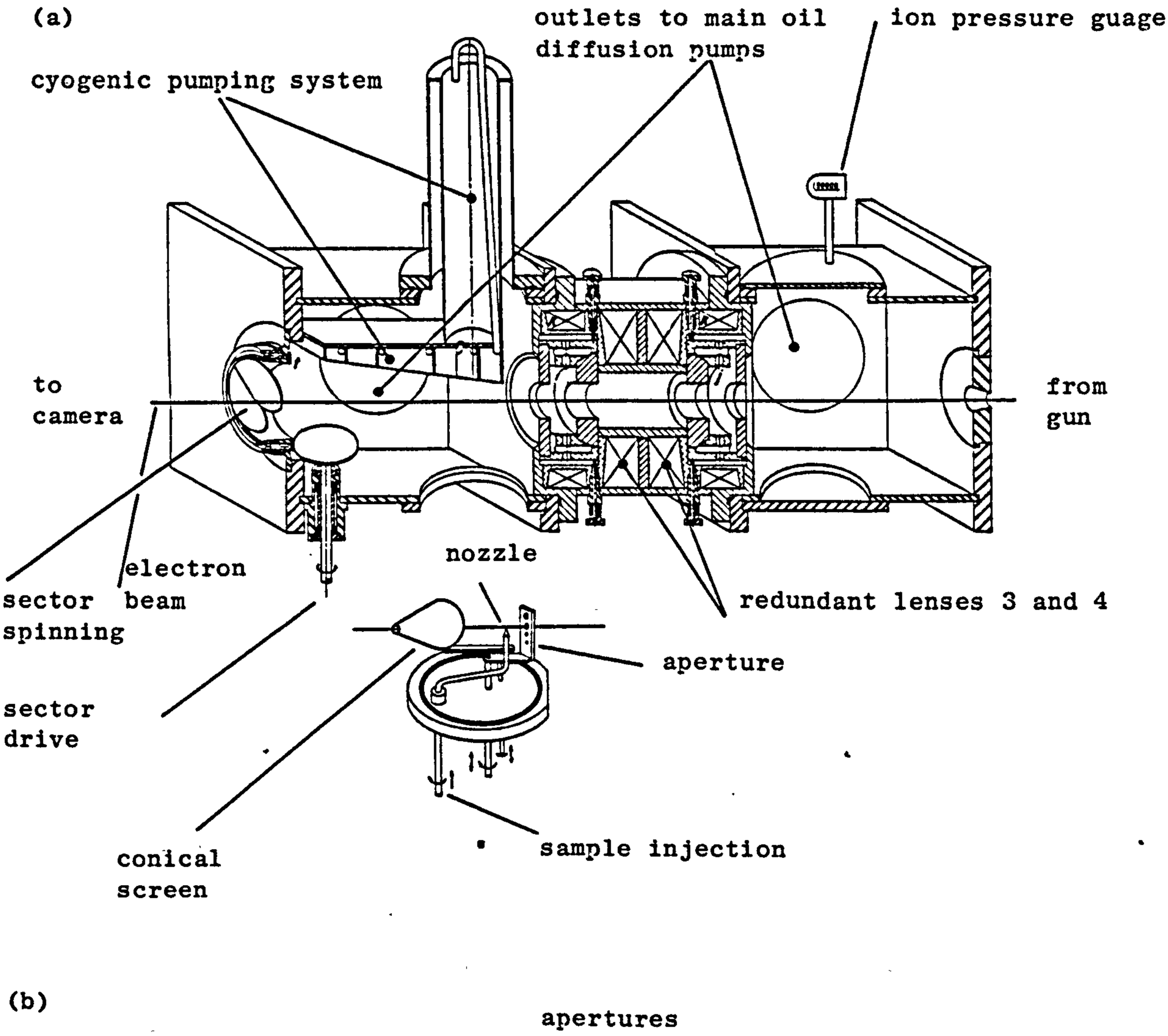

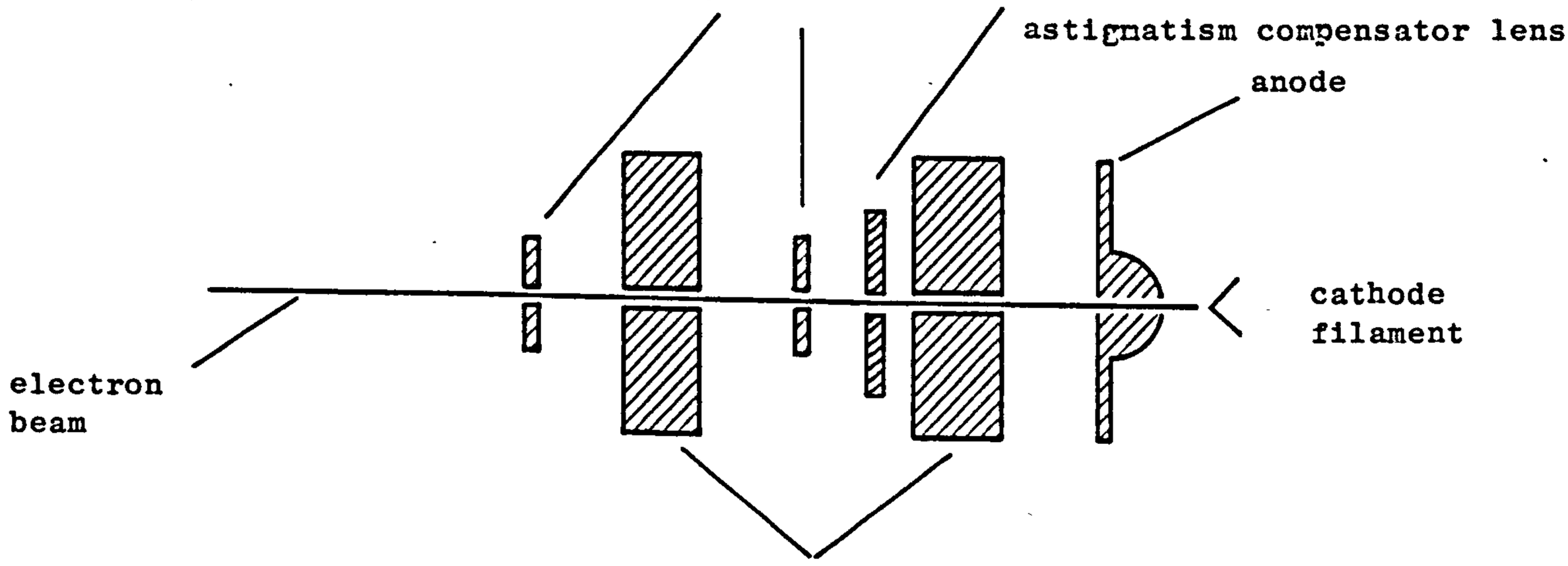

given in Figure 2.1.

2.2 Data Collection

Before running the electron diffraction apparatus the chamber must be evacuated to $<10^{-6}$ torr. The high voltage power supply may then be switched on and gradually raised to operating potential. Finally the filament current can be increased until saturation has just been reached and alignment of the emergent beam checked. A valve which connects the gun to the main chamber by a fast pumping route (cf. the beam aperture) must be closed before injecting a sample,to minimise contamination of the gun. The nozzle is then aligned at one of the two available distances by the method described previously. If any non-conducting contaminants are present on any part of the apparatus which is adjacent to the beam, i.e. apertures, beam stop and nozzle, these will become charged and deflect the beam and the experiment will be necessarily delayed while the offending items are cleaned. Once alignment is completed satisfactorily, the beam is cut off by means of a lever-operated shutter and a photographic plate inserted into the camera in readiness for the first exposure. This is accomplished by a gravity mechanism, possible because of the horizontal mode of operation of the apparatus.

In order to facilitate centering the diffraction

pattern during analysis the plate is first exposed to the undiffracted beam, necessarily for a very short time to avoid fogging the plate by moving a shutter lever partially through its arc until a small slit in the shutter has traversed the beam. At this point the sector, calculated to correspond to the reciprocal scattering of atomic carbon, is made to rotate rapidly, thus activating the centrifugal shutter of the beam stop, and the apparatus is ready to record scattering intensity. Once again cleanliness is of utmost importance, this time in the case of the sector opening, which should increase smoothly from ca. 5 mm from the centre to the perimeter of the diffraction pattern. Since the opening near the centre is small, any dirt present will drastically alter the sector function, and hence negate data at small s values.

An exposure is taken thus: the previously degassed sample is injected by means of the throttle valve through the nozzle, and the shutter is opened for a duration commensurate with the pressure increase as monitored on the ion gauge and the expected scattering power of the sample. Benzene is used to provide calibration of the scale of the experiment, which depends on the nozzle-to-plate distance and wavelength of electrons used, ie accelerating voltage. During a run at one distance the nozzle is undisturbed, and so the former parameter remains constant. The high voltage is monitored by means of an Amplicon Electronics digital voltmeter, and any fluctuations are noted for successive exposures. Often

these are small enough to be ignored. Benzene generates a well resolved radial distribution pattern and has had its structure accurately determined[31]; therefore it is a useful calibrant in scaling the data for an unknown structure.

In benzene refinements physically measured values are initially used for nozzle-to-plate distances and accelerating potential, and corrected values thereafter for these parameters are applied to the structure determination being undertaken.

After exposure the beam and sample flow are shut off, and the plate dropped into a box below the camera. Usually five plates are taken at each distance, two of benzene and three of the molecule being studied. Once removed the exposed plates are developed for 12 minutes in Kodak D19/D19R developer solution using nitrogen bubble burst agitation, and washed for 1 minute in running water prior to immersion in Kodak "Kodafix" fixer solution for ca. 20 minutes. The plates are then thoroughly washed in water, dipped in Kodak Photo-Flo solution and allowed to dry prior to tracing on the microdensitometer.

2.3 Digitisation

The digitisation of the analogue radial intensity pattern is accomplished using a Jarrell-Ash double beam spinning plate microphotometer coupled to an analogue to

digital converter.

Plates are centred in the spinning platter using the image of the undiffracted electron beam as a guide, and a photocell is made to traverse a diameter of the spinning pattern. Voltages are recorded at 100 micron intervals and put onto punch tape, together with a reference voltage recorded at 1 mm intervals to allow for any variations in lamp intensity. Vernier readings are taken from a scale on the microdensitometer at the start and finish of a traverse, and these are later used to check for correspondence with the number of 100 micron data points recorded. Values are also recorded for the reference and 100% transmission voltages prior to tracing in order to scale the data with respect to the reference signal.

If the optical density of the exposed plate differs substantially from the optimum of ∿0.6D, the signal to noise ratio will decline. If the plate is too dark the transmittance voltage may be multiplied by some factor prior to digitisation so that the deterioration in signal quality is not compounded by the analogue to digital converter, by adjusting a sensitivity control on the microdensitometer.

The punch tape which contains the intensity data in digital form is then sent off, together with the appropriate leader tape and identification card, to the Edinburgh Regional Computing Centre, where the information is loaded onto a computer data file. The procedure for data collection described above is developed from that outlined in

R.L. Hildebrandt's PhD thesis.

2.4 Data Reduction

The data reduction program used derives from an established program[33]. Various subroutines are called sequentially from the master electron diffraction programs to perform consecutive stages in the reduction of the raw data loaded into the computer. These are initiated by use of the command ED8O (XYZ) where XYZ is a three letter mnemonic assigned to a molecule. The resulting prompt requires identification of the subroutine required, and these are indexed by a single letter. A brief description of the functions of each subroutine is given in Table 2.1.

2.5 Refinement

Once data reduction has been completed the data are in a form which may be compared with theoretical molecular intensities derived from a mathematical structure formulation. This is done first by constructing a model which assigns atoms normal coordinates, taking an input of geometrical parameters. An example of a molecular model is listed in Appendix 1. Once the compiled version of this model is inserted, the ED8O master refinement program

Table 2.1:

ED80(XYZ) SUBROUTINE	BRIEF DESCRIPTION
A	Sets up scattering factors for all elements in the molecule, scaled to the accelerating potential
C	Converts punch tape binary input into columnar data file which can convert to a character file for editing.
D	Checks character file C for errors
E,F	Each intensity data file is assigned to two numbered job locations, one corresponding to each side of the diffraction pattern. Reference and 100% voltages, and both Vernier scale readings are read in. Blackness and flat-plate corrections are applied. The data is adjusted for fluctuations in lamp intensity during tracing by comparison with movements in the reference voltage. The difference between the two Vernier readings is checked for correspondence with the total number of 100 micron data points. Uphill curves are plotted for visual inspection.
G	Data is interpolated at uniform S units, being 2 and 4 nm^{-1}, for long and short camera distances respectively. Uphill curves are combined for each camera distance, and atomic scattering subtracted, the accomplishment of which requires an input of the number of atoms of each type, scattering factors having been calculated in the 'A' subroutine and minimum S values and weighting points, which can be changed after inspection of the combined intensity curves, and subjected to a smooth quadratic background subtraction. The resultant intensity curves are plotted.
H	Further background and data set limit alterations offered

Note: The procedures outlined above have recently been updated to handle data from a Joyce-Loebl microdensitometer 6[57].

will automatically refer to it. The first refinement undertaken, accessed by the command ED80 (XYZ) followed by the letter R in answer to the next prompt requires an input, among other things, of all geometrical parameters (name and value) and all independent interatomic distances and associated amplitudes of vibration and anharmonicities, giving the multiplicities of each independent distance. The total number of interatomic distances is given by solving (N-1)! where N is the total number of atoms in a molecule. (N-1)! should therefore equal the sum of all multiplicities.

Once the information has been inserted it is possible to improve the calculated fit to the observed structure, either by manual discrete parameter adjustments, or by utilising the method of least squares refinement. The least squares analysis seeks to minimise the difference between the squares of the observed scattering and that calculated according to Equation 5. This is accomplished using a modified version of an established program[34] which allows for correlation between data points by utilising an off diagonal weight matrix $\underline{W}$. The elements of this matrix are given by Equations 12a-12e.

$$(12)\quad a)\quad w_{ii} = (s_i - s_{min})/(sw_1 - s_{min}) \qquad s_{min} < s_i < sw_1$$

$$b)\quad w_{ii} = 1 \qquad sw_1 < s_i < sw_2$$

c) $w_{ii} = (s_{max}-s_i)/(s_{max}-sw_2)$ $\quad sw_2<s_i<s_{max}$

d) $w_{ij} = 0$ $\quad i \neq j \pm 1$

e) $w_{ij} = 0.5(w_{ii}+w_{jj})(p/h)_k$ $\quad i = j \pm 1$

sw_1 and sw_2 are weighting points for the distance k., chosen by inspecting the intensity data, and (p/h) corresponds to the correlation parameter. Correlation between data usually ensures that the number of independent observations is substantially less than the number of observations in the electron diffraction or any other single or combined experimental structural analysis technique. It has been shown that for combined electron diffraction and spectroscopic data this correlation can be minimised by choosing suitable relative weights for the two sets of data[35].

Quantification of the degree of fit of observed to calculated intensity data is expressed as a general R factor given by Equation 13.

(13) $R_G = (\underline{D}'\underline{\underline{W}}\underline{D} \;/\; \underline{I}'\underline{\underline{W}}\underline{I})^{\frac{1}{2}}$

where $\underline{D}$ is the difference vector composed of elements d_i for each value of s_i, and $\underline{I}$ a similar vector of intensities. If the off diagonal elements of the weight matrix are ignored the so-called diagonal R factor may be obtained using Equation 14.

$$(14) \qquad R_D = \frac{\sqrt{\Sigma w_{ii} d_i^2}}{\Sigma w_{ii} i_i^2}$$

If data from other sources such as microwave spectroscopy[14,35,36,37,38], liquid crystal nmr[39,40] or predicate observations[27,41] are to be used, the matrix need be extended by diagonal elements only, chosen with weights inversely proportional to the squared uncertainty of the observation, stated to the standard deviation of the fit of the electron diffraction data points. A structure may then be refined using combined data, or even entirely on non electron diffraction data.

The ED80 programs are accessed interactively from any ERCC computing terminal, and real time or queued operations are possible. Where the variation in R_G (a measure of the difference between experimental and calculated data) with changing a parameter value is small, correspondingly larger estimated standard deviations, or esds, are associated with the refining parameter. In extreme cases the R_G factor minimum may be so shallow as to preclude meaningful refinement altogether. In such cases it is possible to make use of a facility, hereafter described as an "R-factor loop", whereby the parameter is required to adopt a series of fixed values at uniform intervals, a few cycles of refinement carried out at each value, and the minumum R_G factor obtained taken to correspond to the best value for the non-refining parameter.

Care must be taken during a structure determination that all possibilities are considered. It may be possible to get a local minimum in the difference between observed and experimental intensities which does not correspond to the true geometry. An example of this is the structure of $N(PF_2)(SiH_3)_2$ where two different conformations give similar scattering patterns[27]. Various operations can be called while setting up a refinement by using the appropriate index command number, such as altering parameter values or the number of parameters refining. Appendix 2 gives a list of these command numbers and their functions.

2.6 Calibrations, Corrections and Errors

Various calibrations and corrections must be applied if systematic errors are to be reduced. The derivation of these errors has been extensively analysed by Kuchitsu[42]. Calibration of the scale of the experiment has already been described, which uses known values for interatomic distances in benzene to fix values for the same in the sample being studied. The rotating sector must be periodically calibrated to check for any disturbance of its geometry and this is accomplished by examining the scattering pattern of argon.

The dynamic range of the photographic emulsion may be non-linear with the optical density of the exposed

plate. A Blackness Correction must be applied, determined by examining molecular scattering data over a range of exposures and correcting for variations in the relative difference between peaks and troughs at different exposures in the intensity patterns. For Kodak Electron Image plates correction is applied to the photocell voltage, V, according to Equations 15a and 15b.

(15) a. $B = 1-V/4.5$

b. $V = -A\log(B)x4.5$

A further correction to the data takes account of the fact that for a flat photographic plate the nozzle-to-plate distance varies with s, as does the cross-section of the incident beam, which is circular only on axis, and becomes progressively more elliptical thereafter with increasing scattering angle.

Errors may arise from incorrect calibrations. In addition, they may arise from sources such as neglect of beam cross-sectional area, non-monochromaticity of electron source, extraneous (background) scattering, sample impurities, etc. A list of possible sources of error, and parameters likely to be affected, is given in Table 2.2.[43]

When quoting errors in the results from electron diffraction structure determinations undertaken at Edinburgh, the esds derived from the least-squares correlation matrix are arbitrarily increased to attempt to allow for systematic errors. The scheme adopted is as follows:

Table 2.2 Sources of errors in the structural parameters determined by electron diffraction

Systematic errors	Parameter type affected
1. Error in the wavelength	r
2. Error in the nozzle-to-plate distance	r
3. Error in the scale on the microdensitometer	r
4. Error in the sector correction	u
5. Error in blackness correction	u
6. Further errors in the photographic process	u
7. Error in the position of the centre of the diffraction pattern	u
8. Deviations from radial symmetry in the diffraction pattern	u
9. Extraneous scattering	u
10. Neglect of (or wrong correction for) non-zero molecular beam cross-section	u
11. Sample impurities	r,u
12. Wrong background	u
13. Errors in the scattering amplitudes	u
14. Failure of approximations in the applied theory	u
15. Errors in the assumptions about the molecular symmetry or in the assumed parameters	r,u

Note: r = distances; u = amplitudes of vibration.

distances have the values of their esds increased by ca. 0.1%, bond angles by 0.2%, and amplitudes of vibration by 1% of the associated interatomic distance.

CHAPTER 3

THE GAS PHASE MOLECULAR STRUCTURES OF METHYLAMINODIFLUOROPHOSPHINE AND BIS-(DIFLUOROPHOSPHINO)AMINE DETERMINED BY ELECTRON DIFFRACTION

3.1 Introduction

Electron diffraction studies of $NMe(PF_2)_2$[23] and $N(PF_2)_3$[18] have revealed planar arrangements of ligands about nitrogen, and in the case of $NH(PF_2(SiH_3)$[24] the existence of a wide PNSi angle again suggests that the bonds around nitrogen are coplanar. Similarly, while the electron diffraction studies of $NMe_2(PF_2)$ and $NH_2(PF_2)$[13] show that there are perhaps pyramidal arrangements of ligands about nitrogen, with the angles between the P-N bonds and NR_2 planes being 32^o and 35^o respectively, microwave studies of both molecules[28,44] and a determination of the solid phase structure of the former[45] again show planar nitrogen groupings. It was therefore interesting to study the structure of $NHMe(PF_2)$ with a view to determining how the geometry of the PNHC skeleton compares with those found for other PNR_2 skeletons.

Since of the three difluorophosphino amines, only the tertiary[18] and primary[13] have had their gas phase molecular structures determined, a study of bis(difluorophosphino)amine was undertaken. In the tertiary amine the conformation is such that the overall symmetry is C_{3h} with lone pairs on phosphorus as far apart as possible, whereas in the case of $NMe(PF_2)_2$ the lone pairs lie cis to each other. The conformation adopted by $NH(PF_2)_2$ would therefore be of prime interest. The skeletal NHP_2 group would be expected to show a planar configuration as is the case in $NMe(PF_2)_2$ for the NCP_2 group.

The vibrational spectra of $NH(PF_2)_2$ in the gas phase[46] show two N-H stretching and two in-plane N-H deformation modes, suggesting that two conformers are present. However, a study[47] of the crystalline solid at 160 K indicates that only one conformer is present, the molecules having almost exact C_{2v} symmetry. The molecular structure of the secondary amine has therefore been investigated in the gas phase to see whether two distinct conformers could be distinguished.

The infrared spectrum of $NH(PF_2)(SiH_3)$[24] in the gas phase shows two distinct N-H stretching vibrations, implying that two conformers are present in significant abundance. This was confirmed by a gas phase electron diffraction study, which revealed that the two conformers differed from each other in the orientation of the $-PF_2$ group. The infrared spectrum[48] of $NHMe(PF_2)$ also shows two N-H stretching vibrations, with relative intensities of ca. 10:1, and so the electron diffraction structure determination undertaken on the compound was again used to investigate whether two conformers could be identified.

3.2 Experimental

A sample of $NHMe(PF_2)$ was prepared by reacting $PBrF_2$ with monomethylamine[48] in a two-bulb apparatus in the absence of air and under reduced pressure, according to Equation 16.

(16) $PBrF_2 + NH_2Me + NMe_3 \rightarrow NHMe(PF_2) + [NMe_3H]^+[Br]^-$

The driving force for the reaction is the stability of the quaternary ammonium salt. The product was purified by fractional condensation in vacuo and its purity checked by infrared spectroscopy.

Photographic intensities were recorded on Kodak Electron Image Plates using a Balzers' KD.G2 gas diffraction apparatus at nozzle-to-plate distances of 1000, 500 and 250 mm. The sample was maintained at a temperature of 250 K, while the nozzle was at room temperature (296 K). The value of 5.673 $\pm$ 0.003 pm for the electron wavelength was obtained from the analysis of the scattering pattern of gaseous benzene. The photographic intensities were converted to digital form using a Joyce-Loebl automatic microdensitometer.

With the exception of the initial conversion to uphill curves the data reduction and least-squares refinements were carried out, using established programs, on an ICL 4-75 computer[34,49].

Of the three difluorophosphino amines the bis species is the most difficult to prepare. The mono-substituted species is formed by the reaction described by Equation 17.

(17) $PBrF_2 + 2NH_3 \xrightarrow[\text{1 atm.}]{\text{gas phase}} NH_2(PF_2) + [NH_4]^+[Br]^-$ (15 mins)

The reaction goes readily and cleanly. However, in order to increase the number of difluorophosphine substituents on nitrogen, a stronger base is required to abstract bromide from $PBrF_2$, and trimethylamine is added to the reaction mixture. Unfortunately, both the bis and tris species are formed, and are inseparable by fractional condensation in vacuo. The tris species may be prepared by using a sufficient excess of $PBrF_2$ and NMe_3[50], and the published procedure for making $NH(PF_2)_2$[46] suggests acid cleavage of one N-P bond occurs in the presence of agents such as HCl, HBr or H_2S. However, all attempts to do this in the gas or liquid phase, including leaving $N(PF_2)_3$ in the presence of an excess of each reagent in turn for periods of up to four days, produced no reaction. Since the original spectra characterising $NH(PF_2)_2$ are perfectly satisfactory, it must be assumed that some impurity in that case catalysed the acid cleavage.

The secondary amine was therefore prepared according to Equation 18:

(18) $$4NH_2(PF_2) + PBrF_2 + NMe_3 \rightarrow 3NH_2(PF_2) + NH(PF_2)_2 + [NMe_3H]^+[Br]^-$$

By treating a four-fold excess of aminodifluorophosphine with bromodifluorophosphine and trimethylamine, and destroying the excess of primary amine from the mixture of primary and secondary amines with hydrogen bromide, yields of up to 15% of product were recorded relative to

difluorophosphino amine. The purity of the sample prepared in this way was checked by ir and nmr spectroscopy.

Electron-diffraction scattering intensities were recorded photographically using the Cornell University diffraction apparatus[30], now installed at the University of Edinburgh. The apparatus was operated in the conventional convergent beam mode, with a sector designed to give uniform scattering intensity from carbon atoms. With an accelerating potential of 44 kV and nozzle-to-plate distances of 128 and 285 mm, data were obtained over a range of the scattering variable s of 30-350 mm^{-1}. Data were recorded on Kodak Electron Image plates (three plates at each camera distance were used), with the sample at 228 K and the nozzle at 295 K.

Values of 5.707 and 5.719 pm were obtained for the electron wavelength used for the short and long distance wavelengths, by examining the scattering pattern of gaseous benzene.

The photographic intensities were obtained in digital form using a Jarrell-Ash double-beam microphotometer[51], with spinning plates. All calculations were carried out using an ICL 2970 computer at the Edinburgh Regional Computing Centre. The data reduction program used was a version of an established program[33] modified to handle data from the Jarrell-Ash microdensitometer. The least-squares refinement program is a new version of an

established program[34] which uses an off-diagonal weight matrix to allow for correlation between data points.

In all calculations for both species the complex scattering factors of Schafer[9] were used. The weighting points used in setting up the correlation matrices for $NHMe(PF_2)$ and $NH(PF_2)_2$ are given, together with other experimental details, in Table 3.1.

3.3 Refinement of $NHMe(PF_2)$

In the least-squares refinements of $NHMe(PF_2)$ local C_{3v} and C_s symmetries were assumed for the CH_3N and PF_2N groups respectively. The hydrogen bound to nitrogen was assumed to lie in the PNC plane. With these assumptions, the molecular structure could be defined by 12 independent parameters, taken to be the P-F, P-N, N-H, C-N and C-H bonds, the angles FPF, FPN, PNC, PNH and NCH, and two twist angles, defining the conformations of the $-PF_2$ and $-CH_3$ groups. The $-PF_2$ twist angle was defined to be zero when the FPF angle bisector was cis to the N-H bond, and the $-CH_3$ twist angle was taken to be zero when one C-H bond eclipsed the N-H bonds. In the later stages of refinement a variable amount of a second conformer differing only in $-PF_2$ twist angle from the first conformer was introduced.

All three heavy atom bonded distances lie beneath the peak at 160 pm in the radial distribution curve

(Figure 3.1a) and so are strongly correlated. Although the P-F, P-N and N-C distances refined satisfactorily, their amplitudes of vibration would not, and had to be assigned reasonable values.

The major skeletal angles, FPF, PNC and FPN, refined satisfactorily, as did the amplitudes of vibration for the non-bonded distance P...C. The amplitudes of vibration for the F...F and F...N distances refined as a single parameter. Of the parameters involving hydrogen only the C-H bonded distance and the NCH angle could be refined. The methyl group torsion angle was found by performing an R factor loop.

Assuming the presence of only one conformer, the PF_2 twist angle refined satisfactorily to ca. 171^{o}, with the two C...F amplitudes of vibration refining as a single parameter. After completing refinements with one conformer only, a series of refinements was carried out with fixed small amounts of a second conformer, the $-PF_2$ twist angle of which was fixed initially at values in the range 0 to 180^{o}, and latterly in the range 65^{o} to 105^{o}. The variation of R factor with amount of second conformer and twist angle is shown in Figure 3.2. Some refinements were carried out with the $-CH_3$ twist angle fixed at values other than 0^{o}. Altering this angle proved to have no significant effect on the refining parameters.

The final molecular parameters are listed in Table 3.2 and the least square correlation matrix in Table 3.3a.

The molecular scattering intensity curves are shown in Fig. 3.3. and the structures of the two conformers of PF_2-(NHMe) are depicted in Fig. 3.4, with possible H...F interactions shown by broken lines.

3.4 Refinement of $NH(PF_2)_2$

In the early stages of refinement the molecular model used allowed for the presence of only a single conformer. The basic structure had C_{2v} symmetry and was defined in terms of P-F, P-N, and N-H distances, and FPF, FPN and PNP angles. The hydrogen atom was assumed to lie in the PNP plane. Distortion from C_{2v} symmetry (with the FPF angle bisectors eclipsing the N-H bond) was possible by twisting the PF_2 groups around the P-N bonds. These two twists could be constrained to be equal, or equal and opposite, giving structures of C_2 or C_s symmetry. Using this model, the principal bond lengths and angles refined readily, and the best fit (R_G = 0.061) was obtained for a C_2 structure, with PF_2 groups twisted 5^o from the C_{2v} positions.

The model was then modified so that a variable amount of a second conformer, differing from the first only in the PF_2 twist angles, could be included. As it was not feasible to investigate all combinations of the four twist angles defining two conformations and the relative proportions of the two, some constraints on the twist angles were applied. All possible mixtures of conformation

that could be described by two twist angles and a proportionality factor were explored. There was no significant reduction of the R factor for any amount of a second conformer with C_2 or C_s symmetry, including those forms (of C_s and C_{2v} symmetry respectively) in which one or more of the phosphorus lone pairs eclipsedthe N-H bond. However, a considerable improvement was obtained when it was assumed that the second conformer had one angle which was the same as those in the major form, and the second angle was treated as a variable. In Fig 3.5. the variations of the R factor with this angle and with the percentage of the second conformer are shown. The lowest R factor (0.05) was obtained for 27.5% of a form with twist angles of 5 and 58°.

The results of the final refinement are given in Table 3.4. All distances quoted are r_a, and errors are estimated standard deviations obtained in the least-squares analysis, increased to allow for systematic errors. The final least-squares correlation matrix (Table 3.3b) shows several strong correlations between parameters caused by overlap of the P-F and P-N and F...F and F...N peaks in the radial distribution curve (Figure 3.1b).The intensity data and final weighted difference curves are shown in Figure 3.6.

3.5 Results and Discussion

(a) $NHMe(PF_2)$

The parameters found for the skeletal group F_2PN are

in good agreement with those found for closely related compounds (see Table 3.5).The P-N bond length is towards the lower end of the expected range, and the P-F distance is similarly long. However, the non-bonded distances F...F and F...N have values consistent with Bartel hard sphere radii[52] and as a consequence the FPF angle is fairly small and the FPN angle is quite wide. The wide PNC angle can similarly be accounted for in terms of P...C contacts.

No evidence could be obtained regarding the location of the imino hydrogen, but considering the wide PNC angle found (ca. 125^{o}), it is possible that the assumption that the bonds to nitrogen are coplanar is correct.

The twist angle of the $-PF_2$ group of the major conformer refined to 171.4 (20)^{o}. It is probable that the average twist angle of this conformer is 180^{o}, and that torsional vibration about the mean position is giving rise to a substantial shrinkage effect. In this configuration, fluorine atoms lie close enough to methyl protons for there to be some stabilizing effect from weak H...F interactions. The shortest H...F distances for a $-PF_2$ twist angle of 170^{o} vary between 250 pm and 279 pm, depending on the orientation of the CH_3 group. This compares with the sum of the van der Waals' radii for hydrogen and fluorine of 255 pm.

Two N-H stretching vibrations are evident in the room temperature infrared spectrum of $NHMe(PF_2)$, the major

peak occurring at 3467 cm^{-1} and the other at 3417 cm^{-1}. The infrared spectrum of the solid phase at 77 K shows the presence of only one N-H stretching vibration at 3430 cm^{-1}. From the evidence presented in Figure 6 we deduced that the data are consistent with the possible existence of a second conformer, with a $-PF_2$ dihedral angle of ca. 85° and an abundance of up to 20% at room temperature.

In this second conformer there are contacts of 260 pm for one fluorine atom and the proton on nitrogen, and between 263 pm and 296 pm for one fluorine and the closest methyl proton, depending on the $-CH_3$ group twist angle. This configuration corresponds to that of the major conformer found for the compound $NH(PF_2)(SiH_3)$ which has a $-PF_2$ twist angle of 90° and one (Si) H...F contact at 267 pm and one (N) H...F contact at 252 pm. However, in that case the second conformer has a twist angle of 26° which gives rise to only (N) H...F contacts. The absence of a 180° conformer can be explained in terms of the longer Si-H and Si-N bonds in conjugation with the wide PNSi angle, precluding any close (Si)H...F contact.

(b) $NH(PF_2)_2$

From Table 3.5 it can be seen that there is very little variation of P-F distances and FPF and FPN angles in the series of primary, secondary and tertiary difluorophosphino amines, but that the P-N bond lengths increase from around

165 pm in amines with one PF_2 group, to 168 pm in amines with two PF_2 groups; to 171 pm in $N(PF_2)_3$. This may be interpreted in terms of $(p\rightarrow d)\pi$ bonding, with competition between phosphorus atoms for the nitrogen lone pair of electrons, or in terms of non-bonded contacts between phosphorus atoms. The P...P distance in $NH(PF_2)_2$ is 295 pm, with a PNP angle of 122°, but in $N(PF_2)_3$ the maximum possible PNP angle is 120° and as the P...P distance of 296 pm is essentially the same the long P-N bond length may be explained. However the short P...P distance (285 pm) in $NMe(PF_2)_2$[23] associated with a PNP angle of 116° and similarly short P...P distance (289 pm) and narrow PNP angle (118°) found for $N(SiH_3)(PF_2)_2$[27], coupled with the fact that the increments in going from the primary to secondary, and secondary to tertiary difluoro-phosphino amine are approximately equal, tends to suggest that steric crowding is not severe in the molecule studied here.

There is close agreement between X-ray[47] and electron diffraction results for the main geometrical parameters, indicating that although the conformation may change between gaseous and crystalline phases, there is very little distortion of bond lengths and inter-bond angles. This is to be expected, as the X-ray study showed that there were no strong intermolecular contacts.

The conformations adopted by bis(difluorophosphino)amine are of particular interest. The predominant gas-phase

form is very similar to that found in the crystalline solid. It seems highly likely that the gas-phase form has C_{2v} symmetry, and that the apparent 5^{o} twist angles observed are shrinkage effects caused by torsional vibrations of the PF_2 groups. In this form there are four intramolecular F...H contacts of 263-270 pm, and these may provide the weak attractive forces that stabilise this arrangement. In the solid there are additional intermolecular F...H contacts; these do not appear to affect the structure of individual molecules, but only the packing arrangement.

The existence of two N-H stretching and two N-H in-plane deformation bands in the gas-phase ir spectrum of $NH(PF_2)_2$[46] indicated that two conformers probably existed in the gas phase. This has now been confirmed by the structural study. In the less abundant form, one PF_2 group is twisted about 60^{o} from the C_{2v} position. Why this particular structure should be favoured is not clear, but it should be noted that one F...H contact is now at 250 pm, which is slightly less than the sum of the Van der Waals' radii of fluorine and hydrogen. Figure 3.7 shows the conformations adopted by $NH(PF_2)_2$ in the gas phase, with possible attractive H...F interactions indicated by broken lines.

It is not possible to draw conclusions about the conformation in solution of bis(difluorophosphino)amine from the present work, but it is interesting to note that the nmr

coupling constant $^2J(PP')$ is much smaller for this compound[46] than for substituted bis(difluorophosphino)-amines[53,54,55] and that large couplings have been associated with strong interactions between lone pairs of electrons on phosphorus atoms[56]. The existence of a conformer in which this interaction is reduced by the twisting of one PF_2 group away from the position giving maximum lone-pair interaction may provide a rationalisation of the observed nmr coupling constants. The Raman spectrum of liquid $NH(PF_2)_2$ shows two N-H stretching bands at 3315 and 3355 cm^{-1}, with an intensity ratio of ca. 5:1. Thus it seems likely that in condensed fluid phases the conformational properties relate more closely to those in the vapour than to those in the crystal.

3.6 Conclusions

The vibrational spectra of both molecules studied here (Figure 3.8) indicated that two conformers were present in the gas phase, and this has now been confirmed by gas phase electron diffraction, the conformations being directed by intramolecular H...F attractive interactions. Both molecules show expected shortening of the P-N bond relative to the Shomaker-Stevenson[17] estimate for a P-N single bond, commensurate with the number of difluorophosphino groups around nitrogen, and in all other respects the geometrical parameters compare with those found for previously determined difluorophosphino amine structures.

Table 3.1: Weighting functions, correlation parameters and scale factors

Compound	Camera Height mm	Δs nm^{-1}	s_{min} nm^{-1}	s_{max} nm^{-1}	sw_1 nm^{-1}	sw_2 nm^{-1}	p/h	Scale factor
(a) $NHMe(PF_2)$	250	4	60	306	80	265	0.456	1.87(5)
	500	2	27	153	45	135	0.498	1.78(5)
	1000	1	10	78	20	67.5	0.499	1.27(5)
(b) $NH(PF_2)_2$	128.47	4	60	80	300	340	0.126	0.847(9)
	284.76	2	34	44	118	146	0.496	0.797(11)

Table 3.2: Molecular parameters for $PF_2(NHMe)$

	Distances / pm	Amplitude / pm
(a) Independent distances		
r_1(P-F)	159.3(4)	4.9(fixed)
r_2(P-N)	164.8(7)	4.5(fixed)
r_3(N-H)	100.0(fixed)	7.5(fixed)
r_4(C-N)	144.8(12)	4.4(fixed)
r_5(C-H)	107.8(20)	7.7(fixed)
(b) Independent angles (^{o})		
<1 F-P-F	94.1(8)	
<2 F-P-N	100.6(4)	
<3 P-N-C	125.3(20)	
<4 N-C-H	113.8(25)	
<5 P-N-H	118.0(fixed)	
<6 PF_2 twist[a]	171.4(20)	
<7 PF_2 twist[b]	85.0(fixed)	
<8 CH_3 twist	0.0(fixed)	
(c) Dependent Distances		
d_6 (F...F)	233.2(15)	8.8(12)
d_7 (F...N)	249.5(10)	8.8(tied to u_6)
d_8 (F...(N)H)[a]	334.3(18)	15.0(fixed)
d_9 (F...(N)H)[a]	343.3(30)	15.0(fixed)
d_{10}(C...F)[a]	295.1(40)	16.2(30)
d_{11}(C...F)[a]	328.1(30)	16.2(tied to u_{10})
d_{12-17}(F...(C)H)[a]	270-405(3)	16.0(fixed)
d_{18}(P...(N)H)	229.5(10)	11.0(fixed)
d_{19}(P...C)	275.2(15)	8.0(10)
d_{20-22}(P...(C)H)	308-367(4)	12.0(fixed)
d_{23}(N...(C)H)	212.3(25)	11.0(fixed)
d_{24}(C...(N)H)	209.7(13)	11.0(fixed)
d_{25}((C)H...(C)H)	170.8(50)	12.0(fixed)
d_{26}((N)H...(C)H)	233.2(50)	18.0(fixed)
d_{27}((N)H...(C)H)	284.3(29)	18.0(fixed)
d_{28}((N)H...(C)H)	284.3(25)	18.0(fixed)
d_{29}(C...F)[b]	300.7(23)	16.2(tied to u_{10})
d_{30}(C...F)[b]	381.2(18)	16.2(tied to u_{10})

Note: Quoted errors are estimated standard deviations derived from the least squares analysis and increased to allow for systematic errors.

[a]major conformer only; [b]minor conformer only.

Table 3.3: Least squares correlation matrices multiplied by 100

(a) $NHMe(PF_2)$

r_1	r_2	r_4	r_5	<1	<2	<3	<4	<6	u_6	u_{10}	u_{19}	k_1	k_2	k_3	
100	-85	71				-41						-83	-63		r_1
	100	-54				42						81	63	70	r_2
		100				-43						-75	-63		r_4
			100				-41					42			r_5
				100	-42	-41									<1
					100				-63						<2
						100	-80					55	61		<3
							100	-41				-49	-54		<4
								100							<6
									100						u_6
										100					u_{10}
											100				u_{19}
												100	70		k_1
													100		k_2
														100	k_3

(b) $NH(PF_2)_2$

r_1	r_2	r_3	<1	<2	<3	<4	u_1	u_3	u_4	u_6	u_7	u_{11}	u_{12}	u_{17}	k_1	k_2	
100		-27			41		54										r_1
	100		-23	54	-21	-47			-34	33	25			56			r_2
		100															r_3
			100	-47		-66	-24			-28		33	27	-35			<1
				100	-37				48	42				81	28		<2
					100		49							-23	-27		<3
						100			22			-49		-22			<4
							100								43		u_1
								100									u_3
									100					39	36	26	u_4
										100				58			u_6
											100	26			21		u_7
												100					u_{11}
													100				u_{12}
														100			u_{17}
															100	32	k_1
																100	k_2

Note (a) Only elements with absolute values of ≥40 are included.
(b) Only elements with absolute values of ≥20 are included.

Table 3.4: Molecular parameters for $NH(PF_2)_2$

	Distance/pm	Amplitude/pm
(a) Independent geometrical parameters		
r_1(P-F)	158.4(3)	5.6(4)
r_2(P-N)	168.4(8)	6.8(tied to u_1)
r_3(N-H)	97.3(23)	5.7(24)
	Angle/°	
Angle 1 (F-P-F)	95.6(10)	
Angle 2 (F-P-N)	98.3(7)	
Angle 3 (P-N-P)	122.1(7)	
Angle 4 (twist 1)[a]	5.3(13)	
Angle 5 (twist 2)[b]	58[c]	
% of conformer 2	27.5[e]	
(b) Dependent distances		
d_4 (F...F)	234.8(9)	7.4(7)
d_5 (F...N)	247.3(11)	9.2(tied to u_4)
d_6 (P...P)	294.8(14)	10.0(7)
d_7 (P...F)[d]	387.6(27))	
d_8 (P...F)[d]	395.5(30))	12.4(6)
d_9 (P...F)[e]	333.0(25))	
d_{10}(P...F)[e]	409.7(24))	
d_{11}(F...F)[f]	436(4)	15.7(20)
d_{12}(F...F)[f]	494(2)	13.4(20)
d_{13}(F...F)[e]	379(3)	15.7(tied to u_{11})
d_{14}(F...F)[e]	469(3)	13.4(tied to u_{12})
d_{15}(F...F)[e]	470(3)	13.4(tied to u_{12})
d_{16}(F...F)[e]	485(4)	15.7(tied to u_{11})
d_{17}(P...H)	231.7(22)	11.0(fixed)
d_{18}(F...H)[d]	250-310	18.4(80)

[a]Twist angle for both PF_2 groups of major conformer, and for one group of second conformer; [b]Twist angle for one PF_2 group of second conformer; [c]See text; [d]Both conformers; [e]Minor conformer only; [f]Major conformer only.

Table 3.5: Important geometrical parameters for some aminodifluorophosphines

Compound	Technique	Ref.	r(P-N)	r(P-F)	r(C-N)	<(F-P-F)	<(N-P-F)	<(M-N-P)	Shortest r(M)H...F)
$NMe(PF_2)_2$	Electron diffraction	23	168.0(6)	158.3(2)	147.9(17)	95.1(3)	99.6(3)	122.0(4)	
$NMe_2(PF_2)$	Electron diffraction	13	168.4(8)	158.9(3)	144.8(6)	99 (3)	97 (4)	118.3(6)	253(6)
	Microwave	44	166	157	148[a]	95.3	99.8	(121.3[b] (124.5[c]	
$PF_2(NH_2)$	Electron diffraction	13	166.1(7)	158.1(3)		95.3(11)	101.1(11)		262.3(15)
	Microwave	28	165.0(4)	158.7(4)		94.6(2)	100.6(2)		
$PF_2NH(SiH_3)$	Electron diffraction	24	165.4(6)	157.5(3)		100.8(12)	95.6[d]	127.9(7)	267(3)
$N(PF_2)_3$	Electron diffraction	18	171.1(4)	157.4(2)		96.9(3)	99.2(3)		
$NH(PF_2)_2$	Electron diffraction	26	168.4(8)	158.4(3)		95.6(10)	98.3(7)		250[e]
$PF_2(NHMe)$	X-ray diffraction	47	166.7(10)	157.8(5)		95.7(4)	99.4(4)		
	Electron diffraction	25	164.8(7)	159.3(4)	144.8(12)	94.1(8)	100.6(4)	125.3(20)	250[e]

Note: distances in pm, angles in degrees

[a] assumed; [b] fluorines trans to carbons; [c] fluorines cis to carbons; [d] see ref 24; [e] two conformers - see text

Figure 3.1: Final and observed radial distribution curves for (a) $NHMe(PF_2)$ and (b) $NH(PF_2)_2$. Before Fourier inversion data were multiplied by $s^2.exp[(-0.00015\ s^2)(Z_P-f_P)(Z_F-f_F)]$.

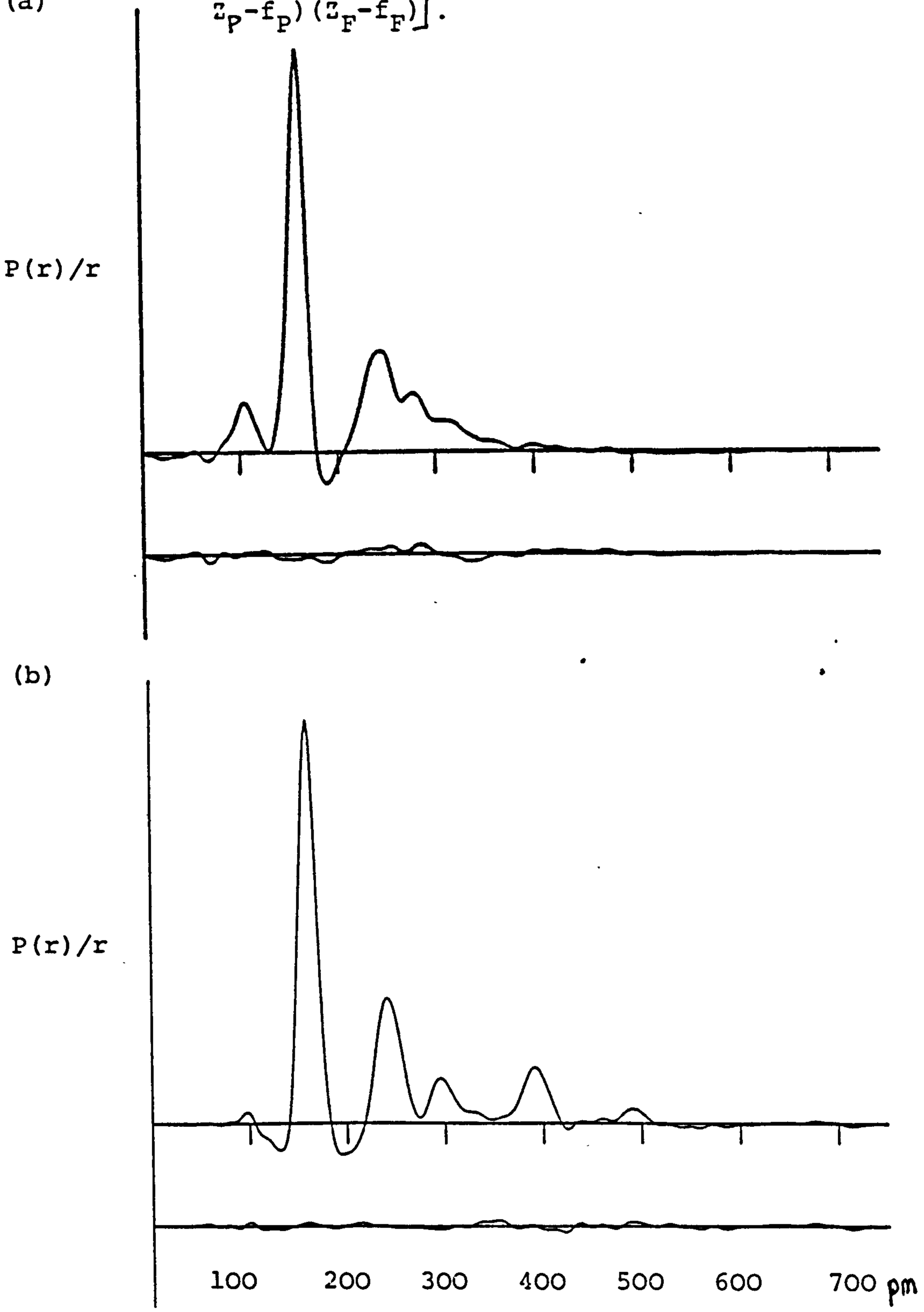

Figure 3.2 : Variation of R_G factor with proportion and twist angle of second conformer of $NHMe(PF_2)$ (b) fixed percentages and varying angles and (a) fixed angle and varying percentages

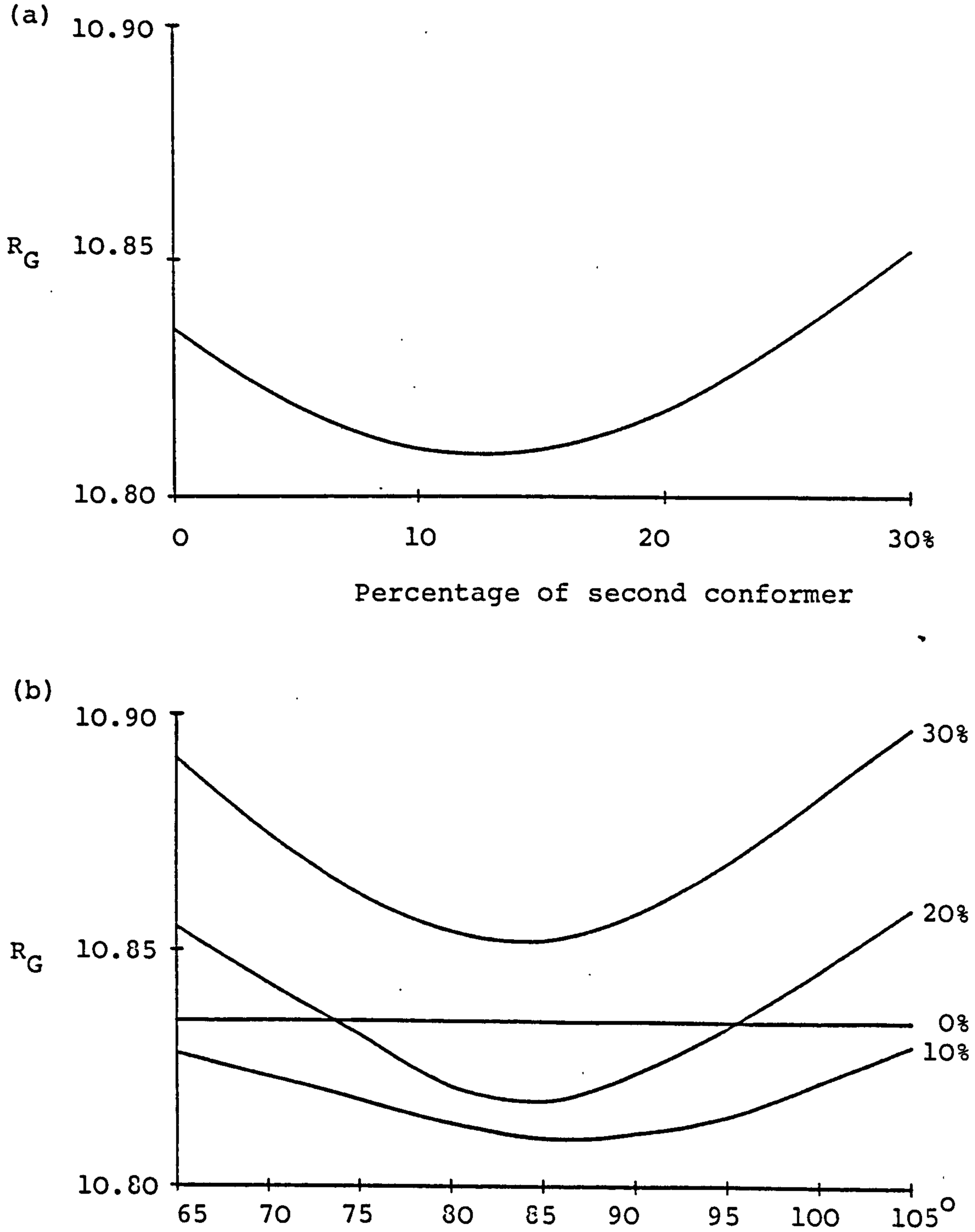

Figure 3.3 : Observed and final weighted difference molecular intensity curves for $NHMe(PF_2)$ for nozzle-to-plate distances of (a) 250, (b) 500 and (c) 1000 mm.

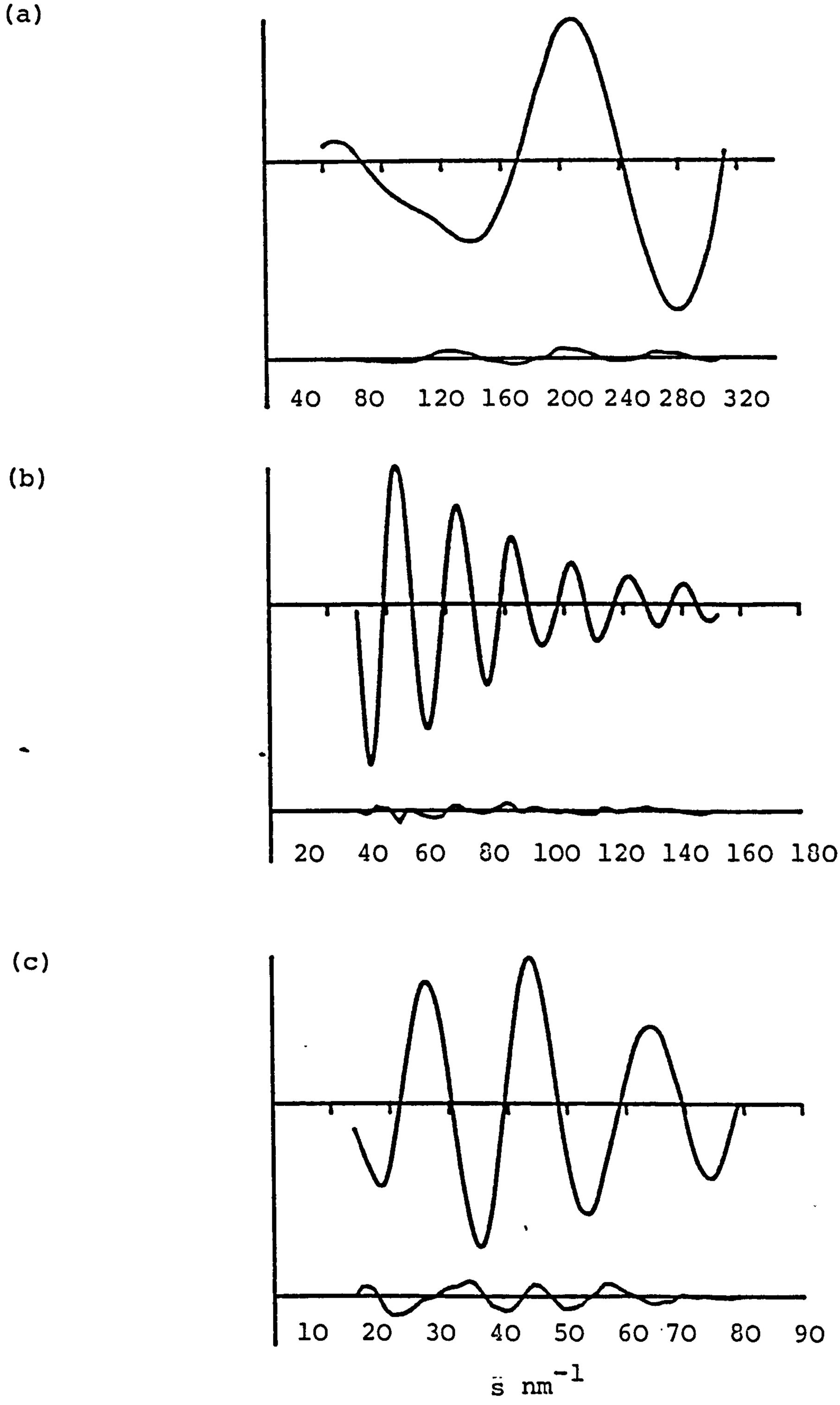

Figure 3.4 : Molecular structures of $NHMe(PF_2)$
(a) major conformer
(b) minor conformer

(a)

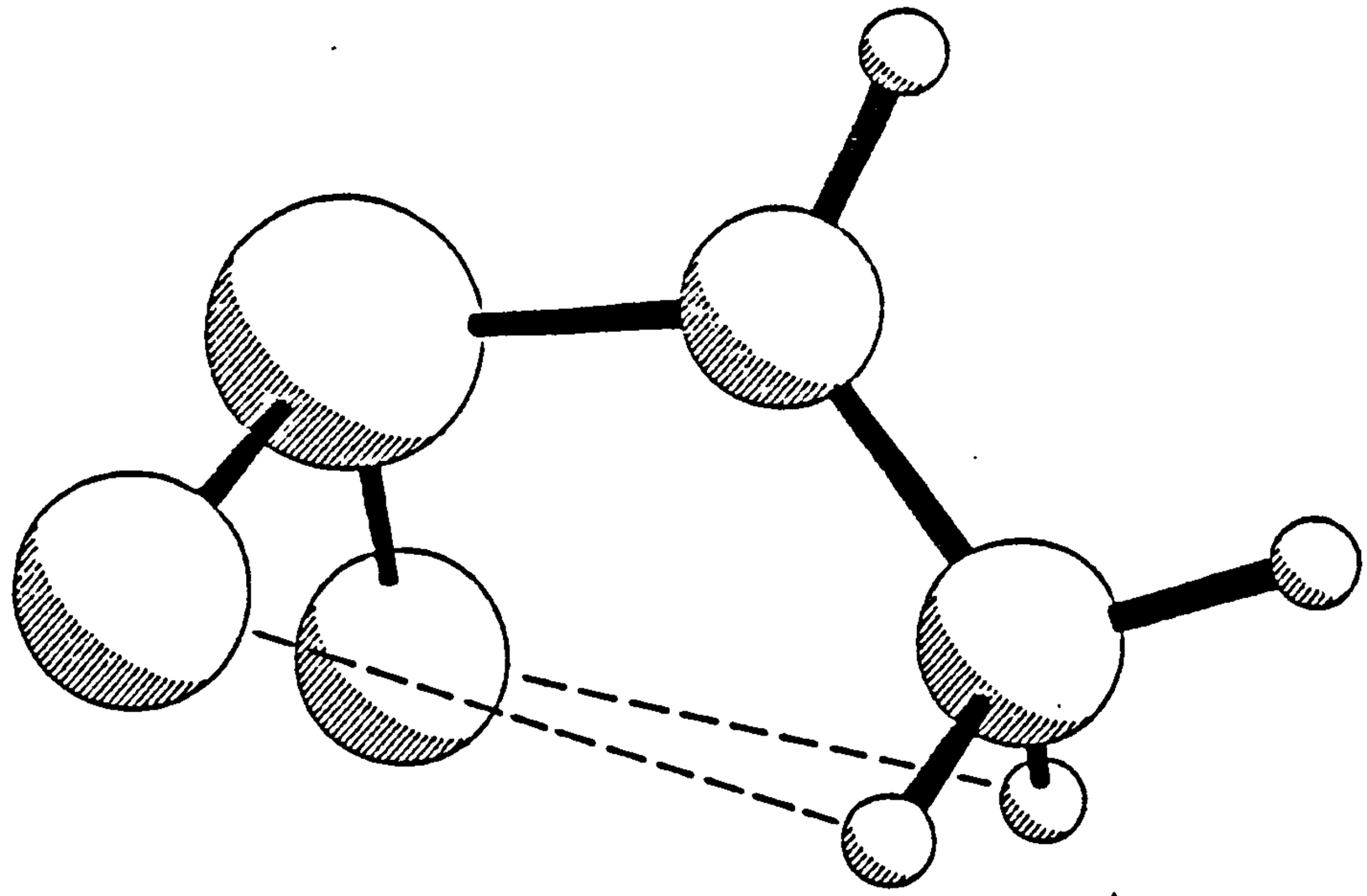

(b)

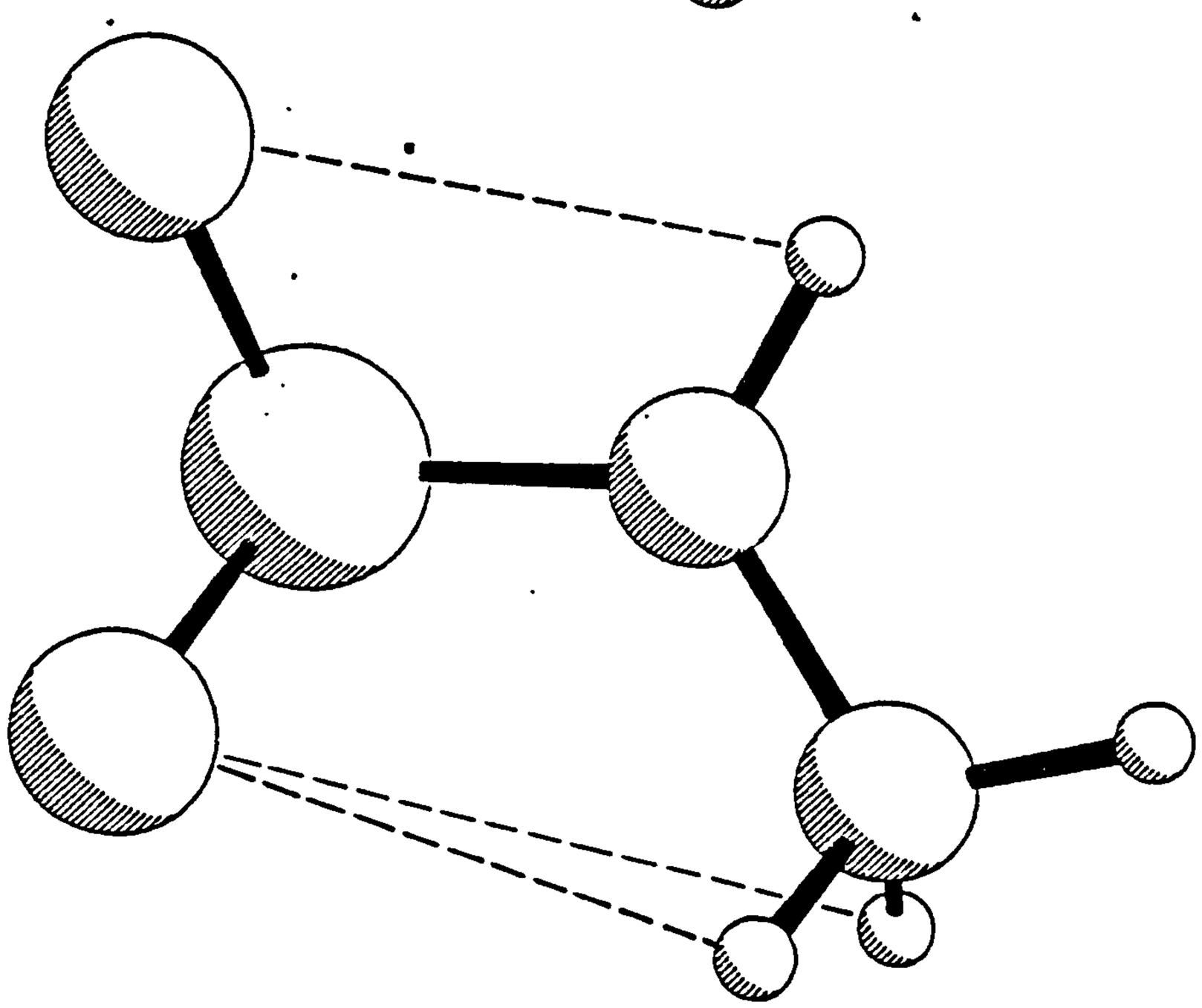

Note: hydrogen to fluorine attractive interactions are shown by broken lines

Figure 3.5 : Variations of the R_G factor with (a) percentage of second conformer present and (b) second twist angle in the second conformer of $NH(PF_2)_2$

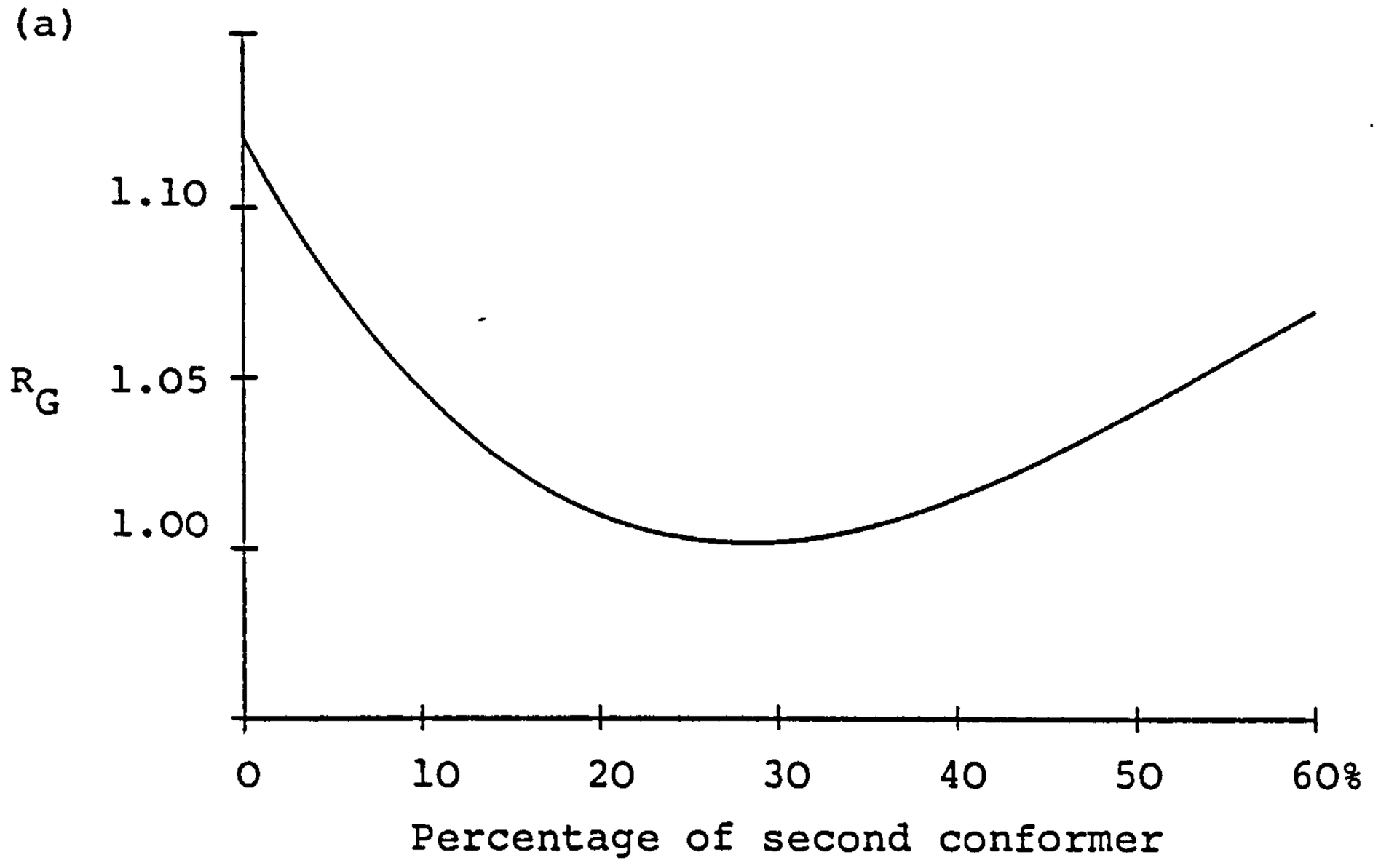

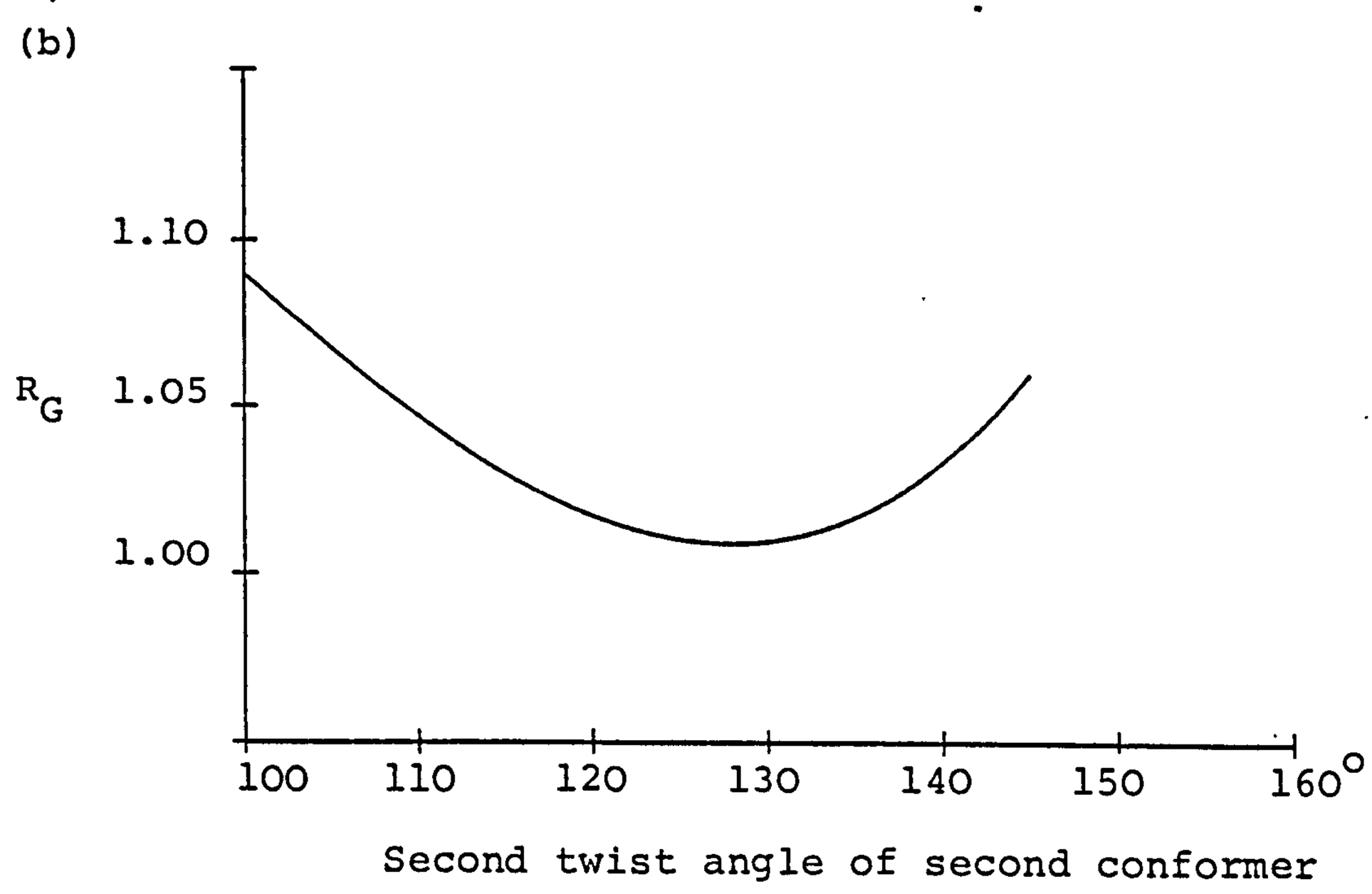

Figure 3.6 : Observed and final weighted difference molecular-intensity curves, for nozzle-to-plate distances of (a) 128 and (b) 285 mm

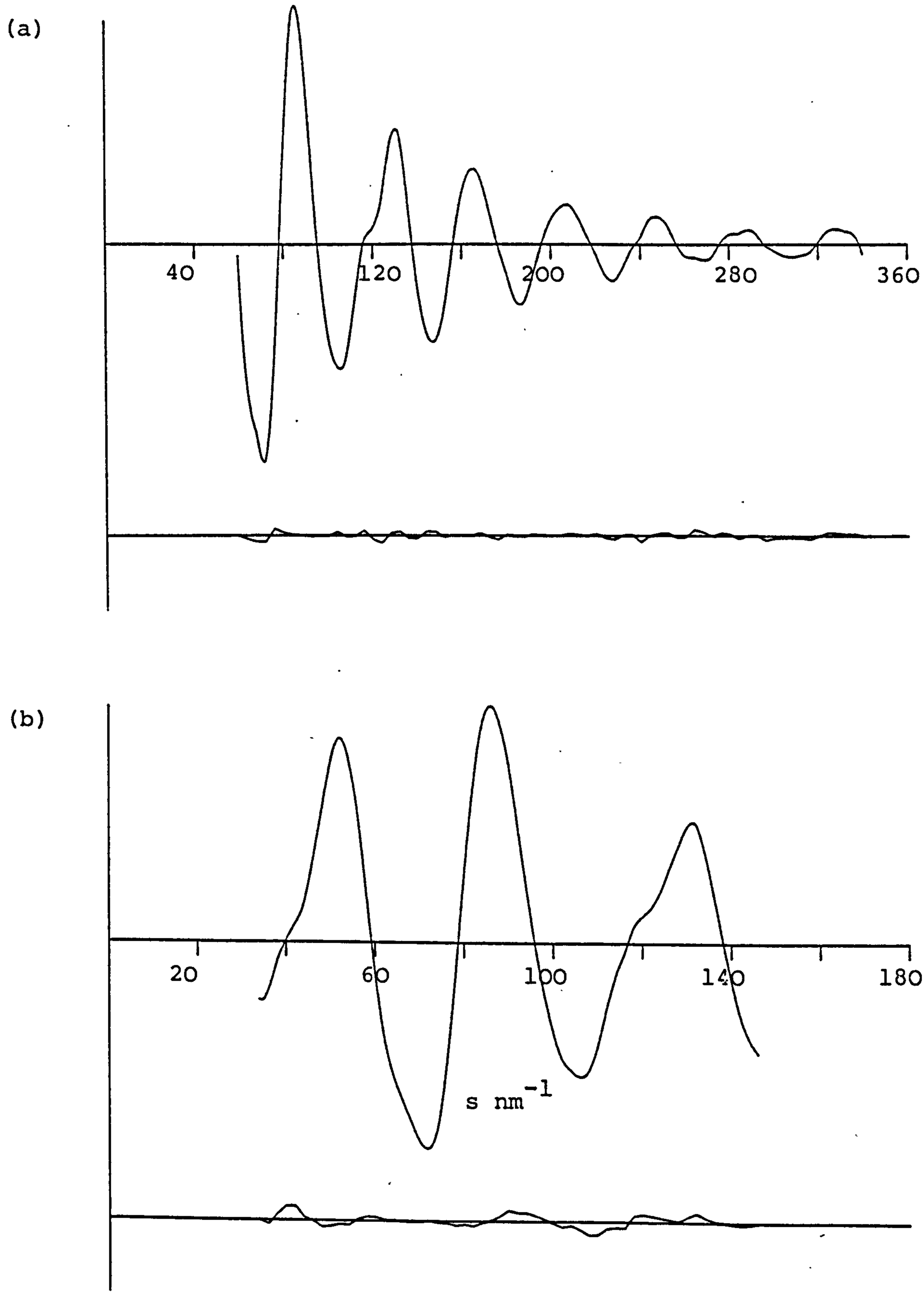

Figure 3.7 : The molecular structures of $NH(PF_2)_2$
(a) major conformer
(b) minor conformer

(a)

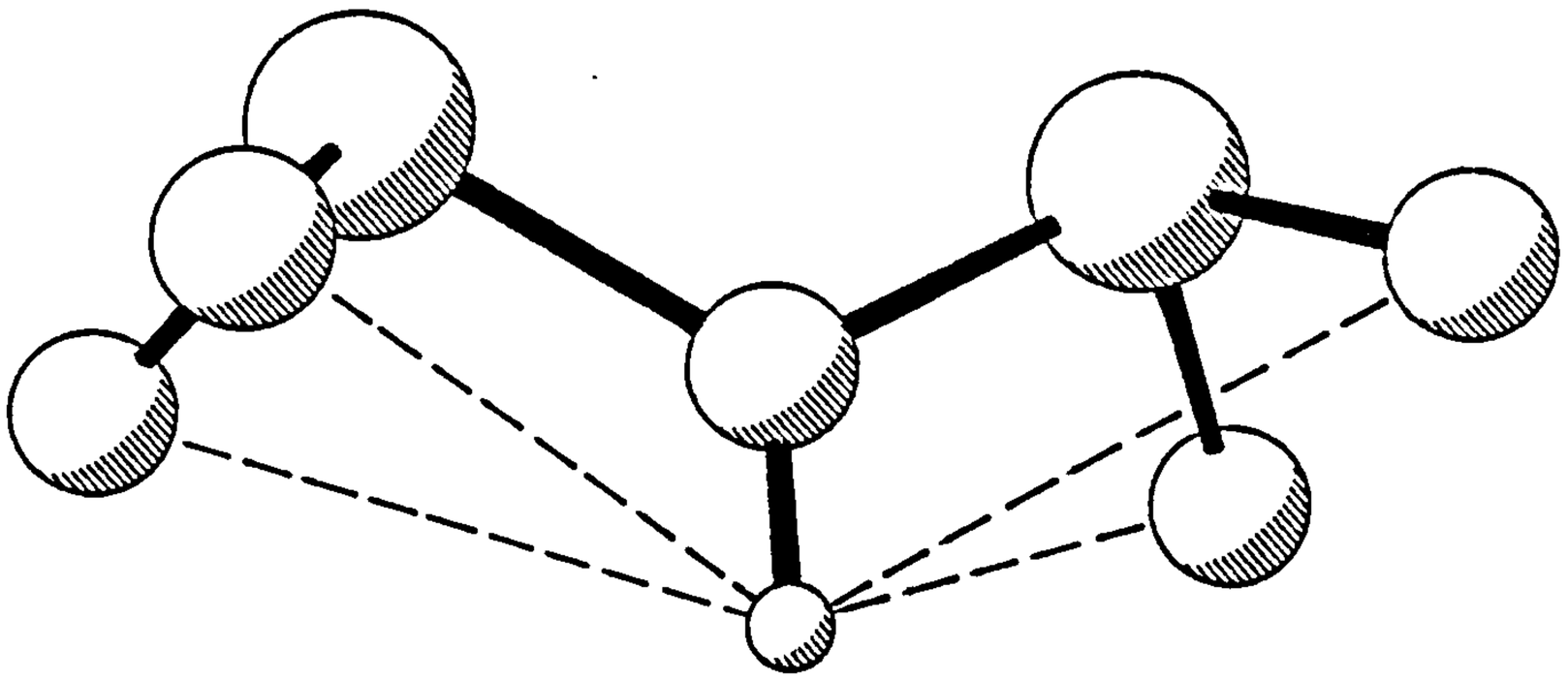

(b)

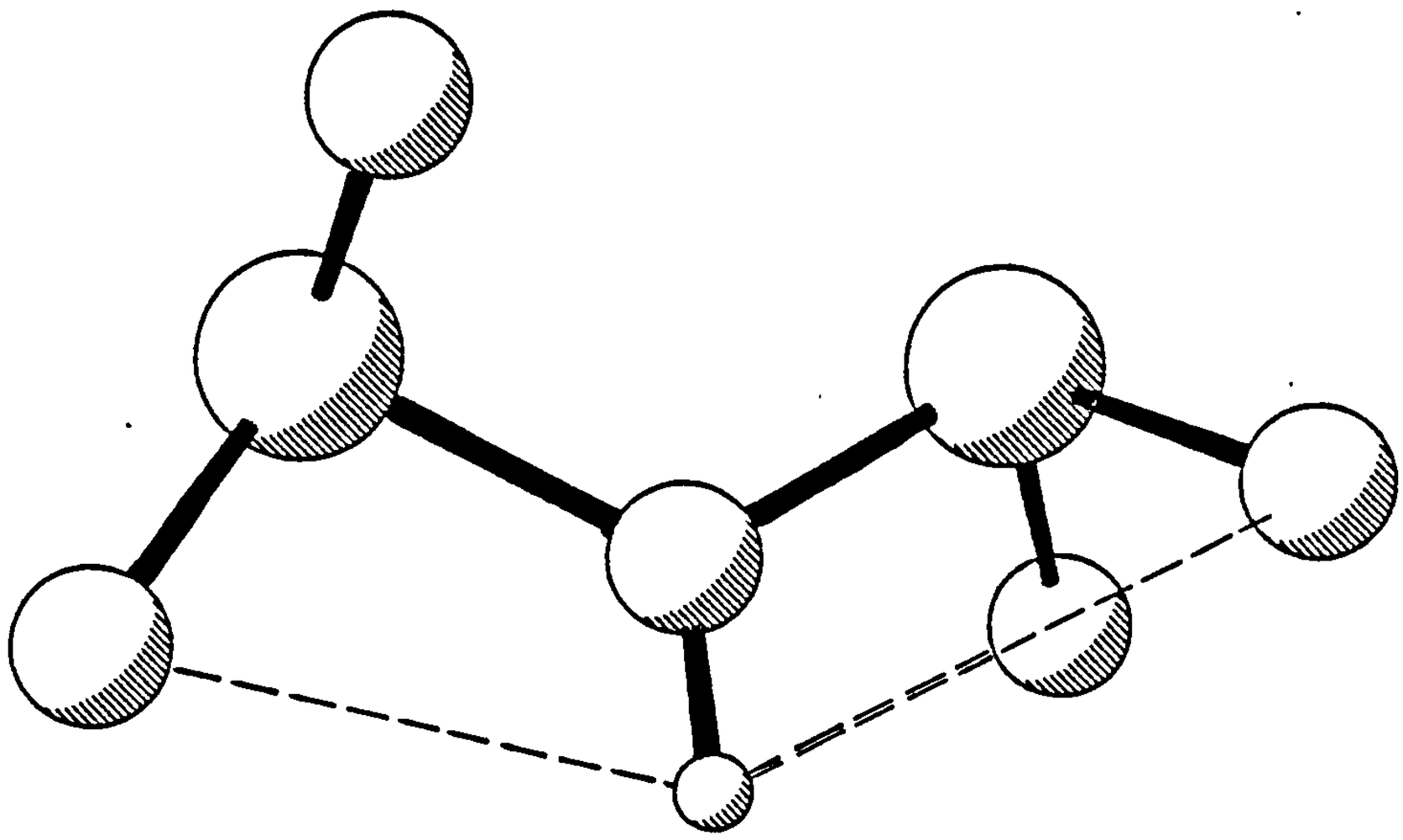

Note: possible hydrogen to fluorine attractive interactions are shown by broken lines

Figure 3.8: Infrared spectra of (a) $NHMe(PF_2)$ and (b) $NH(PF_2)_2$. N-H bands are indicated in s and d for stretch and deformation modes respectively.

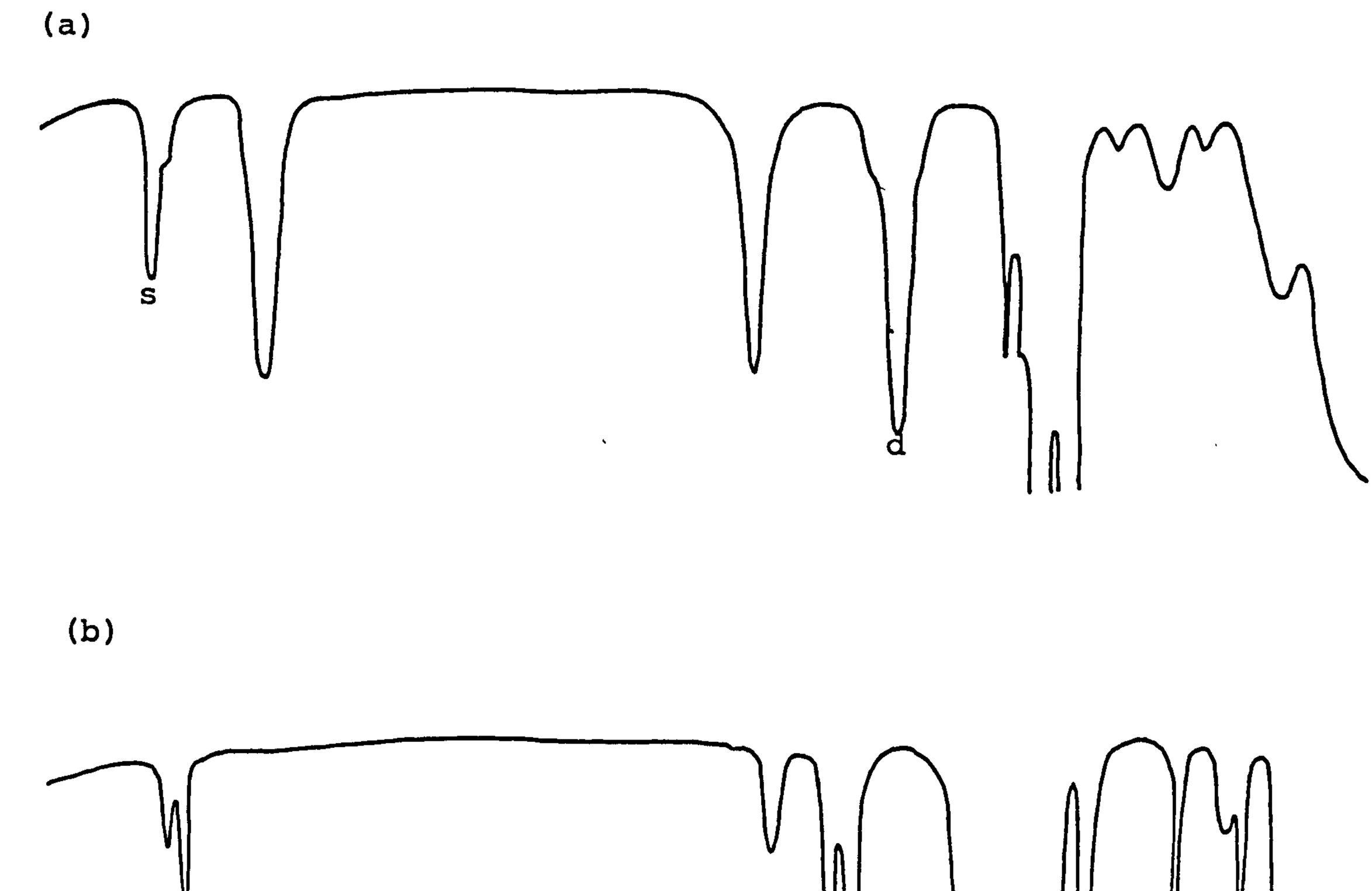

CHAPTER 4

THE GAS PHASE MOLECULAR STRUCTURES OF DIFLUOROPHOSPHINO(DISILYL)AMINE AND BIS(DIFLUOROPHOSPHINO)SILYLAMINE DETERMINED BY ELECTRON DIFFRACTION

4.1 Introduction

The molecular geometries of silicon- and phosphorus-substituted amines have been extensively studied. The silyl amines show a significant shortening of the Si-N bond compared with the Shomaker-Stevenson estimate[17] with the higher substituted trisilylamine[15,16] having a longer bond (173.4(2) pm) than disilylamine (172.5(3) pm)[21], which is correspondingly longer than that for dimethyl(silyl)-amine (171.5(4) pm)[23], due to p→d π-bonding from the lone pair on nitrogen to vacant d orbitals on silicon. As with the difluorophosphino amine series[13,18,26], the decreasing Si-N bond length with number of silyl ligands is seen to be a result of the lone pair on nitrogen being directed towards fewer sites. Only dimethyl(silyl)amine shows any deviation from a planar arrangement of ligands at nitrogen, and, as for the corresponding difluorophosphino amines, this may be due to a low-frequency out-of-plane deformation, which would give a large shrinkage effect.

However, of the three amines containing both silyl and difluorophosphino substituents, only one, $NH(PF_2)-(SiH_3)$, has been the subject of a structural study[24]. It was therefore important to study the other two, $N(PF_2)_2(SiH_3)$ and $N(PF_2)(SiH_3)_2$, as these would be expected to have planar arrangements of the bonds to nitrogen. It was also of interest to see whether there was any evidence of competition between phosphorus and silicon for the nitrogen lone pair of electrons, leading

to a shortening of one type of bond to nitrogen at the expense of the other type. Finally, the conformations adopted by the difluorophosphino groups were of interest, as predictions about these had been made on the basis of nmr coupling constants[53].

4.2 Experimental

A sample of difluorophosphino(silyl)amine was prepared[53] from first reacting $NH_2(PF_2)$ with SiH_3Br at 250 K under reduced pressure according to Equation 19.

(19) $$SiH_3Br + NH_2(PF_2) \xrightarrow[255\ K]{1\ hour} NH(PF_2)(SiH_3) + HBr$$

$$2HBr + NH_2(PF_2) \xrightarrow[255K]{fast} [NH_4]^+ [Br]^- + PF_2Br$$

$NH(PF_2)(SiH_3)$ was isolated by fractional condensation in vacuo. The driving force in the above reaction is the formation of ammonium bromide. Further silylation was accomplished by mixing equal amounts of $NH(PF_2)(SiH_3)$ and SiH_3Br, adding NMe_3 under reduced pressure, and allowing the mixture to warm to room temperature for ca. 10 seconds prior to recondensing remaining volatiles in clean glassware, according to Equation 20.

(20) $$NH(PF_2)(SiH_3) + SiH_3Br + NMe_3 \xrightarrow[298K]{10\ sec} N(PF_2)(SiH_3)_2 + [NHMe_3]^+[Br]^-$$

The final product was purified by fractional condensation in vacuo and its purity checked by infrared spectroscopy. Yields up to 75% of the theoretical were recorded.

Bis(difluorophosphino)silyl amine was prepared[53] from the reaction between $NH(PF_2)_2$ and silyl bromide in the presence of trimethylamine, according to Equation 21.

$$(21)\quad NH(PF_2)_2 + SiH_3Br + NMe_3 \xrightarrow[10\ secs]{298K} N(SiH_3)(PF_2)_2 + [NHMe_3]^+[Br]^-$$

Up to 70% yields were recorded for this reaction. (The preparation of bis(difluorophosphino)amine is described in Chapter 3). Again the product was purified by fractional condensation in vacuo and its purity checked spectroscopically.

Electron diffraction scattering intensities were recorded using the Cornell/Edinburgh diffraction apparatus[25,30], with nozzle-to-plate distances of 128 and 285 mm, and an accelerating voltage of ca. 43 kV. During exposures samples were maintained at 250 K, and the nozzle at room temperature, 293 K. Data were recorded on Kodak Electron Image plates, and obtained in digital form using a Jarrell-Ash double beam microphotometer, with spinning plates[51]. The electron wavelengths were determined from the scattering patterns of gaseous benzene, recorded immediately before or after the sample plates.

All calculations were carried out on an ICL 2970 computer at the Edinburgh Regional Computing Centre, using established data reduction[26] and least-squares refinement programmes[34]. Weighting points used in setting up the off-diagonal weight matrices are given, together with other experimental data, in Table 4.1.In all calculations the complex scattering factors of Schafer et al[9] were used.

4.3 Refinement

Difluorophosphino(disilyl)amine - In refinements of the structure of $N(PF_2)(SiH_3)_2$ it was assumed that the NPF_2 group had local C_s symmetry, and that the two $NSiH_3$ groups had local C_{3v} symmetry. The $N(SiH_3)_2$ group was assumed to have C_2 symmetry, with the two SiH_3 groups twisted away from the conformation in which one Si-H bond of each group was trans to the further N-Si bond. The $PNSi_2$ group was initially assumed to be planar, with C_{2v} symmetry, but distortions of the P-N bond, both in the plane and perpendicular to it, were subsequently permitted: in the final refinements the distortion in the plane was the only one allowed. Finally, the PF_2 group was allowed to twist, about the P-N bond, with zero twist angle defined for the conformation in which the FPF angle bisector lay perpendicular to the NSi_2 plane.

With these assumptions, the structure was defined by

eleven geometrical parameters. Although there were strong correlations between parameters (Table 4.2) caused by overlap of peaks in the radial distribution curve (Figure 4.1a), it was soon clear that the $PNSi_2$ skeleton was planar, and that the three angles at nitrogen were equal, within experimental error. Most of the other heavy-atom parameters refined easily, but the three bonded distances, P-F, P-N and Si-N, were strongly correlated, and occasionally the relative positions of the P-F and P-N distances would reverse. On the basis of the known bond lengths in other difluorophosphino amines[13,18,22,23,24,25,26], the ratio r(P-N)/r(P-F) was assumed to be 1.060 $\pm$ 0.002, and this 'predicate observation'[41] was used as an additional experimental datum in subsequent refinements. Similarly, the ratio <(FPN)/<(FPF) was taken to be 1.035 $\pm$ 0.015, and this mild constraint was sufficient to stabilise the refinements.

The conformation adopted by the $-PF_2$ group was found by fixing the twist angle at various values, and comparing the R factors obtained. By coincidence, the radial distribution curves for twist angles of 10 and 80° are extremely similar but the 80° form gives a significantly lower R factor, and other parameters refine to more reasonable values with the larger twist angle. The silyl twist angle was also found by a similar process, but other parameters associated with hydrogen atom positions could not be refined, and were fixed at

reasonable values.

The results of the final refinement, for which R_G was 0.08 and R_D was 0.06, are given in Table 4.3. Errors quoted are estimated standard deviations obtained in the least squares analysis, increased to allow for systematic errors. The radial distribution curve for this molecule is shown in Figure 4.1a; observed and final weighted difference molecular scattering intensities are shown in Figure 4.2.

Bis(difluorophosphino)silylamine - In the molecular model used for the refinements of this structure it was assumed that the two NPF_2 groups were identical, and had C_s symmetry, that the $NSiH_3$ group had C_{3v} local symmetry, and that the P_2NSi skeleton had C_s symmetry. It was soon apparent that the bonds to nitrogen were coplanar, and in the later refinements this was assumed, with a single angle (PNP) describing the coordination at nitrogen.

The conformation was described by three angles. The SiH_3 twist angle was taken to be zero when one Si-H bond lay in the skeletal plane. The two PF_2 twist angles were defined to be zero when the FPF angle bisectors lay cis to the N-Si bond. These two angles could be constrained to be equal, or equal and opposite, giving C_2 or C_s symmetry to the $N(PF_2)_2Si$ unit, or they could be varied independently.

Of the eleven geometrical parameters, only the NSiH

and the SiH_3 twist angles could not be refined. The latter was fixed at 50°, this value giving the lowest R factor in a series of test refinements. The PF_2 twist angles were varied over a wide range, but the lowest R factors were obtained when both angles were close to zero; a small C_s distortion was preferred to a C_2 distortion.

The results of the final refinement, for which R_G was 0.06 and R_D was 0.04 are listed in Table 4.4, and the least-squares correlation matrix is given in Table 4.5. The intensity data are shown in Figure 4.3 and the radial distribution curve in Figure 4.1.

4.4 Discussion

The gas phase structures of $N(PF_2)(SiH_3)_2$ and $N(PF_2)_2(SiH_3)$ in both cases reveal an entirely planar arrangement of ligands around nitrogen. The absence of any apparent shrinkage due to out-of-plane deformations of the NR_3 group may be attributed to the fact that the atoms bound to nitrogen in all cases contact each other at distances approximating to the sums of their Bartell hard sphere radii[52], precluding closer approach.

The angles at nitrogen are 120° within experimental error in the case of $N(PF_2)(SiH_3)_2$. A slight narrowing of the <PNP angle in $N(PF_2)_2(SiH_3)$ from 120° ($118.2(10)^{\circ}$) may be due to the absence of steric crowding between neighbouring PF_2 groups, since the fluorines tend to point

away from each other in the preferred conformation.

In both molecules r(Si-H) was fixed at a reasonable value and r(P-F) refined to a value consistent with those expected for the F_2PN moiety, as shown in Table 13. Since some π character can be assigned to the R-N bonds, which are in all cases shorter than those expected for a corresponding single bond, some interest lay in investigating the effect of PF_2 and silyl groups competing for the lone pair on nitrogen. It was found that while the P-N bond lengths for the mono and bis PF_2 species, being 168.0(4) pm and 169.1(4) pm respectively, were substantially shorter than those found in $N(PF_2)_3$ (171.1(4) pm)[18], the Si-N bond lengths in both cases were some 2-3 pm longer than that measured in trisilyl-amine[15,16]. This clearly demonstrates that the PF_2 group has a greater propensity for accepting electron density from the p-orbital on nitrogen than the silyl group, and this is almost certainly due to the electron withdrawing effect of the fluorines bonded to phosphorus. It has been shown that replacing hydrogens with fluorines on silyl groups bound to nitrogen shortens the Si-N bond, from 171.5 pm in $NMe_2(SiH_3)$[20] to 165 pm in $NMe_2(SiF_3)$[58]. A gas phase study of the molecule $NH(PMe_2)_2$[59] may therefore be expected to show P-N bonds substantially longer than those found for $NH(PF_2)_2$.

The angles at phosphorus require no special comment: <FPF and <FPN in both cases give expected values for the F_2PN group (Table 4.5). Typical values for these parameters

range from 95-97° and 98-100° respectively. In the case of $NH(PF_2)(SiH_3)$[24] it may be that these strongly correlated angles have been reversed in the refinements.

The conformation of the PF_2 groups in PF_2 amines is generally of some interest, since they can be directed by two factors: lone pair repulsions between P and P or P and N; and attractive interactions between F and H, the latter being important for all NR_3 compounds (R = PF_2, SiH_3, CH_3 or H) containing PF_2 groups, except $N(PF_2)_3$. It has been suggested in Chapter 3 that in general fluorine-hydrogen interactions predominate over lone pair repulsions, as is evident in the cases of $NMe(PF_2)_2$[23] and $NH(PF_2)_2$[26], where attractive H...F interactions force the phosphorus lone pairs, although orthogonal to that on nitrogen, to lie <u>cis</u> to each other in the major conformer for each molecule. For $N(PF_2)_2(SiH_3)$ and $N(PF_2)_2(SiH_3)$ nmr studies had already been used to predict the likely orientations of the PF_2 groups[53]. It has been suggested[56,60] that some two or three bond couplings to three coordinate phosphorus are sensitive to conformation, with large couplings resulting from atoms lying cis to the lone pair on phosphorus. In $N(PF_2)_2(SiH_3)$ both $^3J(^{31}P^1H)$ and $^2J(^{21}P^{29}Si)$ are small (3.5 and 7 Hz respectively), indicating that the <FPF bisectors lie <u>cis</u> to the silyl group. In $N(PF_2)(SiH_3)_2$, nmr couplings have been explained in terms of the average of one <u>cis</u> and one <u>trans</u> J(PX) (X = ^{29}Si or ^1H), indicating fast rotation of the PF_2 group on the nmr timescale. These

predictions have been verified by the present study.

In $N(PF_2)_2(SiH_3)$ the PF_2 torsions refined as a single parameter, with the best fit being for a conformation where the $N(PF_2)_2$ group adopts a local C_s symmetry with the FPF angle bisectors lying 3^o away from being cis to the Si-N bond. This result is identical in principle to those found for $NH(PF_2)_2$, $NMe(PF_2)_2$ and $N(GeH_3)(PF_2)_2$[29,55]. In $N(PF_2)(SiH_3)_2$ the <FPF bisector was found to lie 14^o away from the skeletal plane, corresponding to a substantially larger torsional vibration than that found for $N(PF_2)_2SiH_3$.

In both molecules studied here, attractive H...F interactions almost certainly play the major part in determining the conformations of the PF_2 groups. $N(PF_2)(SiH_3)_2$ contains H...F contacts from 255.5 pm and $N(PF_2)_2SiH_3$ similar contacts from 260.5 pm. The lower valuesin both cases correspond to the sum of Van der Waals' radii for fluorine and hydrogen, and represent the optimum distance for maximum H...F interaction. Molecular illustrations, with possible H...F interactions indicated by broken lines, are given in Figure 4.4.

Table 4.1: Weighting functions, correlation parameters and scale factors

Compound	Camera Height mm	Wave-length pm	Δ_s nm^{-1}	s_{min} nm^{-1}	sw_1 nm^{-1}	sw_2 nm^{-1}	s_{max} nm^{-1}	p/h	Scale Factor
(a) $N(PF_2)(SiH_3)_2$	128.5	5.799	4	60	80	230	260	0.146	0.806(14)
	284.3	5.799	2	26	40	120	144	0.469	0.727(13)
(b) $N(PF_2)_2(SiH_3)$	128.4	5.854	4	64	80	240	316	0.348	0.960(18)
	285.6	5.854	2	26	30	120	142	0.446	0.900(13)

Table 4.2: Least squares correlation matrix x100 for $N(PF_2)(SiH_3)_2$

r_1	r_2	r_3	<1	<2	<4	<5	<7	u_2	u_5	u_6	u_{11}	u_{14}	u_{26}	k_1	k_2	
100	42							56								r_1
	100							69								r_2
		100					-53							51		r_3
			100	-45	-40				67							<1
				100					-62		-55					<2
					100	-57					-79		-45			<4
						100										<5
							100			43			46	-42	-43	<7
								100								u_2
									100							u_5
										100	46					u_6
											100	-44				u_{11}
												100				u_{12}
													100			u_{24}
														100		k_1
															100	k_2

Note: only elements with absolute values ⩾40 are included.

Table 4.3: Molecular parameters for $N(PF_2)(SiH_3)_2$

Independent distances	Distance/pm	Amplitude/pm
r_1(P-F)	158.5(3)	4.7(fixed)
r_2(P-N)	168.0(4)	5.3(5)
r_3(Si-N)	175.5(4)	5.3(tied to u_2)
r_4(Si-H)	149.0(fixed)	8.8(fixed)
Dependent distances		
d_5(F...N)	249.1(12)	10.8(11)
d_6(F...Si)	407.3(15)	11.3(12)
d_7(F...Si)	385.4(21)	11.3(tied to u_6)
d_8(F...Si)	295.7(22)	11.3(tied to u_6)
d_9(F...Si)	324.0(19)	11.3(tied to u_6)
d_{10}(F...F)	237.3(18)	10.8(tied to u_5)
d_{11}(Si...Si)	304.0(25)	10.1(6)
d_{12}(Si...P)	296.7(13)	10.1(tied to u_{11})
d_{13}(Si...P)	298.1(23)	10.1(tied to u_{11})
d_{14-25}(F...H)	255.5 - 514.7(30)	11.1(39)
d_{26-28}(P...H)	309.9 - 402.2(18)	11.9(39)
d_{29}(N...H)	266.2(15)	12.0(fixed)
d_{30-32}(Si...H)	339.5 - 428.4(30)	11.9(tied to u_{26})
d_{33}(H...H)	242.5(fixed)	12.0(fixed)
d_{34-39}(H...H)	296.7 - 530.8(35)	20.0(fixed)
Independent angles/°		
<1(F-P-F)	96.9(10)	
<2(F-P-N)	99.4(7)	
<3(N-Si-H)	110(fixed)	
<4(Si-N-Si)	120.0(15)	
<5(P-N in plane def.)	0.5(9)	
<6(SiH_3 twist)	8(fixed)	
<7(PF_2 twist)	76.0(12)	

Note: all distances are r_a

Table 4.4: Molecular parameters for $N(PF_2)_2(SiH_3)$

Independent distances	Distance/pm	Amplitude/pm
r_1(P-F)	157.0(2)	4.7(3)
r_2(P-N)	169.1(4)	5.2(tied to u_1)
r_3(Si-N)	176.7(7)	5.2(tied to u_1)
r_4(Si-H)	145.8(30)	8.8(fixed)
Dependent distances		
d_5(N...F)	248.7(5)	8.1(8)
d_6(F...F)	233.5(8)	8.1(tied to u_5)
d_7(F...F)	496.5(8)	21.2(25)
d_8(F...F)	431.2(7)	21.2(tied to u_7)
d_9(F...F)	445.2(7)	21.2(tied to u_7)
d_{10}(F...Si)	316.2(31)	25.6(25)
d_{11}(F...Si)	309.6(30)	25.6(tied to u_{10})
d_{12}(P...Si)	301.2(6)	11.5(7)
d_{13}(P...F)	386.5(24)	14.0(7)
d_{14}(P...F)	391.8(21)	14.0(tied to u_{13})
d_{15}(P...P)	289.3(11)	11.5(tied to u_{12})
d_{16-27}(F...H)	260.5 -455.8(40)	22(fixed)
d_{28}(H...H)	237.3(50)	18(fixed)
d_{29-31}(P...H)	328.6 -419.0(20)	18(fixed)
d_{32}(N...H)	264.7(21)	15(fixed)
Independent Angles/°		
<1(F-P-F)		96.1(5)
<2(F-P-N)		99.3(3)
<3(P-N-P)		117.6(7)
<4(N-Si-H)		110(fixed)
<5(PF_2 twist)		-3.3(27)
<6(SiH_3 twist)		50(fixed)

Note: all distances are r_a

Table 4.5: Least squares correlation matrix x100 for $N(PF_2)_2(SiH_3)$

r_1	r_2	r_3	r_4	<1	<2	<3	<5	u_1	u_5	u_7	u_{10}	u_{12}	u_{13}	k_1	k_2	
100		51						40								r_1
	100	-43			-57											r_2
		100				46		40			46					r_3
			100											-49	-47	r_4
				100					66							<1
					100				-45		-43					<2
						100						65				<3
							100			48	48		69			<5
								100						47		u_1
									100							u_5
										100			48			u_7
											100			48	48	u_{10}
												100				u_{12}
													100			u_{13}
														100	64	k_1
															100	k_2

Note: only elements with absolute values ≥40 are included.

Table 4.6: Important geometrical parameters for some difluorophosphino and silyl amines derived from electron diffraction analyses

	Reference	r(P-F)	r(P-N)	r(Si-N)	<FPF	<FPN
$N(PF_2)_3$	18	157.4(2)	171.1(4)		96.9(3)	99.2(3)
$N(PF_2)_2(SiH_3)$	27	157.0(2)	169.1(4)	176.7(7)	96.1(5)	99.3(3)
$N(PF_2)(SiH_3)_2$	27	158.5(3)	168.0(4)	175.5(4)	96.9(10)	99.4(7)
$N(SiH_3)_3$	16			173.4(2)		
$NH(PF_2)_2$	26	158.4(3)	168.4(8)		95.6(10)	98.3(7)
$NH(PF_2)(SiH_3)$	24	157.5(3)	165.4(6)	172.4(7)	101.6(12)	95.2
$NH(SiH_3)_2$	21			172.5(3)		
$NMe_2(SiH_3)$	a			171.9(3)		

[a]G. Gundersen and D.W.H. Rankin, personal communication. (See also Reference 106)

Figure 4.1 : (a) Observed and difference radial distribution curves for $N(PF_2)(SiH_3)_2$

(b) Observed and difference radial distribution curves for $N(PF_2)_2(SiH_3)$.

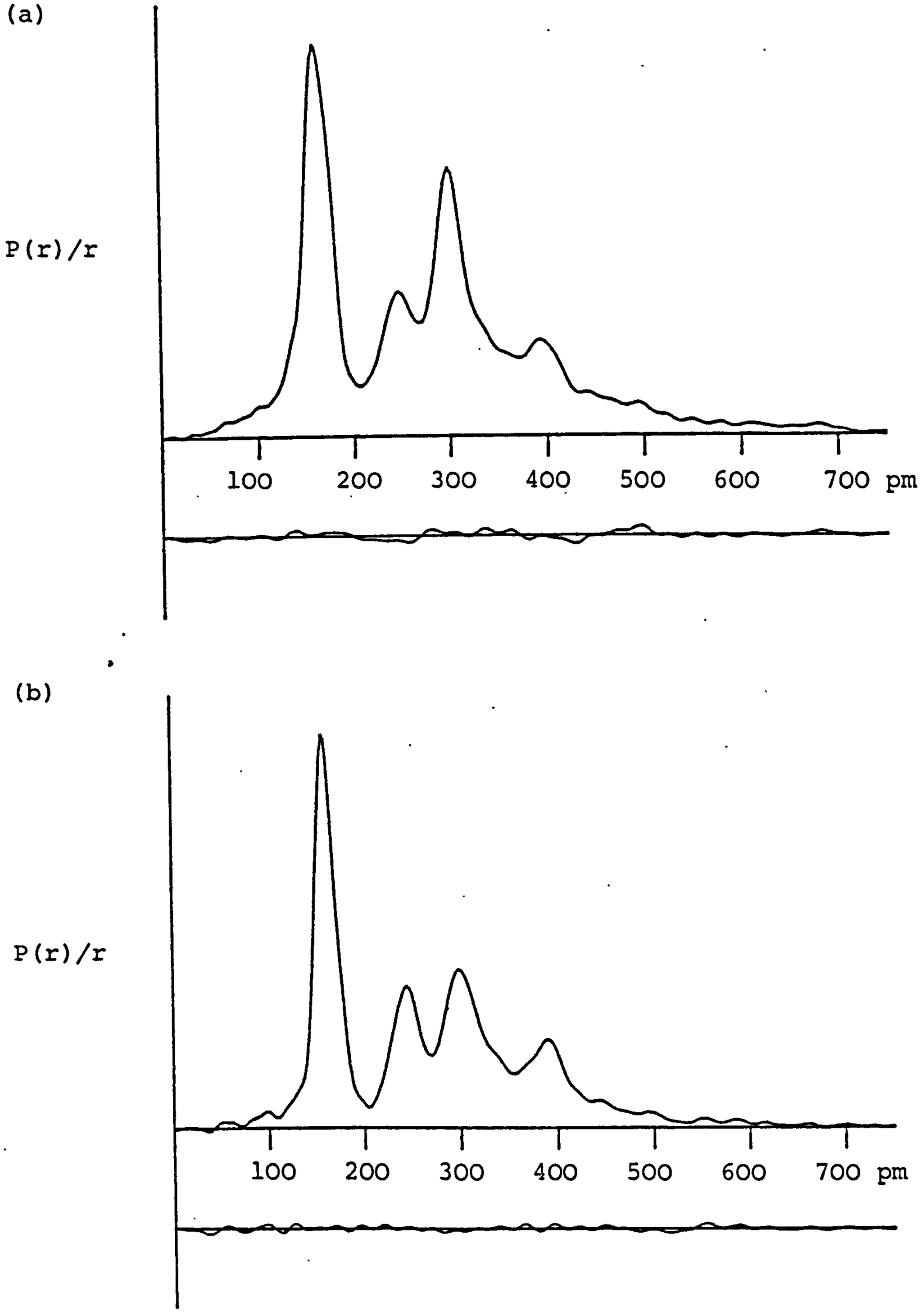

Note: Before Fourier inversion the data were multiplied by $s.\exp[-0.000015s^2/(Z_P-f_P)(Z_F-f_F)]$.

Figure 4. 2 : Observed and final weighted difference molecular scattering intensities for $N(PF_2)(SiH_3)_2$ at nozzle-to-plate distances of (a) 128 and (b) 284 nm

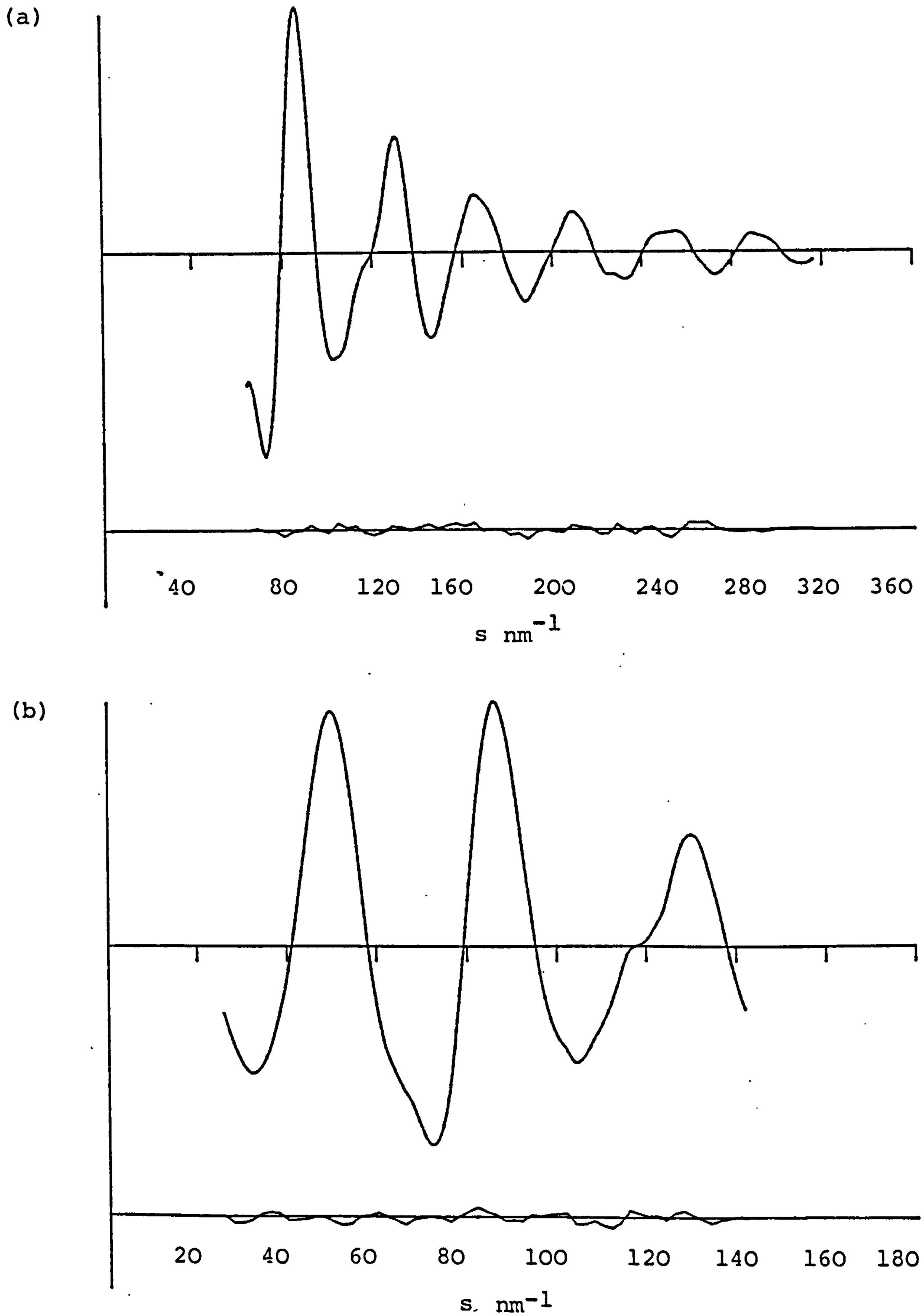

Figure 4.3 : Observed and final weighted difference molecular scattering intensities for $N(PF_2)_2(SiH_3)$ at nozzle-to-plate distances of (a) 128 and (b) 285 nm

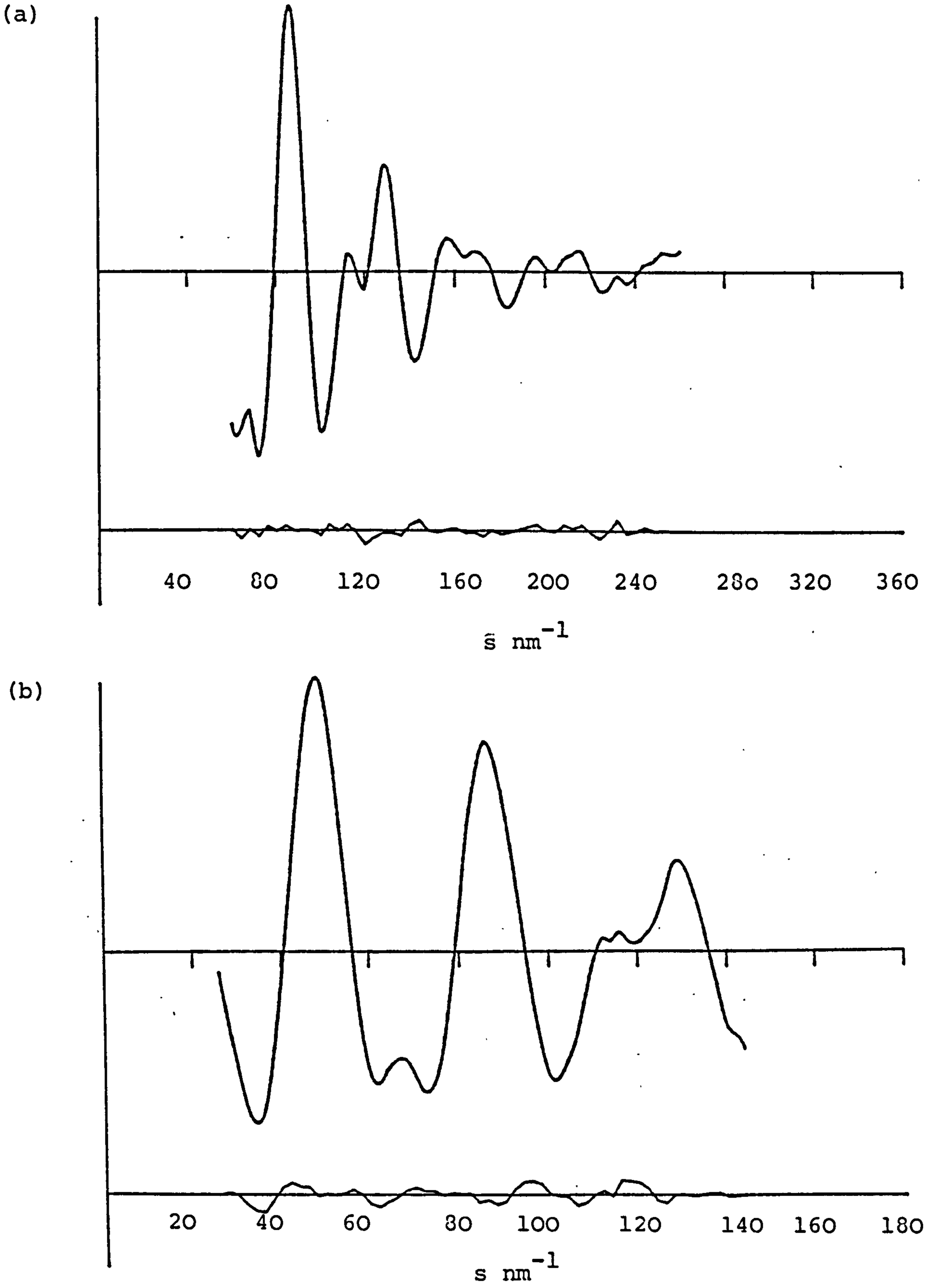

Figure 4.4 : Molecular structure of (a) $N(PF_2)(SiH_3)_2$ and (b) $N(PF_2)_2(SiH_3)$

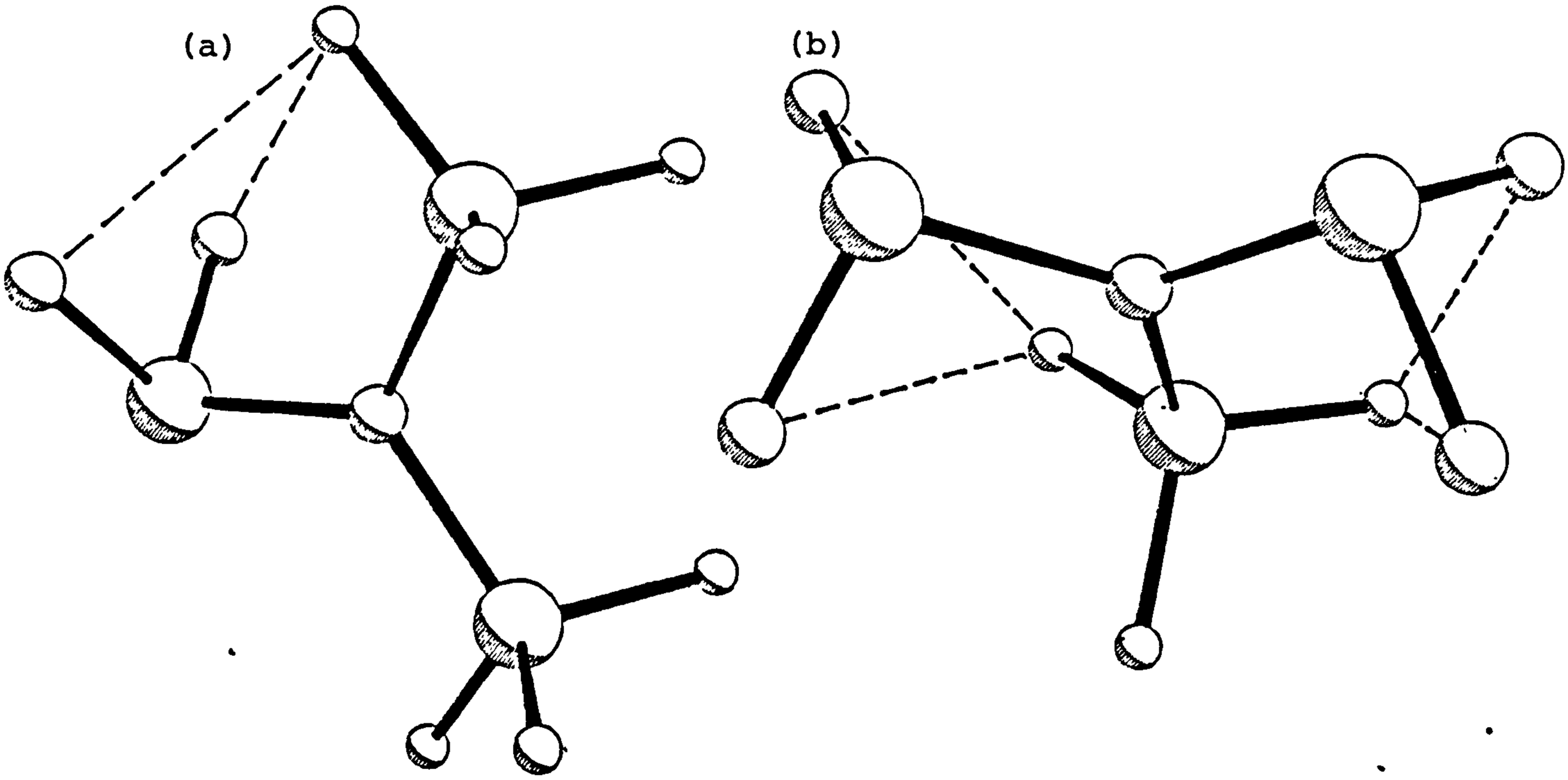

Note: broken lines indicate hydrogen fluorine attractive Interactions

CHAPTER 5

THE GAS PHASE MOLECULAR STRUCTURE OF BIS(DIFLUOROPHOSPHINO)GERMYLAMINE DETERMINED BY ELECTRON DIFFRACTION

5.1 Introduction

Of the five amines with germyl groups bound to nitrogen so far reported[55,61] only one, the very unstable trigermylamine, has been the subject of a gas phase structure investigation[62]. An electron diffraction structural study of the molecule $N(GeH_3)(PF_2)_2$ has therefore been undertaken, the stability of which relative to trigermylamine appears to be increased by the presence of the two difluorophosphino groups.

Certain geometrical features likely to be exhibited by this molecule could be predicted from previously determined structures of other amines. Firstly, in all R_3N compounds (R = PF_2, SiH_3 or GeH_3) studied the skeletal group was found to be planar, arguably due to delocalisation of the lone pair from the p orbital on nitrogen, and the short M-N bonds found in these compounds have been attributed to some increase in bond order due to p→d π bonding from the donor p orbital on nitrogen to vacant d orbitals on the ligands. Therefore it would be surprising if $N(GeH_3)(PF_2)_2$ showed significant distortion from planarity of the $NGeP_2$ skeleton.

Furthermore, in the previous chapter it was shown that where PF_2 and SiH_3 groups are bound to the same central nitrogen atom,the electronegative PF_2 groups cause the bonds from nitrogen to silicon to lengthen. Thus we would expect the Ge-N bond to be substantially longer here than in trigermylamine.

Predictions on the likely conformation of the difluorophosphine groups have been made on the basis of the very low $^{3}J(^{31}P^{1}H)$ coupling constant (2 Hz) found in the initial study of this molecule[55]. It has been suggested that a maximum coupling constant would be obtained when the lone pair on phosphorus lay cis to a germyl proton Therefore it has been concluded that it is the fluorine atoms which must lie cis to the germyl group. The value for $^{2}J(^{31}P^{31}P)$ of 405 Hz at room temperature lends further support to this theory, since the two phosphorus lone pairs lying cis to each other would generate a large coupling. A similar effect is observed in $NMe(PF_2)_2$[54] and in other bis(difluorophosphino) compounds.

The conformation suggested by the above evidence would be exactly analogous to that found for $N(PF_2)_2(SiH_3)$[27]; therefore the predicted conformation seems entirely reasonable.

5.2 Experimental

A sample of bis(difluorophosphino)germylamine was prepared by the liquid phase reaction between bis(difluorophosphino)amine and germyl iodide, in the presence of trimethylamine[55], according to Equation 22.

(22) $$NH(PF_2)_2 + GeH_3I + NMe_3 \rightarrow N(GeH_3)(PF_2)_2 + [NHMe_3]^+[I]^-$$

The product was purified by repeated fractional condensation undertaken on a vacuum line, and the purity was checked by infared and nmr spectroscopy.

Electron diffraction scattering intensities were recorded using the Cornell/Edinburgh diffraction apparatus[26,30], with nozzle-to-plate distances of 182 and 288 mm, and an accelerating voltage of ca. 44 kV. During exposures samples were maintained at 283 K, and the nozzle at room temperature, 298 K. Data were recorded on Kodak Electron Image plates, and obtained in digital form using a Jarrell-Ash double beam microphotometer, with spinning plates[51]. The electron wavelengths were determined from the scattering patterns of gaseous benzene, recorded immediately before or after the sample plates.

Calculations were carried out on ICL 2970 and 2980 computers at the Edinburgh Regional Computing Centre, using the usual data reduction and least-squares refinement programme[26]. Weighting points used in setting up the off-diagonal weight matrices are given, together with other experimental data, in Table 5.1. In all calculations the complex scattering factors of Schafer et al[9] were used.

5.3 Refinement

In refinements of the structure of $N(GeH_3)(PF_2)_2$ the

$GeNP_2$ skeleton was initially assumed to be planar, although an out of plane distortion of the germyl group was subsequently permitted. Local C_s and C_{3v} symmetries were assumed for the NPF_2 and $NGeH_3$ groups respectively. Furthermore the torsion angles of the two PF_2 groups, defined as zero when the <FPF bisectors lay cis to the germyl group, were constrained so as to maintain either C_s or C_2 local symmetry for the $N(PF_2)_2$ moiety. The germyl torsion angle was defined as zero when one Ge-H bond lay in the skeletal plane, and in all cases positive torsion angles corresponded to clockwise rotations about the M-N bonds viewed from M to N. With the adoption of these assumptions, the structure could be defined by 11 geometrical parameters.

The conformation of the germyl group was found by varying the torsion angle and observing the R factors obtained. A plot showing this variation in R factor with torsion angle is given in Figure 5.1. Of the other parameters involving hydrogen <NGeH was fixed at the tetrahedral angle of 110° and r(Ge-H) refined to a reasonable value, albeit with a large estimated standard deviation. All other parameters refined satisfactorily, and it was subsequently found that a somewhat lower R factor was obtained when the $N(PF_2)_2$ fragment was constrained to C_s symmetry, than when it had C_2 symmetry.

Results of the final refinement, for which Rg was 0.12 and Rd was 0.08, are given in Table 5.2. Errors

quoted are estimated standard deviations derived from the least squares analysis increased to allow for systematic errors. The observed and final weighted difference molecular scattering intensity curves are shown in Figure 5.2.

The radial distribution curve is shown in Figure 5.3. Finally, the correlation matrix derived from the final least-squares analysis is given in Table 5.3.

5.4 Results and Discussion

The P_2NGe skeletal group was found to be entirely planar with no apparent shrinkage, a result also found for $N(PF_2)_2(SiH_3)$[27]. Any deviation from planarity resulted in a large increase in R factor.

The geometrical parameters of the NPF_2 groups, r(P-N), r(P-F), <FPN and <FPF, all refined to expected values, commensurate with those found in other bis-(difluorophosphino) amines (Table 5.4a). The value found for r(P-N) of 169.8(8) pm is close to that found in $N(PF_2)_2(SiH_3)$ (169.1(4) pm), indicating that steric crowding due to the bulkier germyl group is not severe.

The Ge-N bond length in this study deserves special comment: compared to trigermylamine this parameter is over 5 pm longer. A similar difference has been observed for the analogous silyl amines (Table 5.4b). This has been attributed to the electronegative $-PF_2$ group having

greater π-acceptor capability than the silyl group[27]. Since the difference is greater in the germyl than the silyl case, it could be argued that the former is a weaker π-acceptor than the latter.

The PNP angle of 114.0(8)° is somewhat small, and the P...P non-bonded contact (285 pm) is at the small end of a range of values found for other bis(difluorophosphino)-amines (Table 17a). Using the formula a(P...Ge) = ½[d(Ge...Ge) + d(P...P)], and assuming values for d(Ge...Ge)[62] and d(P...P)[18] of 316 and 290 pm respectively, the expected value for the germanium-phosphorus distance would be 303 pm. The value of 315 pm found suggests that the narrow PNP angle found is not a result of steric crowding due to the germyl group. By comparing the results tabulated for all bis(difluorophosphino)-amines it can be seen that d(P...P) here is similar to that found in the methyl case, and less than 5 pm smaller than that found for $N(PF_2)_2(SiH_3)$. In the silyl case, it may be that the PNP angle is marginally wider because the fluorine atoms are attracted to the silyl protons, whereas in $N(CH_3)(PF_2)_2$ optimum H...F contact would be possible with a narrower PNP angle. In the germyl case the shortest H...F distance is too long (297 pm) for any strong interaction to take place, as the optimum distance for this lies in the region 250-265 pm[23-27], and it appears here that the PNP angle relaxes back to a smaller value.

The conformation of the PF_2 groups can be deduced

directly from the form of the radial distribution curve, since only a configuration in which the FPF angle bisectors lay <u>trans</u> to each other would give rise to F...F distances up to 500 pm. The apparent distortion of c. 8^{o} away from C_{2v} symmetry for the $N(PF_2)_2$ moiety probably represents torsional shrinkage away from the higher symmetry. The torsional shrinkage in the case of the silyl analogue is 3^{o}; the large value in the present study may be due to the lack of attractive H...F interactions to help pin the conformation down. In the case of $NMe(PF_2)_2$ [23] refinements based on the assumption of low-frequency torsional vibrations led to shrinkage of up to 11^{o} away from C_{2v} symmetry for the $N(PF_2)_2$ group. This larger shrinkage may be explained in terms of H...F crowding. The orientation of the methyl group is suggested as being one in which C-H and N-H bonds are not eclipsed. If the PF_2 groups were to adopt conformations in which every H...F contact was equal, this would correspond to a significant C_s torsion away from C_{2v} local symmetry for the $N(PF_2)_2$ moiety.

The arguments used here to explain torsional shrinkages in $NMe(PF_2)_2$ [23], $N(PF_2)_2(SiH_3)$ [27] and $N(GeH_3)(PF_2)_2$ coincide with those used to explain the values for respective PNP angles and non-bonded P...P distances discussed earlier.

In broad terms, therefore, the structure of $N(GeH_3)(PF_2)_2$ conforms to expectations. An illustration of the molecule is given in Figure 5.4.

Table 5.1: Weighting functions, correlation parameters and scale factors for $N(GeH_3)(PF_2)_2$

Camera Height nm	Wavelength pm	ΔS nm^{-1}	s_{min} nm^{-1}	sw_1 nm^{-1}	sw_2 nm^{-1}	s_{max} nm^{-1}	p/h	Scale Factor
128.16	5.811	4	68	100	240	320	0.363	0.750(35)
288.31	5.811	2	34	44	120	140	0.442	0.724(24)

Table 5.2: Molecular parameters for $N(GeH_3)(PF_2)_2$

Independent distances	Distance/pm	Amplitude/pm
r_1(P-F)	159.2(5)	4.9(11)
r_2(P-N)	169.8(8)	3.4(28)
r_3(N-Ge)	188.9(13)	6.2(15)
r_4(Ge-H)	153.6(43)	8.8(fixed)
Dependent distances		
d_5(N...F)	251.3(6)	7.4(15)
d_6(P...F)	237.6(16)	7.4(tied to u_5)
d_7(F...F)	499.6(11)	10.2(15)
d_8(F...F)	458.4(23)	10.2(tied to u_7)
d_9(F...F)	421.4(28)	10.2(tied to u_7)
d_{10}(F...Ge)	318.8(11)	17.7(17)
d_{11}(F...Ge)	335.3(12)	17.7(tied to u_{10})
d_{12}(F...Ge)	315.3(6)	8.4(6)
d_{13}(P...F)	394.8(9)	10.3(13)
d_{14}(P...F)	381.2(12)	10.3(tied to u_{13})
d_{15}(P...P)	284.7(10)	7.0(12)
d_{16-27}(F...H)	296 - 467	22.0(fixed)
d_{28}(H...H)	250(7)	18.0(fixed)
d_{29-31}(P...H)	343 - 435	18.0(fixed)
d_{32}(N...H)	281(4)	15.0(fixed)
Independent angles/°		
<1 FPF		96.5(11)
<2 FPN		99.6(5)
<3 PNP		114.0(8)
<4 Ge-N (out-of-plane def.)		0(see text)
<5 NGeH		110(fixed)
<6 PF_2 twist		8.2(10)
<7 GeH_3 twist		28.0(see text)

Note: all distances are r_a

Table 5.3: Least squares correlation matrix x100 for $N(GeH_3)(PF_2)_2$

r_1	r_2	r_3	r_4	<1	<2	<3	<6	u_1	u_2	u_3	u_6	u_7	u_{10}	u_{12}	u_{13}	u_{15}	k_1	k_2	
100	-60	-64						74	85								51	60	r_1
	100	-79	-50		-59	-72		-85	-79										r_2
		100				82		81	78										r_3
			100			50													r_4
				100							68								<1
					100														<2
						100		66	61										<3
							100								-70				<6
								100	92								57	61	u_1
									100	57							50	58	u_2
										100									u_3
											100								u_6
												100							u_7
													100					54	u_{10}
														100			59		u_{12}
															100				u_{13}
																100			u_{15}
																	100	71	k_1
																		100	k_2

Note: only elements with absolute values >50 are included.

Table 5.4

(a) Important geometrical parameters for some bis(difluorophosphino)amines

$RN(PF_2)_2$	r(P-F)	r(P-N)	<FPF	<FPN	<PNP	d(P...P)	Shortest d(F...H)	Ref
R = H	158.4(3)	168.4(8)	95.6(10)	98.3(7)	122.1(7)	294.8(14)	250	26
R = CH_3	158.4(2)	168.1(7)	95.2(5)	99.8(4)	115.9(10)	285.1(11)	(not given)	23
R = SiH_3	157.0(2)	169.1(4)	96.1(5)	99.3(3)	117.6(7)	289.3(11)	260(4)	27
R = GeH_3	159.2(5)	169.8(8)	96.5(11)	99.6(5)	114.0(8)	284.7(10)	297(3)	29
R = PF_2	157.4(2)	171.1(4)	96.9(3)	99.2(3)	120(fixed)	296.4(6)	-	18

(b) r(M-N), M = Si or Ge), for some germyl and silyl amines

Compound	r(M-N)	Ref
$N(GeH_3)_3$	183.6(5)	62
$N(SiH_3)_3$	173.4(2)	15,16
$N(GeH_3)(PF_2)_2$	188.9(13)	29
$N(SiH_3)(PF_2)_2$	176.7(7)	27

Note: all distances in pm; all angles in degrees.

Figure 5. 1: Variation of R_G with methyl torsion angle

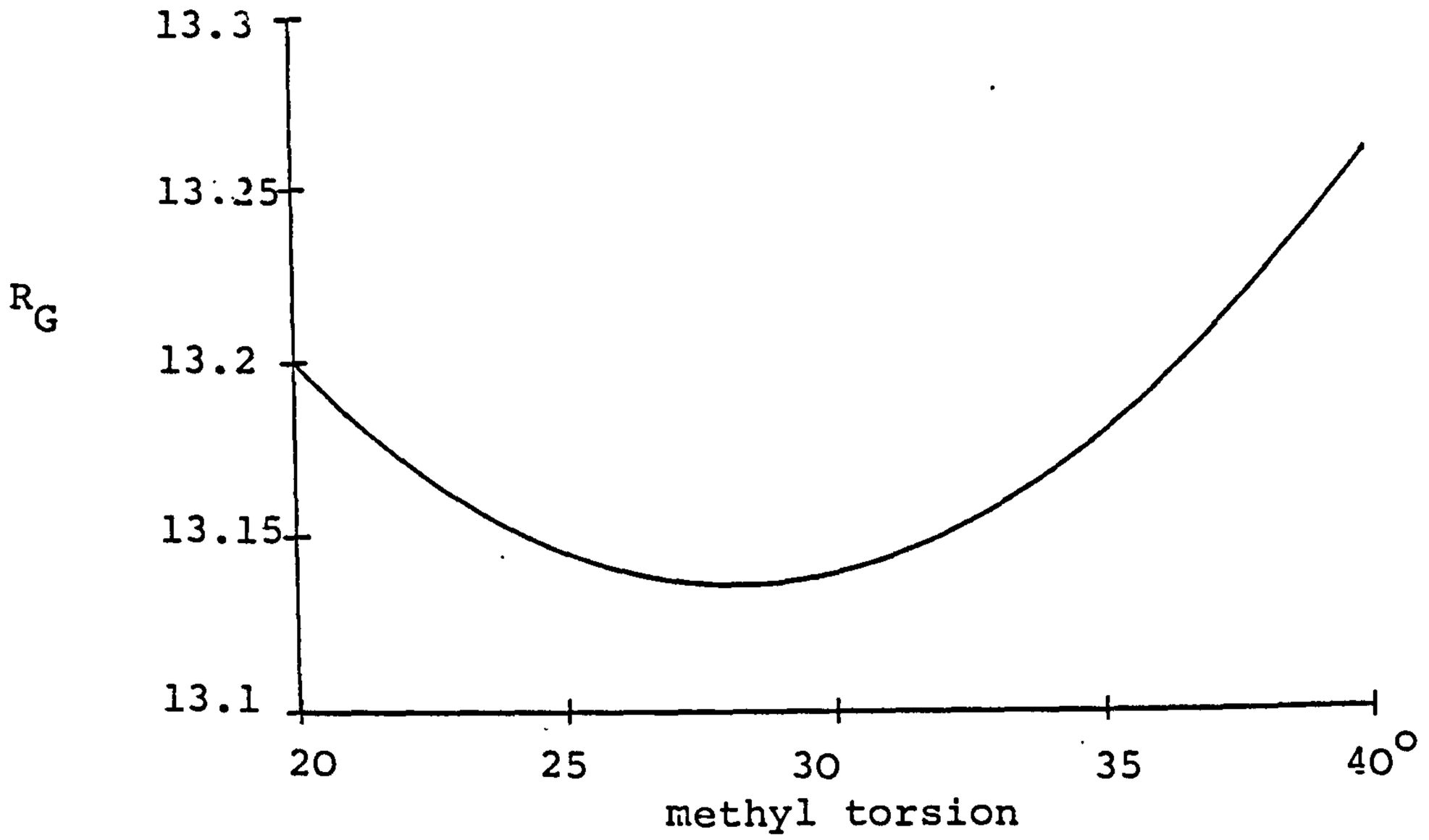

Note: l = defined in text

Figure 5.2 : Observed and final weighted difference molecular scattering intensities at nozzle-to-plate distances of (a) 128 and (b) 288 mm

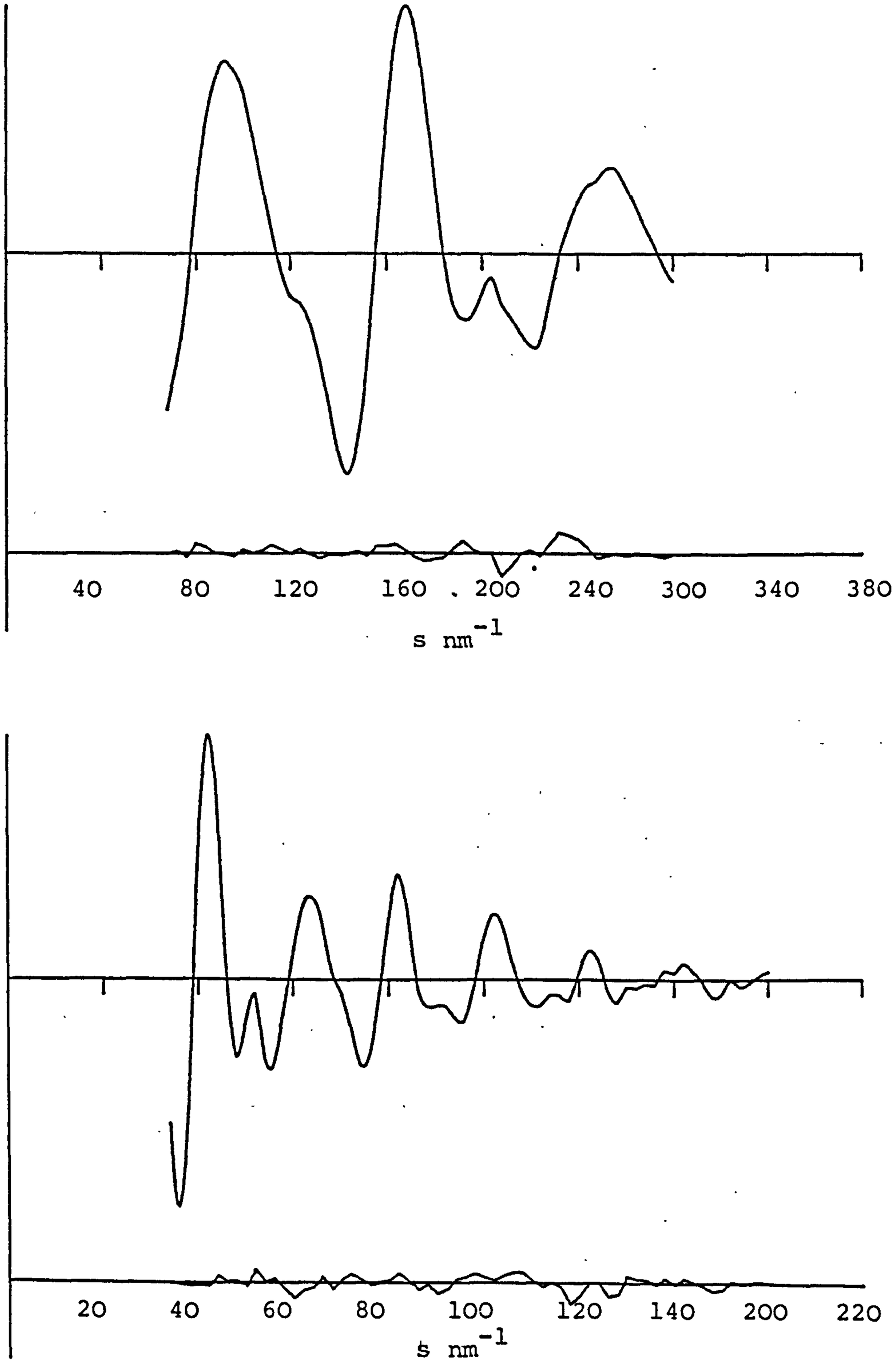

Figure 5.3: Observed and difference radial distribution curve, P(r)/r. Before Fourier inversion the data were multiplied by $s.\exp[-0.000015\ s^2/(Z_{Ge}-f_{Ge})(Z_F-f_F)]$.

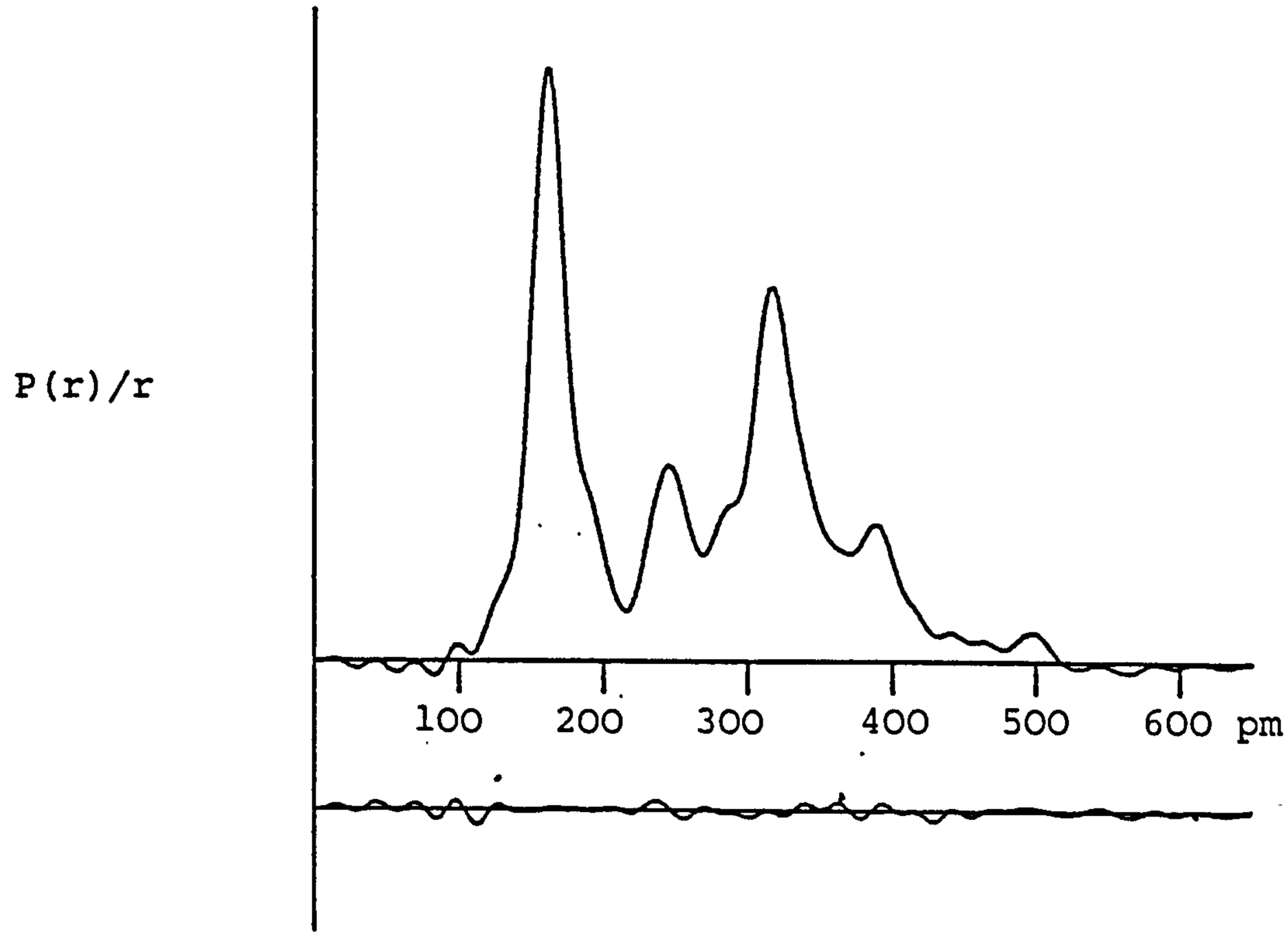

Figure 5.4 : The molecular structure of $N(GeH_3)(PF_2)_2$

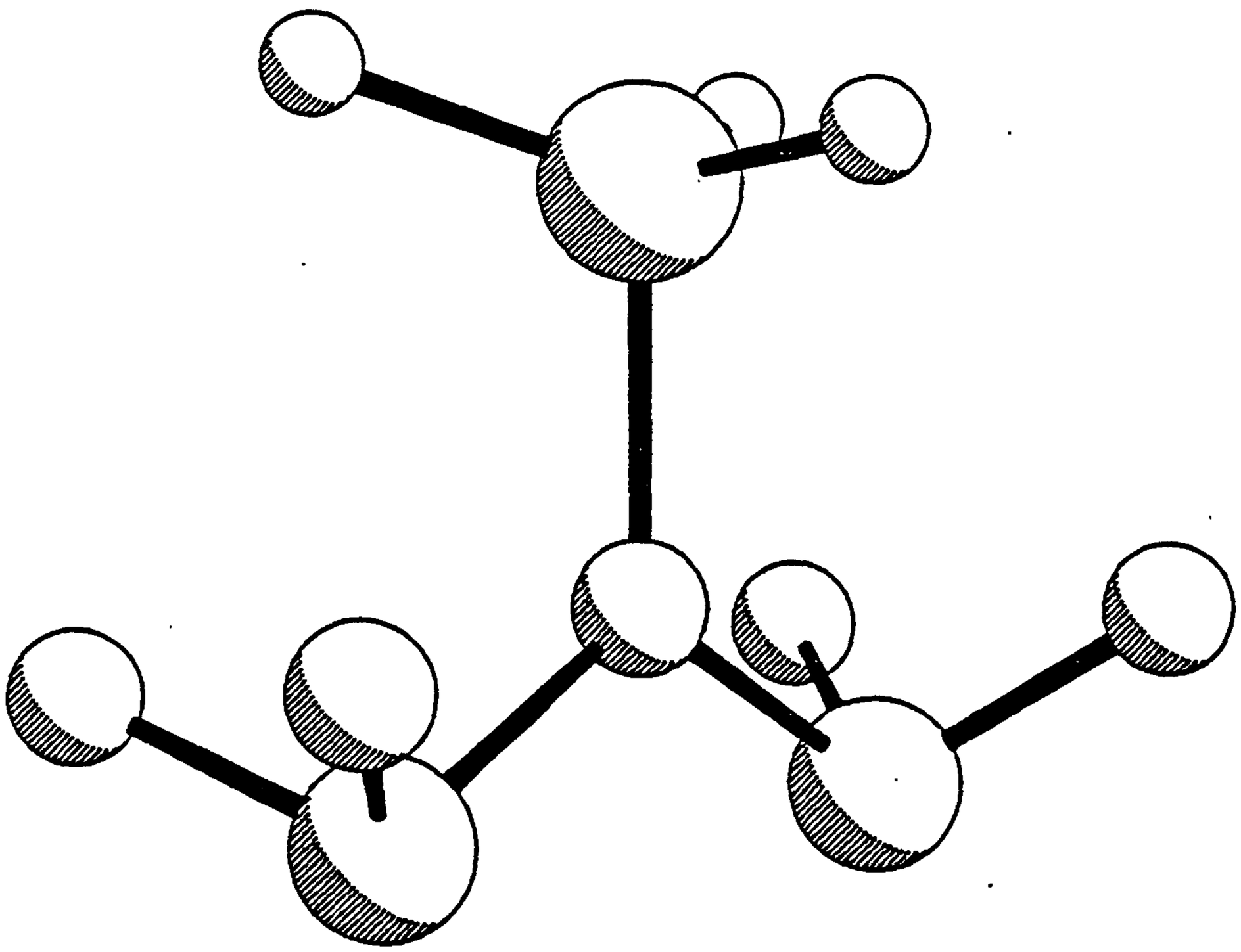

CHAPTER 6

THE GAS PHASE MOLECULAR STRUCTURE OF DIFLUORO(ISOSELENOCYANATO)PHOSPHINE DETERMINED BY ELECTRON DIFFRACTION

6.1 Introduction

Electron diffraction structure determinations have been carried out on PF_2NCO and PF_2NCS[63]. These molecules show short P-N bonds and wide angles at nitrogen characteristic of aminodifluorophosphines. These features have been explained in terms of some π-bonding between the lone pair of electrons on nitrogen and vacant d orbitals on phosphorus. It is therefore of interest to see whether the structure of PF_2NCSe follows the pattern set by the two difluoro-phosphine pseudohalides.

In the cases of PF_2NCO and F_2PNCS, complications arose because both molecules exhibit a significant shrinkage effect in the electron diffraction (r_a) structure determination due to low frequency bending modes. Spectroscopic data were used in these cases to calculate perpendicular amplitude coefficients and linear shrinkage corrections which yielded average (r_α) structures when applied to the refined electron diffraction (r_a) structure. The infrared spectrum of PF_2NCSe[64] similarly exhibits a low frequency bending mode, at 55 cm^{-1}, and in this case the necessary corrections from spectroscopic data were applied to the refining structure, as the computer programs used offer the facility to refine either r_a or r_α structures. Results are quoted here for both, since it is worth noting the major differences with respect to geometrical parameters obtained from either structure.

6.2 Experimental

A sample of PF_2NCSe was prepared by condensing 10 mMol $PBrF_2$ onto 50 mMol of the silver pseudohalide salt[64], allowing the reaction mixture to warm to room temperature and quickly recondensing volatiles into clean glassware (Equation 23).

(23) $PBrF_2 + [Ag]^+[NCSe]^- \rightarrow [Ag^+][Br]^- + PF_2NCSe$

A yield of 80% PF_2NCSe with respect to $PBrF_2$ was obtained. The product was separated from unchanged starting material and subsequently purified by fractional condensation in vacuo; the purity was checked by infrared spectroscopy.

Electron diffraction scattering intensities were recorded photographically using the Cornell/Edinburgh diffraction apparatus[26,30]. With an accelerating potential of 43 kV and nozzle-to-plate distances of 128 and 285 mm, several sets of data were obtained covering an s range of 34 to 268 nm^{-1}. The sample and the nozzle were held at room temperature (293 K). The background pressure was 4×10^{-7} torr and during a run this increased to 2×10^{-6} torr. The ion guage responsible for the above measurements is situated in the main chamber but removed somewhat from the nozzle.

Photographic intensities were convered to digital form using a Jarrell-Ash double beam microphotometer[51] with spinning plates. The electron wavelength was determined from the scattering pattern of gaseous benzene recorded

immediately before the sample exposures. The weighting points used in the setting up of the off-diagonal weight matrix employed in the least squares refinement program, together with correlation parameters and other experimental details, are shown in Table 6.1.

All calculations were done on the Edinburgh Regional Computing Centre's ICL 2970 computer, using established data reduction[26] and least squares refinement[34] programs. The scattering factors of Schafer et al[9] were used throughout.

6.3 Calculated Amplitudes of Vibration and K Values

These were obtained using our program GTRIP, based on Schachtschneider's[65] GMAT routines for generating inverse kinetic energy matrices (G) for a molecular system or for each symmetry block. A versatile routine FGRUM calculates eigenvalues and allows an initial trial potential energy matrix (F) to be modified interactively in one of three ways:

(a) specified F elements may be assigned new values;

(b) specified F elements may be included in a least-squares refinement based on the differences between observed and calculated frequencies and between observed and calculated isotope shifts; the required derivatives $\frac{\delta\nu}{\delta F_{ij}}$ are not calculated analytically but obtained numerically by altering F_{ij} to $F + \Delta F$ and rediagonalising to obtain eigenvalues $\lambda + \Delta\lambda$;

(c) the entire F matrix may be altered in such a manner as to fit the observed frequencies for one isotopic species by the so-called "direct fit" procedures; this has the unfortunate property of leading to a solution with the same L vectors as the initial trial F matrix, so we have modified the procedure by eliminating any off-diagonal elements in the new F matrix below a specified threshold. The modified F matrix is then used as the starting point for a new "direct fit" plus elimination cycle, and the process continues until convergence on the observed frequencies is achieved. It is usually convenient to begin with a high threshold (1.0 or 0.5 mdyn/Å) and to reduce it progressively if convergence is slow; in this way most of the changes are forced into the diagonal F elements, and only a limited number of non-zero off-diagonal elements remain in the final F matrix, which now has L vectors that may differ substantially from those of the original trial.

The L vectors corresponding to the final F matrix, chosen to reproduce observed frequencies and isotope shifts (where available) are then used to generate the mean-square Cartesian displacements for specified pairs of atoms. These are summed over all symmetry species and finally converted into u and K values by coordinate rotations appropriate to the atom pair. The amplitudes are calculated for 0 K and any specified higher temperature. GTRIP also includes facilities for calculation of Coriolis

coupling terms and centrifugal distortion constants for symmetric top molecules.

6.4 Normal Coordinate Analysis

The published values[64] for the fundamental vibration frequencies of PF_2NCSe were used in the normal coordinate analysis. Figure 20 shows the applied molecular model and definition of valence coordinates. The normal modes of vibration are distributed into the symmetry species of the C_s symmetry group according to $\Gamma = 8a' + 4a''$. The following set of symmetry coordinates was constructed.

$$S_1(A') = t$$

$$S_2(A') = s$$

$$S_3(A') = d$$

$$S_4(A') = 2^{-\frac{1}{2}}(r_1 + r_2)$$

$$S_5(A') = R\alpha$$

$$S_6(A') = (RD/2)^{\frac{1}{2}}(\beta_1 + \beta_2)$$

$$S_7(A') = (DS)^{\frac{1}{2}}\gamma$$

$$S_8(A') = (ST)^{\frac{1}{2}}\phi$$

$$S_1(A'') = 2^{-\frac{1}{2}}(r_1 - r_2)$$

$$S_2(A'') = (RD/2)^{\frac{1}{2}}(\beta_1 - \beta_2)$$

$$S_3(A'') = (ST)^{\frac{1}{2}}\theta$$

$$S_4(A'') = (RS)^{\frac{1}{2}}\tau$$

Here R, D, S and T designate the equilibrium distances of $R_{15} = R_{16}$, R_{12}, R_{23} and R_{34} respectively (cf Figure 6.1 for the numbering of atoms).

An harmonic force field for PF_2NCSe was developed which exactly fitted the observed vibrational frequencies. Table 6.2 shows the final results in terms of the symmetry F matrix. Table 6.3 gives the potential energy distribution terms calculated from the developed force fields, together with approximate descriptions of the normal modes of vibration, although mixing is so pronounced in some cases as to make simple assignments inadequate. Table 6.4 shows the calculated mean amplitudes of vibration for the normal modes of PF_2NCSe, at O K and 298 K together with calculated K values at 298 K as used in the following r_α structure determination.

6.5 Refinement

Molecular model - The molecule was assumed to have local C_s symmetry for the PF_2N group with the geometry being defined by the P-F, P-N, N=C and C=Se distances, the angles FPF, FPN, PNC and NCSe, and a torsion angle. The last was defined to be zero when the FPF angle bisector was trans to the N=C bond.

Initial refinements of the r_a structure indicated that the NCSe angle could lie anywhere between 170 and 180°, and that it was strongly correlated with the PNC angle, which lay between 139 and 145°. This showed that there could be a large shrinkage arising from bending at nitrogen and carbon. The predominance of the P...Se peak in the radial distribution curve (Figure 6.2) would ensure that

this effect was pronounced. The geometrical parameters obtained during a final r_a structure refinement are given in Table 6.5. It was subsequently decided to concentrate on refinements of the r_α structure. This would also take account of the effects of the torsional vibration on any apparent distortion from C_s symmetry.

Average structure parameters (r_α) are related to those measured in the electron diffraction experiment (r_a) by the expression given by equation 11, reproduced below

$$(11) \quad r_\alpha = r_a + \frac{u^2}{r_e} - K$$

where u is the root mean square amplitude of vibration and K is the perpendicular amplitude correction coefficient. Thus, using r_a instead of r_e in the second term, and calculated values for u and K, we have been able to refine the r_α structure directly.

The final r_α parameters found for PF_2NCSe, together with r_a values for all distances from the same refinement are shown in Table 6.6. The P-N=C angle has widened from an r_a value of 144°, obtained assuming a linear N=C=Se chain, to 149°. In the r_α structure the symmetry now became exactly C_s with the N=C=Se chain exactly linear, and so only seven parameters were subsequently used to define the molecular geometry.

In the final stages of the refinement, all independent

geometrical parameters and amplitudes of vibration, with the exceptions of u(P-N) (= 1.2 x u(C-Se)) and u(F...F) (= 1.0 x u(F...N)) were free to refine.

Table 6.6 shows the final parameter set (r_α) for PF_2NCSe: the least squares correlation matrix is given in Table 6.7, and the observed and difference molecular scattering curves are shown in Figure 6.3.

6.6 Discussion

In most structure determinations carried out on compounds containing the PF_2N group[25,26,27,63] the P-F and P-N distances were so close that refinement of all four parameters associated with these bonded distances was impossible, and u(p-F) and u(P-N) usually constrained to refine together. In the case of PF_2NCSe, r(P-F) and r(P-N) are comparatively well resolved, whereas the peaks associated with r(C=Se) and r(P-N) are coincident, and the two amplitudes associated with these distances were refined as a single parameter. The correlation between r(P-N) and r(C=Se) is clearly shown in the least squares correlation matrix (Table 6.7). The correlation would have been more severe but for the fact that the sum of r(C=N) and r(C=Se) is well defined by the N...Se distance in the linear pseudohalide moiety. Thus r(C=Se) is equal to d(Se...N) - r(C=N).

The angle found at nitrogen [149.0(15)°] is the

widest yet reported for two coordinate nitrogen bound to phosphorus[66], but this value is not unexpected when compared to those for PF_2NCO, PF_2NCS and $(PF_2N)_2C$[67]. In fact, all r_α structural parameters and r_a distances yield values consistent with those found for the two comparable pseudohalides. Parameters for PF_2NCSe, PF_2NCS, PF_2NCO and $(PF_2N)_2C$, together with those for SiH_3NCSe[68] are compared in Table 6.8. Most amplitudes of vibration were found to be within experimental error of those calculated in the normal coordinate analysis, despite the fact that this was undertaken prior to the gas phase structure investigation and utilised slightly different parameters.

The final R_G and R_D factors were 0.10 and 0.08 respectively. These are somewhat higher than usual for structures of small molecules undertaken at Edinburgh. This can be attributed to the rapid decay with increasing angle in the short distance intensity data, arising from destructive interference caused by the superposition of scattering from many differing interatomic distances of comparable scattering power, a feature illustrated by the form of the radial distribution curve (Figure 6.2).

However, the R factors compare well with those obtained in the analyses of PF_2NCO and PF_2NCS.

Table 6.1: Weighting functions, correlation parameters and scale factors for PF_2NCSe

Camera height mm	Δs nm^{-1}	s_{min} nm^{-1}	sw_1 nm^{-1}	sw_2' nm^{-1}	s_{max} nm^{-1}	p/h	Scale Factor
128	4	60	80	200	268	0.014	0.919(31)
285	2	34	50	110	140	0.366	0.863(22)

Table 6.2: Non-zero symmetry force constants $x10^{-2}$ (mdyn pm^{-1}) for PF_2NCSe

A'	1	5.72						
	2	1.10	13.50					
	3	-0.06		5.32				
	4	0.01			4.22			
	5					0.73		
	6				0.48		0.12	
	7				0.12			0.58
	8				-0.05			
A"	1	4.58						
	2		0.64					
	3		-0.01	0.23				
	4				0.01			

Table 6.3: Frequency assignment, potential energy distribution and approximate description of normal modes for PF_2NCSe

Species	Frequency (cm^{-1})	Potential Energy Distribution	Approximate Description
A'	1972	90s	N=C stretch
	920	23t + 29d + 42r	C=Se stretch
	851	26t + 72d + 49r	P-F sym. stretch
	569	22t + 41d + 49β	P-N stretch
	429	80α	NCSe bend
	396	21γ + 66ψ	PF_2 bend
	262	15t + 20d + 49β	PF_2 deform.
	77	74d + 156γ + 21ω	PNC bend
A"	851	95r	P-F asym. stretch
	490	39β + 52θ	NCSe bend
	347	54β + 41θ	PF_2 deform.
	54	91τ	torsion

Table 6.4: Calculated amplitudes of vibration at OK and 298K and K values at 298K

	u OK (pm)	u 298K (pm)	K 298K (pm)
P-F	4.10	4.18	1.78
P-N	4.59	5.39	2.31
N=C	3.67	3.69	1.18
C=Se	3.83	3.98	2.06
F...F	6.03	6.77	2.36
F...N	6.15	7.42	3.72
F...C	7.07	11.98	13.88
F...Se	7.79	17.30	0.04
P...C	5.14	6.80	0.62
P...Se	5.60	10.73	0.14
N...Se	3.91	4.15	2.35

Table 6.5: Molecular parameters (r_a) for PF_2NCSe

Independent distances/pm	
r_a(P-F)	154.9(3)
r_a(P-F)	169.2(18)
r_a(N-C)	122.4(8)
r_a(C-Se)	168.2(10)

Independent angles(°)	
<F-P-F	98.1(16)
<F-P-N	97.5(8)
<P-N=C	141.1(30)
<N=C=Se	175.4(48)

Notes:

1. Figures in brackets are esds derived from the least squares analysis increased to allow for systematic errors.
2. In this refinement a distortion from a linear arrangement for the N=C=Se moiety, maintaining C_s symmetry for the molecule, was allowed. The minimum R_G factor (0.9) was obtained when the bend at carbon was such that selenium lay cis to phosphorus.

Table 6.6: Molecular parameters for PF_2NCSe

Independent distances/pm

r_α(P-F)	153.0(4)
r_α(P-N)	164.9(12)
r_α(N=C)	121.2(8)
r_α(C=Se)	168.1(10)

Angles(°)

<F-P-F	97.9(14)
<F-P-N	98.8(8)
<P-N-C	149.0(15)

		Electron diffraction	Vibrational spectroscopy
	r_a/pm	u/pm	u/pm
r(p-F)	154.7(4)	4.7(11)	4.2
r(P-N)	167.0(12)	3.6(17)	5.4
r(C=N)	122.0(8)	5.9(12)	3.7
r(C=Se)	170.0(10)	3.0(tied to u_2)	4.0
d(Se...N)	291.3(9)	6.7(17)	4.2
d(Se...P)	438.7(8)	12.8(8)	10.7
d(Se...F)	513.5(14)	21.4(13)	17.3
d(C...P)	276.4(11)	5.5(23)	6.8
d(C...F)	353.2(13)	17.3(23)	12.0
d(N...F)	245.0(11)	7.2(21)	7.4
d(F...F)	233.2(11)	7.2(tied to u_{10})	6.8

Note: Figures in brackets are esds derived from the least square analysis increased to allow for systematic errors.

Table 6.7: Least squares correlation matrix x100

r_1	r_2	r_3	r_4	<1	<2	<3	u_1	u_2	u_3	u_5	u_6	u_7	u_8	u_9	u_{10}	k_1	k_2	
100								76										r_1
	100	53	-74		-62	-66												r_2
		100			-58	-67												r_3
			100							-70			-63					r_4
				100											89			<1
					100										-56			<2
						100	52											<3
							100	84								74	65	u_1
								100								63	55	u_2
									100									u_3
										100			79					u_5
											100							u_6
												100						u_7
													100					u_8
														100				u_9
															100			u_{10}
																100	66	k_1
																	100	k_2

Note: only elements with absolute values ≥50 are included.

Table 6.8: Important geometrical parameters for some two-coordinate nitrogen compounds

	F_2PNCO[a]	F_2PNCS[a]	F_2PNCSe	$(F_2PN)_2C$[b]	SiH_3NCSe[c]
r_a(P-N)	168.3(6)	168.6(6)	167.0(12)	168.0(6)	
r_aP-F	156.3(3)	156.6(3)	154.7(4)	156.2(2)	
r_aN=C	125.6(6)	122.1(6)	122.0(8)	124.0(5)	118.1(8)
r_aC=Se			170.0(10)		175.9(7)
<MNC(r_α)	134.8(8)	144.0(7)	149.0(15)		180
<MNC(r_a)	130.6(8)	140.5(7)	143.9(13)[d]	132.8(5)	158.9(6)

Note: all distances are in pm; angles are in degrees

[a]Ref 63; [b]Ref 67; [c]Ref 68; [d]linear N=C=Se assumed.

Figure 6.1 : The trans-PF_2NCSe model with linear NCSe chain, symmetry C_s. Valence coordinates are indicates. ϕ is a linear bending in the symmetry plane, and θ is perpendicular to it. τ is a twisting coordinate generated by two torsions as $2^{-\frac{1}{2}}$ $(\tau_{3216} + \tau_{3215})$.

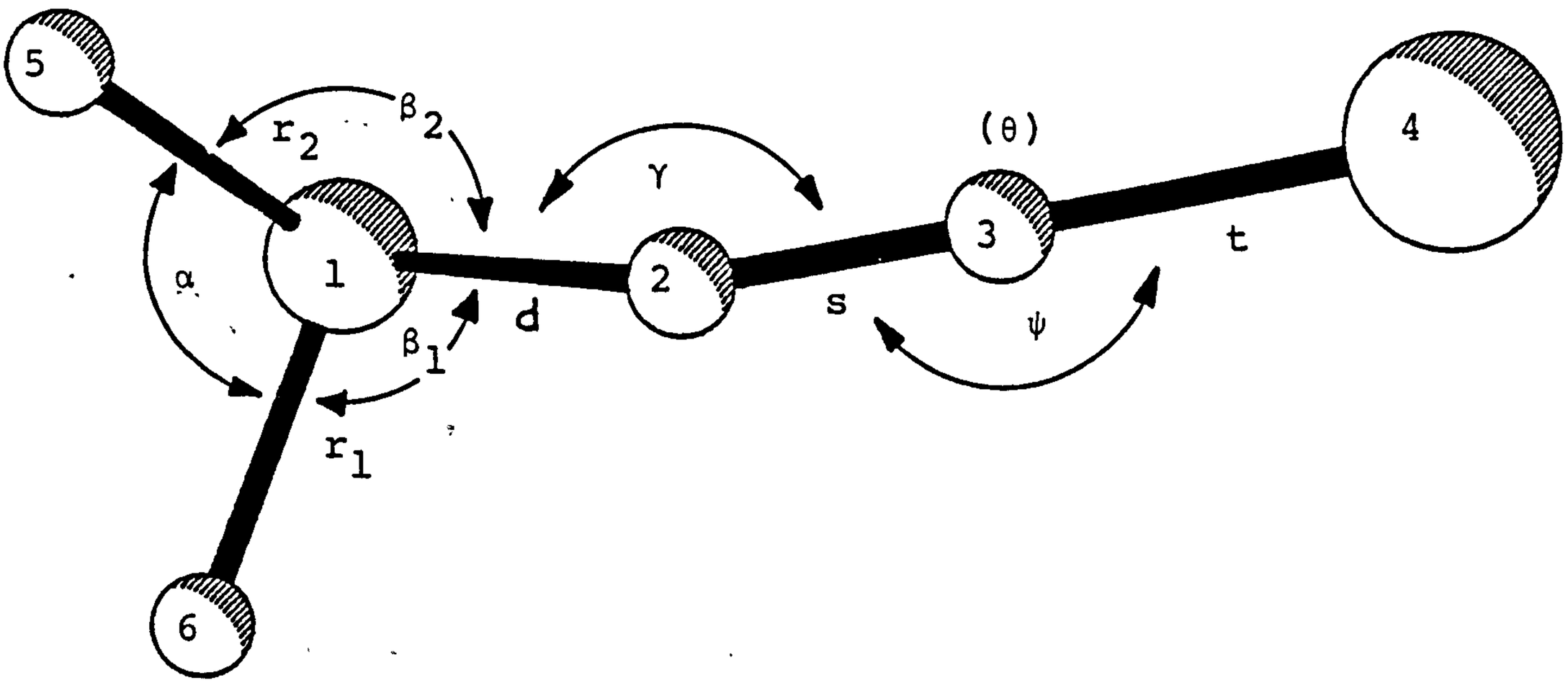

Figure 6. 2 : Observed and difference radial distribution curves, P(r)/r, for PF_2NCSe. Before Fourier inversion the data were multiplied by $s.\exp[(-0.00002\ s^2)/(Z_{Se}-f_{Se})(Z_F-f_F)]$.

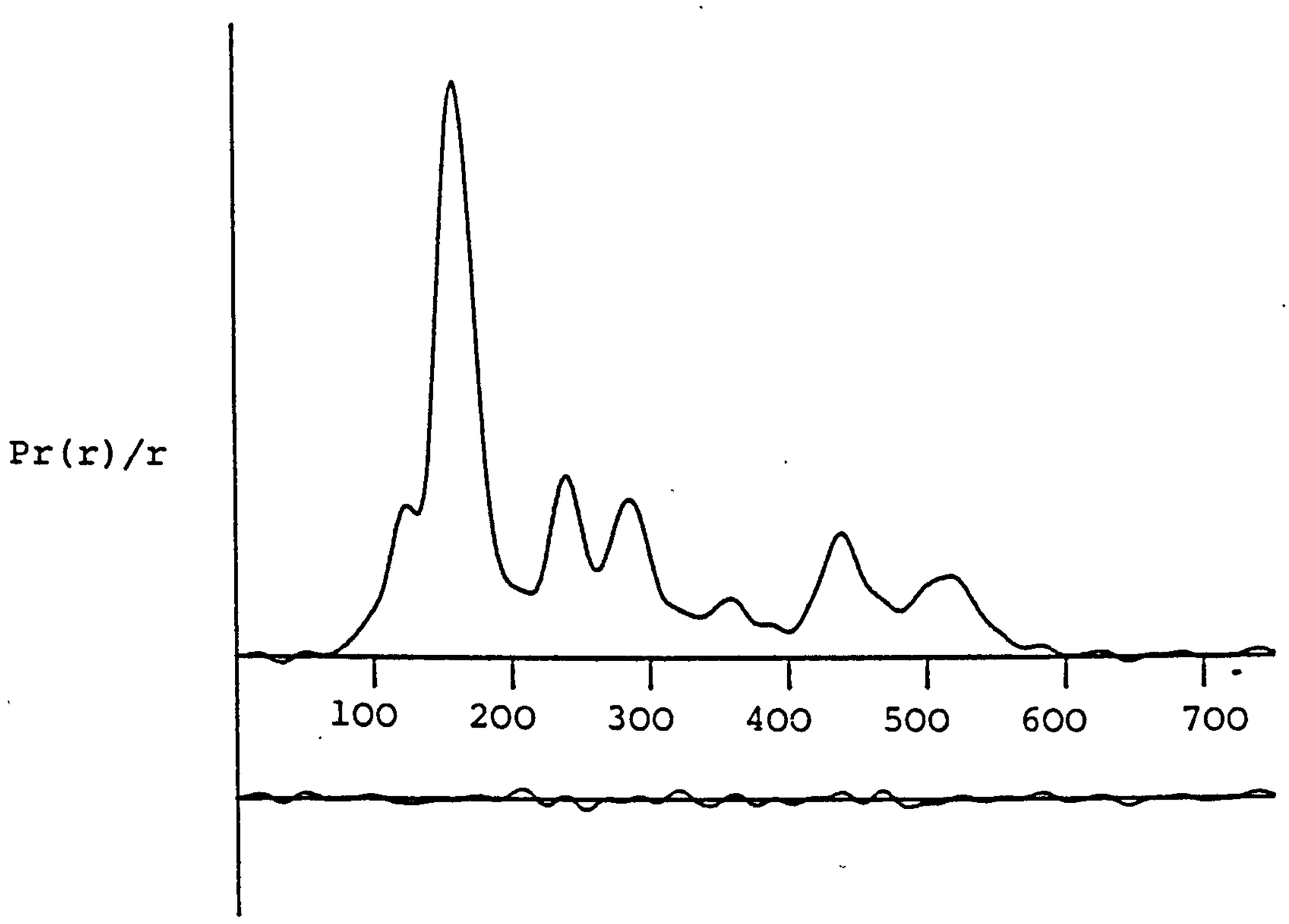

Figure 6.3 : Observed and final weighted difference molecular scattering intensities for nozzle-to-plate distances of (a) 120 and (b) 205 mm

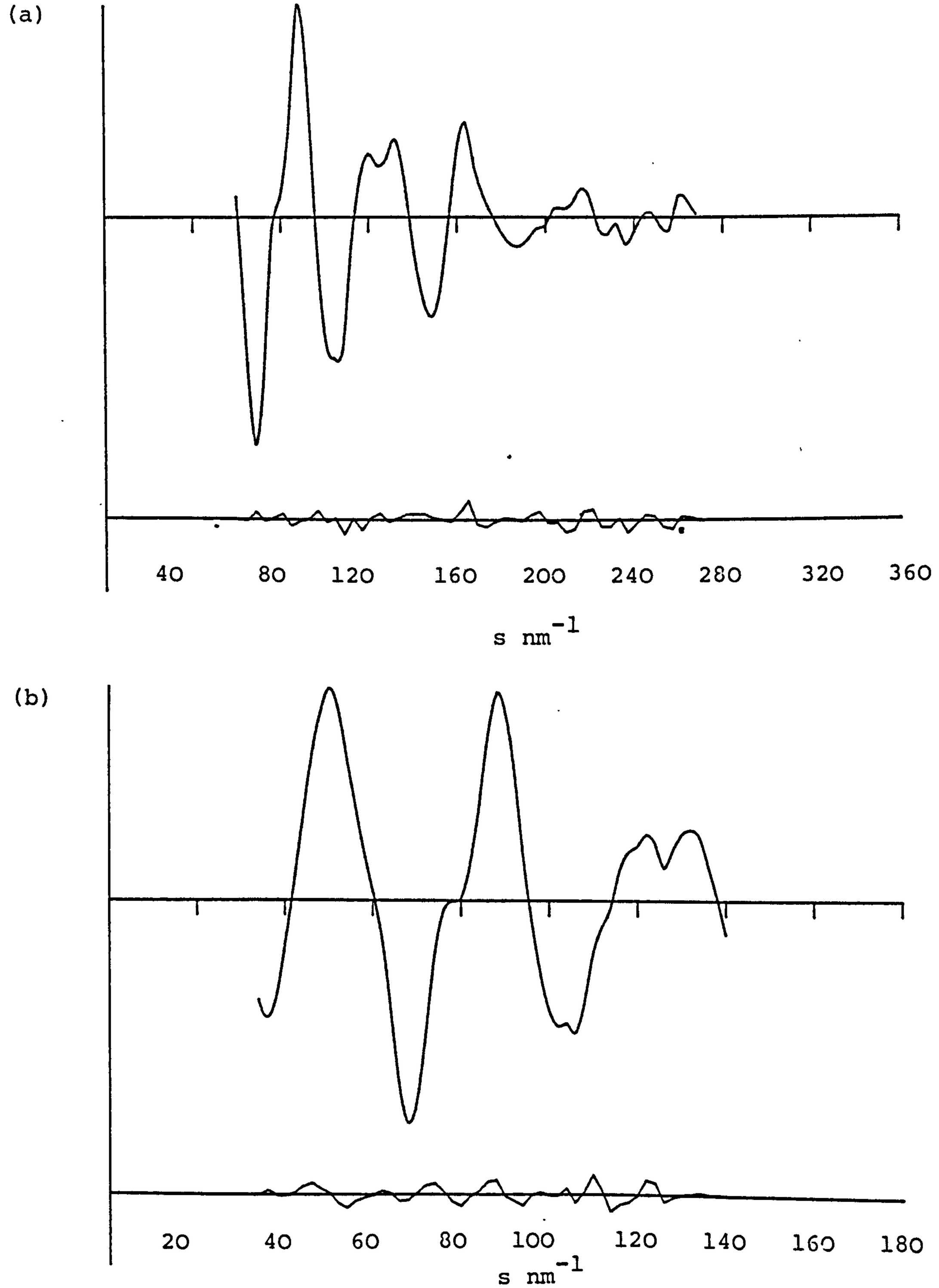

CHAPTER 7

PRINCIPLES OF LIQUID CRYSTAL NMR SPECTROSCOPY

7.1 Introduction

In general nmr couplings comprise two components. The first of these is a scalar quantity resulting from a through-bond interaction between spinning nuclei referred to as the indirect or 'J' coupling. To a first approximation this is invariant with sample orientation with respect to an applied magnetic field. A second component, the direct or 'D' coupling, is a through-space interaction derived from the trace of a set of second rank tensors. Due to random molecular motion, in normal solution nmr experiments this usually averages to zero. In the solid phase, through-space coupling is observed. Although this phenomenon has long been understood, its usefulness as an analytical technique has been limited by intermolecular contributions hopelessly complicating the spectra obtained[69]. Other methods of orienting molecules with respect to an applied magnetic field have been tried with limited success[70,71], but it was not until the use of compounds known as liquid crystals in the capacity of orienting solvents that direct couplings became readily measurable[72,73].

7.2 Liquid Crystals

In 1888 a class of compounds now known to constitute 5% of all naturally occurring organic substances was discovered, which showed two distinct phase transitions

between the isotropic liquid and solid phases[74]. Compounds exhibiting this "mesophase" were subsequently designated liquid crystals[75]. In this liquid crystalline state a compound appears to be a viscous but turbid fluid. In general, molecules which show such mesophases are comparatively rigid, linear, and contain aromatic rings[76,77].

Intermolecular dispersion forces cause neighbouring molecules in a liquid crystal to align parallel to each other[78,79]. If a magnetic field from an nmr spectrometer is applied to such a sample, this "short range" order can be extended over the entire bulk of the material, since the direction of smallest magnetic susceptibility (usually the longest molecular axis) will align parallel to the applied field.

Liquid crystals sub-divide into three basic types corresponding to differences in molecule packing: smectic; nematic; and cholesteric[80] (Figure 7.1). Of these the nematic mesophase is the most widely used in lcnmr spectroscopy, being the most mobile,and therefore the least susceptible,of all phases to temperature, or concentration, gradients within a given sample. Nematic liquid crystal solvents are the only type considered hence, and were exclusively used in all lcnmr experiments.

Figure 7.1: Schematic representation of packing in liquid crystal types.

(a) nematic

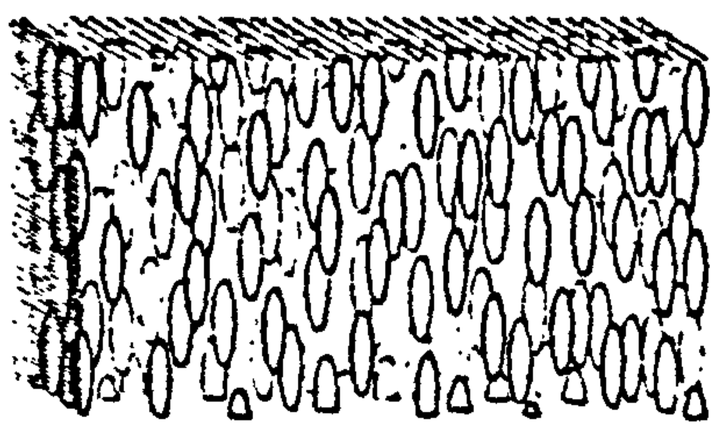

(b) smectic a

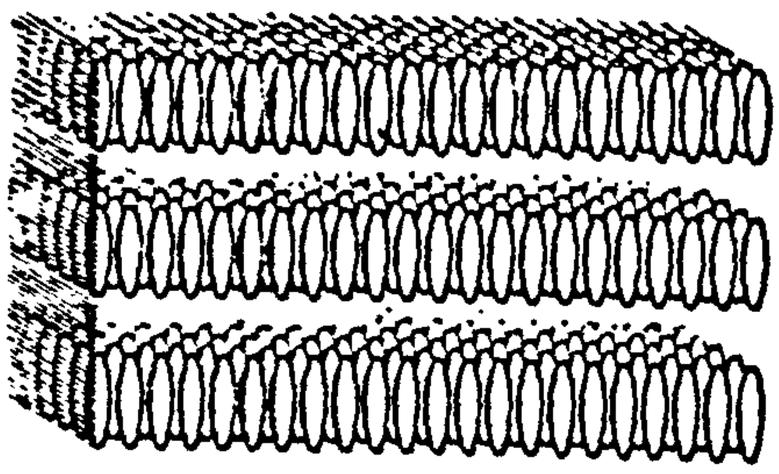

(c) smectic b

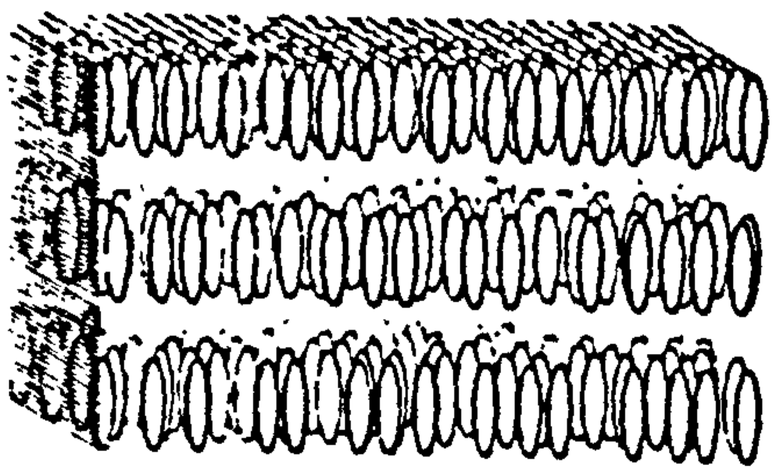

(d) cholesteric

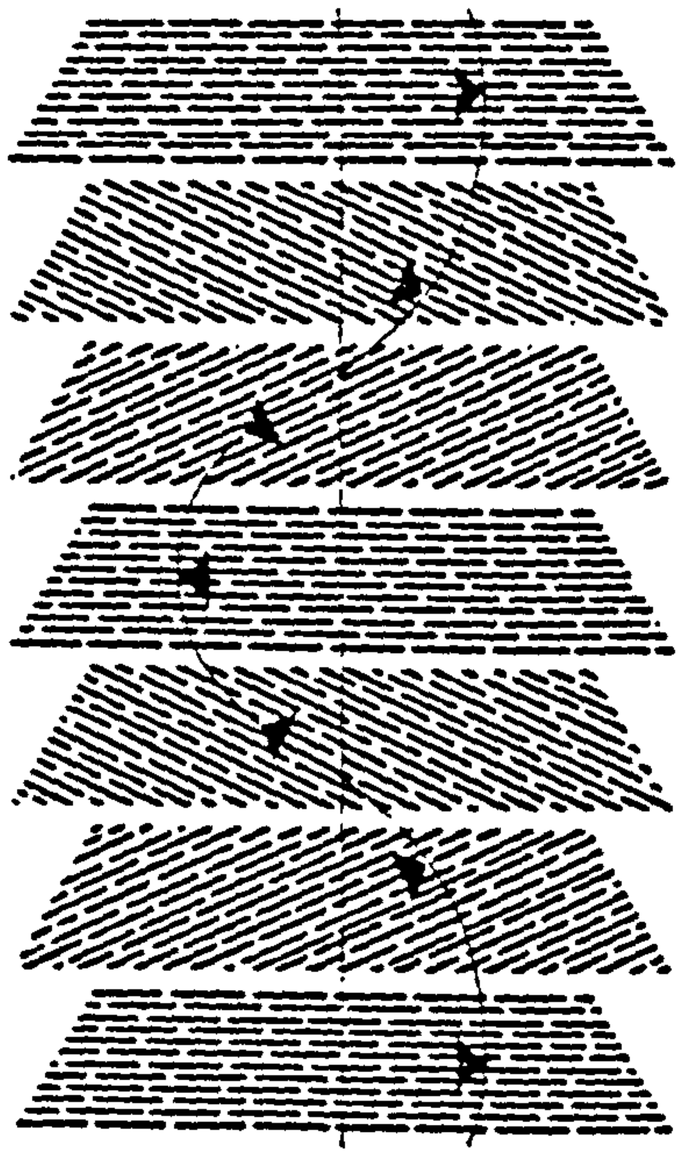

7.3 NMR of Solutes Dissolved in Nematic Mesophases

Molecules dissolved in liquid crystals experience restricted molecular motion corresponding to partial orientation by the solvent. They are matriced in a mobile phase and nmr measurements are limited to intramolecular interactions. The observed couplings in a nematic mesophase, henceforward designated by Δ, comprise partly direct and partly indirect coupling. Δ is defined to a first approximation by Equations 24a and 24b.

$$(24a) \quad \Delta_{ij} = J_{ij} + 2D_{ij}$$

$$(24b) \quad \Delta_{ii'} = 3D_{ii'}$$

Equation 24b corresponds to the interaction between two magnetically equivalent nuclei, which has only a direct dipole-dipole component, giving rise to an extra coupling over those seen in isotropic spectra of the same species. The direct coupling D_{ij} is defined by Equation 25,

$$(25) \quad D_{ij} = -\frac{h\gamma_i\gamma_j}{4\pi^2}\left(\tfrac{1}{2}\right)\left\langle\frac{3\cos^2\theta_{ij}-1}{r^2_{ij}}\right\rangle$$

where θ_{ij} is the angle between the applied magnetic field and the vector connecting atoms i and j, r_{ij} is the inter-atomic distance, γ is the magnetogyric ratio, and the angle brackets denote averaging over vibrational and molecular motions. Equation 25 is in turn derived from

the nuclear spin Hamiltonian for solutes in orienting media, and may be rewritten as Equation 26.

$$(26) \quad D_{ij} = \frac{h\gamma_i\gamma_j}{4\pi^2 r_{ij}^3} \cdot S_{ij}$$

where S_{ij} is the degree of orientation of the vector joining the atoms i and j: here vibrational averaging of r_{ij} has been neglected. Orientation has been described in terms of a 3x3 symmetric and traceless matrix by Saupe[81]. The elements, corresponding to a molecular-fixed cartesian co-ordinate system of orthogonal x, y and z axes are given by Equation 27.

$$(27) \quad S = \begin{bmatrix} S_{xx} & S_{xx} & S_{zx} \\ S_{xy} & S_{yy} & S_{zy} \\ S_{xz} & S_{yz} & S_{zz} \end{bmatrix}$$

The five independent elements of this ordering matrix are conveniently defined as S_{zz}, $S_{xx}-S_{yy}$, S_{xy}, S_{yz} and S_{xz}. The elements of this matrix are calculated by expression 28.

$$(28) \quad S_{pq} = (\tfrac{1}{2}) \ \langle 3\cos\theta_p\cos\theta_q - \delta_{pq}\rangle$$

$$p,q = x,y,z.$$

where δ_{pq} is the Kronecker delta (= 1 for p=q, otherwise = 0), and θ_x, θ_y and θ_z represent the angle made between the cartesian molecule-fixed axes x, y and z and the

magnetic field vector. Equation 28 defines the range of values available to S as -0.5 → 1.0. The molecule-fixed axis system is most usefully chosen to coincide with the maximum number of high order symmetry axes within the molecule: under this condition the number of independent elements in the orientation matrix S may be reduced. Table 7.1 gives the relationship between these and the symmetry of the spin system being observed[82]. (Note the molecule PF_2Cl has C_s symmetry overall, but the spin system has the higher C_{2v} symmetry).

Once the molecule-fixed axis system has been established, it is possible to relate it to any other axis, for example the direction of an interatomic distance, by a coordinate transformation, given by Equation 29.

$$(29) \quad S_{(\text{any axis})} \equiv S_a \sum_{p,q} \cos \alpha_p{}^a \cos \alpha_q{}^a \cdot S_{pq}$$

Here $\alpha_x{}^a$, $\alpha_y{}^a$ and $\alpha_z{}^a$ are the angles between the a axis and the molecule-fixed axes x, y and z. Hence if the S matrix is known, the degree of orientation of any other axis can be derived. Conversely, the S matrix may be derived if enough S_a values are known. S_a can adopt the same range of values as S_{pq}: if $S_a = 1$ the a axis and applied field vector are parallel; if $S_a = -0.5$ then they are perpendicular.

The liquid crystal nmr experiment may therefore yield information about the relative orientations of vectors

joining pairs of atoms, hence about bond angles and ratios of interatomic distances.

The dipolar couplings measured are related to the five independent orientation parameters by an expansion of Equation 26 given below (Equation 30).

$$(30)\quad D_{ij} = \frac{\gamma_i\gamma_j h}{8\pi^2 r_{ij}^3}\ [S_{zz}(3\cos^2\theta_{ijz}-1) + (S_{xx}-S_{yy})(\cos^2\theta_{ijx}-\cos^2\theta_{ijy}) + 2S_{xz}(\cos\theta_{ijx}.\cos\theta_{ijz}) + 2S_{yz}(\cos\theta_{ijy}.\cos\theta_{ijz}) + 2S_{xy}(\cos\theta_{ijx}.\cos\theta_{ijy})]$$

Here θ_{ijx}, θ_{ijy} and θ_{ijz} represent angles made between the vector joining atoms i and j and the fixed-molecular axis system. Equation 30 relates dipolar couplings to orientation, and molecular geometrical, parameters. For an AB_3 molecule, with C_{3v} symmetry the appropriate relationships simplify according to Equations 31a and 31b.

$$(31a)\quad D_{BB} = \frac{K_{BB}}{r_{BB}}\ S_{zz}\quad (K_{xy} = \gamma_x\gamma_y h/8\pi^2)$$

$$(31b)\quad D_{AB} = \frac{K_{AB}}{r_{AB}^3}\ [S_{zz}(3\cos^2\theta_{ABz} -1)]$$

and the ratio D_{AA}:D_{AB} given by Equation 31c.

$$(31c)\quad \frac{D_{BB}}{D_{AB}} = \frac{K_{BB}}{K_{AB}}.\ \left(\frac{r_{AB}}{r_{BB}}\right)^3.\ S_{zz}.\ \frac{1}{(1-3\cos^2\theta_{ABz})}$$

Since $\cos\theta_{ABz}$ can be replaced by $(r_{AB}^2 - \frac{3}{4}r_{BB}^2)r_{AB}$, the above equation shows that the ratio of the two couplings observed can be directly used to calculate the ratio of the two interatomic distances r_{AB} and r_{BB}, and hence the value of the included angle <BAB, thus determining the shape, but not the size, of the molecule AB_3.

7.4 Compatability between Electron Diffraction and LCNMR

In the most favourable cases, such as that outlined above, lcnmr experiments may solve fully the structural shape of a molecule, or part thereof. However, most molecules without high symmetry or small size do not meet the following requirement for a complete solution:

(32) No. of observable couplings $\geq$ no. of independent geometrical parameters plus no. of independent orientation parameters.

Simple molecules without high symmetry would be unlikely to yield geometrical information by lcnmr techniques alone, even if all nuclei had spin ½. This is illustrated by the molecule PF_2HSe, discussed in Chapter 9.

In order to relate lcnmr data to that derived from other sources it must be assumed that the structure is invariant between the molecular gas and liquid crystalline solvated state, or allowances must be made for reorientation and other distortions from the gas phase structure, induced by

the effect of the orienting medium on the solute. Rigid molecules are least likely to show different geometries for the two phases considered. In the cases of trifluorophosphine[83] and phosphine[84-86], favourable comparisons have been made between the gas phase and liquid-crystalline solvated state structures. However, phosphoryl fluoride, having only a single oxygen in addition to the atomic constituents of trifluorophosphine, shows a discrepancy between the lcnmr and electron diffraction results, attributed to reorientation distortion[87,88]. An elegant example of solvent-induced distortion is afforded by the observation of a small deuterium quadrupole splitting in the molecule $C(CD_3)_4$[89], indicating a loss of the tetrahedral symmetry of the free molecule. Furthermore, it has been noted that the geometry of a solvated species can alter with change in temperature[90] or nature[91] of solvent used. It is evident that consideration must always be given to solvent effects when solving structures in whole or in part by lcnmr techniques.

Information can be obtained from the use of lcnmr methods, not only about bond angles but also, where appropriate, concerning internal motion in non-rigid molecules. Table 7.2 lists some lcnmr studies which have yielded geometries for molecules, or moieties of molecules, containing spinning nuclei[92a-h].

Table 7.1: Non-zero, independent elements of the ordering matrix $S_{\alpha\beta}$ for groups of interacting nuclei according to point group symmetry

Point Group	$S_{\alpha\beta}$
C_1, C_i	S_{zz}, $(S_{xx}-S_{yy})$, S_{xy}, S_{xz}, S_{yz}
C_2, C_{2h}, C_s	S_{zz}, $(S_{xx}-S_{yy})$, S_{xy}
C_{2v}, D_2, D_{2h}	S_{zz}, $S_{xx} - S_{yy}$
C_3, C_{3h}, C_{3v}	S_{zz}
C_4, C_{4h}, C_{4v}	S_{zz}
C_5, C_{5h}, C_{5v}	S_{zz}
C_6, C_{6h}, C_{6v}	S_{zz}
$C_{\infty h}$	S_{zz}
D_{2d}	S_{zz}
D_3, D_{3d}, D_{3h}	S_{zz}
D_4, D_{4d}, D_{4h}	S_{zz}
D_5, D_{5d}, D_{5h}	S_{zz}
D_6, D_{6h}	S_{zz}
$D_{\infty h}$	S_{zz}
S_4, S_6	S_{zz}
K_h, O, O_h, T, T_d	all $S_{\alpha\beta}$ zero

Table 7.2: Some examples of molecules whose molecular shape has been wholly or partly determined by lcnmr

Point Group	Molecule	Formula	Results	Reference
C_{3v}	trifluorophosphine	PF_3	<FPF	83,90
C_{3v}	phosphoryl fluoride	PF_3O	<FPF	87,88
C_{3v}	phosphine	PH_3	<HPH	84,85,86
C_{3v}	methyl fluoride	$^{13}CH_3F$	All distance ratios	92a
C_{3v}	methyl halides	$^{13}CH_3X$ X=Cl,Br,I	<HCH	92b
C_{3v}	acetonitrile	$^{13}CH_3{}^{13}C{\equiv}N$	All distance ratios	92c
D_{3h}	2,4,6-trifluorobenzene		All distance ratios	92d
D_{2h}	tetrafluoroethylene	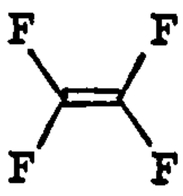	All distance ratios	92e
C_{3v}	propyne	$CH_3C{\equiv}CH$	All distance ratios (from ^{13}C satellites	92f
C_{3v}	cyanopropyne	$CH_3C{\equiv}C-C{\equiv}N$	All distance ratios (from ^{13}C satellites	92g
C_{3v}	furan	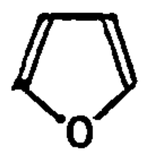	interproton distance ratios	92h

7.5 Vibrational Averaging

The effect of vibrational averaging on an interatomic distance has been discussed for electron diffraction in Chapter 1, where it was shown that the distance measured, r_a, was equal to $\langle r_{ij}^{-1} \rangle^{-1}$, where square brackets indicate time-averaging of the instantaneous distance between atoms i and j. Similarly by examining the form of Equation 26, modified to account for vibrational averaging according to Equation 33,

$$(33) \quad D_{ij} = - \frac{h\gamma_i\gamma_j}{4\pi^2} \langle r_{ij}^{-3} \rangle \langle S_{ij} \rangle$$

it can be seen that the distance being measured, defined as r_d[39], is given by the expression $r_d = \langle r_{ij}^{-3} \rangle^{-\frac{1}{3}}$. The two quantities r_a and r_d may then be related by using the general relationship

$$(34) \quad \langle r^k \rangle^{1/k} = r_e + 3au^2/2 + (k-1)u^2/2r_e$$

to give

$$(35) \quad r_d = r_a + u^2/r_e$$

Here u represents the mean amplitude of vibration of atoms i and j and r_e the interatomic equilibrium distance. Since the correction term u^2/r_e is small, r_e may be adequately replaced by r_a. Thus, to a first approximation, only a very simple correction utilising easily accessible

parameters is required to ensure compatability between r_a and r_d.

7.6 Combining LCNMR Data with those obtained from Gas Phase Techniques

For most molecules studied by lcnmr no unique solution is possible for the structure, since the number of independent geometrical and orientation parameters usually exceeds the number of independent dipolar couplings observed. In these cases certain geometrical parameters may be assigned fixed, reasonable values until the relationship defined by Equation 32 holds.

In some cases, where molecules with low symmetry are studied, the orientation parameters alone may be investigated, by fixing structural parameters at reasonable values[93a-e]. The assumed parameters may take values derived from an electron diffraction or microwave experiment. However in Chapter 2 it was described how data external to the electron diffraction experiment may be used to supplement electron diffraction data and so help to determine a molecular structure. Furthermore, it was possible to refine a structure, using electron diffraction least squares analysis programs, entirely on non -ed data. Liquid crystal nmr data are eminently suitable for this purpose, and we have already described how to calculate r_a values from dipolar couplings. As previously described, these new data were added to the

electron diffraction data points. The weight matrix had to be extended diagonally to include weights for each new data point; i.e. dipolar coupling constant, and these were usually chosen to be inversely proportional to the squared uncertainty of the observation. From the limited experience gathered so far from combined electron diffraction/lcnmr refinements, it would appear that the well defined parameters in the electron diffraction structure determination remain essentially unchanged by the inclusion of new data, whereas parameters which were previously poorly determined, such as those involving hydrogen, become very much better determined.

7.7 Complementation of LCNMR and Electron Diffraction Data

Frequently, when two interatomic distances have values less than ca. 5-10 pm apart, they may not be independently resolved in the electron diffraction structure determination[13,23-27,94a-c], and only the mean of the two (or more) distances may be accurately known. Since that which is unknown constitutes a ratio of distances, lcnmr may provide exactly the information required to remove correlations between interatomic distances with similar values.

Secondly, parameters involving hydrogen are difficult to ascertain accurately from electron diffraction experiments, particularly in the presence of heavy atoms[13,25-27,39,95a,b], due to the weak scattering power

of the proton, and H...H interatomic distances are almost never seen in radial distribution plots, except for very small and light molecules[96a-f]. Once again, lcnmr may provide the answer, since protons with 100% abundance spin ½ give rise to excellent nmr signals.

By choosing to undertake combined ed/lcnmr refinements we hoped in the case of PF_2HSe to look for the previously poorly determined location of the hydrogen atom. In the case of PF_2NH_2 we hoped to resolve the distances P-N and P-F, which show strong correlation in the ed experiment.

CHAPTER 8

LIQUID CRYSTAL NMR EXPERIMENTAL PROCEDURES

8.1 LCNMR Experimental

Many examples of liquid crystals have been used as orienting solvents for the purposes of obtaining nmr spectra of solutes (Table 8.1), but most of these are fairly reactive, many containing the N=N functional group. While these are suitable to act as solvents for most organic molecules, the difficulties in obtaining spectra for such species as trifluorophosphine[83] and other fluorophosphine compounds[84-88] in these solvents have been documented.

Initially, trials were carried out dissolving trifluorophosphine in a variety of liquid crystal solvents, mostly originally intended for use in liquid crystal displays such as those used in digital watches. 10% molar solutions of PF_3 were prepared in each case using previously degassed solvents in sealed 5 mm glass nmr tubes. In all cases decomposition of the solute was rapid at the nematic temperature; as a consequence of this in most cases no ^{31}P or ^{19}F nmr spectra were obtained. Figure 8.1 shows the result of a successful attempt to obtain a ^{31}P spectrum of PF_3 in the nematic phase of MBBA.

Fortunately, in response to a request to British Drug Houses, samples were obtained of a range of liquid crystals of the type of compound illustrated below.

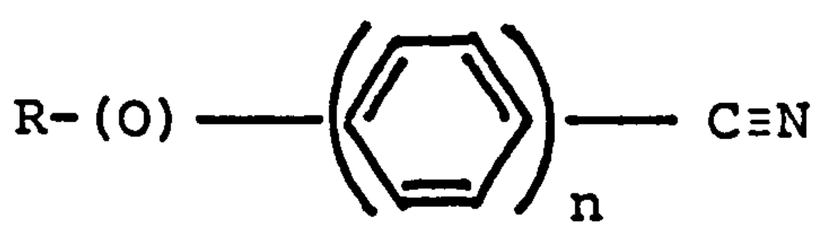

n = 2 or 3

Table 8.1: Some nematic solvents tried

Type	Formula	Approx Nematic Range (K)
British Drug Houses E1	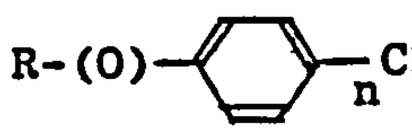	271-311
British Drug Houses E8	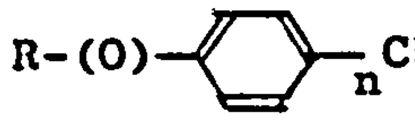	261-344
Schiffs base MBBA	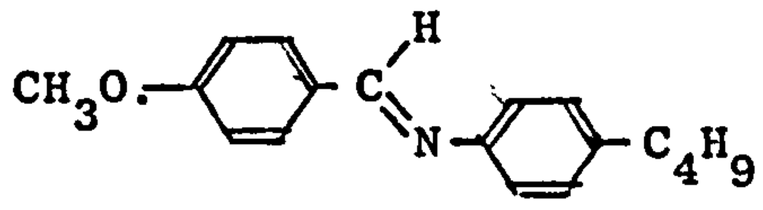	294-319
Schiffs base EBBA	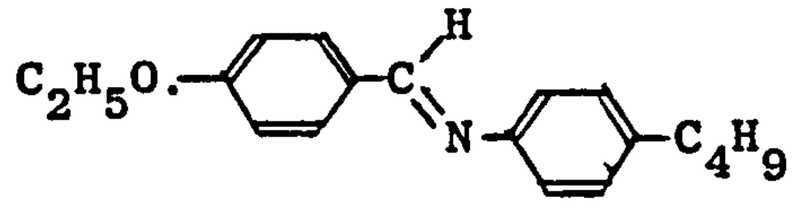	308-352
Various Kodak Nematic Mixtures	not known	ca.273-373

Note: The nematic range of solvents is depressed by addition of solute: hence E8 with 10% solute added exhibits a range of ca. 250 to 320 K.

Figure 8.1: ^{31}P Spectrum of PF_3 dissolved in MBBA

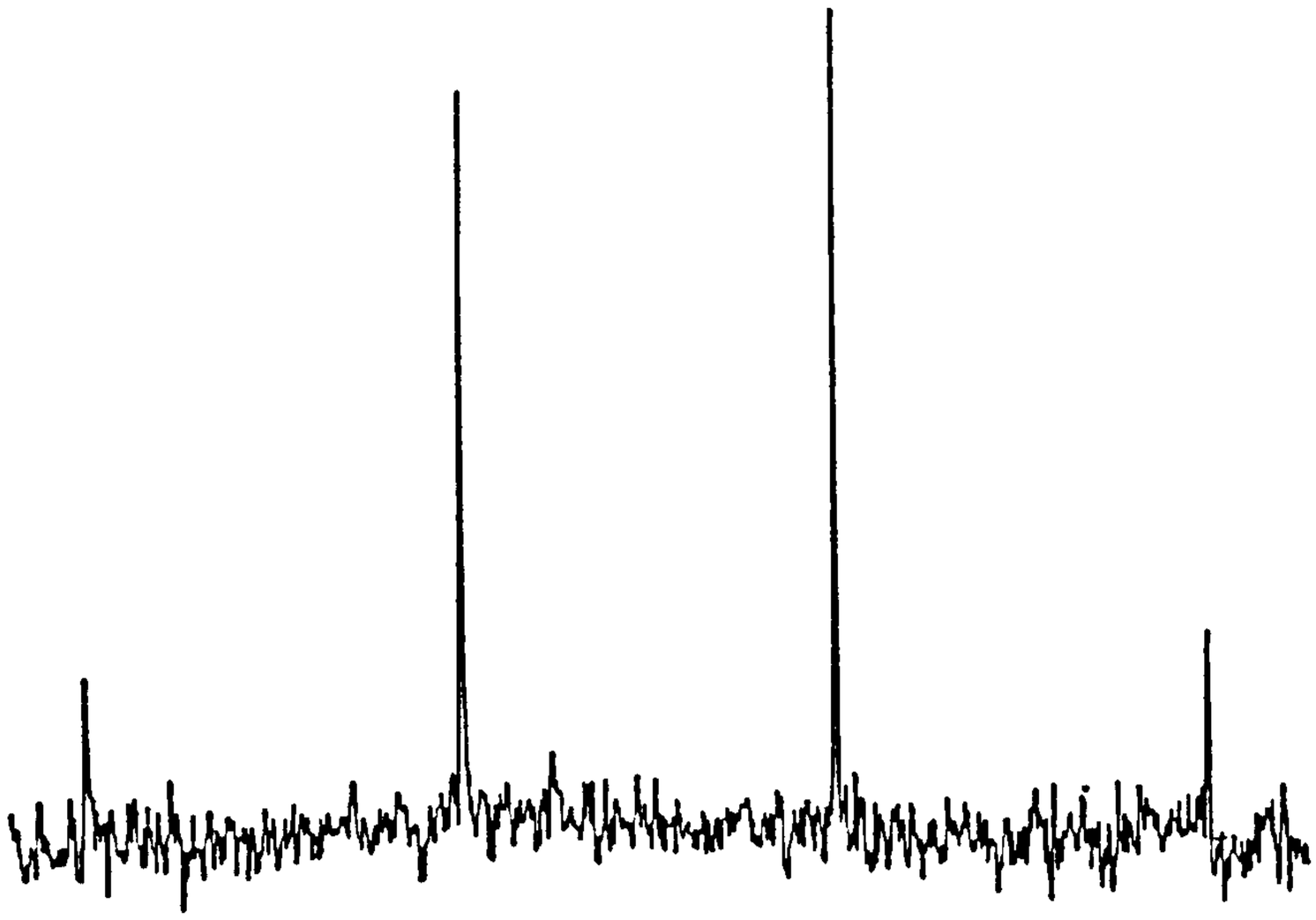

These are mixtures of 4-alkyl or alkoxy-4-cyano bi- or terphenyls.

The samples, code-named "E1" and "E8" by British Drug Houses, proved especially suitable, being unreactive to all unstable volatile species subsequently dissolved therein including SiH_3F, $SiH_3C{\equiv}N$, PF_3, $PF_2(NH_2)$, $Se(PF_2)_2$, PF_2HSe and SiF_3H. Furthermore, the compound E8, with ca. 10% molar solute added, had an unusually wide and low temperature range for its nematic phase, between 235 and 325 K, and also gave higher orientation parameters than other solvents tried.

In all subsequent work nmr samples were prepared in the following way. Molar concentrations of >20% reduce the isolation between solute molecules to give significant line broadening in the lcnmr spectrum, whereas low concentration solutions give sharp splittings but with reduced signal-to-noise ratio[97]. As a compromise, the molar concentrations used were chosen to be ca. 10%. These gave spectra with both good signal-to-noise ratios and line definitions, provided various physical parameters such as temperature stability and homogeneity of sample and field were given due consideration. Usually 0.2 mMol of solute was added to ca. 0.3 ml of a previously degassed sample of E8, thus giving the minimum required depth of sample in a 5 mm nmr tube to match the probe of a Varian Associates XL100 MHz spectrometer, on which most spectra were recorded. Keeping the volume of sample small ensured a minimum temperature gradient throughout the

sample; essential if sharp couplings were to be observed in the nematic phase, since both chemical shift and dipolar couplings vary with the degree of orientation of the solute molecule, which is itself dependent on temperature. Figures 8.2a and 8.2b show how the Δ coupling constants and chemical shifts change with temperature for the molecules PF_2HSe and $PF_2(^{15}NH_2)$ in the nematic phase of E8.

Since chemical shifts and coupling constants vary with temperature, it is important that the temperature during the acquisition of data in a fast Fourier-transform nmr experiment be held constant, and this was best achieved on the XL100 by allowing thermal equilibrium to be attained. This was considered to have occurred when two successive spectra gave the same line positions. The variable temperature control on the spectrometer utilises the technique of warming pre-cooled air to the required temperature. Normally liquid nitrogen is used as a coolant, but better stability was obtained using a solid CO_2 methanol slush bath, since this reduced the extent of heating required with a subsequent improvement in stability. This modification had not been implemented when the spectra used to derive Figure 8.1 were recorded. Definitive spectra used in the structure analysis of all compounds did benefit from this improved thermal stability. A digital thermometer was used to monitor the temperature in the probe of the spectrometer, calibrated against the standard methanol thermometer[98]. With care temperatures

Figure 8.2: Variation of Δ and chemical shift with temperature for solutes dissolved in liquid crystal E8. Plots were drawn from successive ^{19}F spectra of each solution recorded at different temperatures, including some above nematic range of the solutions
(a) $SePF_2H$ - selenium satellites not included.
(b) $PF_2(^{15}NH_2)$

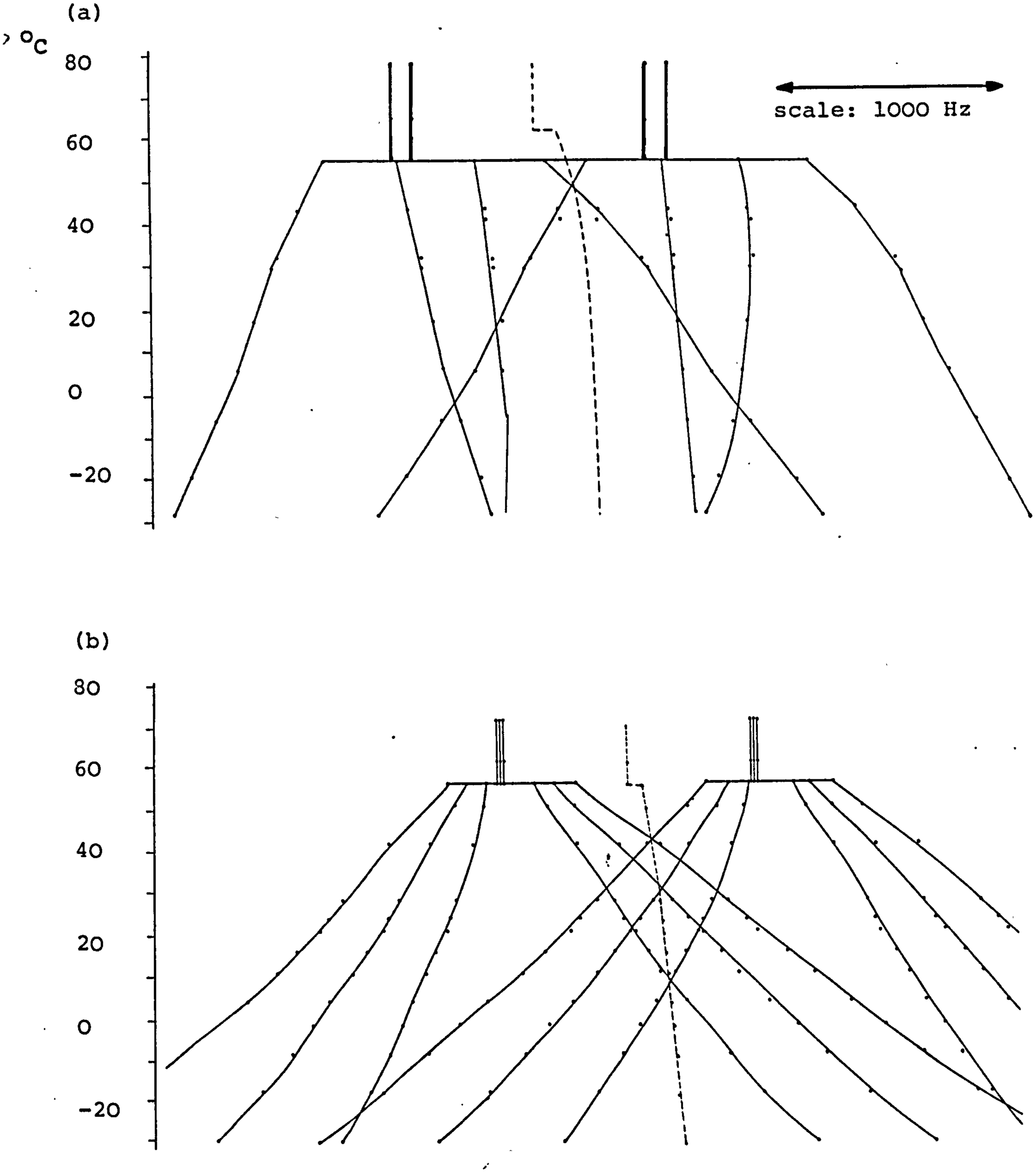

Note: broken lines indicate chemical shift.

were reproducible within $\pm$ 0.5^{o} using the digital thermometer.

In the Varian Associates XL100 MHz spectrometer, which has a conventional electromagnet, the sample remained stationary throughout data collection. When recording spectra on a Bruker WH360 MHz spectrometer with a superconducting magnet, the perpendicular applied field allowed the sample tube to be spun, since sample alignment remained parallel to the tube. However, on this machine, temperature control proved to be inferior to that found on the XL100, and on balance the latter yielded better spectra in lcnmr experiments.

Unlike the Bruker WH360 spectrometer, whose magnetic field is inherently stable, the XL100 requires to lock on to a nucleus to ensure that the field cannot drift. Usually an internal reference compound, such as a deuterated solvent, is used for this purpose. In nematic solvents, however, the lock would align and show direct couplings; therefore this method could not be used. In some cases, glass capillaries containing solvents have been inserted, into nmr tubes containing nematic solutions[83], for the purpose of providing an internal lock, but this must increase inhomogeneity in both the sample temperature and the applied field. The Varian Associates machine is equipped with proton and fluorine external locks, and these were used throughout. As a consequence, decoupling experiments involving the observation of one

of these nuclei while irradiating the other were ruled out.

Since, in order to determine all Δ couplings within most molecules more than one nucleus needed to be observed, the temperature had to be exactly reproducible. This was done by adjusting the temperature of the sample until values for ΔMX obtained by observing the M and X spectra were equal.

8.2 Obtaining Values for Direct Coupling Constants

In order to derive direct coupling constants from Δ splittings, it was necessary to observe nuclei in isotropic as well as anisotropic media. Where possible, this was accomplished by looking at nmr spectra at two temperatures above the nematic phase of the solvent used; otherwise values had to be taken from those found in other isotropic solvents.

Whenever there are several different similar multiple splittings within a spectrum, it may be difficult to assign couplings, since Δ values may be grossly different from well-known J values, although in the cases of enriched or <100% abundance samples, identification is facilitated by observing the lines due to unenriched sample in the first case, and by the known intensity ratios of the satellites to the central peaks in the latter. If a Δ splitting is seen to diminish with a reduction in temperature, this must correspond to a coupling with both J and D components, of

opposite sign, and furthermore the relationship $|2D|<|J|$ must hold, since it is known that $|D|$ must increase with decreasing temperature.Identification of couplings in some cases may be possible by observing several nuclei and comparing splittings. In the last resort, however, double resonance experiments can resolve the assignments of Δ couplings to observed splittings.

8.3 Weights and Errors for Direct Couplings

Once a self-consistent set of direct coupling constants has been assembled, each is given an estimated standard deviation. These correspond partly to the uncertainty in measuring line positions. Their error is minimised by taking previously described precautions to ensure maximum thermal equilibrium of the sample and homogeneity of the applied field, and minimum temperature gradient within the sample. However, two other major sources of error may occur, and allowance for these must also be made in calculating the esd for a dipolar coupling.

The first of these arises when, due to thermal instability, spectra of a sample may be unobtainable in the temperature at which the nematic solvent used becomes anisotropic, in which case values from other isotropic solutions must be used, which may differ by up to a few Hz from the true values. A similar compromise must be made in the case of some proton spectra, since isotropic

solutions of liquid crystals give strong and complex spectra which may mask the solute peaks.

The second major source of error is impossible to allow for since it involves an unmeasurable parameter, the anisotropic contribution to J in the nematic phase. Any anisotropy in J will affect the value of the measured direct coupling, and the only way in which a value for J_{aniso} can be estimated is to constrain the value of an errant dipolar coupling to conform to a known geometrical structure; the error between the observed and calculated D coupling may then be attributed to an anisotropic component of the indirect J coupling. This approach is far from satisfactory, since differences between D observed and D calculated on the basis of a known molecular structure may also indicate a distortion in the molecular geometry imposed by the orienting medium.

Lcnmr experiments yielding satisfactory geometrical parameters show that,at least in these cases,any anisotropy in J must be negligible. In general, couplings involving light atoms only would not be expected to show significant anisotropic indirect coupling, as in the examples given in references 83-86 and 92. This observation is supported by theoretical considerations. Direct couplings derived for heavier elements coupling to hydrogen or other heavier elements must be treated even more cautiously; for example significant J_{aniso} components have been frequently found,or suspected,to contribute to measured $^{2}D_{FF}$ values[87,88,100], while the ^{13}C-H and ^{13}C-F indirect

couplings in enriched methyl fluoride have been reported to have a large anisotropic component, although the errors in the measurements in this case are high[101], and the claimed large anisotropy in the indirect coupling has been shown to have no theoretical foundation[102].

8.4 The Equivalence of Molecular Structures in the Gas Phase and Nematic Solution

In order to investigate the equivalence of structures determined in molecules dispersed in gas or nematic solvent media, attempts were made to acquire lcnmr data for several small molecules, including PF_3 and SiH_3F. Other molecules currently being studied include SiF_3H $SiH_3C{\equiv}N$, $SiH_3C{\equiv}CH$, and other simple silyl compounds. Trifluorophosphine showed good agreement between lcnmr, microwave[103], and electron diffraction data[104], both from our own measurements at two temperatures and from previously published measurements[83]. Silyl fluoride proved to be too insoluble for any recognisable spectra to be recorded. The results of the studies undertaken on the structure of PF_3 are documented in Table 8:2.

Table 8.2

a) Couplings measured for PF_3 in various nematogens and at various temperatures.[a]

Solvent	Temperature (K)	J_{PF} [b]	Δ_{PF}	D_{PF}	Δ_{FF}	D_{FF}
(i) E8	283	1400	1520.9	60.45	567.2	189.05
(ii) E8	253	1400	1535.6	67.8	665.6	221.85
(iii) E1	301	1400	1493.2	46.6	427.4	142.45
(iv) MBBA[c]	301	1400	1440	20	122	40.65

Notes: a) all couplings are given in Hertz; b) taken from measurements of isotropic solutions of E1 and MBBA; c) results derived from very poor quality spectra.

b) Structural parameter <FPF calculated for PF_3 by various methods.

Source	Method	<FPF (degrees)
This work (i)	lcnmr	96.45[d](20)[e]
This work (ii)	lcnmr	96.20[d](20)[e]
This work (iii)	lcnmr	96.55[d](25)[e]
This work (iv)	lcnmr	99[d](3)[f]
Ref.83	lcnmr	97.8
Ref. 103	microwave	96.9(7)
Ref. 104	ed	97.8(2)

Notes: d) Calculated using the expression

$$\frac{\gamma_F}{\gamma_P} - \frac{D_{PF}}{D_{FF}} = \left(\frac{r_{PF}}{r_{FF}}\right)^2 \left[\left(\frac{r_{PF}}{r_{FF}}\right)^2 - 2\right]$$

e) Derived from an nmr spectral line width of 0.25 Hz;

f) Derived from an nmr spectral line width of 1 Hz.

CHAPTER 9

THE MOLECULAR STRUCTURE OF DIFLUOROPHOSPHINE SELENIDE, DETERMINED USING A COMBINATION OF GAS ELECTRON DIFFRACTION AND LIQUID CRYSTAL NMR DATA

9.1 Introduction

Although the molecule PF_2HSe is a simple one, its structure determination by electron diffraction only is complicated by the fact that scattering from bonded and non-bonded distances associated with the proton is not only of relatively low intensity, but also that the distances approximately coincide with other much more intense peaks in the radial distribution curve, shown in Figure 9.1. Thus the structure is only incompletely determined, an occurrence also frequently found in both microwave spectroscopy, where only a limited number of rotational constants may be measured, and in nmr studies of solutes dissolved in liquid crystals, where only a few examples of molecular shape being entirely determined are known. Unless certain assumptions are made about structures thus studied, it is necessary to include data from more than one source, a more acceptable means of completely determining a structure. There have been successful structure determinations carried out using a combination of rotational constant and electron diffraction data[105], while rotational constants have been used to provide overall scaling factors in liquid crystal nmr studies[86]. The determination of the molecular structure of difluorophosphine selenide represents the first attempt to marry electron diffraction data with those obtained from lcnmr experiments.

9.2 Experimental

A sample of PF_2HSe was prepared by the reaction between hydrogen selenide and PF_2Br in the presence of mercury, under reduced pressure, by vigorously shaking a glass bulb containing the reagents for a prolonged period until ca. 50% conversion to product had been attained.[107]

$$PBrF_2 + H_2Se \xrightarrow{Hg} PF_2HSe + [HBr]$$

The product was purified by fractional condensation in vacuo and its purity monitored by infrared spectroscopy.

a. Electron diffraction: Electron diffraction intensities were recorded photographically on Kodak Electron Image plates using the Cornell/Edinburgh diffraction apparatus[26,30] operating at 42 kV. The sample was maintained at 250 K and the nozzle and room temperature (293 K) during exposures. Data were collected using two camera distances, 128 mm (3 plates) and 287 mm(3 plates), and were converted to digital form using a Jarrell-Ash double-beam micro-photometer[51] with spinning plates. The electron wavelength, 5.822 ± 0.003 pm, was determined from the diffraction pattern of gaseous benzene.

b. Liquid crystal nmr: In this work, samples were prepared containing 0.2 mMol of PF_2HSe in ca. 0.3 ml of 'E8' in 5 mm tubes, and these solutions had a nematic phase between 235 and 325 K.

All nmr experiments were carried out using a Varian Associates XL100 spectrometer in the pulsed Fourier transform mode. Double resonance experiments were carried out using the instrument's built-in decoupler. Temperature control was maintained by using the Varian machine's temperature system in the usual way, but with the liquid nitrogen cooling reservoir replaced by one containing an acetone/CO_2 mixture, the benefits of which have been previously outlined.

Values of indirect coupling constants were measured in the isotropic phase at 333 K. In order to check on any temperature variation of the indirect couplings, attempts were made to record spectra at 353 K, but the solute was thermally unstable, and only poor quality ^{19}F spectra could be obtained. However, the PF and FH couplings showed no temperature variation, and the couplings observed at 333 K have been used in derivation of all dipolar couplings.

The relative signs of the couplings observed in spectra of the nematic phase were determined by double resonance experiments. The spectra thus obtained are illustrated by Figures 9.2-6 and the results listed in Table 9.1. As J(PF) is known to be large and negative in all fluorophosphines, it was assumed that $J_{PF} + 2D_{PF}$ was negative, and other signs were related to this. The signs of indirect couplings were taken from reference 108.

c. Refinement of electron diffraction structure: Calculations were performed on ICL 2970 and 2980 computers, using an established data reduction programme[26], and the complex scattering factors of Schafer et al[9]. In all structural refinements it was assumed that the PF_2HSe molecule had C_s symmetry. The geometry was then defined by six parameters, chosen to be the P-Se, P-F and P-H bonded distances, and the angles <SePF, <PFP and <SePH. The values of the weighting functions used, correlation parameters and scale factors, are given in Table 9.2..

d. Combined electron diffraction/nmr analysis: For the combined structural analysis the modified least squares refinement programme[34] was used, so that any experimental data relating to geometrical parameters or amplitudes of vibration could be included. For each problem studied a specific routine must be provided, so that theoretical values equivalent to the experimental data may be calculated. The derivatives of these with respect to the refining parameters are then evaluated numerically. In the case of liquid crystal nmr, the addition data are dipolar couplings, which may be calculated using Equation 30.

$$(30)\quad D_{ij} = \frac{-\gamma_i\gamma_j h}{8\pi^2 r_{ij}^3}\,[S_{zz}(3\cos^2\theta_{ijz}-1) + (S_{xx}-S_{yy})(\cos^2\theta_{ijx}-\cos^2\theta_{ijy}) + 2S_{xz}(\cos\theta_{ijx}\cdot\cos\theta_{ijz}) + 2S_{yz}(\cos\theta_{ijy}\cdot\cos\theta_{ijz}) + 2S_{xy}(\cos\theta_{ijx}\cdot\cos\theta_{ijy})]$$

D_{ij} is the dipolar coupling between atoms i and j, with magnetogyric ratios γ_i and γ_j and separation r_{ij}: the angles of the i-j vector with respect to the molecular axes are θ_{ijx}, θ_{ijy} and θ_{ijz}, and the orientation parameters are S_{zz}, $S_{xx}-S_{yy}$, S_{xz}, S_{yz} and S_{xy}. In the present case the x axis was defined as parallel to the Se-P bond, and the z axis was perpendicular to the plane of symmetry. Thus S_{xz} and S_{yz} are zero, and the other three orientation parameters were included in the list of refineable parameters. When dipolar couplings recorded at two temperatures were used, three more orientation parameters were included, and the number of additional observations was doubled. For the additional observations, the weight matrix was extended with diagonal terms only, chosen so that weights were inversely proportional to the squared uncertainty of the observation and scaled to the standard deviation of the fit of the electron diffraction data points.

Vibrational averaging: As molecules at about ambient temperature are involved in vibrational motions with periods (10^{-12} to 10^{-14} s) much shorter than the nmr time scale ($\sim 10^{-5}$ s), it is necessary to average all the quantities in Equation 30 over vibrational motions. Provided the molecular reorientation rate in the solution is slow compared to the vibration rate, the two motions are uncorrelated, and the distance determined in the experiment is simply $\langle r_{ij}^{-3} \rangle^{-1/3}$, or r_d. A correction is applied to this distance to equate it to that measured

in the electron diffraction experiment, according to Equation 36, derived from Equation 35 by substituting r_a for r_e in the smaller term.

$$(36) \quad r_d = r_a + {}^{u^2}/_{r_a}$$

The derivation of the above equation is given in Chapter 7. All refinements were carried out on an r_a structure.

9.3 Results and Discussion

a. Nmr spectra: Two self-consistent sets of nmr data were obtained by the method described previously from ^{1}H, ^{19}F and ^{31}P spectra recorded at 253 and 293 K. The splittings observed in the first order spectra and indirect couplings measured from spectra of isotropic solutions were used to calculate the direct couplings using Equations 24a and 24b.

$$(24a) \quad \Delta_{ij} = J_{ij} + 2D_{ij}$$

$$(24b) \quad \Delta_{ii'} = 3D_{ii'}$$

Details of the spectra recorded for each nucleus at each temperature are given in Table 9.1,together with those parameters obtained in the isotropic temperature range of the solvent used. Values for Δ, J and D obtained for each nucleus are given in Table 9.3.

b. Refinement of structure using only electron diffraction data: Using only electron diffraction data, it was a straightforward matter to refine the four geometrical parameters defining the heavy-atom structure, and four associated amplitudes of vibration, as there are four distinct peaks in the radial distribution curve (Figure 9.1). However, the parameters involving the hydrogen atom would refine only with an unreasonably large esd, as shown in the final refinement, the results of which are listed as refinement A in Table 9.4. The final R factors were 0.10 (R_G) and 0.09 (R_D): the least squares correlation matrix is given in Table 9.5a and the molecular scattering intensity data are shown in Figure 9.7.

c. Combined structure analysis: The liquid crystal nmr data provided seven additional observations at each temperature, and three parameters were required to define the molecular orientation at each temperature. It was soon apparent that the two sets of dipolar couplings gave essentially identical results, and in subsequent work all the couplings were considered simultaneously. Thus it is clear that there can be no significant change in structure with temperature over the range studied. The coupling constants were given weights dependent on their uncertainties (standard deviations of the measurements), with two exceptions. It proved to be impossible to obtain a value for J(SeH) in isotropic solution, as the compound was too unstable at 333 K for a long run, necessary to observe a ^{77}Se spectrum, and the weak selenium satellites could not

be detected in a ^{1}H spectrum which was dominated by solvent resonances. It was therefore necessary to use a value measured for a solution in cyclohexane[108] and the uncertainty in D(SeH) was arbitrarily assumed to be 2 Hz. Secondly, it was found consistently that calculations did not reproduce the PSe coupling, the errors being 40-60 Hz. This was not entirely unexpected, as it is well known that for heavier elements there may be a sizeable anisotropic component of the indirect coupling[87], and there is no way that this can be estimated. A large anisotropy arising from the non-spherical nature of the indirect coupling tensor for $^{1}J(^{31}P^{77}Se)$ has previously been postulated to account for the unreasonably long (227 pm) P=Se bond length calculated from lcnmr measurements undertaken on the molecule Me_3PSe[109].

The phosphorus-selenium direct couplings found for $SePF_2H$ were therefore assigned a high uncertainty of 10 Hz in the refinements, which then converged to give the results listed as refinement B in Table 9.4. The observed and calculated dipolar couplings and their uncertainties are listed in Table 9.1. The least squares correlation matrix for refinement B is given in Table 9.5b. It should be noticed that the inclusion of the nmr data has greatly increased the correlations between geometrical parameters, and there are strong correlations between geometrical and orientation parameters, but amplitudes of vibration have not become correlated with other parameters.

The improvement in the precision of the geometrical

parameters involving hydrogen in refinement B is most striking, especially since the erroneous value and huge esd obtained from electron diffraction only showed that the single technique effectively could not locate the hydrogen atom. Furthermore, the other geometrical parameters, well determined by electron diffraction, are unperturbed by the inclusion of lcnmr data, indicating that the structures observed are essentially the same in both the gas and nematic solution. The amplitudes of vibration similarly remain unaffected by the inclusion of liquid crystal data.

The geometrical parameters are in themselves unremarkable. The structure of the PF_2 unit is very similar to those in difluorophosphine sulphide[110] and difluorohalophosphine sulphides[111]. The P = Se distance, 202.6(4) pm, is substantially shorter than those in trialkyl- or aryl-phosphine selenides, which typically have bond lengths between 209 and 212 pm[112-114]; such shortening is commonly found when the phosphine has electronegative substituents. The P-H bond distance is slightly greater than that found by microwave spectroscopy for PF_2HS [139.2(5) pm][110], but the SePh angle (118.6°) is very close to the SPH angle (119.2°) in PF_2HS. Figure 9.8 gives a perspective view of PF_2HSe.

Table 9.1:

(a) Dipolar couplings[a]

Nuclei	293 K			253K		
	Observed	Calculated	Uncertainty	Observed	Calculated	Uncertainty
$^{31}P-^{19}F$	87.4	87.3	0.3	9.6	9.8	0.4
$^{31}P-^{1}H$	1035.6	1035.5	0.6	893.1	893.5	1.1
$^{77}Se-^{31}P$	-88.9	-151.7	10.0	-64.2	-108.1	10.0
$^{19}F-^{19}F$	438.2	438.4	1.0	260.3	260.3	0.2
$^{19}F-^{1}H$	676.2	676.2	0.3	509.4	509.4	0.2
$^{77}Se-^{19}F$	-82.4	-82.4	0.3	-60.2	-60.8	0.5
$^{77}Se-^{1}H$	-56.1	-62.2	2.0	-36.5	-40.1	2.0

[a]All couplings are in Hz

(b) Double resonance experiments

Experiment	Couplings related	Relative signs
$^{1}H-\{^{31}P\}$	FH and PF	Opposite
	SeP and SeH	Equal
$^{19}F-\{^{31}P\}$	FH and PH	Equal
	SeF and SeP	Equal
	FF and PF	Opposite
$^{19}F-\{^{77}Se\}$	PF and SeP	Equal
	FH and SeH	Opposite
	FF and SeF	Opposite

Table 9.2: Weighting functions, correlation parameters and scale factors for PF_2HSe

Camera Height mm	Δs nm^{-1}	s_{min} nm^{-1}	sw_1 nm^{-1}	sw_2 nm^{-1}	s_{max} nm^{-1}	p/h	Scale Factor
128.2	4	64	80	240	272	0.046	0.870(16)
287.4	2	32	50	110	136	0.483	0.874(36)

Table 9.3: Couplings in PF_2HSe[a]

Nuclei	J 333 K	J 353 K	Δ[b] 253 K	Δ[b] 293K	D 253K	D 293 K
$^{31}P-^{19}F$	-1193.0(1)	-1193.0(1)	-1018.2(4)	-1173.8(5)	+87.4(3)	+9.6(4)
$^{31}P-^{1}H$	+720.2(1)	c	+2791.4(10)	+2506.3(20)	+1035.6(6)	+893.1(11)
$^{77}Se-^{31}P$	-1029.5(1)	c	-1207.3(10)	-1157.8(6)	-88.9(6)	-64.2(4)
$^{19}F-^{19}F$	-	-	+1314.7(30)	+781.0(7)	+438.2(10)	+260.3(2)
$^{19}F-^{1}H$	+91.3(1)	+91.3(1)	+1443.7(2)	+1110.0(4)	+676.2(3)	+509.4(2)
$^{77}Se-^{19}F$	-97.5(1)	c	-262.3(4)	-217.8(8)	-82.4(3)	-60.2(5)
$^{77}Se-^{1}H$	-13(1)[d]	c	-125.2(20)	-86.0(15)	-56.1(11)	-36.5(8)

[a]All couplings in Hz. Estimated standard deviations are given in parentheses. [b]J + 2D or 3D. [c]Not studied.
[d]Taken from ref. 107b.

Table 9.4: Molecular parameters[a] for PF_2HSe

	Refinement A (ed-only)		Refinement B(ed + nmr)	
	Distance/pm	Amplitude/pm	Distance/pm	Amplitude/pm
r_1P=Se	202.3(3)	4.9(5)	202.6(4)	4.8(6)
r_2P-F	155.8(2)	4.8(5)	155.7(3)	4.7(6)
r_3P-H	142.3(39)	8.5(fixed)	142.2(7)	8.5(fixed)
r_4Se...F	306.6(7)	8.3(6)	306.1(6)	8.4(7)
r_5F...F	234.6(8)	4.1(15)	235.2(10)	4.8(16)
r_6Se...H	313.1(110)	12.0(fixed)	298.0(8)	12.0(fixed)
r_7F...H	218.3(75)	13.0(fixed)	231.2(10)	13.0(fixed
	Angle(°)		Angle (°)	
<1 SePF	117.2(4)		116.8(3)	
<2 FPF	97.7(5)		98.1(7)	
<3 SePH	129.8(75)		118.6(7)	
			Orientation parameter	
s_1S_{zz}	(253K)		-0.0535(5)	
$s_2S_{xx}-S_{yy}$	(253K)		0.2173(23)	
s_3S_{xy}	(253K)		0.0675(30)	
s_4S_{zz}	(293K)		-0.0318(3)	
$s_5S_{xx}-S_{yy}$	(293K)		0.1612(17)	
s_6S_{xy}	(293K)		0.0581(21)	

[a]All distances are r_a. Quoted errors are estimated standard deviations determined in the least squares analyses, increased to allow for systematic errors.

Table 9.5a: Least squares correlation matrix x100, Refinement A[a]

r_1	r_2	r_3	<1	<2	<3	u_1	u_2	u_4	u_5	k_1	k_2	
100												r_1
	100		-40	-40								r_2
		100	-49		-42							r_3
			100		-70							<1
				100								<2
					100			-47	-53			<3
						100	58		-43	72		u_1
							100			70		u_2
								100		47		u_4
						100						u_5
							100					k_1
								100				k_2

[a]Only elements with absolute values ≥40 are included.

Table 9.5b: Least squares correlation matrix x100, Refinement B[a]

r_1	r_2	r_3	>1	>2	>3	s_1	s_2	s_3	s_4	s_5	s_6	k_1	k_2	
100														r_1
	100													r_2
		100	58		-75		92	-66		92	-60			r_3
			100		-96		74	-94		77	-97			>1
				100		-92	-59		-95	-55				>2
					100		-84	94		-86	94			>3
						100	57	-52	96	54				s_1
							100	-84	55	99	-78			s_2
								100	-50	-85	98			s_3
									100	52	-42			s_4
										100	-81			s_5
											100			s_6
												100		k_1
													100	k_2

[a]Only elements with absolute values ≥50 are included. There were no strong correlations between amplitudes of vibration and other refining parameters.

Figure 9.1 : Radial distribution curve, P(r)/r. Before Fourier inversion the data were multiplied by $s.\exp\left[(-0.00002s^2)(Z_{Se}-f_{Se})(Z_F-f_F)\right]$.

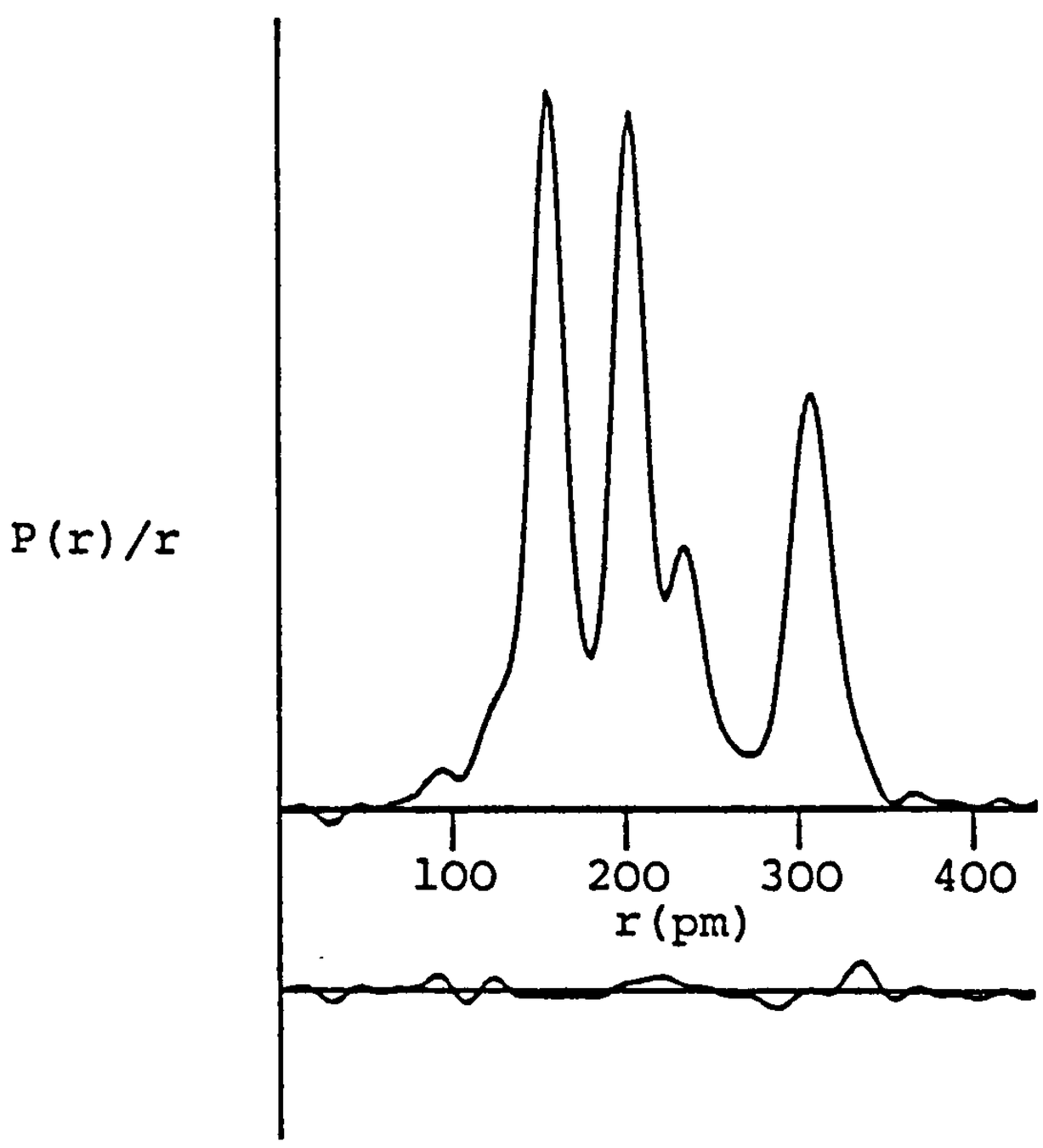

Figure 9.2: H-{P} double resonance experiment

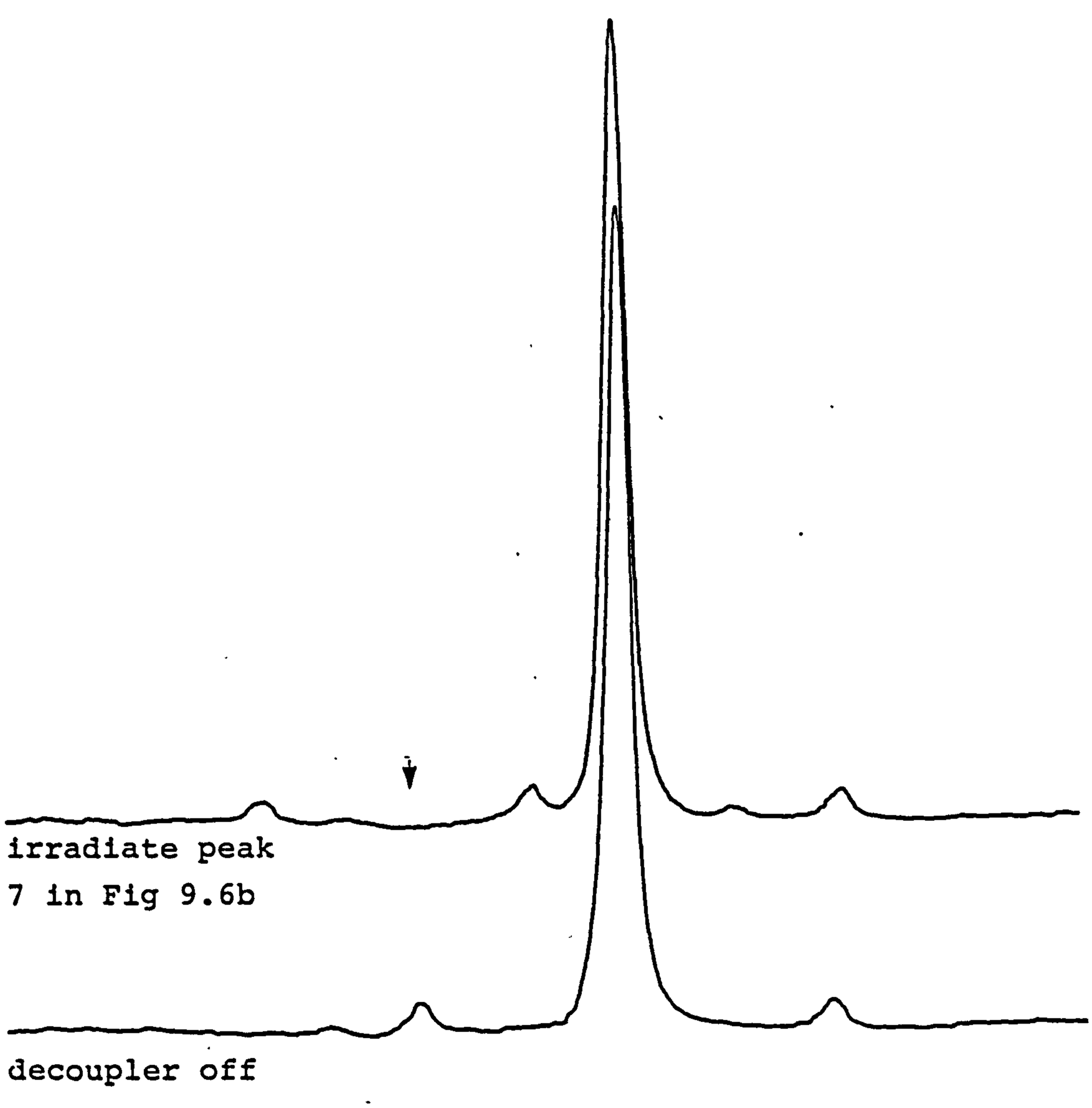

Figure 9.3: H- {P} double resonance experiment

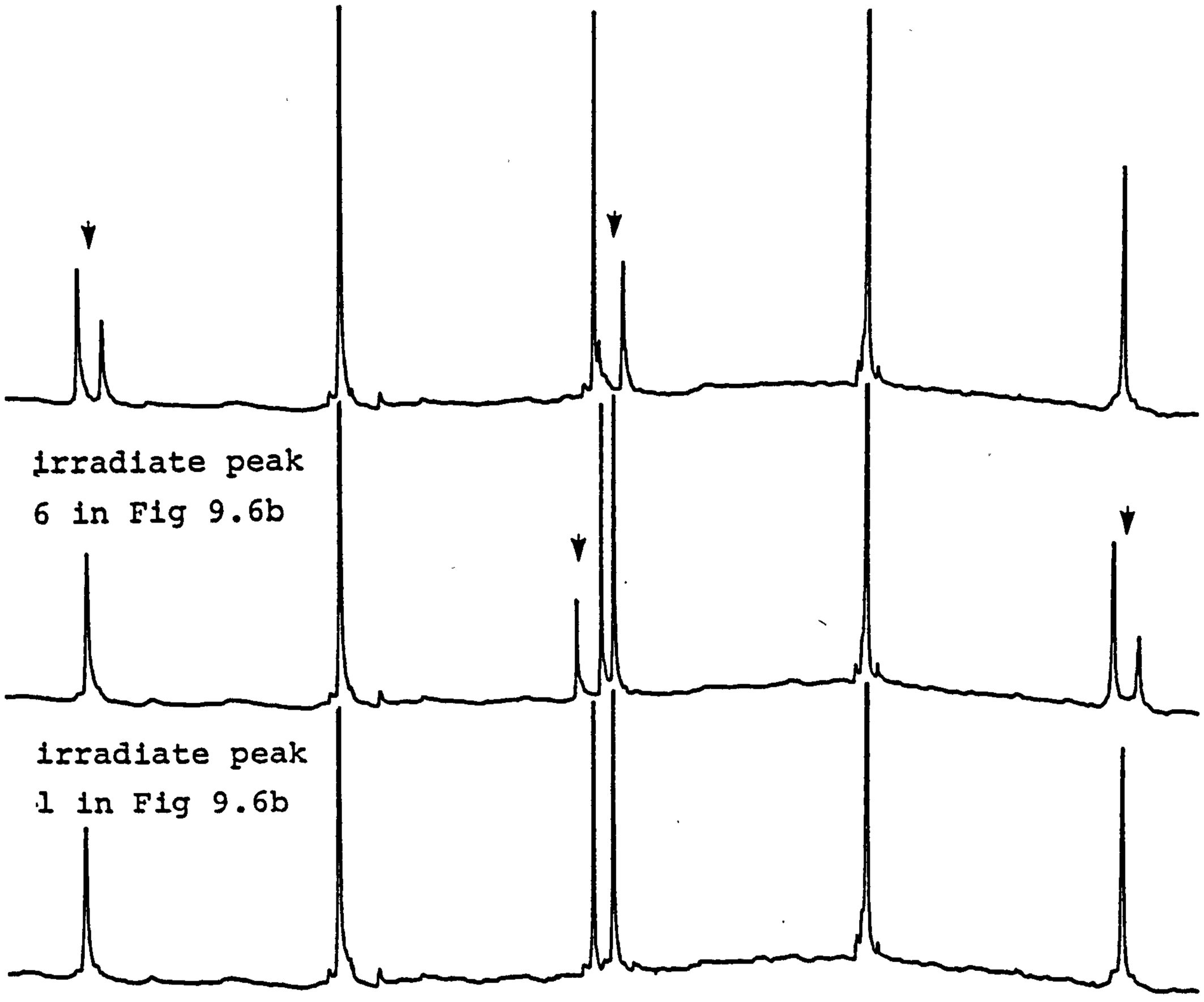

Figure 9.4: F- {Se} double resonance experiment

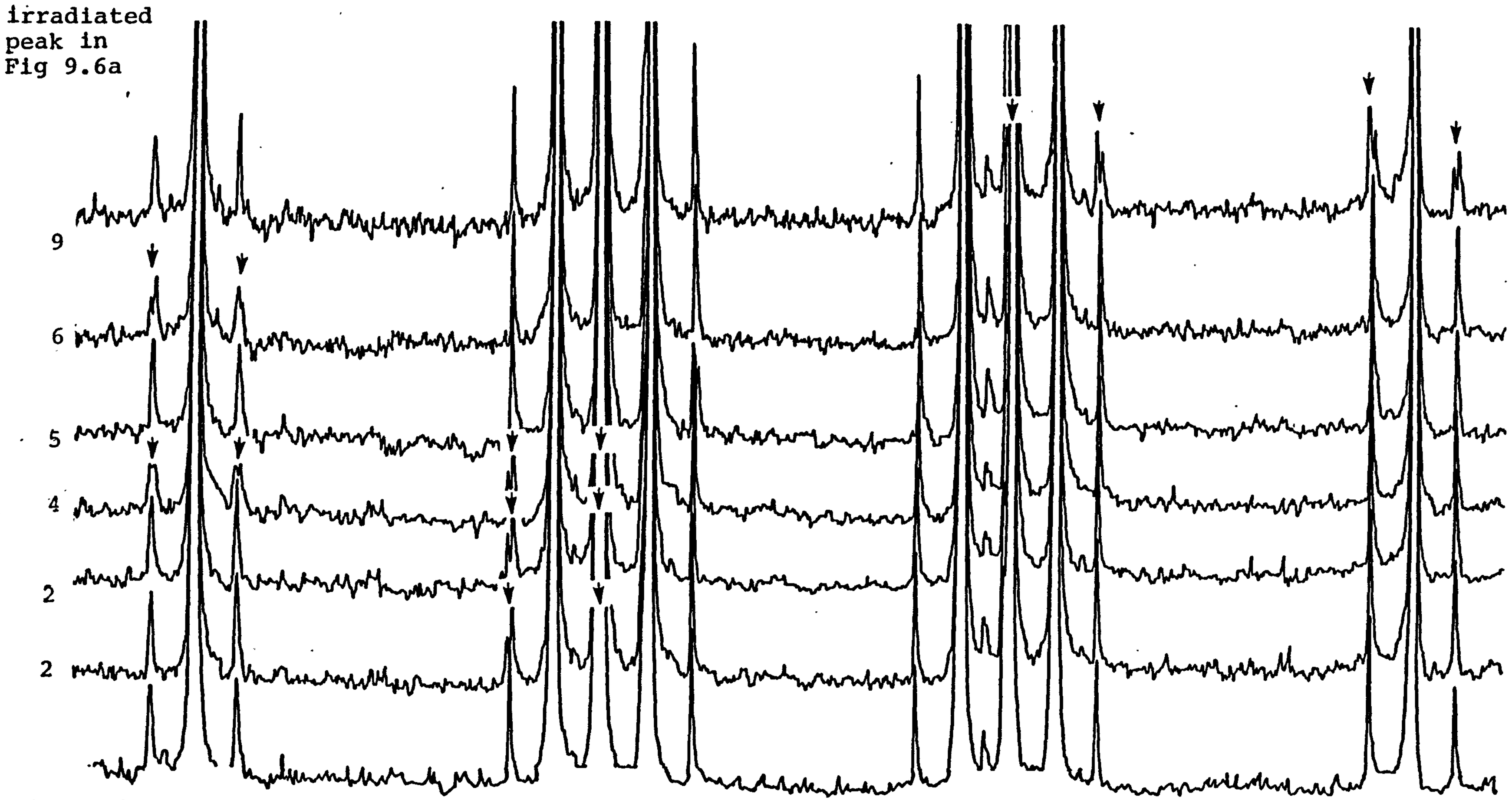

Figure 9.5: F- {P} double resonance experiment

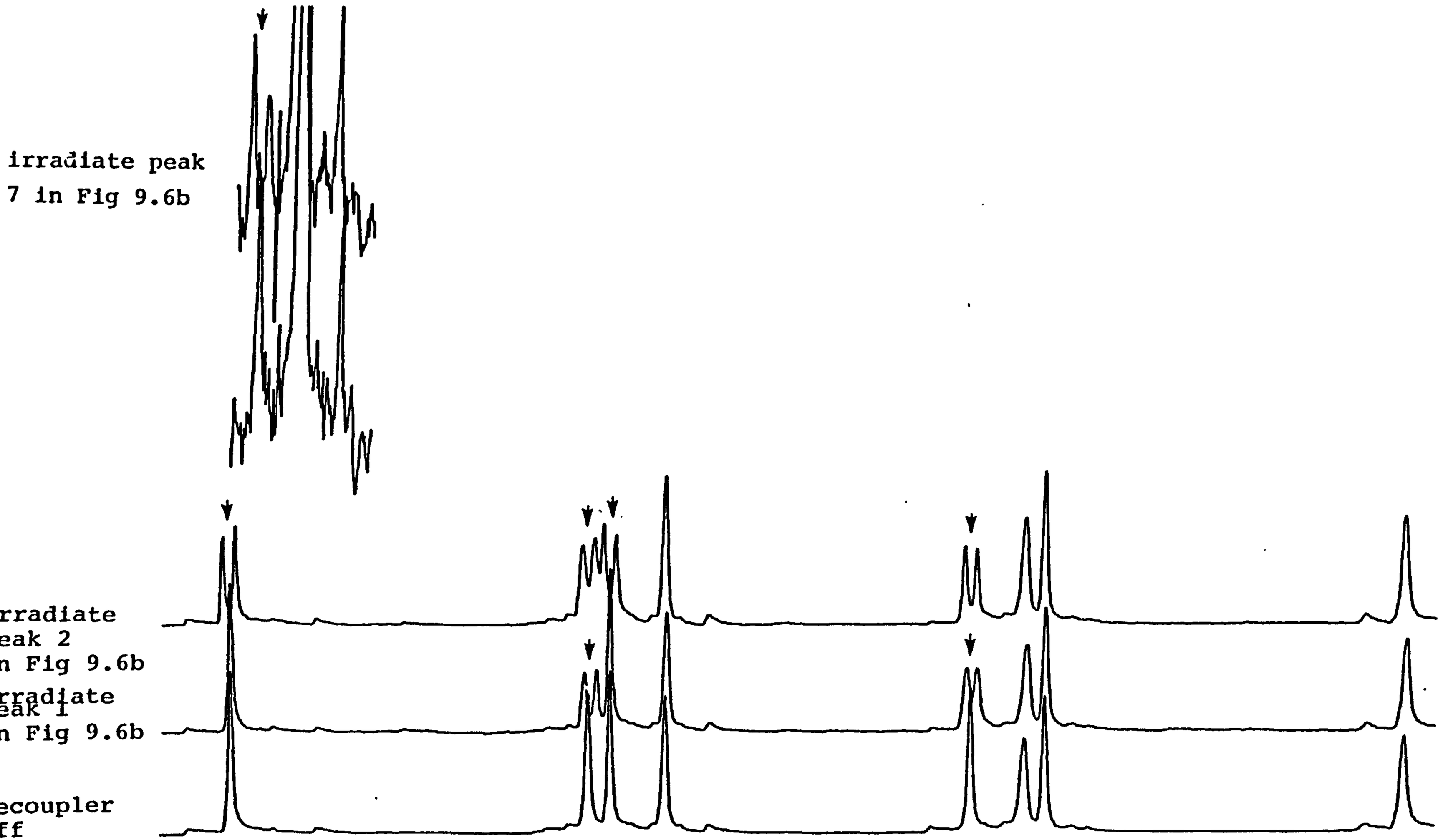

Figure 9.6: Representations (not necessarily to scale) of (a) ^{77}Se and (b) ^{31}P lcnmr spectra of PF_2HSe. Peaks irradiated in any of the four preceding double-resonance experiments are annotated here for easy identification.

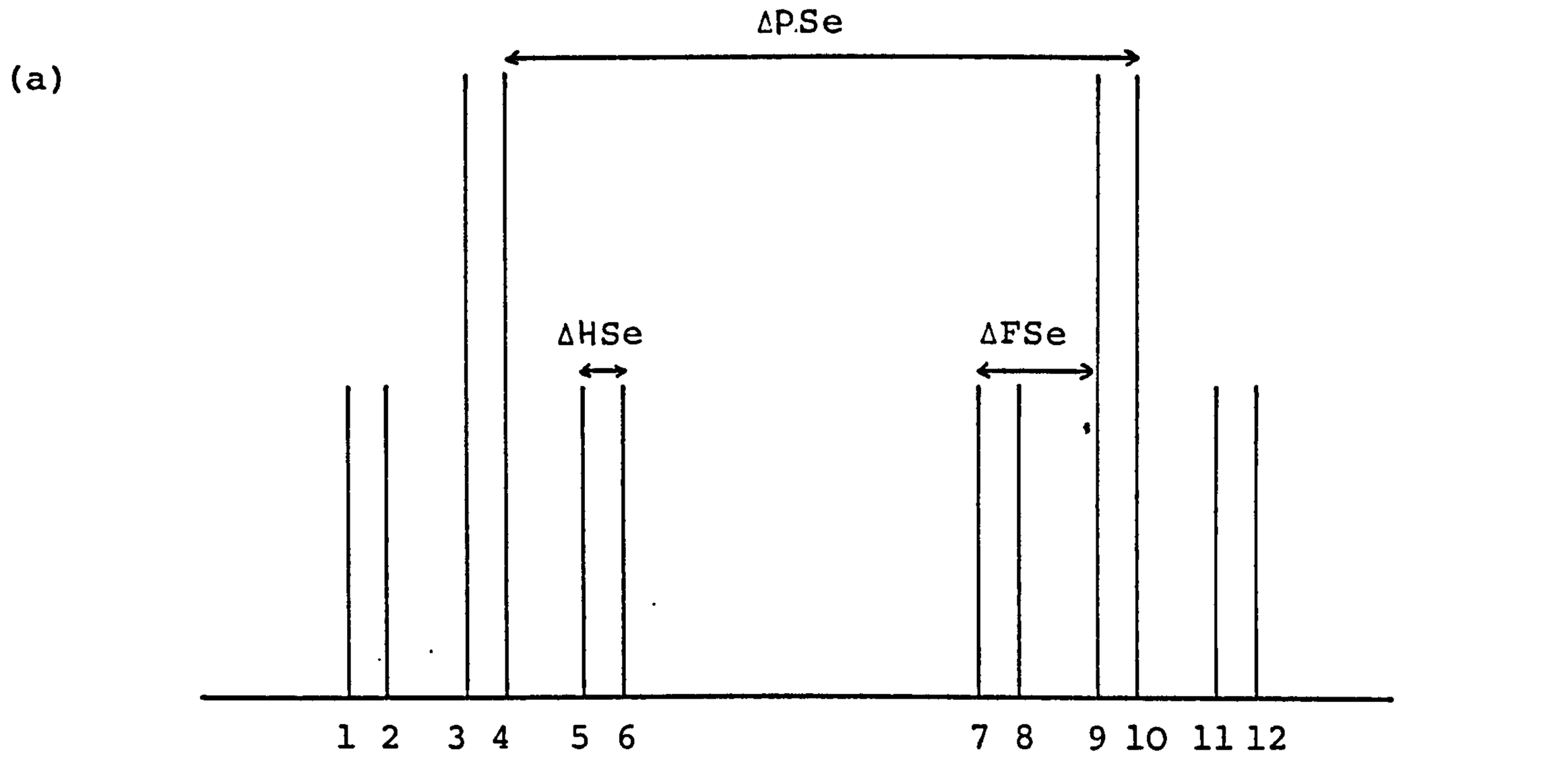

Figure 9.7 : Observed and final weighted difference molecular intensities for nozzle-to-plate distances of (a) 128 and (b) 287 mm

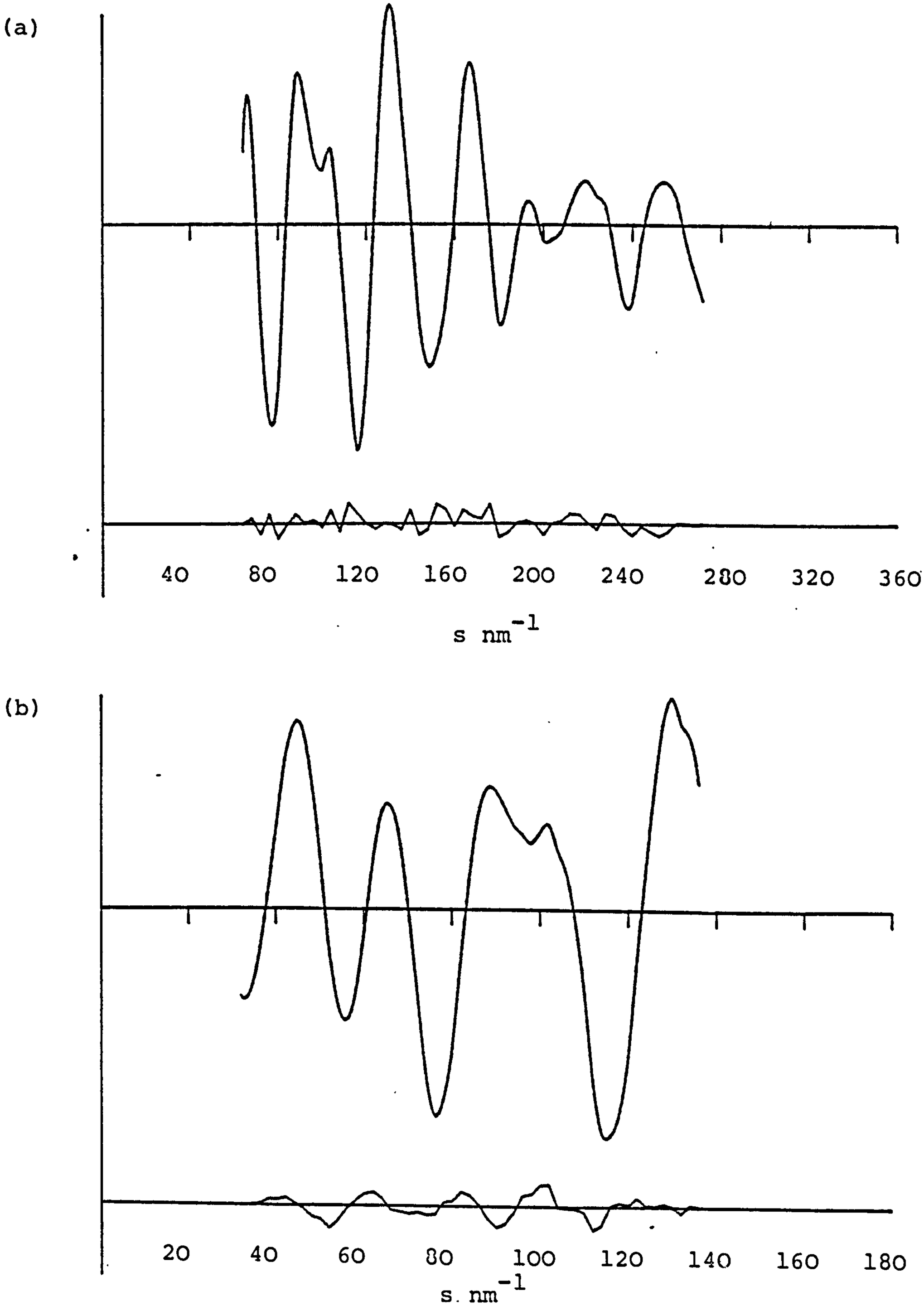

Figure 9.8 : The molecular structure of $SePF_2H$

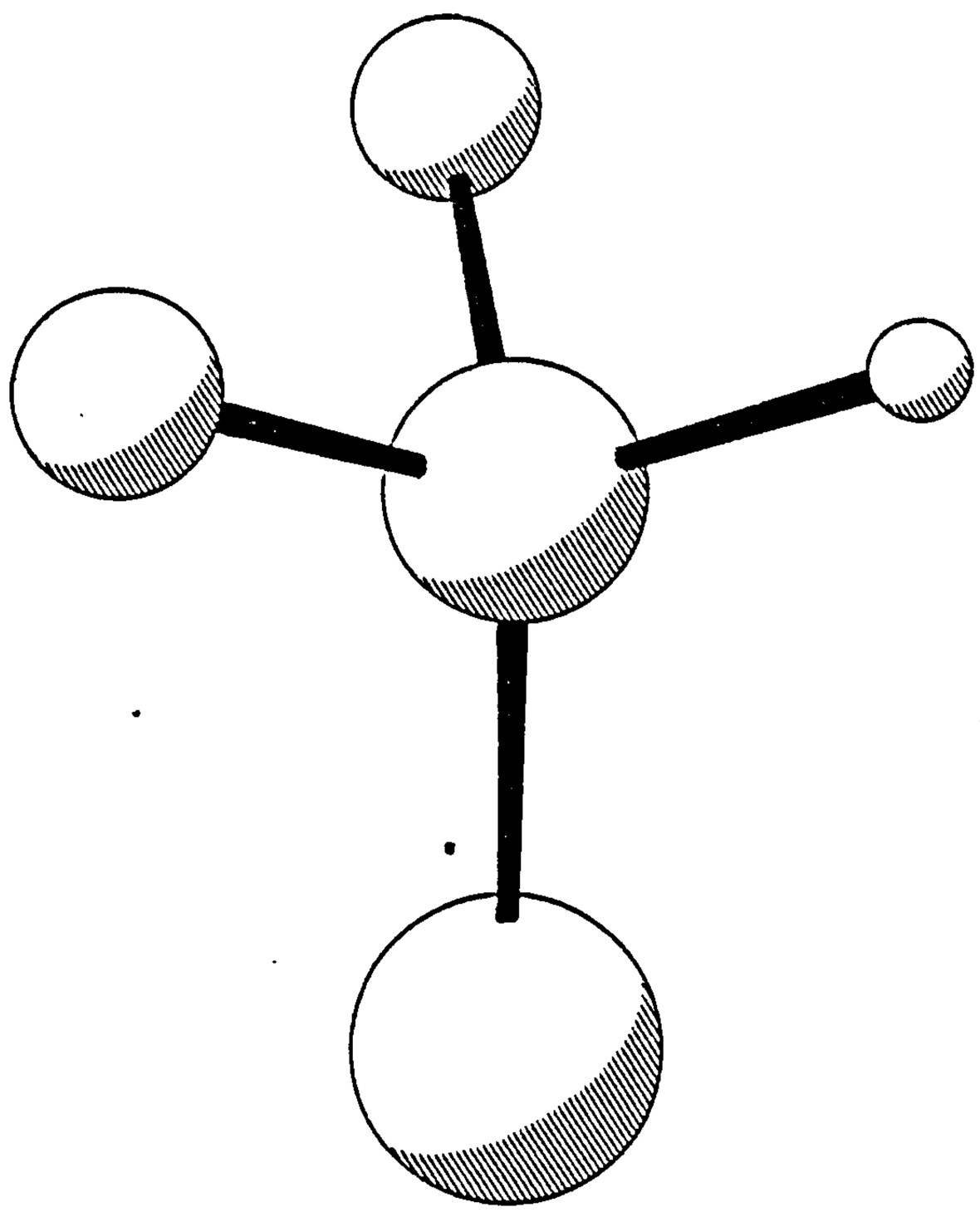

CHAPTER 10

THE MOLECULAR STRUCTURE OF AMINODIFLUOROPHOSPHINE DETERMINED BY USING A COMBINATION OF GAS PHASE ELECTRON DIFFRACTION AND LIQUID CRYSTAL NMR DATA

10.1 Introduction

The molecule $(PF_2)NH_2$ has been studied in the gas phase by both electron diffraction[13] and microwave[28] techniques. The wide discrepancy concerning the degree of planarity at nitrogen in this compound, manifesting itself in the calculation of included angles at nitrogen of 346(6)° and 360(1)° from the former and latter determinations respectively, has resulted in much discussion among structural chemists concerning the barriers to inversion of the PNH_2 moiety, and to rotation about the P-N bond. Calculations estimating that the barriers may be as low as or lower than ca 0.4 Kcal mol^{-1} in either case[115/116] lend weight to the prevailing view that the PNH_2 skeleton is essentially planar but floppy. Thus the discrepancy between the ed and microwave structures may be accounted for, since the apparent ease of motion of the amino protons would give rise to a substantial shrinkage effect (see Figure 1 .2) in the ed experiment, which looks at the average position of atoms, whereas since microwave spectroscopy examines mean structures a planar grouping of bonds to nitrogen would be observed. However, further controversy on the gas phase structure of $(PF_2)NH_2$ is bound to be raised by a recent X-ray structure determination of the molecule undertaken in Edinburgh[117]. Among other interesting results to be discussed later it was found that bonds to nitrogen in the crystalline phase were not coplanar, and that the included angles at nitrogen summated to 349(5)°.

Here intermolecular H...F attractive interactions have been invoked to account for the amino protons lying out of the plane including P,N and the <FPF bisector, although it could easily be postulated that the solid phase has trapped out an average geometry for a mobile $-NH_2$ moiety undergoing a wide amplitude vibration out of this plane.

A difficulty arose in the acceptance of existing electron diffraction data in that parameters involving hydrogen were determined with extremely low precision. In the electron diffraction experiment, as was outlined in the introductory chapters to this thesis, the intensity of a distance peak in the radial distribution curve varies as a function of the product of the atomic weights of the atom pair considered. For aminodifluorophosphine the peaks corresponding to d(H...H) and d(F...H) have intensities of <0.4% and <2% respectively of that for the main r(P-F) peak. The problem is compounded by close overlap of three of the four d(F...H) distances, and also because the high vibrational amplitude values associated with non-bonded distances to hydrogen atoms tend to lower peak heights.

A new electron diffraction study of the molecule $(PF_2)NH_2$ has therefore been undertaken for two major reasons. Firstly, since methods of ed data collection and analysis have improved somewhat since the original investigation, it was hoped to obtain more accurate values

for all parameters than had been possible previously. Secondly, it was hoped to combine ed data with that from lcnmr studies of the same molecule dissolved in a suitable orienting solvent, in order to see if the additional information thus obtained would help to reduce esds for refining parameters.

10.2 Experimental: ED

A sample of $(PF_2)NH_2$ was prepared by the gas phase reaction of difluorophosphine bromide with ammonia at room temperature[118]. $(PF_2)NH_2$ is itself a common starting material for a variety of preparative chemistry undertaken at Edinburgh, and is readily prepared in yields approaching 100% by the simple reaction,

$$F_2PBr(g) + 2NH_3(g) \rightarrow \left[NH_4^+\right] \; Br^-(s) + (PF_2)NH_2(g)$$

The product was purified by repeated fractional condensation, and as usual had its purity checked by ir spectroscopy both before and after the collection of gas phase structural data.

Electron scattering intensities were recorded photographically using the Cornell/Edinburgh University diffraction apparatus in the usual mode[30]. An accelerating potential of 45.1 kV was used to obtain data at nozzle-to-plate distances of 128 and 285 mm with the bulk

sample held at 273 K. Pressure during an exposure was recorded at ca $5x10^{-6}$ torr while that for background was measured to be $3x10^{-7}$ torr. The electron wavelength used was derived from the scattering pattern of benzene, recorded immediately before experimental data collection at each distance. Photographic intensities were digitised and data were reduced in the usual manner[26,34]. Table 10.1 shows the weighting points used in setting up the off-diagonal weight matrix, together with other experimental details. As usual, the complex scattering factors of Schafer et al were used in all theoretical molecular scattering computations[9]. Observed and difference scattering intensities are given in Figure 10.1.

10.3 Experimental: LCNMR

Solutions of 0.2 mmol of $(PF_2)NH_2$ in ca 3 mmol of a suitable orienting solvent were prepared in 5 mm nmr tubes. British Drug Houses liquid crystal E8 is now almost exclusively used as the orienting medium in lcnmr experiments at Edinburgh, for reasons outlined in Chapter 8, and was employed in this case.

All data collection was carried out on a Varian Associates XL100 spectrometer in the pulsed Fourier transform mode, with stationary sample tube. Temperature stabilisation was as usual enhanced by replacing the normal liquid notrogen cooling reservoir with one comprising an acetone/CO_2 mixture. As before the variation of dipolar

couplings with temperature was used to ensure that a self-consistent set of couplings was recorded for all observed nuclei, by adjusting operating conditions until ΔMX was seen to be identical in both M and X spectra. By subtracting isotropic nmr data, recorded above the nematic temperature of the solution and extrapolated to each of the two nematic temperatures studied, it was possible to obtain two sets of Δ couplings, defined by equation 24,

$$(24a) \quad \Delta_{ij} = J_{ij} + 2D_{ij}$$

$$(24b) \quad \Delta_{ii} = 3D_{ii}$$

at both 253 and 293 K. The relative signs of couplings observed in the nematic phase were elicited from a series of double resonance experiments.. The spectra thus obtained are illustrated by Figures 10.2-5;the results are listed in Table 10.2. As J(PF) is known to be large and negative on all fluorophosphines $\Delta_{PF} \equiv J_{PF} + 2D_{PF}$ was assumed to be negative; other signs were then related to this. The signs of indirect couplings were taken from reference 119.

10.4 Refinement of Structure

(a) Using ed data only: a number of mathematical structural formulations were used to calculate theoretical intensity data in an attempt to duplicate that found by experiment.

The models used differed in permitted freedom of movement of the imino protons. Neither wag of the $-NH_2$ group, maintaining C_s symmetry for the PNH_2 moeity, nor a torsion of a planar $-NH_2$ group, yielded a satisfactory fit of observed to theoretical data. A reasonable correspondence between calculated and experimental scattering intensities was finally afforded by the adoption of a model in which either hydrogen atom was allowed to move independently out of the plane prescribed by P,N, and the bisector of <FPF. Two different PNH angles were allowed, but in the absence of lcnmr data, r(N-H) and r(N-H'), arranged cis and trans respectively to the bisector of <FPF, were constrained to be equal. The molecule could then be completely specified by 9 geometrical parameters, given in Table 10.3a. This table gives all parameters for $(PF_2)NH_2$ together with the results and esds of two separate final refinements, A and B. The significance of these two parameter sets will be discussed later.

(b) combining ed + lcnmr data: the usual least squares refinement program was modified to include dipolar couplings as extra data HPF_2Se, calculated according to equation 30.

$$(30)\quad D_{ij} = \frac{-\gamma_i\gamma_j h}{8\pi^2 r_{ij}^3}\Big[S_{zz}(3\cos^2\theta_{ijz}-1) + (S_{xx}-S_{yy})(\cos^2\theta_{ijx}-\cos^2\theta_{ijy}) + 2S_{xz}(\cos\theta_{ijx}\cos\theta_{ijz}) + 2_{yz}(\cos\theta_{ijy}\cos\theta_{ijz}) + 2S_{xy}(\cos\theta_{ijx}\cos\theta_{ijy})\Big]$$

Terms in the above equation have been adequately defined previously. In this case the axes were defined so that r(P-N) lay on the x axis and the z axis lay perpendicular to the C_s plane, passing through nitrogen. Thus s_{xz} and s_{yz} were zero, and the other three orientation parameters were included in the set of refinable parameters. Although dipolar couplings were measured at two temperatures, initial refinements showed similar results for the sets recorded at the two temperatures. Since at the higher temperature lcnmr spectral line widths were noticeably narrower on average, only this data set was used in the final refinements.

The additional observations were interfaced with ed data using an off diagonal weight matrix with the elements described in Chapter 2.

For additional (lncmr) observations, the weight matrix was extended using only diagonal terms, with weights chosen so that the lcnmr data did not over-rule the ed data causing diverging refinements. In final refinements all dipolar couplings were given equal weights, since all were readily measurable to a good degree of accuracy. The molecular model used in these refinements differed from that used for calculating theoretical intensities from ed-only data in that r(N-H) and r(N-H') were allowed independent values.

Since the timescale of the ed experiment (10^{-17}s)

is faster than that for molecular vibrations (10^{-12}s) whereas that for the nmr experiment is much longer (ca 10^{-5}s), it follows that molecular vibrations do not correlate with either measurement. The former looks at an average of all instantaneous structures, resulting in a molecule apparently removed from C_s symmetry by shrinkage whereas the latter averages over all vibrational orientations to give a net C_s structure. To allow for this, C_s symmetry had to be maintained in the molecular model used for the liquid crystal. This was achieved by considering halves of each hydrogen atom displaced equally and oppositely out of the P.N-(<FPF bisector) plane. <HNH and<H'NH' were used to denote the separations between the two halves of each hydrogen (H and H' lie cis and trans to <FPF bisector respectively).

Otherwise the model used here was unchanged from the ed-only case, as were the procedures, trials and general results which led to the adoption of this model as giving the most satisfactory fit between observed and calculated scattering intensities.

In order to equate the ed and lcnmr measurements, a vibrational correction was applied to the calculated dipolar couplings yielding r_d from the measured r_a values, by application of equation 36, described in the previous chapter.

(36) $r_d = r_a + u^2/ r_a$; since $r_a \simeq r_e$.

In all refinements an r_a structure has been used.

10.5 Results and Discussion

Two self consistent nmr data sets were obtained as outlined above, from ^{1}H, ^{19}F and ^{31}P spectra recorded at 253 and 293 K. In addition ^{19}F and ^{31}P isotropic spectra were recorded at 313 and 333 K in the same solvent. The ^{1}H spectra thus recorded proved not to submit to analysis, due to a preponderance of in number and intensity of peaks due to solvent protons: thus $^{1}J_{NH}$ had to be assigned a reasonable value. The observed splittings from the first-order spectra, together with indirect couplings from spectra of isotropic solutions at higher temperatures extrapolated to yield isotropic couplings at the required nematic temperature, and derived direct couplings, are shown in Table 10.4.

Since both the ed-only and ed + lcnmr refinements yielded essentially similar results, general discussion of these and conclusions drawn therefrom, may be taken to apply to both analyses, unless otherwise stated. All geometrical parameters refined satisfactorily, except for <HNH and <H'NH', which were fixed by R factor loops. In the ed-only case, <H'NH' was fixed at a value where considerations of minimum Rg factor were offset against a reluctance to allow the dependent <HNH' to fall below 100^{o}.

Stable refinements were not possible with all parameters associated with the heavy atom bonded distances refining: u(P-N), r(P-N) and r(P-F) were allowed to refine simultaneously with u(P-F) fixed at a reasonable value. Subsequently three refined parameter values were fixed and u(P-F) allowed to adopt a refined value. In final refinements, u(P-F) was again fixed at its refined value, u(N-H) and u(N-H') were constrained to a single value, and u(F...F) and u(F...N) also refined independently while some of the non-bonded amplitudes of vibration involving protons refined as groups.

A consequence of allowing all heavy-atom parameters to refine was that the geometrical parameters tended to-wards a different set of values corresponding to alternative minimum Rg structures, albeit with, in some cases, unrealistic vibrational amplitudes (Tables 10.3a and b, refinement B). For the duration of most of the calculations performed on $(PF_2)NH_2$ data, these alternatives were deemed unreasonable, since the major feature was a movement of r(p-F) from ca 159 pm to ca 160 pm, and of r(P-N) from ca 163 pm to ca 161 pm, the latter value being in each case substantially different from the broad agreement for the values of these parameters derived from other sources (Table 10.5).

Examining this, it can be seen that in refinement ed/A, while r(P-N) agrees well with the value derived from the microwave analysis, it is some 1.3 pm longer than

that found by X-ray diffraction , and r(P-F), while again agreeing with the microwave value, corresponds only to the shorter of two phosphorus-fluorine bond lengths in the X-ray analysis. In refinement ed + lcnmr/A, however, there is much closer agreement between the fluid phase and X-ray results. On the basis of this comparison, taking into account that the values found for ed/<FPF and X-ray/<FPF, and for ed/<FPN and X-ray/ average <FPN, lie within their respective esds of each other, it would be possible to argue that in the ed + lcnmr and X-ray geometrical results for the F_2PN moiety are essentially similar, except for the lengthening of one P-F bond in the crystal by ca 2 pm, a result of intermolecular H...F interactions in the packing arrangement . However, in the B refinements there is a tendency for r(P-F) to approach the higher X-ray value for this parameter, while r(P-N) tends to move to an unreasonably low value. This last effect may compensate for the enforced lengthening of one r(P-F), a consequence of models chosen to represent the structure of $(PF_2)NH_2$ constraining both P-F bond lengths to be equal. Why any deviation from C_s symmetry for the NPF_2 moiety should manifest itself is not clear, unless the H' proton in its average position interacts in some way with the closest fluorine atom. It would therefore be interesting to try to refine a structure on a model with discrete r(P-F) distances.

Refinements designated A will be exclusively considered from now on. The values found for r(N-H) seem unreasonably low, but were well defined according to their esds. Similarly <PNH and <PNH', especially the former (cis to <FPF bisector) adopting very wide (134-136(6)^{o}) values, diverge somewhat from those derived from other sources, although only in the X-ray(where gas-phase motional amplitudes do not apply), and in MNDO calculations (with no esds given), were two angles <PNH allowed. Indeed, the latter of these methods gave the angles PNH closest of all to this work. Values for heavy atom inter-bond angles correspond very closely with those found from microwave spectroscopy, as well as with the X-ray structure as described above.

Angles <HNH and <H'NH' were allowed to adopt a series of values, using R factor loops. The results of these examinations can be seen in Figure 10.6 . An average position for the proton <u>trans</u> to the <FPF bisector was found to be 40^{o} away from the C_s plane of the molecule (ed only) and 10^{o} away from that plane (ed + lcnmr), whereas the proton <u>cis</u> to the <FPF bisector showed no sign of motional freedom expected for the floppy molecule predicted earlier.

Values found for amplitudes of vibration were within esds of expected values except for U(F...F) (<u>ca</u> 4.3-5.3 pm) which was somewhat smaller than expected, and U(P-F) slightly high.

10.6 Conclusions

The ed and ed + lcnmr structural analyses of $(PF_2)NH_2$, while requiring some further investigation, have shown the following:

a) The heavy atom ed-only results are in close agreement with those from microwave spectroscopy while those from ed + lcnmr agree well with the X-ray structure.

b) The locations of the amino protons are in disagreement with other gas phase analyses, but this may in part be due to the greater flexibility of the molecular model used in this study.

c) Evidence from both ed and ed + lcnmr indicates that while the trans proton is mobile, the cis proton, subject perhaps to intramolecular H...F interactions, is not.

Tables 10.6a and 10.6b show the least squares correlation matrices for the ed/A and ed + lcnmr/A refinements. Figures 10.7a and 10.7b show the atomic arrangements for the ed/A and ed+lcnmr/A structures respectively, with possible H...F interaction shown by broken lines, while Figure 10.8 shows the radial distribution plot for the molecule.

Table 10.1: Weighting functions, correlation parameters and scale factors for $(PF_2)NH_2$

(a) ed only

Camera Height mm	Δs nm^{-1}	s_{min} nm^{-1}	sw_1 nm^{-1}	sw_2 nm^{-1}	s_{max} nm^{-1}	p/h	Scale Factor
128.3	0.400	6.000	8.000	26.000	34.000	0.3571	0.796
284.5	0.200	2.000	3.000	12.000	14.800	0.2095	0.776

(b) ed + lcnmr

128.3	0.400	6.000	8.000	26.000	34.000	0.4075	0.762
284.5	0.200	2.000	3.000	12.000	14.800	0.3786	0.764

Table 10.2: Double resonance experiments

Experiment	Couplings related	Relative signs
$^{19}F-\{^{31}P\}$	FN and NP	equal
	FH and HP	equal
	FF and FP	opposite
$^{19}F-\{^{15}N\}$	FH and HN	equal
	FP and PN	equal
	FF and FN	opposite
$^{1}H-\{^{31}P\}$	HF and FP	equal
	HN and NP	equal
	HH and HP	equal
deduced from above	HF and FN	equal
	HP and PN	equal
	HH and HN	equal

Table 10.3a: Molecular parameters (ed-only) for $(PF_2)NH_2$

	Refinement A		Refinement B	
	Distance/pm	Amplitude/pm	Distance/pm	Amplitude/pm
r_1P-F	158.8(3)	5.2(fixed)	160.0(5)	6.6(4)
r_2P-N	165.1(5)	4.9(7)	161.3(10)	4.5(fixed)
r_3N-H	89.5(9)	9.5(10)	91.9(8)	8.5(9)
d_4F...N	248.3(5)	8.2(9)	248.7(a)	8.3(8)
d_5F...F	233.1(6)	5.3(9)	233.3(a)	5.4(8)
d_6P...H'	216.4(4)	8.3(b)	217.0(a)	7.8(b)
d_7P...H	237.5(4)	8.3(b)	237.1(a)	7.8(b)
d_8H...H'	137.4(6)	8.3(b)	137.7(a)	7.8(b)
d_9F...H	286.4(3)	16.7(27)	289.6(a)	15.7(24)
d_{10}F...H	329.9(3)	16.7(b)	333.8(a)	15.7(b)
d_{11}F...H'	285.2(6)	16.7(b)	288.4(a)	15.7(b)
d_{12}F...H'	285.2(6)	16.7(b)	288.4(a)	15.7(b)
	Angle(°)		Angle(°)	
<1 FPF	94.4(4)		93.6(4)	
<2 FPN	100.1(4)		101.4(4)	
<3 PNH'	113(4)		115(4)	
<4 H'NH'	80(fixed)		80(fixed)	
<5 PNH	136(6)		137(5)	
<6 HNH	0(fixed)		0(fixed)	
<7 HNH'	100.4(calculated)		97.1(a)	
Rg final	4.8		4.8	

[a]not calculated; [b]tied to u_{11}, quoted esds were derived from the least squares analysis and increased to allow for systematic errors.

Table 10.3b: Molecular parameters (ed + lcnmr) for $(PF_2)NH_2$

	Refinement A		Refinement B	
	Distance/pm	Amplitude/pm	Distance/pm	Amplitude/pm
r_1(P-F)	159.3(3)	5.2(fixed)	160.3(4)	7.2(5)
r_2(P-N)	163.3(7)	4.9(fixed)	160.7(5)	2.9(8)
r_3(N-H)	87.2(7)	9.8(14)	88.3(6)	10.2(17)
r_4(N-HO	86.2(11)	9.8(tied to u_3)	88.7(10)	10.2(tied to u_3)
d_5(F...N)	248. 6(5)	7.5(9)	248.3(a)	8.2(7)
d_6(F...F)	233.2(5)	4.3(10)	233.3(a)	5.3(fixed)
d_7(P...H)	216.8(3)	12(fixed)	217.7(a)	12(fixed)
d_8(P...H)	231.9(5)	12(fixed)	231.1(a)	12(fixed)
d_9(H...H)	140.7(8)	12(fixed)	141.8(a)	12(fixed)
d_{10}(H...H)	140.7(8)	12(fixed)	141.8(a)	12(fixed)
d_{11}(F...H)	311.3(16)	15.2(59)	313.5(a)	15.8(51)
d_{12}(F...H)	322.4(16)	15.2(tied to u_{11})	324.75(a)	15.8(tied to u_{11})
d_{13}(F...H)	282.1(70)	15.2(tied to u_{11})	282.3(a)	15.8(tied to u_{11})
d_{14}(F...H)	282.1(70)	15.2(tied to u_{11})	282.3(a)	15.8(tied to u_{11})
	Angles(°)		Angles(°)	
<1 FPF	94.1(4)		93.4(4)	
<2 FPN	100.8(4)		101.4(4)	
<3 PNH'	117(3)		119(3)	
<4 H'NH'	20(fixed)		20(fixed)	
<5 PNH	134(6)		134(6)	
<6 HNH	0(fixed)		0(fixed)	
<7 HNH'	108.1(calculated)		106.5(calculated)	
	Orientation parameters			
$s_1(s_{zz})$	-0.0619(4)		-0.0620(4)	
$s_1(s_{zz}-s_{yy})$	-0.0238(19)		-0.0196(17)	
$s_2(s_{xx})$	0.1089(22)		0.1063(20)	
$s_3(s_{xy})$				
	Dipolar Couplings (Hz)			
	obs.	calc.	calc.	esds (see text)
D PF	6.7	8.2	7.2	
D PN	27.3	21.6	25.2	
D FF	519.6	520.0	519.8	
D FN	34.0	30.6	30.9	
D NH	498.5	498.5	498.5	
D PH	-127.7	-124.8	-126.8	
D FH	-160.6	-163.4	-161.9	
D HH	-1106.5	-1106.4	-1105.9	
Rg final	6.9		6.4	

[a]not calculated. Quoted errors were obtained in the least squares refinements and increased to allow for systematic error.

Table 10.4: Couplings measured in E8 for $(PF_2)^{15}NH_2$

Nuclei	J_{iso}	Δ^a(293K)	D(293K)
$^{31}P-^{19}F$	-1190.1[b]	-1176.7	+ 6.7
$^{31}P-^{15}N$	+ 71.9[b]	+ 126.5	+ 27.3
$^{19}F-^{19}F$	-	+1558.8	+ 519.6
$^{19}F-^{15}N$	- 6.0[b]	+ 62.0	+ 34.0
$^{15}N-^{1}H$	- 80.4[c]	+ 916.6	+ 498.5
$^{31}P-^{1}H$	+ 18.6[b]	- 236.8	- 127.7
$^{19}F-^{1}H$	+ 13.3[b]	- 307.9	- 160.6
$^{1}H-^{1}H$	-	-3319.5	-1106.5

[a] Δ= J+2D or 3D; [b] measured in E8 above nematic temperature range of solution; [c] taken from ref. 118.

Table 10.5 Some important geometrical parameters resultant from diverse structure determinations and calculations compared for $NH_2(PF_2)$

	Original ed	Microwave	X-ray	MNDO Calculations	This work ed only A	This work ed only B	This work ed + lcnmr A	This work ed + lcnmr B
r(P-N)	166.1(7)	165.0(4)	163.8(1)	163.8	165.1(5)	161.4(10)	163.3(7)	160.7(5)
r(P-F)	158.1(3)	158.7(3)	160.8(1) 159.0(1)	156.1	158.8(3)	160.0(5)	159.3(3)	160.3(4)
r(N-H)	103.1(18)	99.2(5)	86.2(19)	99.2	89.5(9)	91.9(8)	87.2(7) 86.2(11)	88.3(6) 88.7(10)
<FPF	95.3(11)	94.6(2)	93.29(4)	97	94.4(4)	93.6(4)	94.1(4)	93.4(4)
<FPN	101.1(11)	100.6(2)	102.13(5) 99.41(4)	102	100.1(4)	101.4(4)	100.8(4)	101.4(4)
<PNH	119(2)	121.4	118.7(16) 120.7(14)	118 126	113(4) 136(6)	115(4) 137(5)	117(3) 134(6)	119(3) 134(6)
<HNH	108(2)	117.2(4)	109.1(18)	112	100.4	97.1	108.1	106.5

Note: all distances are in pm; angles are in degrees.

Table 10.6a: Least squares correlation matrix x100 for ed-only, refinement A

r_1	r_2	r_3	<1	<2	<3	<5	u_2	u_3	u_4	u_5	u_9	k_1	k_2	
100	-86		-50	30			79					-30		r_1
	100		33	-50	-26		-56					50	38	r_2
		100			-27									r_3
			100		27		-47		54	38			-12	<1
				100	51				-30	-42	-39	-27	-36	<2
					100	24			25	29		-20	-36	<3
						100			43					<5
							100						24	u_2
								100				21	20	u_3
						100	65	38						u_4
							100	25						u_5
								100						u_9
									100					k_1
										100				k_2

Note: only elements $\geq |20|$ are included.

Table 10.6b: Least squares correlation matrix x100 for ed+lcnmr, refinement A

r_1	r_2	r_3	<1	<2	<3	<5	r_4	s_1	s_2	s_3	u_3	u_5	u_6	u_{11}	k_1	k_2	
100	-88		-56				40		35	-31					-58	-41	r_1
	100		47	-45	-31		-48		-40						61	46	r_2
		100				-61	72	-33		50							r_3
			100					-66	-56	61		35			34	23	<1
				100	65	47	40		59								<2
					100	85	47		52			39					<3
						100				-39		53	42				<5
							100		53						-31		r_4
								100	43	-46		-35					s_1
									100								s_2
										100							s_3
											100						u_3
												100	66	41			u_5
													100				u_6
														100			u_{11}
															100	31	k_1
																100	k_2

Note: only elements $\geq|30|$ are included.

Figure 10.1: H-{P} double resonance experiment

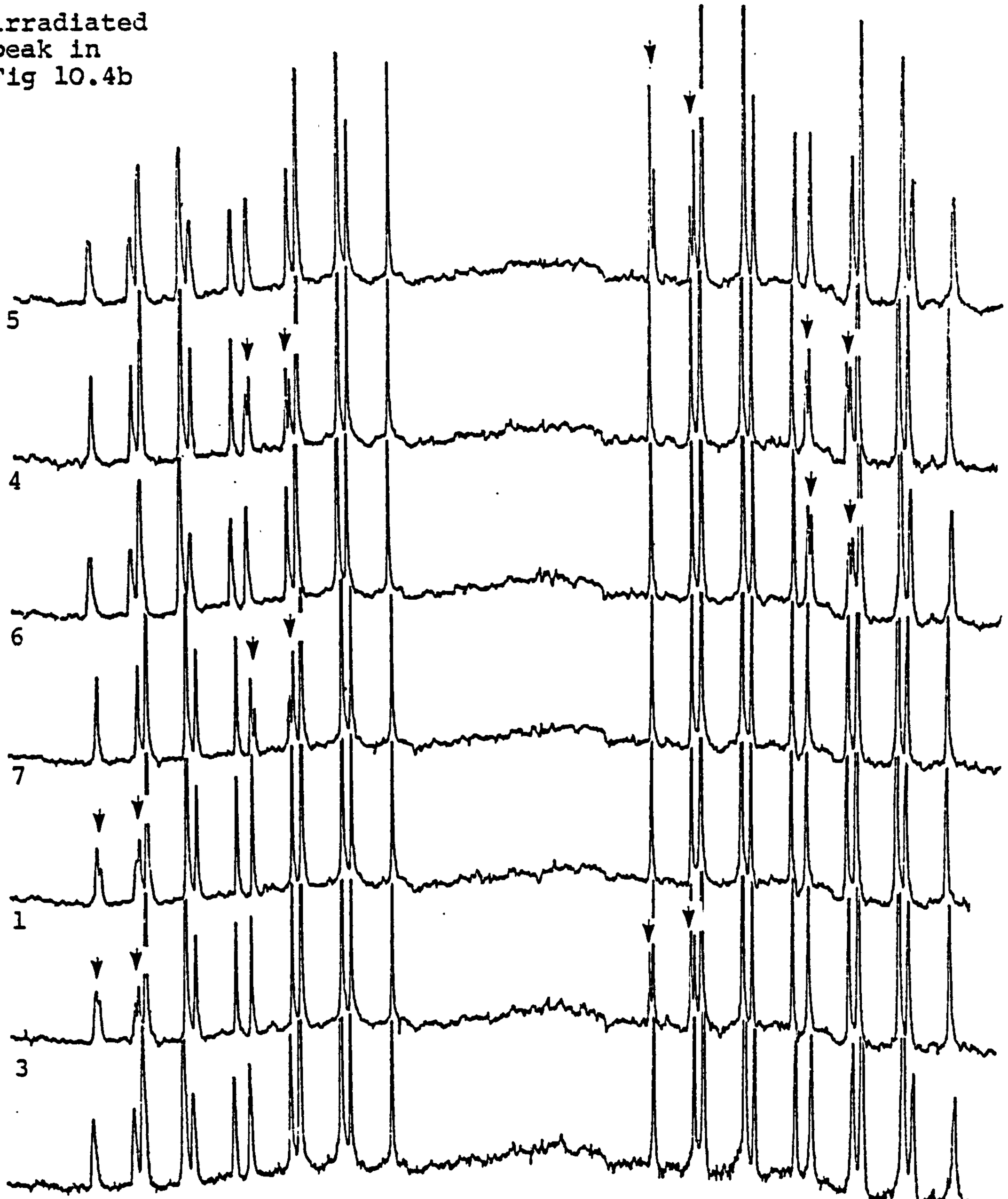

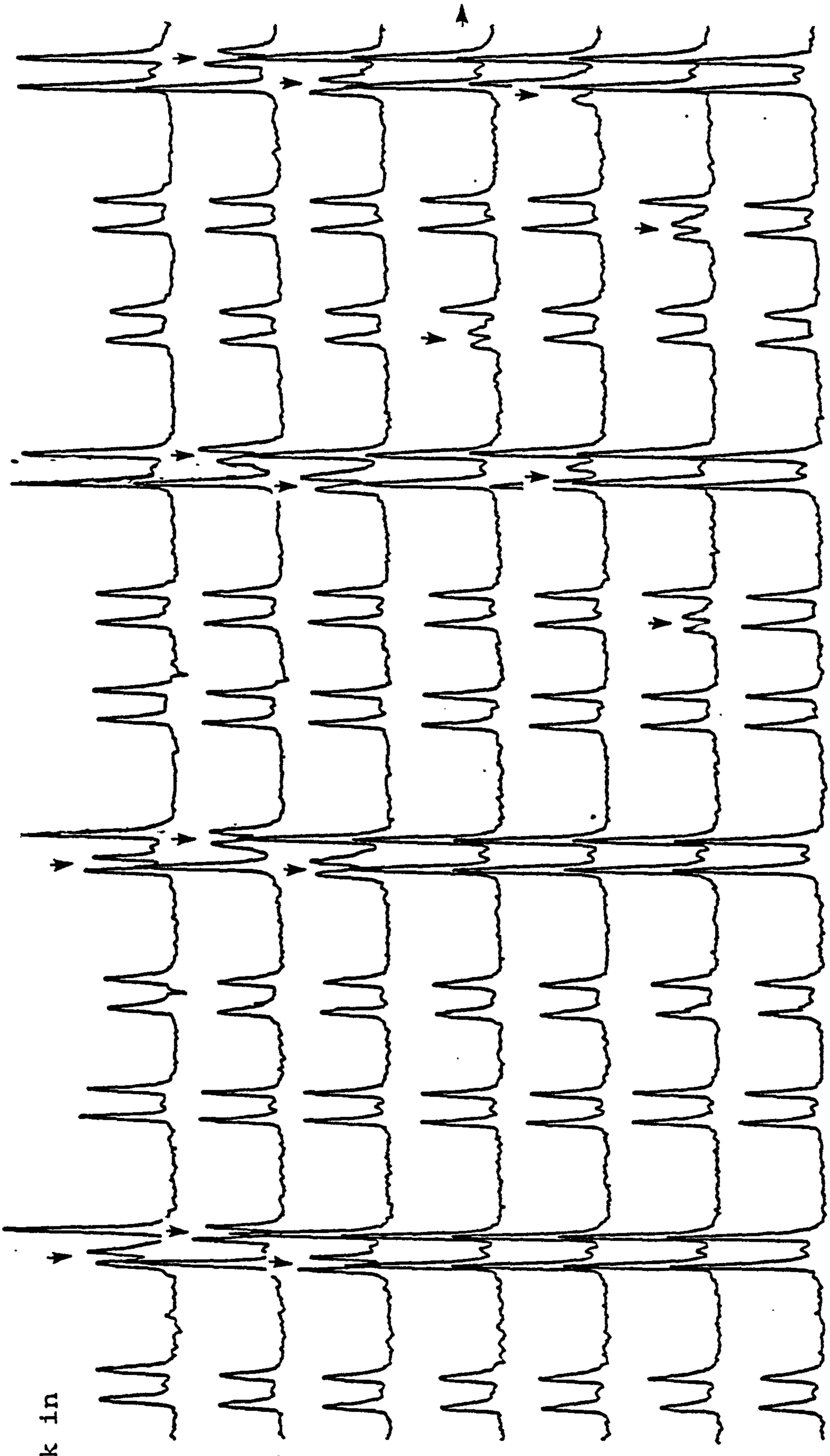

Figure 10.2: F-{P} double resonance experiment

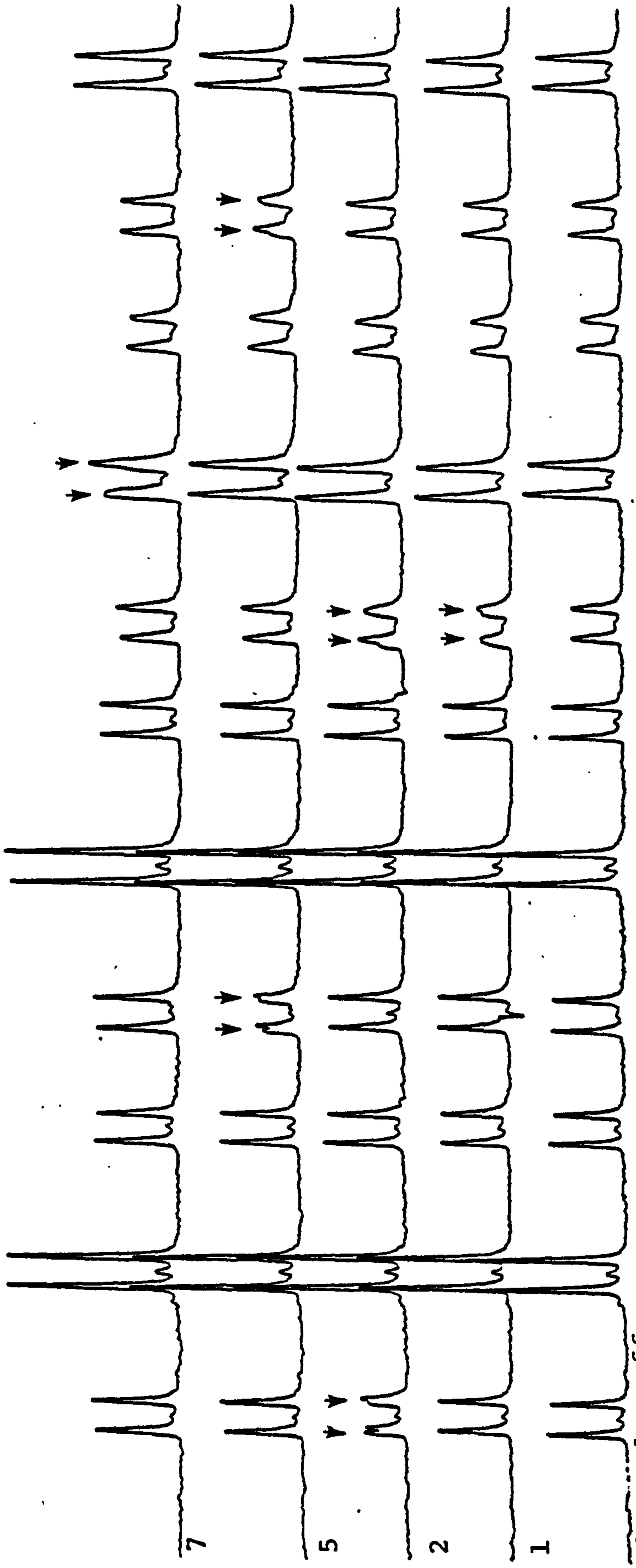

Figure 10.3: F- {N} double resonance experiment

irradiated peak in Figure 10.4a

Figure 10.4: Representations (not necessarily to scale) of (a) ^{15}N and (b) ^{31}P lcnmr spectra of $PF_2(NH_2)$. Peaks irradiated in any of the three preceding double resonance experiments are annotated here for easy identification.

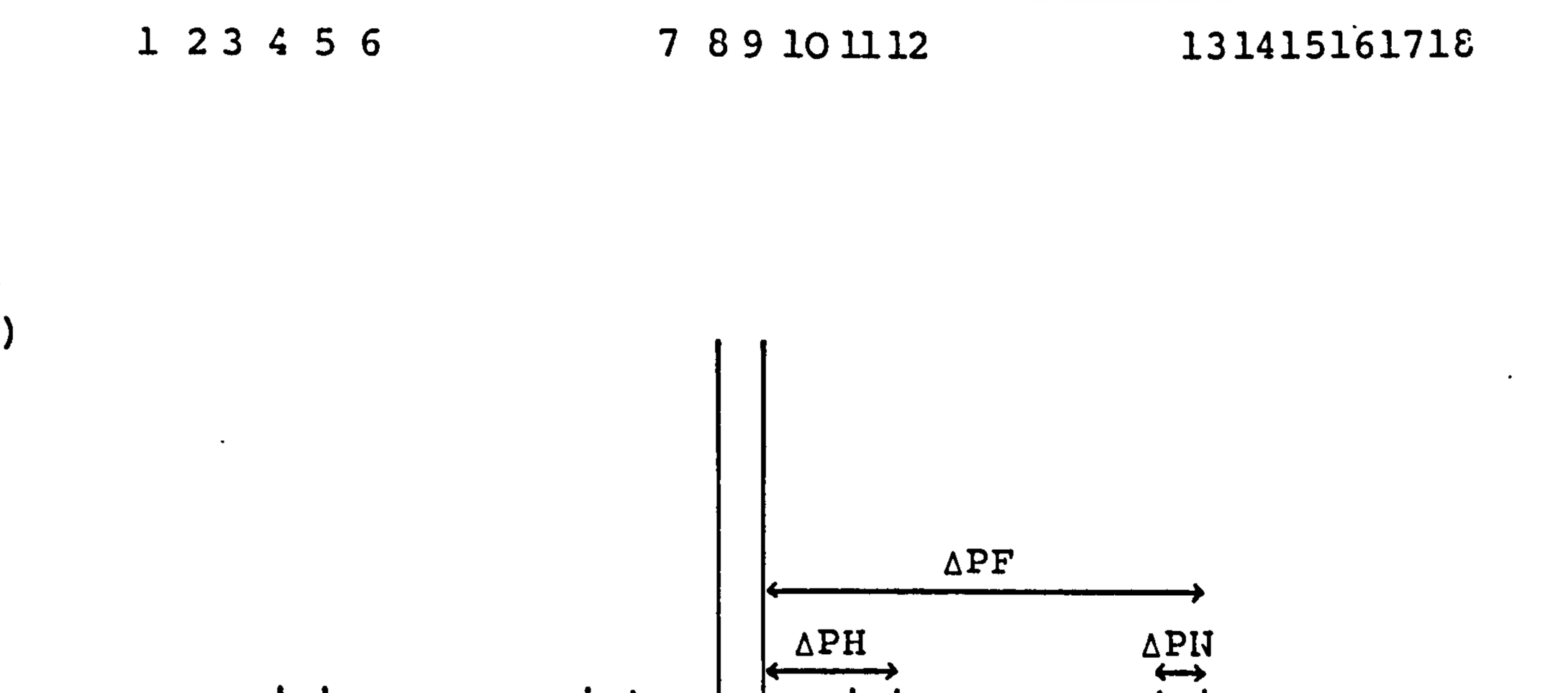

Figure 10.5 : Observed and final difference weighted molecular scattering intensities at nozzle-to-plate distances of (a) 128 and (b) 238 mm.

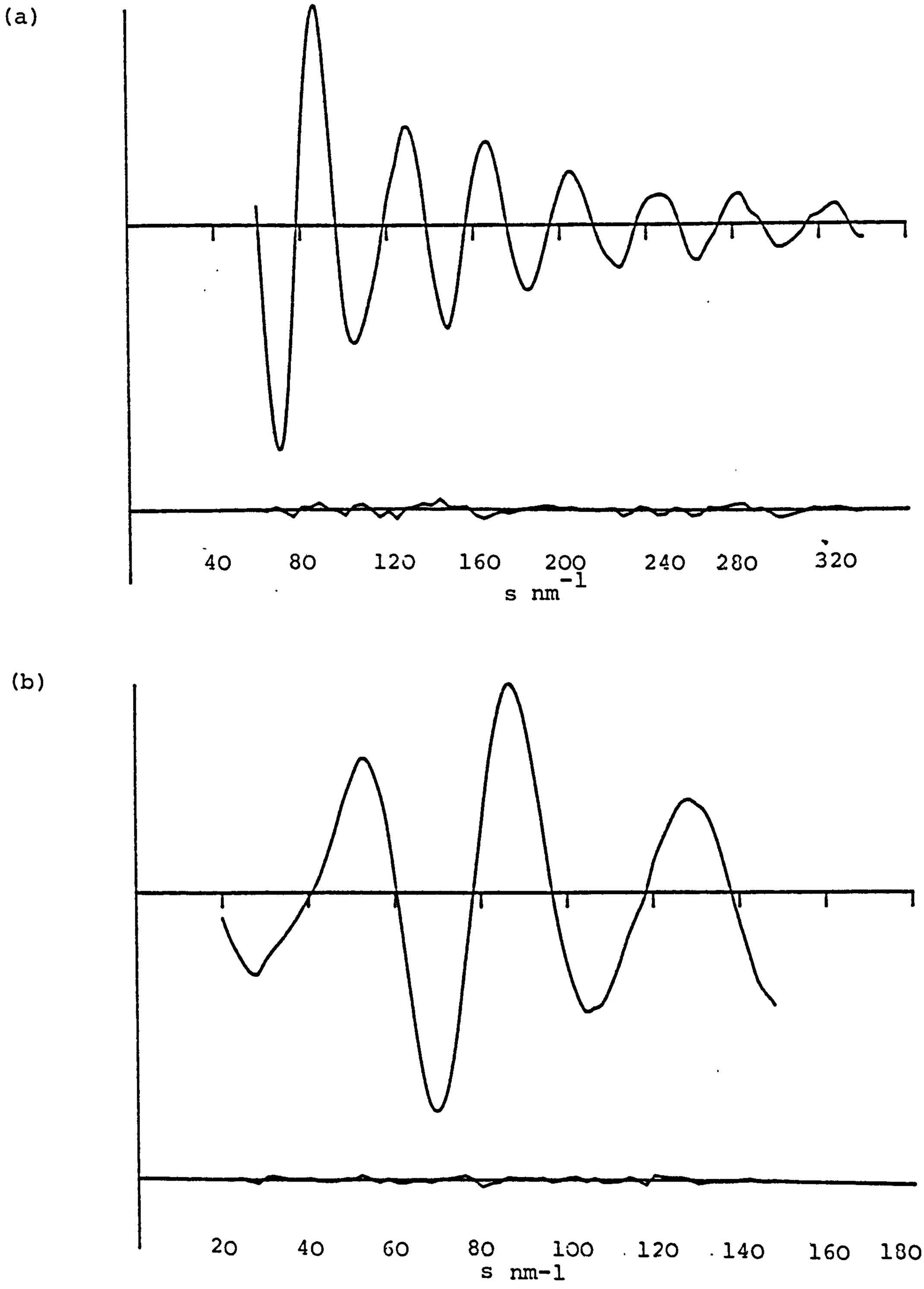

Figure 10.6a: Ed-only - variation of R_G with α for the hydrogen atom (i) cis to nitrogen lone pair; (ii) trans to nitrogen lone pair

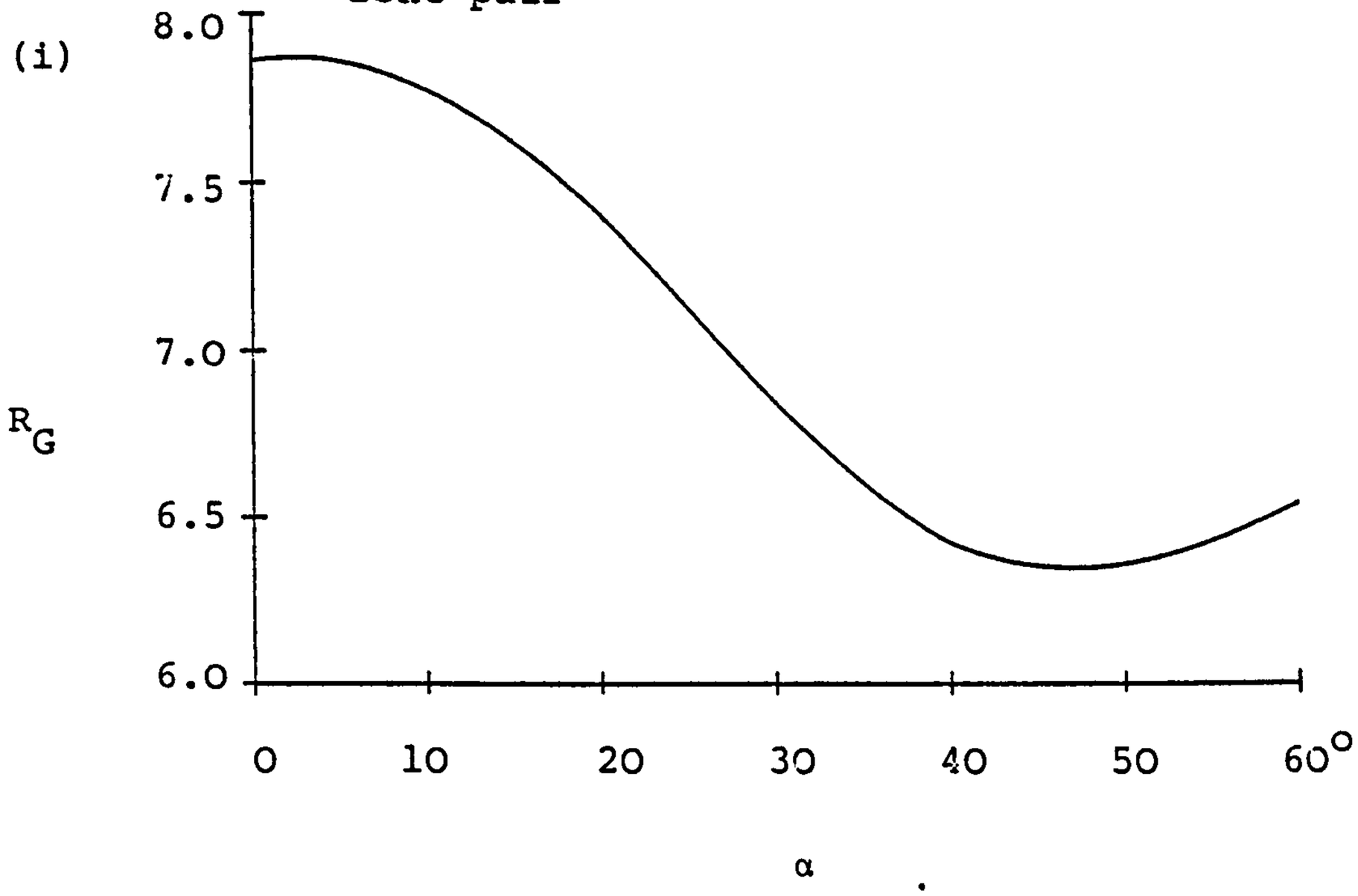

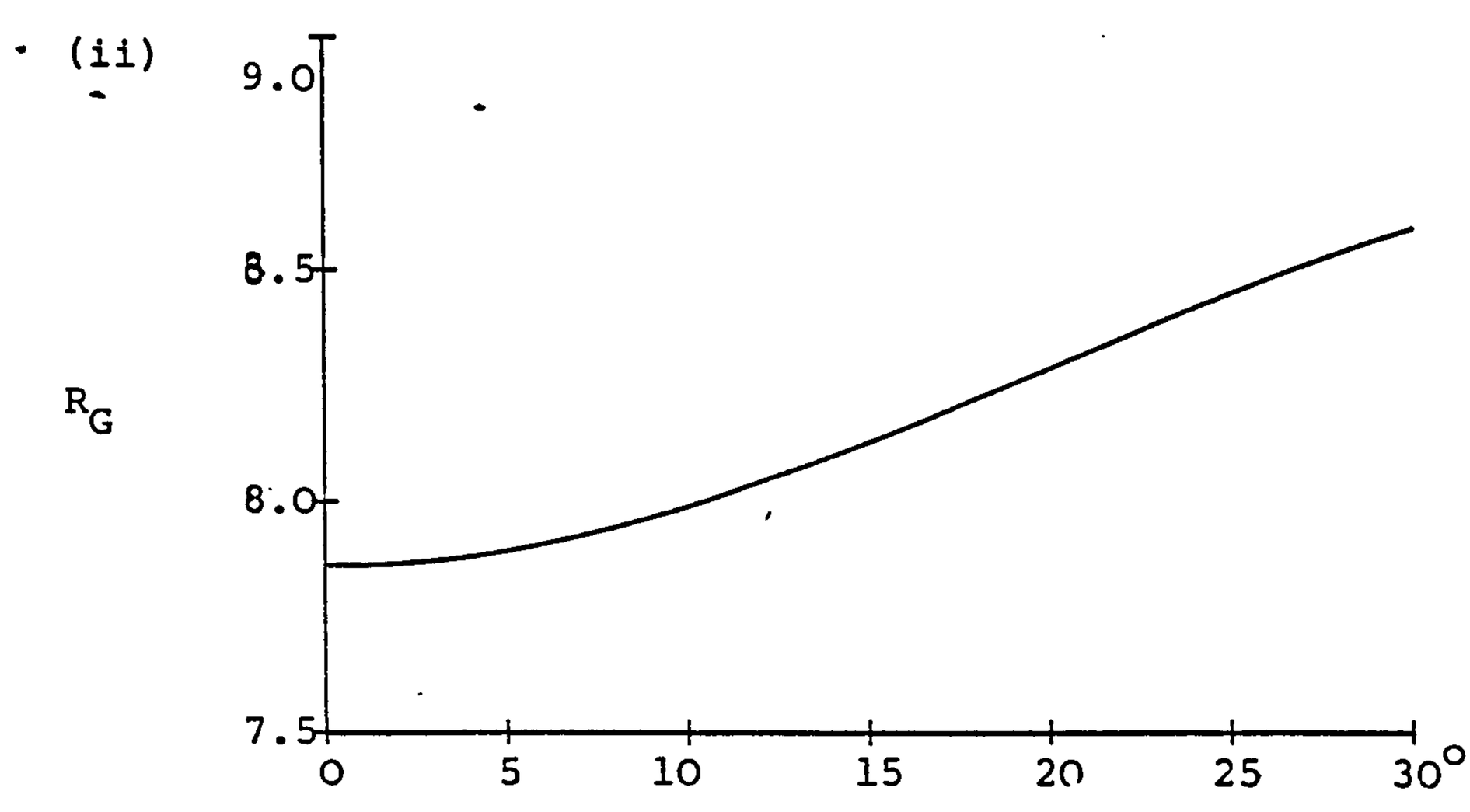

Note: α = angle between r(N-H) and the plane subtended by P, N, and the bisector of <FPF.

Figure 10.6b: Ed+1cnmr variation of R_G with α for the hydrogen atom (i) cis to nitrogen lone pair, (ii) trans to nitrogen lone pair

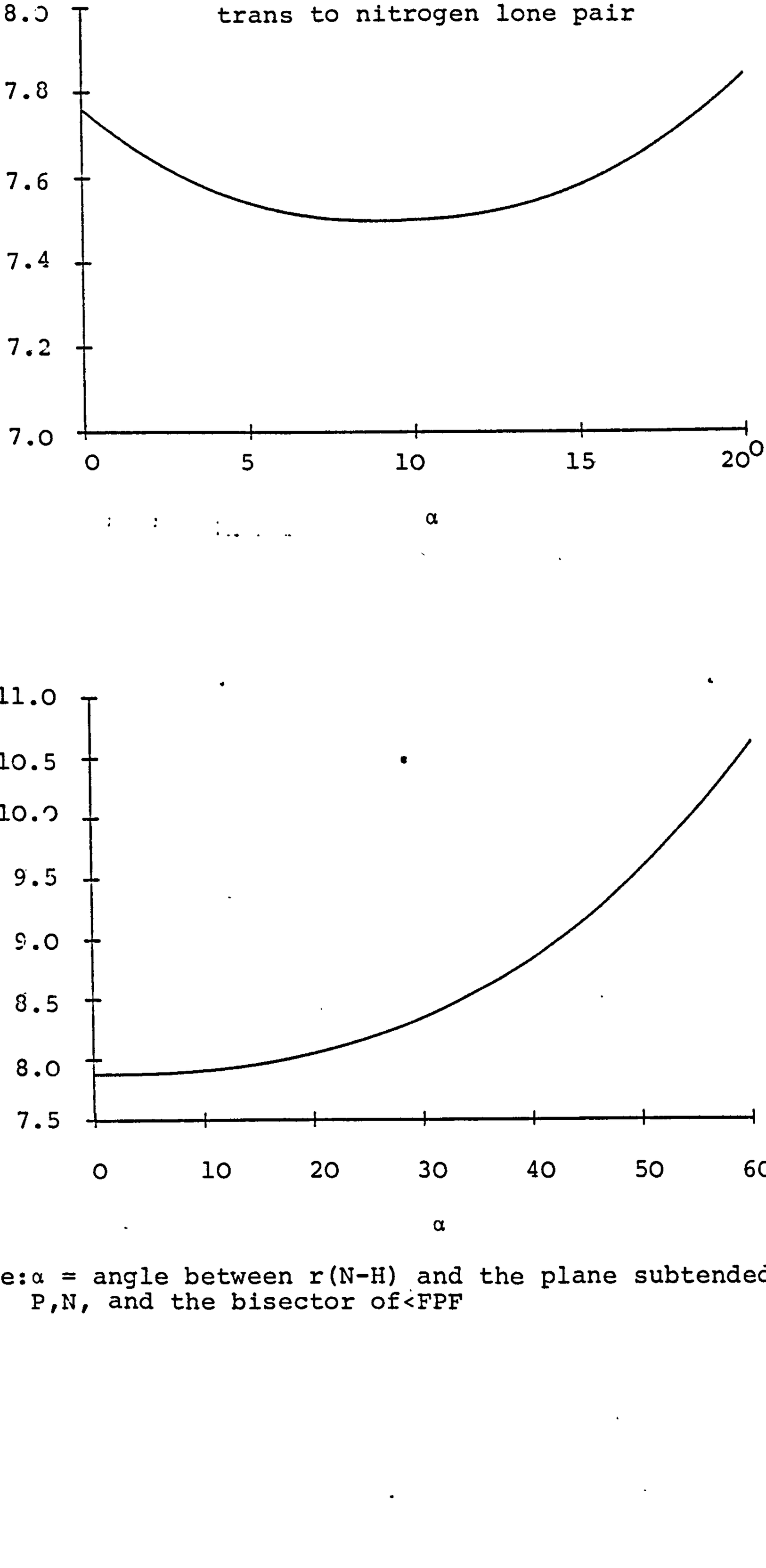

Note: α = angle between r(N-H) and the plane subtended by P,N, and the bisector of<FPF

Figure 10.7 : Molecular structure of $(PF_2)NH_2$
(a) ed-only
(b) ed+lcnmr; the split hydrogen atom cis to the lone pair on phosphorus maintains C_s symmetry overall, while allowing the included angles at nitrogen to fall, on average, to a value $<2\pi$ radians.

(a)

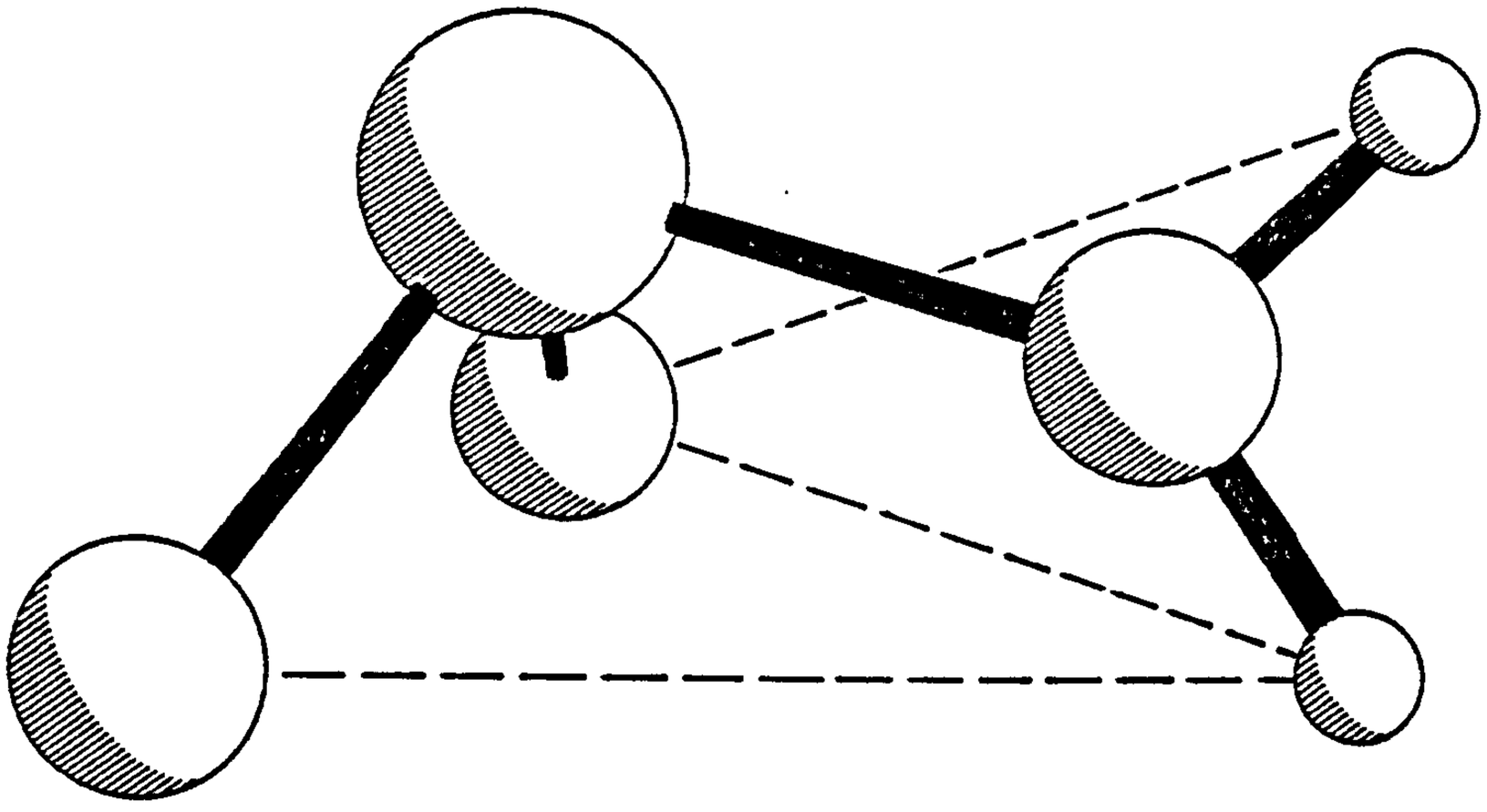

(b)

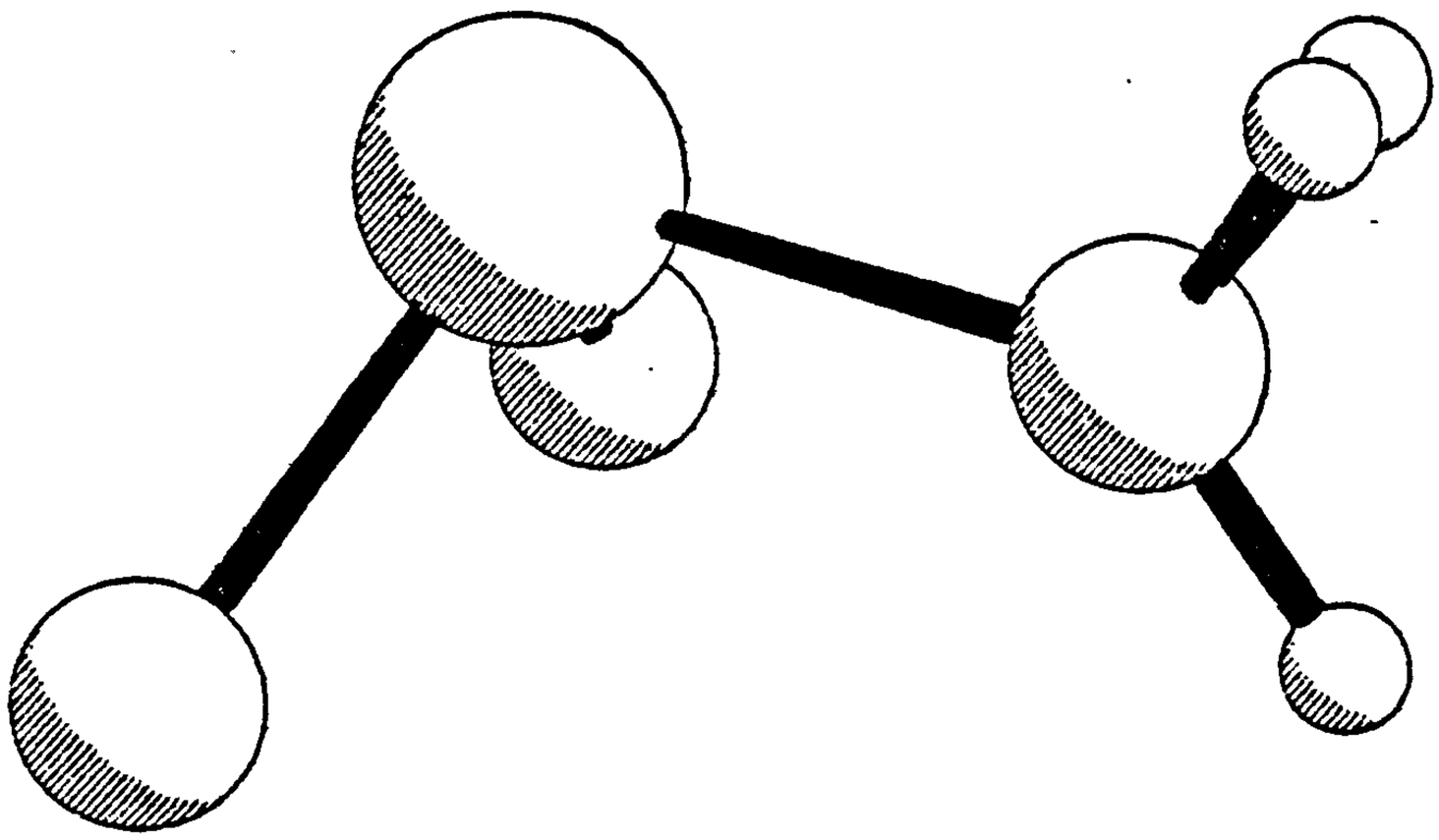

Note: possible hydrogen to fluoride attractive interactions are shown by broken lines, shown in Figure (a) only.

Figure 10.8 : Observed and final difference radii distribution curves.Before Fourier inversion,the data were multiplied by $s.\exp[-0.000015\ s^2/(z_P-f_P)(z_F-f_F)]$.

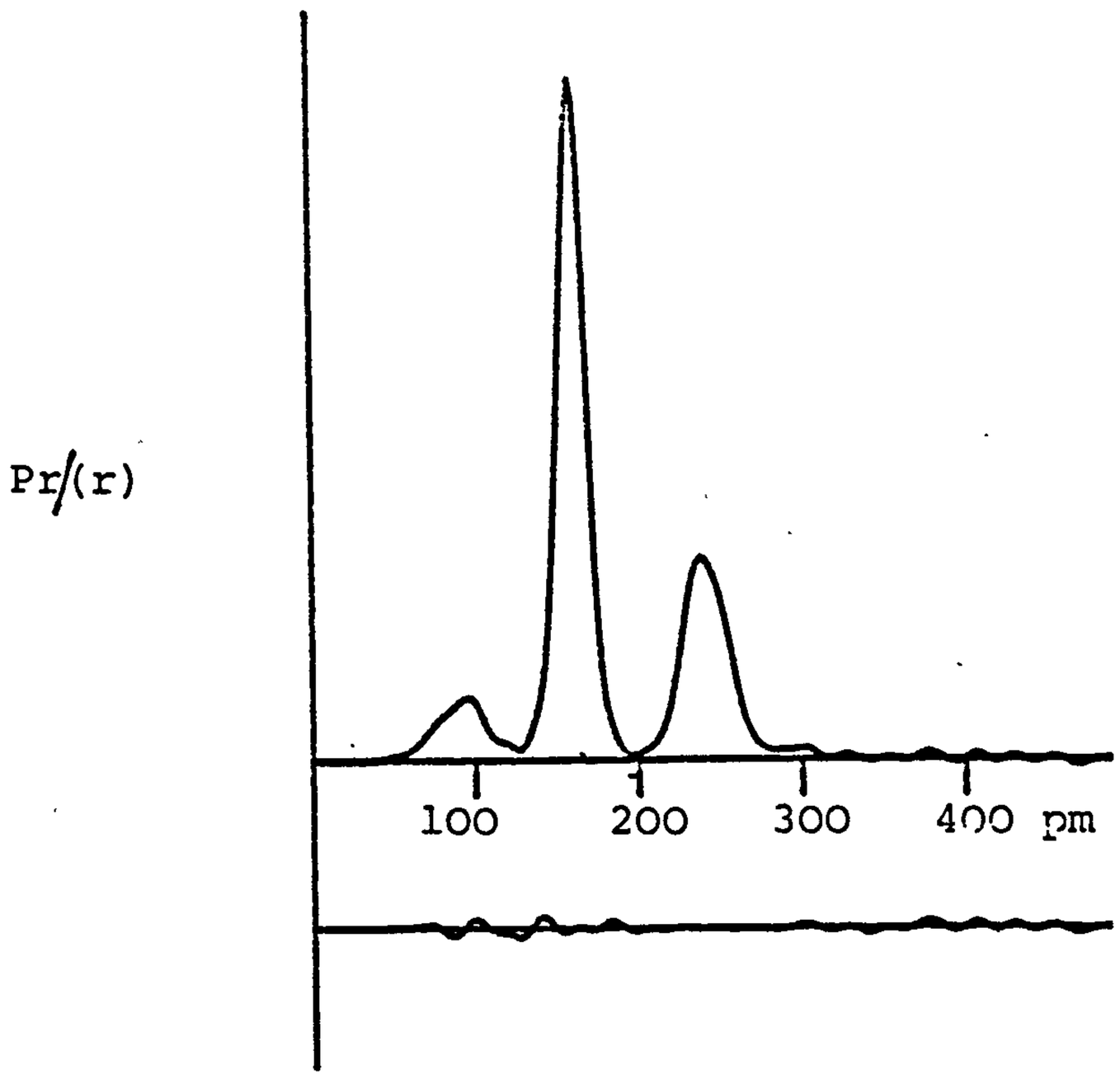

REFERENCES

1. E. Rutherford, Phil. Mag., 1911, 21, 669.

2. a) P. Debye, Ann.Physik., 1915, 46, 809
   b) P. Debye, Phys. Z., 1930, 31, 419.

3. P. Ehrenfest, Amsterdam Acad., 1915, 23, 1132.

4. C. Davisson and L.H. Germer, Phys. Rev., 1927, 30, 705.

5. a) G.P. Thomson, Proc. Roy. Soc., 1928, A117, 600.
   b) G.P. Thomson, Proc. Roy. Soc., 1928, A119, 651.

6. H. Mark and R. Weirl, Naturwiss., 1930, 18, 205.

7. R. Weirl, Ann. Physik., 1931, 8, 521.

8. a) L.S. Bartell, J. Chem. Phys., 1955, 23, 1219.
   b) L.S. Bartell and K. Kuchitsu, ibid., 1961, 35, 1945.
   c) J. Pundgren, Arkiv. Fysik., 1965, 30, 61.
   d) K. Kuchitsu, Bull. Chem. Soc., Japan, 1967, 40, 498.

9. . R.A. Bonham, L. Schafer and A.C. Yates, J. Chem. Phys., 1971, 55, 3055.

10. a) C. Finbak, Avh. No. Vidensk.-Akad., Oslo, Mat. Naturvidensk. Kl.No.13, 1937.
    b) P. Debye, Phys. Z., 1939, 40, 66 and 404.

11. a) I.L. Karle and J. Karle, J. Chem. Phys., 1949, 17, 1052.
    b) H. Hauptman and J. Karle, J. Chem. Phys., 1950, 18, 875.
    c) J. Ainsworth and J. Karle, J. Chem. Phys., 1952, 20, 425.
    d) P.W. Moore, Y. Morino and J. Nakamura, J. Chem. Phys., 1962, 36, 1050.
    e) S.J. Cyvin, K. Kuchitsu, T. Iijimaz and Y. Morino, J. Chem. Phys., 1962, 36, 1109.
    f) W. Freyland, J. Haase and W. Zeil, Z. Naturforsch., 1966, A21, 1945.

12. a) E. Hirota and Y. Morino, J. Chem. Phys., 1955, 23, 737.
    b) Y. Morino and M. Traetteberg, Acta. Crystallogr., 1960, 13, 1108.
    c) S.J. Cyvin, "Molecular Vibrations and Mean Square Amplitudes", 1968, Elsevier, Amsterdam.

13. G.C. Holywell, D.W.H. Rankin, B. Beagley and J.M. Freeman, J. Chem. Soc.(A), 1971, 785.

14.a) H.M. Seip in "Selected Topics in Structure Chemistry", Universitetforlaget, Oslo, 1967, 25.

b) K.Kuchitsu and S. Konaka, J. Chem. Phys., 1966, 45, 4342.

c) K. Kuchitsu, J.P. Guillory and L.S. Bartell, J. Chem. Phys., 1968, 49, 2488.

15. K. Hedberg, J. Amer. Chem. Soc., 1955, 77, 6491.

16. B. Beagley and A.R. Conrad, Trans. Faraday Soc., 1970, 66, 2740.

17. V. Schomaker and D.P. Stevenson, J.A.C.S., 1941, 63, 37.

18. D.E.J. Arnold, D.W.H. Rankin, M.R. Todd and R. Seip, J.C.S. Dalton, 1979, 1290.

19.a) D.E.J. Arnold, D.W.H. Rankin and G. Robinet, J.C.S. Dalton, 1977, 585.

b) H. Oberhammer and R. Schmutzler, J.C.S. Dalton, 1976, 1454.

c) L.S. Khaikin and L.V. Vilkov, Doklady Acad. Nauk, SSSR, 1966, 168, 810.

d) A. Almenningen, B. Andersen and E.E. Astoup, Acta. Chem. Scand., 1969, 23, 2199.

e) M.I. Davis and J.W. Paul, J. Mol. Structure, 1971, 9, 478; ibid. 1972, 12, 259.

f) V.A. Narmov, L.F. Shatrukov and V.N. Shemashko, Doklady Acad. Nauk, SSSR, 1973, 209, 118.

20. C. Glidewell, D.W.H.Rankin, A.G. Robiette and G.M. Sheldrick, J. Mol. Structure, 1970, 6, 231.

21. B.J. Aylett, I.A. Ellis, J.J. Monaghan, D.W.H. Rankin, A.G. Robiette, G.M. Sheldrick and W.S. Sheldrick, J. Chem. Soc.(A), 1969, 1224.

22. L.V. Vilkov et al, Zhur. Stukt. Khim., 1969, 10, 1101.

23. E. Hedberg, L. Hedberg and K. Hedberg, J. Amer. Chem. Soc., 1974, 96, 4417.

24. D.E.J. Arnold, E.A.V. Ebsworth, H.F. Jessop and D.W.H. Rankin, J.C.S. Dalton, 1972, 1681.

25. G.S. Laurenson and D.W.H. Rankin, J. Mol. Struct., 1979, 54, 111.

26. C.M. Huntley, G .S. Laurenson and D.W.H. Rankin, J.C.S. Dalton, 1980, 954.

27. G.S. Laurenson and D.W.H. Rankin, J.C.S. Dalton, 1981, 425.

28. A.H. Brittain, K. Cohn, L. Lee, R.H. Schwendeman and J.E. Smith, J. Amer. Chem. Soc., 1971, 93, 6772.

29. G.S. Laurenson and D.W.H. Rankin, J.C.S. Dalton, 1981, 1047.

30. S.H. Bauer and K. Kimura, J. Phys. Soc. Japan, 1962, 17, 300.

31. T. Iijima, M. Kimura and K. Tamagawa, J. Mol. Struct., 1976, 30, 243.

32. R. Hildebrandt, PhD Thesis, Cornell Univ., 1969.

33. D.M. Bridges, J.M. Freeman, G.C. Holywell and D.W.H. Rankin, J. Organometallic Chem., 1971, 32, 87.

34. B. Beagley, J.M. Freeman, G.C. Holywell and D.W.H. Rankin, J. Chem. Soc. A., 1971, 785.

35. L.S. Bartell, E.J. Jacob and H.B. Thompson, J. Mol. Structure, 1971, 8, 383.

36. Y. Hori, Y. Morino, K. Kuchitsu and M. Tamimoto, Bull. Chem. Soc. Japan, 1968, 41, 2349.

37.a) T. Fukuyama, K. Kuchitsu and Y. Morino, J. Mol. Struct., 1968, 1, 463.

b) ibid, 1969, 4, 41.

38. R.L. Hilderbrandt and J.D. Wieser, J. Chem. Phys., 1971, 55, 4648; ibid., 1972, 56, 1143.

39. A.S.F. Boyd, G.S. Laurenson and D.W.H. Rankin, J. Mol. Struct., 1981, 71, 217.

40. A.S.F. Boyd, G.S. Laurenson and D.W.H. Rankin, unpublished observations.

41. L.S. Bartell, D.J. Romenesko and T.C. Wong, "Molecular Structure by Diffraction Methods", (Specialist Periodical Reports), The Chemical Society, London, 1977, 3, 72.

42. K. Kuchitsu, in "Molecular structure and vibrations", ed. S.J. Cyvin, Elsvier, Amsterdam, 1972.

43. Specialist Periodical Reports, "Molecular Structure by Diffraction Methods", Vol. 1, The Chemical Society, London, 1973, 39.

44. D. Damiani, P. Forti and P.G. Favero, J. Am. Chem. Soc., 1973, 95, 756.

45. E.D. Morris and C.E. Nordman, Inorg. Chem., 8, 1673.

46. D.E.J. Arnold and D.W.H. Rankin, J.C.S. Dalton, 1975, 889.

47. M.J. Barrow, E.A.V. Ebsworth, M.M. Harding and S.G.D. Henderson, J.C.S. Dalton, 1979, 1192.

48. J.S. Harman and D.W.A. Sharp, J. Chem. Soc. A. (1970), 1935.

49. D.M. Bridges, J.M. Freeman, G.C. Holywell and D.W.H. Rankin, J. Organomet. Chem., 1971, 32, 87.

50. D.E.J. Arnold and D.W.H. Rankin, J.C.S. Dalton, 1975, 889.

51. S.H. Bauer and R.L. Hilderbrandt, J. Mol. Struct., 1969, 3, 325.

52. L.S. Bartell, J. Chem. Phys., 1960, 32, 827.

53. E.A.V. Ebsworth, D.W.H. Rankin and J.G. Wright, J.C.S. Dalton, 1979, 1065.

54. J.F. Nixon, J. Chem. Soc. (A), 1969, 1087.

55. E.A.V. Ebsworth, D.W.H. Rankin and J.G. Wright, J.C.S. Dalton, 1977, 2348.

56. D.E.J. Arnold, E.R. Cromie and D.W.H. Rankin, J.C.S. Dalton, 1977, 1999.

57. S. Cradock, J. Kaprowski and D.W.H. Rankin, J. Mol. Struct., 1981, 77, 113.

58. D.E.J. Arnold, E.A.V. Ebsworth, H.F. Jessop and D.W.H. Rankin, J.C.S. Dalton, 1972, 1681.

59. H.H. Karsch and D.W.H. Rankin, personal communication.

60. A.H. Cowley, M.J.S. Dewar, W.R. Jackson and W.B. Jennings, J. Amer. Chem. Soc., 1970, 92, 1085.

61. D.W.H. Rankin, J. Chem. Soc. (A), 1969, 1926.

62. C. Glidewell, D.W.H. Rankin and A.G. Robiette, J. Chem. Soc. (A), 1970, 2935.

63. S.S. Cyvin and D.W.H. Rankin, J. Chem. Soc. Dalton, 1972, 1277.

64. S. Cradock, E.A.V. Ebsworth, M.L. McConnell, D.W.H. Rankin and M.R. Todd, J. Chem. Soc. Dalton, 1977, 20 1925.

65. J.H. Schachtschneider and R.G. Snyder, Spectrochim. Acta., 1963, 19, 117.

66. L.S. Khaikin and L. Vilkov,"Topics in Current Chemistry", 1975, 53, 38.

67. D.W.H. Rankin, J. Chem. Soc. Dalton, 1972, 869.

68. A. Fraser, G.S. Laurenson and D.W.H. Rankin, unpublished observations.

69. P. Deihl and C.L. Khetrapal, "NMR Studies of Molecules Oriented in the Nematic Phase of Liquid Crystals." p3

70. A.D. Buckingham and J.A. Pople, Trans. Faraday Soc., 1963, 59, 2421.

71. P. Ducros, Bull. Soc. Franc. Mineral. Crist., 1960, 83, 85.

72. G. Englert and A. Saupe, Phys. Rev. Letters, 1963, 11, 462.

73. G. Englert and A. Saupe, Z. Naturforsch, 1964, 19a, 172.

74. F. Reinitzer, Monatsh., 1888, 9, 421.

75. O. Lehmann, "Flussige Kristalle, sowie Plastizitat von Kristallen im Allgermeinen, molekulare Umlagerungen und Aggregatzustandsanderungen", Engelmann, Leipzig, 1904.

76. J.W. Emsley and J.C. Lindon,"NMR Spectroscopy using Liquid Crystal Solvents", Pergamon Press, 1975, 3-7.

77. P. Deihl and C.L. Khetrapal, "NMR Studies of Molecules Oriented in the Nematic Phase of Liquid Crystals", 4,5.

78. E. Bose, Z. Physik., 1909, 10, 32.

79. H. Zocher, Trans. Faraday Soc., 1933, 29, 945.

80. G. Friedel, Ann. Phys., 1922, 18, 273.

81. A. Saupe, Z. Naturforsch, 1963, 20a, 572.

82. J.W. Emsley and J.C. Linden,"NMR Spectroscopy using Liquid Crystal Solvents", Pergamon Press, 1975, 16.

83. B.P. Dailey and N. Zumbulyadis, Mol. Phys., 1973, 26, 777.

84. B.M. Fung and I.Y. Wei, J. Amer. Chem. Soc., 1970, 92, 1497.

85. B.P. Dailey and N. Zumbulyadis, Mol. Phys., 1974, 27, 633.

86. H. Spiesecke, Z. Naturforsch, 1970, 25a, 650.

87. J. Bulthius and C.A. de Lange, J. Mag. Resonance, 1974, 14, 13.

88. B.P. Dailey and P.F. Bhattacharyya, Mol. Phys., 1974, 28, 209.

89. R. Ader and A. Loewenstein, Mol. Phys., 1972, 24, 455.

90. G.S. Laurenson and D.W.H. Rankin, unpublished observations

91. E.E. Burnell, J.R. Council and S.E. Ulrich, Chem. Phys. Letters, 1975, 31, 295.

92. a) R.A. Bernheim and T.R. Krugh, J. Amer. Chem. Soc., 1970, 52, 494 (See also Ref. 101).

b) P.K. Bhattacharyya and B.P. Dailey, Mol. Phys., 1973, 26, 1379.

c) G. Englert and A. Sange, Mol. Cryst. and Liq. Cryst., 1966, 1, 503; ibid, 1969, 8, 233; G. Enghert, A. Povh, and A. Saupe,Adv. in Chem., 1967, 63, 51.

d) D.N. Chen, L.W. Reeves, A.S. Tracey and M.M. Tracey, J. Amer. Chem. Soc., 1974, 96, 5349.

e) A. Saupe and H. Spiesecke, Mol. Cryst. and Liq. Cryst., 1970, 6, 287.

f) D. Canet and E. Haloui, Org. Mag. Resonance, 1974, 6(10), 537.

g) ibid, Chem. Phys. Letters, 1974, 26, 261.

h) P. Diehl, H.P. Kellerhals and C.L. Khetrapal, Helv. Chim. Acta., 1968, 51, 529.

93. a) M.S. Gopinathan and P.T. Narasimhan, J. Mag. Res., 1973, 9, 45.

b) A. Azman and M. Zancer, Z. Naturforsch, 1972, 27a, 1535.

c) L.W. Reeves, J.M. Riverco, R.A. Spragg and J.A. Vanin, Mol. Phys., 1973, 25, 9.

d) J. Courtieu and Y. Gounelle, Org. Magn. Resonance, 1971, 3, 533.

e) B.P. Dailey and J. Lindon, Mol. Phys., 1971, 20, 937.

94. a) B. Beagley, A.H. Clark, D.W.J. Cruickshank and T.G. Hewitt, J. Chem. Soc. (A), 1970, 872.

b) A. Robertson, PhD Thesis, University of Edinburgh, 1976.

c) S.H. Bauer and E.A. McNeill, J. Mol. Struct., 1975, 27, 151.

95. a) C.J. Dain, A.J. Downs, G.S. Laurenson and D.W.H. Rankin, J.C.S. Dalton, 1981, 472.

b) M.T. Barlow, C.J. Dain, A.J. Downs, G.S. Laurenson and D.W.H. Rankin, J.C.S. Dalton, 1982, 597.

96. a) L.S. Bartell and B.L. Carroll, J. Chem. Phys., 1965, 42, 1135.

b) L.S. Bartell and H.K. Higginbotham, J. Chem. Phys., 1965, 42, 851.

c) I.L. Karle, J. Chem. Phys., 1952, 20, 63.

d) A. Almenningen, O. Bastiansen and L. Fernholt, Det. Kgl. Norske Videnskab.Selskabs Str., 1958, Nr 3.

e) K. Kimura and K. Kubo, J. Chem. Phys., 1960, 32, 1776.

f) B. Beagley, A.R. Conrad, J.M. Freeman, J.J. Monaghan, B.G. Norton and G.C. Holywell, J. Mol. Str., 1972, 11, 371.

97. P. Diehl and C.L. Khetrapal, Mol. Phys., 1967, 14, 283.

98. Varian Associates Publication, no.87-202-006 B168,p19.

99. a) M. Barfield, Chem. Phys. Letters, 1970, 4, 518.

b) H. Nakatsuji, H. Kato, I. Morishima and T. Yonezawa, Chem. Phys. Letters, 1970, 4, 607.

c) H. Nakatsuji, K. Hirao, H. Kato and T. Yonezawa, Chem. Phys. Letters, 1970, 6, 541.

d) A.D. Buckingham and I. Love, J. Magn. Resonance, 1970, 2, 338.

100. a) J. Gerritsen and C. MacLean, Rec. Trav. Chim., 1972, 91, 1393.

b) ibid, Spectrochim. Acta., 1971, 27A, 1495.

c) J. Degelaen, P. Diehl and W. Niederberger, Org. Magn. Resonance, 1972, 4, 721.

d) J. Gerritsen, G. Koopmans, H.S. Rollema and C. MacLean, J. Magn. Resonance, 1972, 8, 20.

e) G.J. den Otter, J. Gerritsen and C. MacLean, J. Mol. Struct., 1973, 16, 379.

f) G.J. den Otter, W. Heijser and C. MacLean, J. Magn. Resonance, 1974, 13, 11.

g) A. Schumann, H. Dreeskamp and K. Hilderbrand, J. Magn. Resonance, 1975, 18, 97.

h) P. Diehl, S. Sykora and E. Wullschleger, Mol. Phys., 1975, 29, 305.

101. R. Bernheim and T.R. Krugh, J. Am. Chem. Soc., 1969, 91, 2385.

102. S. Meiboom, R.C. Hewitt and L.C. Snyder, Pure Appl. Chem., 1972, 32, 251.

103. K. Kuchitsu, Y. Morino and T. Moritani, Prog. Inorg. Chem., 1969, 8, 867.

104. E. Hirota and Y. Morino, J. Mol. Spect., 1970, 33, 460.

105. L.S. Bartell, J.P. Guillory and K. Kuchitsu, J. Chem. Phys., 1968, 48, 2488.

106. D.W.H. Rankin et al, J. Mol. Struct., 1970, 6, 231.

107. L. Centofanti and R.W. Parry,Inorg. Chem., 1970, 9, 744.

108. D.W.W. Anderson, E.A.V. Ebsworth, G.D. Miekle and D.W.H. Rankin, Mol. Phys., 1973, 25, 387.

109. J.P. Albrand, A. Coyne and J.B. Robert, Chem. Phys. Letters, 1977, 48, 524.

110. C.R. Nare and J. Sheridan, J. Mol. Struct., 1973, 15, 391.

111. L. Acha, E.R. Cromie and D.W.H. Rankin, J. Mol. Struct., 1981, 73, 111.

112. P.J. Carroll and D.D. Titus, J. Chem. Soc. Dalton Trans., 1977, 824.

113. T.S. Cameron and B. Dahlen, J. Chem. Soc. Perkin Trans, 1975, 2, 1737.

114. Z. Galdecki, M.L. Glowka, J. Michalski, A. Okruszek and W.J. Stec, Acta. Cryst., 1977, 33B, 2322.

115. M.C. Bach, C. Brian, F. Crasnier and J.-F. Labarre, C. Leibovia and A. Dargelos, J. Mol. Str., 1973, 17, 23.

116. W.B. Jennings, J.H. Hargis and S.D. Worley, Chem.Comm., 1980, p30.

117. A. Blake, E.A.V. Ebsworth, D.W.H. Rankin and A.J. Welch, personal communication.

118. D.W.H. Rankin, J. Che. Soc. (A), 1971, 783.

119. D.W.W. Anderson, J.E. Bentham and D.W.H. Rankin, J. Chem. Soc. (Dalton), 1973, 1215.

Appendix I: Example of a mathematical model: $PF_2(NH_2)$; this model utilises a subroutine MX_2 which calculates atom coordinates for the atoms M and X in a $Cs(-MX_2)$ molecular fragment. This model also predicts dipolar couplings. Theoretical scattering intensities are calculated by programs elsewhere in the ED80 program library of which this model becomes a subroutine when refining the structure of $PF_2(NH_2)$.

```
C NMREMODEL ; USES MX2 SUBROUTINE TO GENERATE 2X1/2H SPLIT CS
C          E DUMMY N FOR MX2          BY PF2N BISECTOR PLANE TRANS
      SUBROUTINE COORD (X,Y,Z)
C                                     TO F'S AND 2X1/2H CIS TO F'S
C PF2NH2    P F F N H H N H H
C P1 P-F,P2 P-N,P3 N-H',P4 FPF,P5 FPN,P6 PNH',P7 H'NH',P8 PNH ,
C P9 NH,P10 HNH
      IMPLICIT REAL*8 (A-H,O-Z)
      REAL*4 RM
      COMMON/M80/PAR(20),R(100),RM(100),U(100)
      DIMENSION X(50),Y(50),Z(50)
      PI=3.14159265359
      C=1.8D2
      RAD=PI/C
      RM(9)=0.5D0
      RM(10)=0.5D0
      A1=PAR(4)*RAD
      A2=PAR(5)*RAD
      A3=PAR(6)*RAD
      A4=PAR(7)*RAD
      A5=PAR(8)*RAD
      A6=PAR(10)*RAD
      A=PAR(2)
      B=PAR(1)
      C=A2
      D=A1
      E=0.0D0
      F=PI
      G=0.0D0
      N=1
      CALL M80MX2(A,B,C,D,E,F,G,N,X,Y,Z)
      A=0.0D0
      B=PAR(9)
      C=A5
      D=A6
      E=PI
      G=0.0D0
      F=0.0D0
      N=7
      CALL M80MX2(A,B,C,D,E,F,G,N,X,Y,Z)
      A=0.0D0
      B=PAR(3)
      C=A3
      D=A4
      E=0.0D0
      G=0.0D0
      F=0
      N=4
      CALL M80MX2(A,B,C,D,E,F,G,N,X,Y,Z)
      RETURN
      END
```

```
C
      SUBROUTINE EXTRA(X,Y,Z,E)
C      1     2     3     4     5     6     7     8
C     PF    PN    FF    FN    NH    PH    FH    HH
C         P9        P10       P11
C      S1=SZZ  S2=SXX-SYY  S3=SXY
       IMPLICIT REAL*8 (A-H,O-Z)
       REAL*4 RM
       COMMON/M80/P(20),R(100),RM(100),U(100)
       DIMENSION E(20),X(50),Y(50),Z(50),S(5),G(50)
       G(1)=9.919D1
       G(2)=2.30509D2
       G(3)=G(2)
       G(4)=-2.4832D1
       DO 10 J=5,9
   10  G(J)=2.45017D2
       S(1)=P(11)
       S(2)=P(12)
       S(5)=P(13)
       S(3)=0.0D0
       S(4)=0.0D0
       E(1)=(ED8ONA(X,Y,Z,G,S,2,1)+ED8ONA(X,Y,Z,G,S,3,1))/2.0D0
       E(2)=ED8ONA(X,Y,Z,G,S,1,4)
       E(3)=ED8ONA(X,Y,Z,G,S,2,3)
       E(4)=(ED8ONA(X,Y,Z,G,S,2,4)+ED8ONA(X,Y,Z,G,S,3,4))/2.0D0
       E(5)=(ED8ONA(X,Y,Z,G,S,4,5)+ED8ONA(X,Y,Z,G,S,4,6)
     £+ED8ONA(X,Y,Z,G,S,4,8)+ED8ONA(X,Y,Z,G,S,4,9))/4.0D0
       E(6)=(ED8ONA(X,Y,Z,G,S,1,5)+ED8ONA(X,Y,Z,G,S,1,6)
     £+ED8ONA(X,Y,Z,G,S,1,8)+ED8ONA(X,Y,Z,G,S,1,9))/4.0D0
       E(7)=(ED8ONA(X,Y,Z,G,S,2,5)+ED8ONA(X,Y,Z,G,S,2,6)
     £+ED8ONA(X,Y,Z,G,S,2,8)+ED8ONA(X,Y,Z,G,S,2,9)
     £+ED8ONA(X,Y,Z,G,S,3,5)+ED8ONA(X,Y,Z,G,S,3,6)
     £+ED8ONA(X,Y,Z,G,S,3,8)+ED8ONA(X,Y,Z,G,S,3,9))/8.0D0
       E(8)=(ED8ONA(X,Y,Z,G,S,5,8)+ED8ONA(X,Y,Z,G,S,6,8)
     £+ED8ONA(X,Y,Z,G,S,5,9)+ED8ONA(X,Y,Z,G,S,6,9))/4.0D0

       RETURN
       END
C
       DOUBLE PRECISION FUNCTION ED8ONA(X,Y,Z,G,S,I,J)
C      CALCULATES DIPOLAR COUPLING I,J
       IMPLICIT REAL*8 (A-H,O-Z)
       DIMENSION X(50),Y(50),Z(50),S(5),G(50)
       R=DSQRT((X(I)-X(J))**2+(Y(I)-Y(J))**2+(Z(I)-Z(J))**2)
       CX=(X(I)-X(J))/R
       CY=(Y(I)-Y(J))/R
       CZ=(Z(I)-Z(J))/R
```

```
C
C       AMPLITUDE CORRECTIONS FOR PREDICTED D VALUES R=R-U**2/R
C
      DIMENSION DR(9,9)
      DO 1 K=1,9
      DO 1 L=1,9
    1 DR(K,L)=0.0D0
      DR(2,1)=0.0013
      DR(3,1)=0.0013
      DR(1,4)=0.0013
      DR(2,3)=0.0021
      DR(2,4)=0.0023
      DR(3,4)=0.0023
      DO 11 IN=5,9
      DR(4,IN)=0.0036
      DR(1,IN)=0.0098
      DR(2,IN)=0.0133
   11 DR(3,IN)=0.0133
      DR(5,8)=0.0139
      DR(6,8)=0.0139
      DR(5,9)=0.0139
      DR(6,9)=0.0139
      R=R-DR(I,J)
      EDSONA=-G(I)*G(J)*(S(1)*(3.0D0*CZ*CZ-1.0D0)+S(2)*(CX*CX-CY*CY)+2.0
     *D0*S(5)*CY*CX)/R**3
C       WRITE(6,99)EDSONA
99  FORMAT(' EDSONA ',F12.4)
    RETURN
    END
```

Appendix I (contd)

```
      SUBROUTINE MSOMX2(A,B,C,D,E,F,G,N,X,Y,Z)
C Calculates coordinates of MX2 group atoms.
C Atom N is M; atoms N+1 and N+2 are X.
C
C O is origin; A is r(O-M); B is r(M-X); C is <OMX; D is <XMX;
C E is clockwise twist about MX, viewed M to O (zero defined as when
C    XMX bisector is in xy plane with +ve y;
C F is clockwise rotation of MX2 about z axis;
C G is clockwise twist of MX2 about x axis.  All angles are in radian
C M lies on x axis (+ve x) before F and G are applied.
C
      IMPLICIT REAL*8 (A-H,O-Z)
      DIMENSION X(50),Y(50),Z(50)
      X(N)=A
      Y(N)=0.
      Z(N)=0.
      X(N+1)=A-B*DCOS(C)
      X(N+2)=X(N+1)
      R=B*DSIN(C)
      T=D/2.
      S=B*DSIN(T)
      T=S/R
      T=DARSIN(T)
      S=E-T
      T=E+T
      Y(N+1)=R*DCOS(S)
      Y(N+2)=R*DCOS(T)
      Z(N+1)=-R*DSIN(S)
      Z(N+2)=-R*DSIN(T)
      J=N+2
      IF(F.EQ.0.)GO TO 2
      R=DCOS(F)
      S=DSIN(F)
      DO 1 I=N,J
      T=X(I)*R+Y(I)*S
      Y(I)=Y(I)*R-X(I)*S
    1 X(I)=T
    2 IF(G.EQ.0.)GO TO 4
      R=DCOS(G)
      S=DSIN(G)
      DO 3 I=N,J
      T=Y(I)*R+Z(I)*S
      Z(I)=Z(I)*R-Y(I)*S
    3 Y(I)=T
    4 RETURN
      END
```

Appendix II: ED80 command numbers and their functions

```
Command no.: 1
Commands 10-19: parameters in refinement
10  Present state of commands 12-19
11  Clear commands 12-19 ... nothing refines
13  Refine parameters
14  Refine amplitudes
15  Add amplitude constraint
16  Remove amplitude constraints
17  Set up R factor loop
18  Set up 2-dimensional R factor loop
19  Read phase parameters

Command no.: 2
Commands 20-29: refinement conditions
20  Present state of commands 22-29
21  Clear commands 22-29 to standard values
22  Set no. of cycles of refinement
23  Set partial shift
24  Refine r(a), r(g) or r(alpha) parameters
25  Refine on I(s)*s**4 or I(s)*s**5
26  Set up weighting scheme
27  Read extra distance data from file 'XYZDIST'

Command no.: 3
Commands 30-39: printout requirements
30  Present state of commands 32-39
31  Clear commands 32-39 to standard values
32  Print parameters every cycle
33  Omit part of parameter list
34  Print correlation matrix
35  Print table of s limits, etc.
36  Print table of parameters
37  Read new label
38  List atom coordinates
39  Calculate bond lengths and angles

Command no.: 4
Commands 40-49: molecular parameter modification
40  List current parameters
42  Read complete parameter set
43  Read scale factor line
44  Read distance line
45  Read parameter line
46  Remove distance lines
47  Change number of distances
48  Read atomic numbers
49  Change number of indep. and dep. parameters
```

Appendix II (contd)

```
Command no.: 5
Commands 50-59: intensity data modification
50  List s limits and weighting points
52  Change s min
53  Change s max
54  Change lower weighting point
55  Change upper weighting point
56  Ignore or restore data set
57  Subtract background
58  Subtract background (odd point)
59  Subtract background (spline function)

Command no.: 6
Commands 60-69: lineprinter plots
60  Present state of commands 62-69
61  Clear commands 62-69 ... no lineprinter plots
62  Plot intensity curves on lineprinter
63  Plot combined intensity curves on lineprinter
64  Plot P(r)/r on lineprinter
65  Plot P(r) on lineprinter
66  Read radial distribution curve parameters

Command no.: 7
Commands 70-79: non-e.d. data
70  Present state of commands 72-79
71  Clear commands 72-79 ... ignore non-e.d. data
72  Change number of non-e.d. data
73  Change one non-e.d. data line
74  Ignore or include non-e.d. data in refinements

Command no.: 8
Commands 80-89: graphplotter plots
80  Present state of commands 82-89
81  Clear commands 82-89 ... no graphplotter plots
82  Plot intensity curves on graphplotter
83  Plot combined intensity curve on graphplotter
84  Plot P(r)/r on graphplotter
85  Plot P(r) on graphplotter
86  Read radial distribution curve parameters
88  Plot size

Command no.: 9
Commands 90-99: programme termination
90  Present state of commands 92-98
91  Clear commands 92-98 to standard values
92  Set convergence criteria
93  Protect parameter set
99  Store commands
```

Appendix III: List of abbreviations used in the text

ed	gas phase electron diffraction
esd	estimated standard deviation
ir	infrared spectroscopy
lcnmr	liquid crystal nuclear magnetic resonance spectroscopy
nmr	nuclear magnetic resonance spectroscopy
rms	root mean square

APPENDIX IV

Published Papers

Journal of Molecular Structure, 54 (1979) 111—119

AN ELECTRON DIFFRACTION DETERMINATION OF THE GAS PHASE MOLECULAR STRUCTURE OF METHYLAMINODIFLUOROPHOSPHINE

GRAHAM S. LAURENSON and DAVID W. H. RANKIN

Department of Chemistry, University of Edinburgh, West Mains Road, Edinburgh EH9 3JJ (Gt. Britain)

(Received 5 January 1979)

ABSTRACT

The gas phase molecular structure of methylaminodifluorophosphine has been studied by electron diffraction. The data can be interpreted in terms of a single conformer in which the phosphorus lone pair is *trans* to the N—C bond, although the possibility that up to 20% of a second conformer is present cannot be excluded. The principal parameters are: r(P—F) 159.3(4) pm; r(P—N) 164.8(7) pm; r(C—N) 144.8(12) pm; ∠(F—P—F) 94.1(8)°; ∠(F—P—N) 100.6(4)°; ∠(P—N—C) 125.3(20)°. The wide P—N—C angle indicates that the bonds to nitrogen are probably coplanar.

INTRODUCTION

Electron diffraction studies of $NMe(PF_2)_2$ [1] and $N(PF_2)_3$ [2] have revealed planar arrangements of ligands about nitrogen, and in the case of $PF_2[NH(SiH_3)]$ [3] the existence of a wide PNSi angle again suggests that the bonds around nitrogen are coplanar. Similarly, while the electron diffraction studies of $NMe_2(PF_2)$ [4] and $PF_2(NH_2)$ [4] indicate a possible pyramidal arrangement of ligands about nitrogen, with the angles between the P—N bonds and NR_2 planes being 32° and 35° respectively, microwave studies of both molecules [5, 6] and a determination of the solid phase structure of the former [7] again show planar nitrogen groupings. It was therefore interesting to study the structure of $PF_2(NHMe)$ with a view to determining how the geometry of the PNHC skeleton compares with that found in other PNR_2 skeletons.

The infrared spectrum of $PF_2[NH(SiH_3)]$ in the gas phase [3] shows two distinct N—H stretching vibrations, implying that two conformers are present in significant abundance. This was confirmed by a gas phase electron diffraction study, which revealed that the two conformers differed from each other in the orientation of the $-PF_2$ group. There are also two N—H stretching vibrations in the gas phase infrared spectrum of $NH(PF_2)_2$ [8] and two conformers of this compound are believed to be present, but the solid phase infrared spectrum has only one band in the N—H stretching region and an X-ray study shows only one conformer to be present in the crystalline phase [9]. The infrared spectrum of $PF_2[NH(CH_3)]$ also shows two N—H stretching vibrations, with

relative intensities of ca. 10: 1, and so the electron diffraction structure determination carried out on the compound was used to investigate whether two conformers could be identified.

EXPERIMENTAL

A sample of $PF_2(NHMe)$ was prepared by reacting $PBrF_2$ with monomethylamine [10] in a two-bulb apparatus in the absence of air and under reduced pressure. The product was purified by fractional condensation in vacuo and its purity was checked by infrared spectroscopy.

Photographic intensities were recorded on Kodak Electron Image plates using a Balzers' KD.G2 gas diffraction apparatus at nozzle-to-plate distances of 1000, 500 and 250 mm. The sample was maintained at a temperature of 250 K, while the nozzle was at room temperature (296 K). The value of 5.673 ± 0.003 pm for the electron wavelength was obtained from the analysis of the scattering pattern of gaseous benzene. The photographic intensities were converted to digital form using a Joyce-Loebl automatic microdensitometer.

With the exception of the initial conversion to uphill curves, the data reduction and least-squares refinements were carried out, using established programs, on an ICL 4-75 computer [4, 11]. The scattering factors of Schäfer et al. [12] were used throughout. The weighting points used in setting up the off-diagonal weight matrix are given in Table 1, together with scale factors and correlation parameters.

MOLECULAR MODEL

In the least-squares refinements of $PF_2(NHMe)$, local C_{3v} and C_s symmetries were assumed for the CH_3N and PF_2N groups respectively. The hydrogen bound to nitrogen was assumed to lie in the PNC plane. With these assumptions, the molecular structure could be defined by 12 independent parameters, taken to be the P—F, P—N, N—H, C—N and C—H bonds, the angles FPF, FPN, PNC, PNH and NCH, and two twist angles, defining the conformations of the $-PF_2$ and $-CH_3$ groups. The $-PF_2$ twist angle was defined to be zero when the FPF angle bisector was *cis* to the N—H bond, and the $-CH_3$ twist angle was taken to be zero when one C—H bond eclipsed the N—H bond. In the later stages

TABLE 1

Weighting functions, correlation parameters and scale factors

Camera height (mm)	Δs (nm^{-1})	s_{min} (nm^{-1})	s_{max} (nm^{-1})	sw1 (nm^{-1})	sw2 (nm^{-1})	p/h	Scale factor
250	4	60	306	80	265	0.456	1.87(5)
500	2	27	153	45	135	0.498	1.78(5)
1000	1	10	78	20	67.5	0.499	1.27(5)

of refinement a variable amount of a second conformer differing only in $-PF_2$ twist angle from the first conformer was introduced.

REFINEMENT

All three heavy-atom bonded distances lie beneath the peak at 160 pm in the radial distribution curve (Fig. 1), and so are strongly correlated. The P—F, P—N and N—C distances refined satisfactorily, unlike their amplitudes of vibration which had to be assigned reasonable values.

The major skeletal angles, FPF, PNC and FPN, refined satisfactorily, as did the amplitudes of vibration for the non-bonded distance P · · · C. The amplitudes of vibration for the F · · · F and F · · · N distances refined as a single parameter. Of the parameters involving hydrogen, only the C—H bonded distance and the NCH angle could be refined.

Assuming the presence of only one conformer, the PF_2 twist angle refined satisfactorily to ca. 171°, with the two C · · · F amplitudes of vibration refining as a single parameter. After completing refinements with one conformer only, a series of refinements was carried out with fixed small amounts of a second conformer, the $-PF_2$ twist angle of which was fixed initially at values in the range 0—180°, and latterly in the range 65—105°. The variation of R factor with amount of second conformer and twist angle is shown in Fig. 2. Some refinements were carried out with the $-CH_3$ twist angle fixed at values other than 0°. Varying this angle proved to have no significant effect on the refining parameters.

The final molecular parameters are listed in Table 2, and the least-squares correlation matrix in Table 3. The molecular scattering intensity curves are shown in Fig. 3 and the structures of the two conformers of $PF_2(NHMe)$ are depicted in Fig. 4.

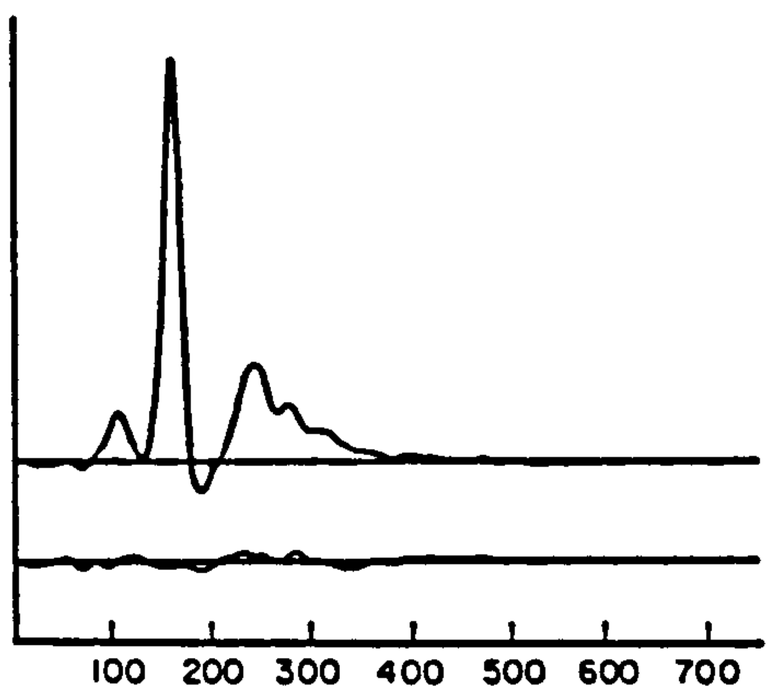

Fig. 1. Observed and final difference radial distribution curve $P(r)/r$, calculated with a damping factor of 0.000015 nm^{-2}.

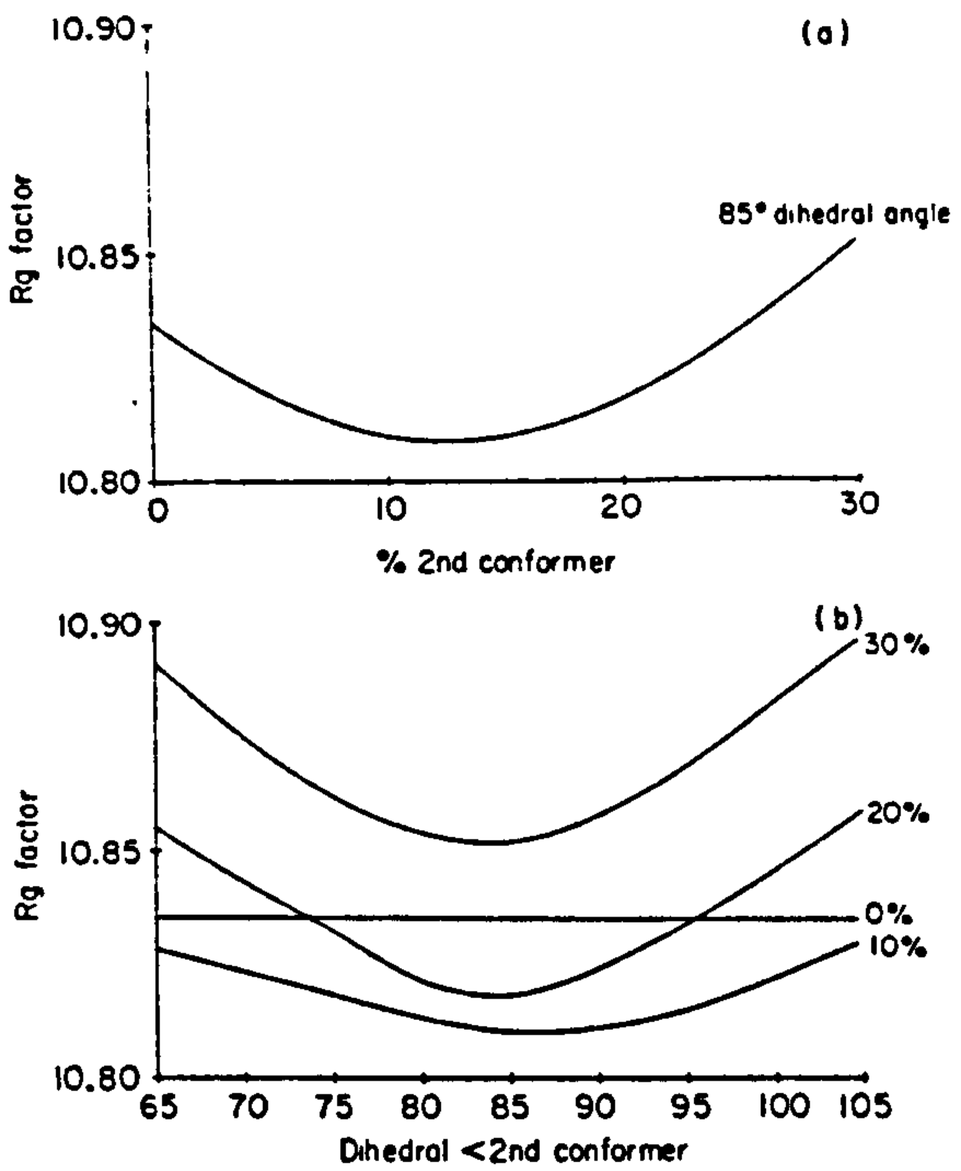

Fig. 2. Variation of R factor (R_g/R_g(min)) with proportion and twist angle of second conformer. (a) Fixed angle and varying percentages. (b) Fixed percentages and varying angles.

RESULTS AND DISCUSSION

The parameters found for the skeletal group F_2PN are in good agreement with those found for closely related compounds (see Table 4). The P—N bond length is towards the lower end of the expected range, and the P—F distance is similarly long. However, the non-bonded distances F · · · F and F · · · N have values consistent with hard sphere radii [13], and as a consequence the FPF angle is fairly small and the FPN angle is quite wide. The wide PNC angle can similarly be explained in terms of P · · · C contacts.

No evidence could be obtained regarding the location of the imino hydrogen, but considering the wide PNC angle found (ca. 125°), we believe that our assumption concerning a planar arrangement of ligands about nitrogen is likely to be correct.

The twist angle of the $-PF_2$ group of the major conformer refined to 171.4(20)°. It is probable that the average twist angle of this conformer is 180°, and that torsional vibration about the mean position gives rise to a substantial shrinkage effect. In this configuration, fluorine atoms lie close enough to methyl protons for there to be some stabilizing effect from weak H · · · F interactions. The shortest H · · · F distances for a $-PF_2$ twist angle of 170° vary between 250 pm and 279 pm, depending on the orientation of the CH_3

TABLE 2

Molecular parameters for $PF_2(NHMe)$[c]

	Distances (pm)	Amplitude (pm)
(A) Independent distances		
$r1$ (P—F)	159.3(4)	4.9(Fixed)
$r2$ (P—N)	164.8(7)	4.5(Fixed)
$r3$ (N—H)	100.0(Fixed)	7.5(Fixed)
$r4$ (C—N)	144.8(12)	4.4(Fixed)
$r5$ (C—H)	107.8(20)	7.7(Fixed)
(B) Dependent distances		
$d6$ (F · · · F)	233.2(15)	8.8(12)
$d7$ (F · · · N)	249.5(10)	8.8 tied to $u6$
$d8$ (F · · · (N)H)[a]	334.3(18)	15.0(Fixed)
$d9$ (F · · · (N)H)[a]	343.3(30)	15.0(Fixed)
$d10$ (C · · · F)[a]	295.1(40)	16.2(30)
$d11$ (C · · · F)[a]	328.1(30)	16.2 tied to $u10$
$d12$ (F · · · (C)H)[a]	397.0(30)	16.0(Fixed)
$d13$ (F · · · (C)H)[a]	405.3(30)	16.0(Fixed)
$d14$ (F · · · (C)H)[a]	327.2(25)	16.0(Fixed)
$d15$ (F · · · (C)H)[a]	283.5(30)	16.0(Fixed)
$d16$ (F · · · (C)H)[a]	270.2(29)	16.0(Fixed)
$d17$ (F · · · (C)H)[a]	353.7(40)	16.0(Fixed)
$d18$ (P · · · (N)H)	229.5(10)	11.0(Fixed)
$d19$ (P · · · C)	275.2(15)	8.0(10)
$d20$ (P · · · (C)H)	367.0(30)	12.0(Fixed)
$d21$ (P · · · (C)H)	308.1(40)	12.0(Fixed)
$d22$ (P · · · (C)H)	308.1(40)	12.0(Fixed)
$d23$ (N · · · (C)H)	212.3(25)	11.0(Fixed)
$d24$ (C · · · (N)H)	209.7(13)	11.0(Fixed)
$d25$ ((C)H · · · (C)H)	170.8(50)	12.0(Fixed)
$d26$ ((N)H · · · (C)H)	233.2(50)	18.0(Fixed)
$d27$ ((N)H · · · (C)H)	284.3(29)	18.0(Fixed)
$d28$ ((N)H · · · (C)H)	284.3(25)	18.0(Fixed)
$d29$ (C · · · F)[b]	300.7(23)	16.2 tied to $u10$
$d30$ (C · · · F)[b]	381.2(18)	16.2 tied to $u10$
(C) Independent angles (°)		
$\angle 1$ F—P—F	94.1(8)	
$\angle 2$ F—P—N	100.6(4)	
$\angle 3$ P—N—C	125.3(20)	
$\angle 4$ N—C—H	113.8(25)	
$\angle 5$ P—N—H	118.0(Fixed)	
$\angle 6$ PF_2 Twist, major conformer	171.4(20)	
$\angle 7$ PF_2 Twist, minor conformer	85.0(Fixed)	
$\angle 8$ CH_3 Twist	0.0(Fixed)	

[a]Major conformer only. [b]Minor conformer only. [c]Quoted errors are estimated standard deviations derived from the least-squares analysis and increased to allow for systematic errors.

TABLE 3

Least-squares correlation matrix multiplied by 100

r1	r2	r4	r5	∠1	∠2	∠3	∠4	∠6	u6	u10	u19	k1	k2	k3	
100	−85	71	−35	−10	20	−41	34	1	−13	−12	−10	−83	−63	−16	r1
	100	−54	31	−3	−21	42	−38	−5	8	13	14	81	63	70	r2
		100	−21	−5	36	−43	27	−11	−12	−8	−8	−75	−63	−17	r4
			100	10	10	39	−41	−2	15	11	6	42	31	4	r5
				100	−42	−41	28	13	14	5	−1	2	−14	−18	∠1
					100	14	−16	−27	−63	−25	−25	−18	−14	−6	∠2
						100	−80	−8	−8	27	12	55	61	26	∠3
							100	−41	2	−32	7	−49	−54	−24	∠4
								100	18	33	−28	6	9	7	∠6
									100	27	29	15	8	−2	u6
										100	10	15	17	6	u10
											100	10	10	8	u19
												100	70	20	k1
													100	22	k2
														100	k3

group. This compares with the sum of the van der Waals' radii for hydrogen and fluorine of 255 pm.

Two N—H stretching vibrations are evident in the room temperature infrared spectrum of $PF_2(NHMe)$, the major peak occurring at 3467 cm^{-1} and the other at 3417 cm^{-1}. The infrared spectrum of the solid phase at 77 K shows the presence of only one N—H stretching vibration, at 3430 cm^{-1}. From the evidence presented in Fig. 2 we deduced that the data are consistent with the possible existence of a second conformer, with a $-PF_2$ dihedral angle of ca. 85° and an abundance at room temperature of up to 20%.

In this second conformer there are contacts of 260 pm for one fluorine atom and the proton on nitrogen, and between 263 pm and 296 pm for one fluorine and the closest methyl proton, depending on the twist angle of the $-CH_3$ group. This configuration corresponds to that of the major conformer found for the compound $PF_2[NH(SiH_3)]$ [3], which has a $-PF_2$ twist angle of 90° and one (Si)H · · · F contact at 267 pm and one (N)H · · · F contact at 252 pm. However, in that case the second conformer has a twist angle of 26° which gives rise to only (N)H · · · F contacts. The absence of a 180° conformer can be explained in terms of the longer Si—H and Si—N bonds, in conjugation with the wide PNSi angle, precluding any (Si)H · · · F contact with the twist angle in this region.

We find, therefore, that weak H · · · F interactions seem to determine the preferred conformation in PF_2—N compounds, with (M)H · · · F contacts appearing to predominate over (N)H · · · F contacts (M = C or Si).

TABLE 4

Structural parameters of some aminodifluorophosphines

Compound	Technique	Ref.	Parameter (distances in pm, angles in degrees)						
			r(P—N)	*r*(P—F)	*r*(C—N)	∠(F—P—F)	∠(N—P—F)	∠(M—N—P)	Shortest *r*((M)H···F)
$NMe(PF_2)_2$	Electron diffraction	1	168.0(6)	158.3(2)	147.9(17)	95.1(3)	99.6(3)	122.0(4)	
NMe_2PF_2	X-ray diffraction	7	162.8(5)	161.0(4)	146.0(9)	91.5(3)	101.6(2)	120.4(5)[a] 123.7(5)[b]	
	Electron diffraction	4	168.4(8)	158.9(3)	144.8(6)	99 (3)	97 (4)	118.3(6)	253(6)
	Microwave	5	166	157	148[c]	95.3	99.8	121.3[a] 124.5[b]	
$PF_2(NH_2)$	Electron diffraction	4	166.1(7)	158.1(3)		95.3(11)	101.1(11)		262.3(15)
	Microwave	6	165.0(4)	158.7(4)		94.6(2)	100.6(2)		
$PF_2[NH(SiH_3)]$	Electron diffraction	3	165.4(6)	157.5(3)		100.8(12)	95.6[d]	127.9(7)	267(3)
$N(PF_2)_3$	Electron diffraction	2	171.1(4)	157.4(2)		96.9(3)	99.2(3)		
$NH(PF_2)_2$	X-ray diffraction	9	166.7(10)	157.8(5)		95.7(4)	99.4(4)		
$PF_2(NHMe)$	Electron diffraction	this work	164.8(7)	159.3(4)	144.8(12)	94.1(8)	100.6(4)	125.3(20)	250[e]

[a]Fluorines *trans* to carbons. [b]Fluorines *cis* to carbons. [c]Assumed. [d]See ref. 3. [e]Two conformers — see text.

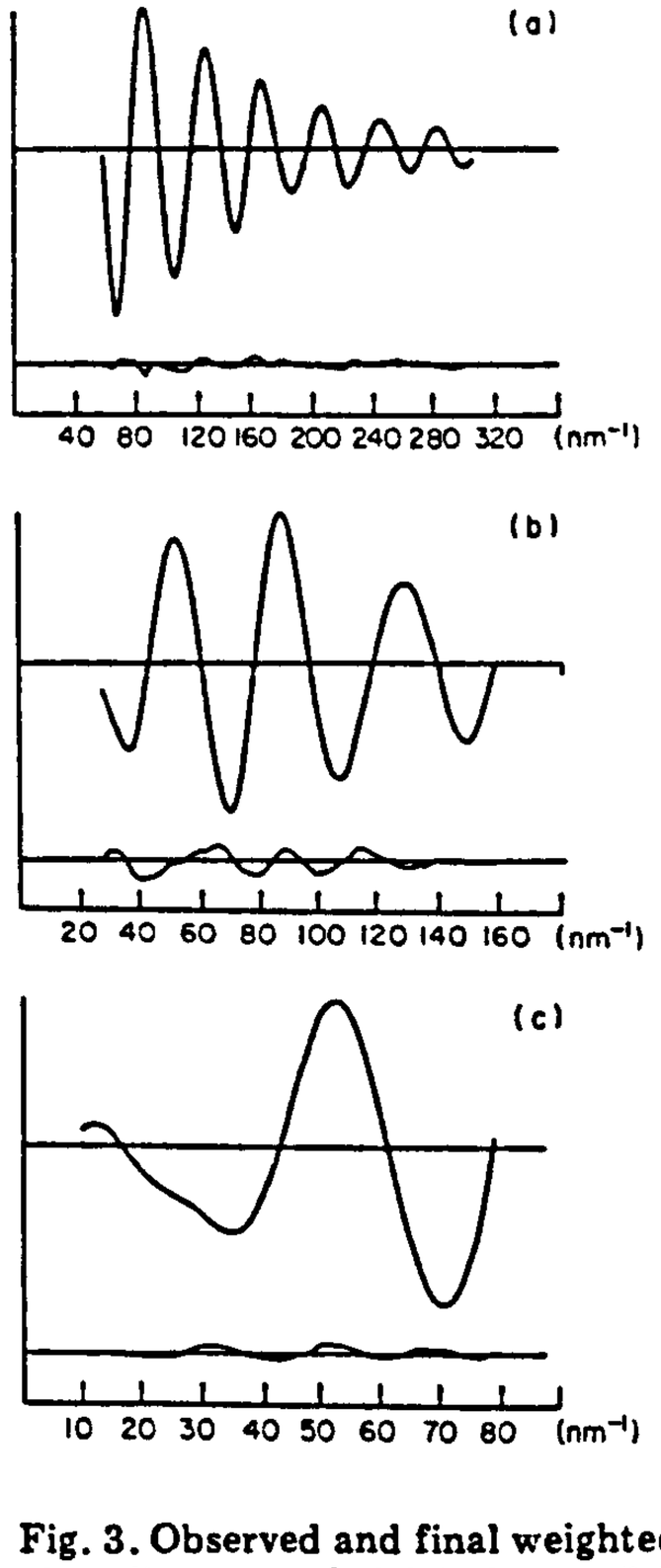

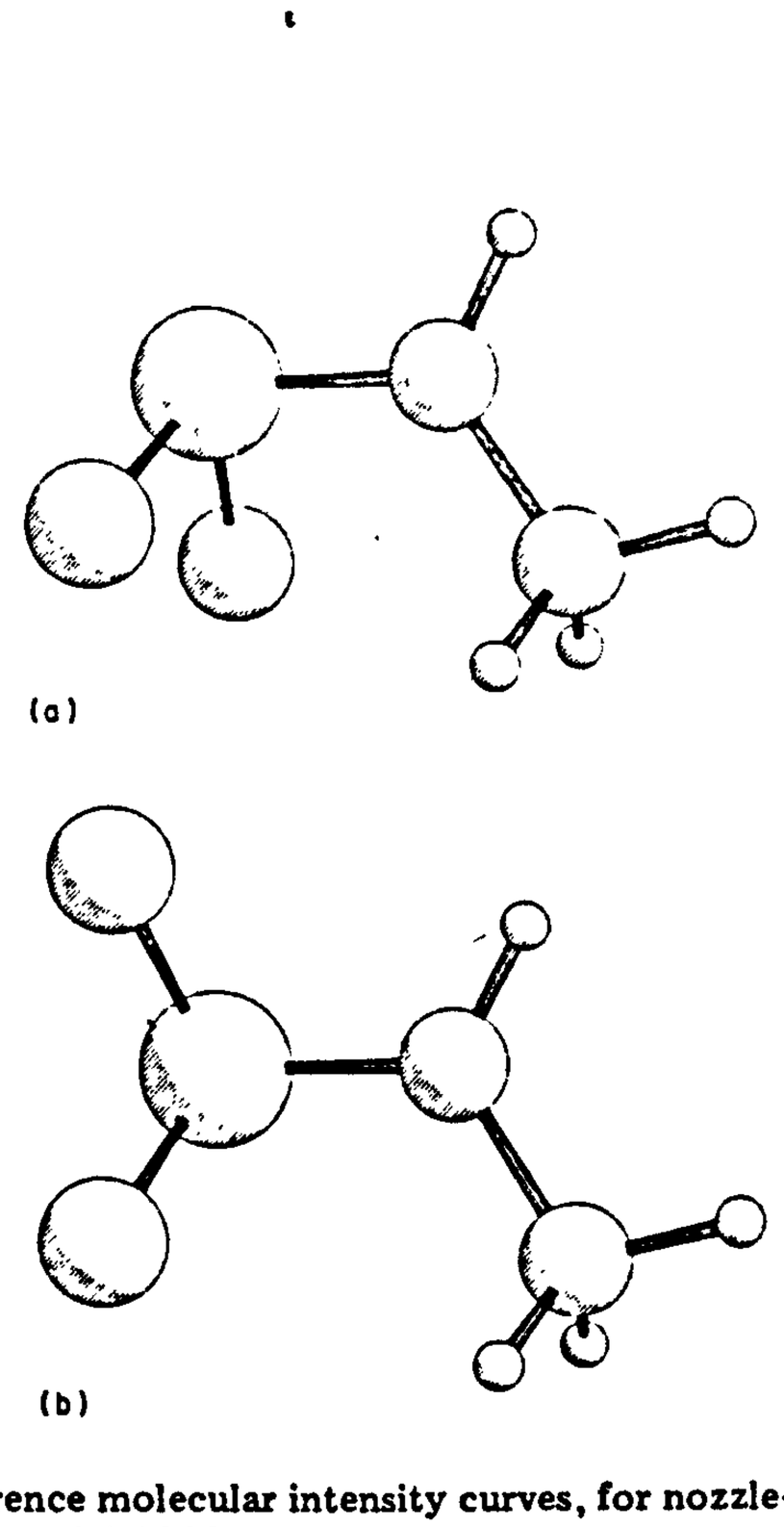

Fig. 3. Observed and final weighted difference molecular intensity curves, for nozzle-to-plate distances of: (a) 250 mm, (b) 500 mm, (c) 1000 mm.

Fig. 4. Structures of $PF_2[NH(CH_3)]$. (a) Major conformer (PF_2 twist 171°). (b) Minor conformer (PF_2 twist 85°).

ACKNOWLEDGEMENTS

We thank Professor D. W. J. Cruickshank and Dr. B. Beagley for provision of experimental facilities, and Mrs. V. Ulbrecht for practical assistance. One of us (G. S. L.) thanks the Science Research Council for a research studentship. We thank Mr. S. G. D. Henderson for preparing the sample of $PF_2(NHMe)$.

REFERENCES

1 E. Hedberg, L. Hedberg and K. Hedberg, J. Am. Chem. Soc., 96 (1974) 4417.
2 D. E. J. Arnold, David W. H. Rankin, R. Seip and M. R. Todd, J. Chem. Soc., Dalton Trans., in press.
3 D. E. J. Arnold, E. A. V. Ebsworth, H. F. Jessep and D. W. H. Rankin, J. Chem. Soc., Dalton Trans., (1972) 1681.

4 G. C. Holywell, D. W. H. Rankin, B. Beagley and J. M. Freeman, J. Chem. Soc. A, (1971) 785.
5 P. Forti, D. Damiani and P. G. Favero, J. Am. Chem. Soc., 95 (1973) 756.
6 A. H. Brittain, J. E. Smith, P. L. Lee, K. Cohn and R. H. Schwendeman, J. Am. Chem. Soc., 93 (1971) 6772.
7 E. D. Morris and C. E. Nordman, Inorg. Chem., 8 (1969) 1673.
8 D. E. J. Arnold and D. W. H. Rankin, J. Chem. Soc., Dalton Trans., 10 (1975) 889.
9 M. J. Barrow, E. A. V. Ebsworth, M. M. Harding and S. G. D. Henderson, J. Chem. Soc., Dalton Trans., to be published.
10 J. S. Harman and D. W. A. Sharp, J. Chem. Soc. A, (1970) 1935.
11 D. M. Bridges, G. C. Holywell, D. W. H. Rankin and J. M. Freeman, J. Organomet. Chem., 32 (1971) 87.
12 L. Schäfer, A. C. Yates and R. A. Bonham, J. Chem. Phys., 55 (1971) 3055.
13 L. S. Bartell, J. Chem. Phys., 32 (1960) 827.

Gas-phase Molecular Structure of Bis(difluorophosphino)amine, determined by Electron Diffraction

By Christopher M. Huntley, Graham S. Laurenson, and David W. H. Rankin,* Department of Chemistry, King's Buildings, University of Edinburgh, Edinburgh EH9 3JJ

Reprinted from

JOURNAL
OF
THE CHEMICAL SOCIETY

DALTON TRANSACTIONS

1980

Gas-phase Molecular Structure of Bis(difluorophosphino)amine, determined by Electron Diffraction

By Christopher M. Huntley, Graham S. Laurenson, and David W. H. Rankin,* Department of Chemistry, King's Buildings, University of Edinburgh, Edinburgh EH9 3JJ

The molecular geometry of bis(difluorophosphino)amine, $NH(PF_2)_2$, in the gas phase has been studied by electron diffraction. Principal parameters are: r_a(P–F) 158.4(3), r_a(P–N) 168.4(8) pm; FPF 95.6(10), FPN 98.3(7), and PNP 122.1(7)°. Two conformers are present in the vapour at room temperature. The predominant form (72%) has almost C_{2v} symmetry, but the PF_2 groups are twisted 5° away from most symmetrical positions. In the less abundant form, one PF_2 group is twisted by 60° from the C_{2v} position but the other only by 5°.

Of the three difluorophosphino-amines, only two have had their gas-phase molecular structures determined. The primary amine, $NH_2(PF_2)$, has been shown by both electron diffraction [1] and microwave spectroscopy [2] to adopt a conformation in which the axes of the phosphorus and nitrogen lone pairs of electrons are orthogonal. The microwave study indicated that the nitrogen atom had planar co-ordination, but in the electron-diffraction results the hydrogen-atom positions were not well defined, although there was some evidence that the PNH_2 group was not planar.

In the case of the tertiary amine, $N(PF_2)_3$, an electron-diffraction study [3] has shown that the NP_3 skeleton is planar, and that each phosphorus lone-pair orbital is orthogonal to the nitrogen lone-pair $2p$ orbital. The conformation of the molecule is such that the overall symmetry is C_{3h}, with the phosphorus lone pairs as far away from each other as possible. This structure contrasts with that of $NMe(PF_2)_2$,[4] which has the lone pairs as close together as possible, with C_{2v} symmetry for the $CN(PF_2)_2$ fragment. The structure of the secondary amine is therefore of particular importance. The vibrational spectra of this compound in the gas phase [5] show two N–H stretching and two in-plane N–H deformation modes, suggesting that two conformers are present. However, a study [6] of the crystalline solid at 160 K indicates that only one conformer is present, the molecules having almost exact C_{2v} symmetry. We have therefore investigated the molecular structure of the secondary amine in the gas phase, to see whether we can identify two distinct conformers.

EXPERIMENTAL

Attempts to prepare bis(difluorophosphino)amine using the published procedure [6] were unsuccessful. Tris(difluorophosphino)amine did not react with HCl, HBr, or H_2S in the gas or liquid phase, over a period of several days at room temperature. Having re-examined the original vibrational spectra, which are perfectly satisfactory, we can only conclude that the acid cleavage of the tertiary amine is catalysed by some material which was not present in recently prepared samples. The secondary amine was therefore prepared by treating a four-fold excess of aminodifluorophosphine with bromodifluorophosphine and trimethylamine, and destroying the excess of primary amine from the mixture of primary and secondary amines with hydrogen bromide. The purity of the sample prepared in this way was checked by i.r. and n.m.r. spectroscopy.

Electron-diffraction scattering intensities were recorded photographically using the Cornell University diffraction apparatus,[7] now installed at the University of Edinburgh. The apparatus was operated in the conventional convergent beam mode, with a sector designed to give uniform scattering intensity from carbon atoms. With an accelerating potential of 44 kV and nozzle-to-plate distances of 128 and 285 mm, data were obtained over a range of the scattering variable s of 30—350 mm^{-1}. Data were recorded on Kodak Electron Image plates (three plates at each camera distance were used), with the sample at 228 K and the nozzle at 295 K. The background pressure was 5×10^{-7} Torr,† and was maintained at 3×10^{-6} Torr during exposures. The electron wavelength was determined from the scattering pattern of gaseous benzene, recorded immediately before the amine patterns were recorded.

TABLE 1

Weighting functions, correlation parameters, and scale factors

Camera height / mm	Wavelength / pm	Scale factor	Δs	$s_{min.}$	s_1	s_2	$s_{max.}$	Correlation parameter
					nm^{-1}			
128.47	5.707	0.847(9)	4	60	80	300	340	0.126
284.76	5.719	0.797(11)	2	34	44	118	146	0.496

The photographic intensities were obtained in digital form using a Jarrell–Ash double-beam microphotometer,[8] with spinning plates. All calculations were carried out using an ICL 2970 computer at the Edinburgh Regional Computing Centre. The data reduction program used was a version of an established program,[9] modified to handle data from the Jarrell–Ash microdensitometer. The least-squares refinement program is a new version of an established program,[1] which uses an off-diagonal weight matrix to allow for correlation between data points. The weighting points used in setting up that matrix are given in Table 1, together with correlation parameters and other experimental details. In all calculations, the complex scattering factors of Schäfer *et al.*[10] were used.

† Throughout this paper: 1 Torr = (101 325/760) Pa.

Refinement.—In the early stages of refinement the molecular model used allowed for the presence of only a single conformer. The basic structure had C_{2v} symmetry and was defined in terms of P–F, P–N, and N–H distances, and FPF, FPN, and PNP angles. The hydrogen atom was assumed to lie in the PNP plane. Distortion from C_{2v} symmetry (with the FPF angle bisectors eclipsing the N–H bond) was possible by twisting the PF_2 groups around the P–N bonds. These two twists could be constrained to be equal, or equal and opposite, giving structures of C_2 or C_s symmetry. Using this model, the principal bond lengths and angles refined readily, and the best fit (R_G = 0.067) was obtained for a C_2 structure, with PF_2 groups twisted 5° from the C_{2v} positions.

The model was then modified so that a variable amount of a second conformer, differing from the first only in the PF_2 twist angles, could be included. As it was not feasible to investigate all combinations of the four twist angles defining two conformations and the relative proportions of the two, some constraints on the twist angles were applied. All possible mixtures of conformations that could be described by two twist angles and a proportionality factor were explored. There was no significant reduction of the R factor for any amount of a second conformer with C_2 or C_s symmetry including those forms (of C_s and C_{2v} symmetry respectively) in which one or more of the phosphorus lone pairs eclipse the N–H bond. However, a considerable

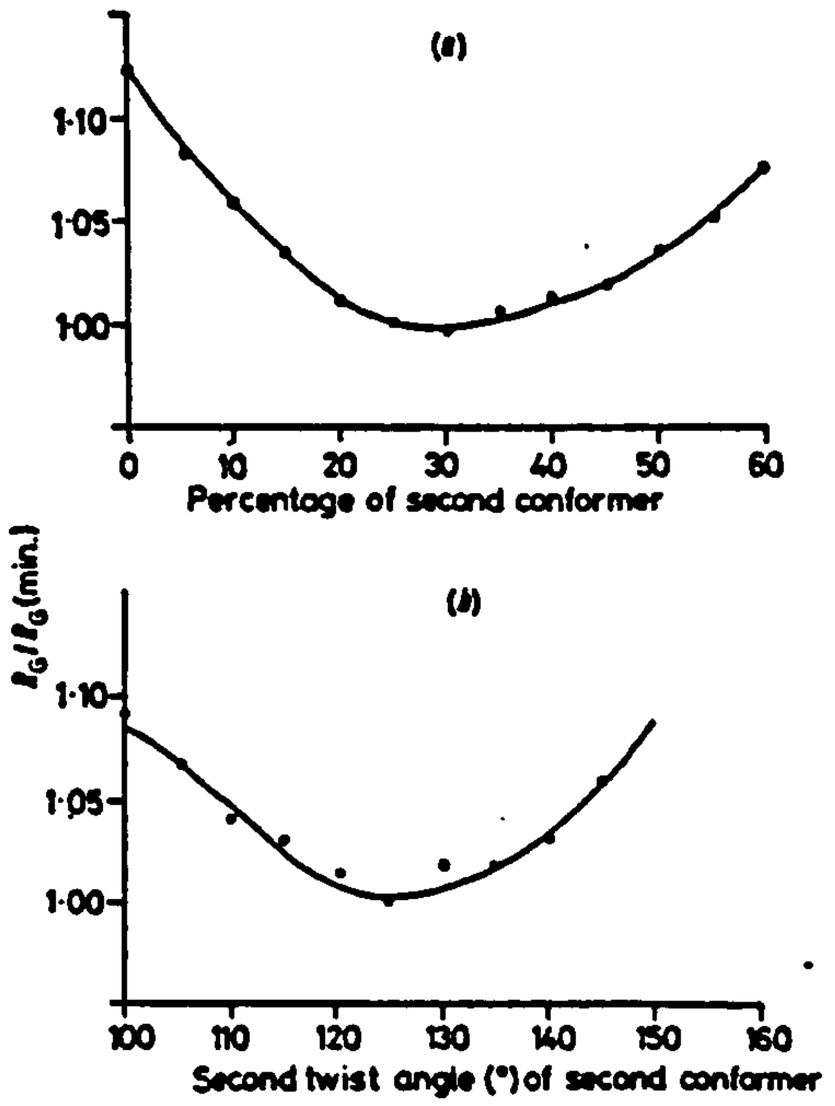

FIGURE 1 Variations of the R factor with (*a*) percentage of second conformer present and (*b*) second twist angle in the second conformer

improvement was obtained when it was assumed that the second conformer had one angle which was the same as those in the major form, and the second angle was treated as a variable. In Figure 1 the variations of the R factor with this angle and with the percentage of the second conformer are shown. The lowest R factor (0.057) was obtained for 27.5% of a form with twist angles of 5 and 58°.

RESULTS AND DISCUSSION

The results of the final refinement are given in Table 2. All distances quoted are r_a, and errors are estimated standard deviations obtained in the least-squares analysis, increased to allow for systematic errors. The

TABLE 2

Molecular parameters for $NH(PF_2)_2$

	Distance/pm	Amplitude/pm
(*a*) Independent geometrical parameters		
r_1(P–F)	158.4(3)	5.6(4)
r_2(P–N)	168.4(8)	6.8 (tied to u_1)
r_3(N–H)	97.3(23)	5.7(24)
	Angle/°	
Angle 1 (F–P–F)	95.6(10)	
Angle 2 (F–P–N)	98.3(7)	
Angle 3 (P–N–P)	122.1(7)	
Angle 4 (twist 1) [a]	5.3(13)	
Angle 5 (twist 2) [b]	58 [e]	
% of conformer 2	27.5 [e]	
(*b*) Dependent distances		
d_6(F ··· F)	234.8(9)	7.4(7)
d_8(F ··· N)	247.3(11)	9.2 (tied to u_4)
d_9(P ··· P)	294.8(14)	10.0(7)
d_7(P ··· F) [d]	387.6(27)	12.4(6)
d_8(P ··· F) [d]	395.5(30)	
d_9(P ··· F) [e]	333.0(25)	
d_{10}(P ··· F) [e]	409.7(24)	
d_{11}(F ··· F) [f]	436(4)	15.7(20)
d_{12}(F ··· F) [f]	494(2)	13.4(20)
d_{13}(F ··· F) [e]	379(3)	15.7 (tied to u_{11})
d_{14}(F ··· F) [e]	469(3)	13.4 (tied to u_{12})
d_{15}(F ··· F) [e]	470(3)	13.4 (tied to u_{12})
d_{16}(F ··· F) [e]	485(4)	15.7 (tied to u_{11})
d_{17}(P ··· H)	231.7(22)	11.0 (fixed)
d_{18}(F ··· H) [d]	250—310	18.4(80)

[a] Twist angle for both PF_2 groups of major conformer, and for one group of second conformer. [b] Twist angle for one PF_2 group of second conformer. [c] See text. [d] Both conformers. [e] Minor conformer only. [f] Major conformer only.

final least-squares correlation matrix (Table 3) shows several strong correlations between parameters caused by overlap of the P–F and P–N and F ··· F and F ··· N peaks in the radial distribution curve (Figure 2). The intensity data and final weighted difference curves are shown in Figure 3.

Some structural parameters for some aminodifluorophosphines are compared in Table 4. It is clear that there is very little variation of P–F distances and FPF and FPN angles in the series of compounds, but that the P–N bond lengths increase from around 165 pm in amines with one PF_2 group to 168 pm in amines with two PF_2 groups to 171 pm in $N(PF_2)_3$. This may be interpreted in terms of $(p\rightarrow d)\pi$ bonding, with competition between phosphorus atoms for the nitrogen lone pair of electrons, or in terms of non-bonded contacts between phosphorus atoms. The P ··· P distance in $NH(PF_2)_2$ is 295 pm, with a PNP angle of 122°, but in $N(PF_2)_3$ the maximum possible PNP angle is 120° and as the P ··· P distance of 296 pm is essentially the same the long P–N bond length may be explained. The short P ··· P distance (285 pm) in $NMe(PF_2)_2$,[4] associated with a PNP angle of 116°, is an enigma.

The very close agreement of X-ray [6] and electron-

diffraction results for the main geometrical parameters indicates that, although the conformation may change between gaseous and crystalline phases, there is very little distortion of bond lengths and inter-bond angles. This is to be expected, as the *X*-ray study showed that there were no strong intermolecular contacts.

The conformations adopted by bis(difluorophosphino)-amine are of particular interest. The predominant gas-phase form is very similar to that found in the crystalline

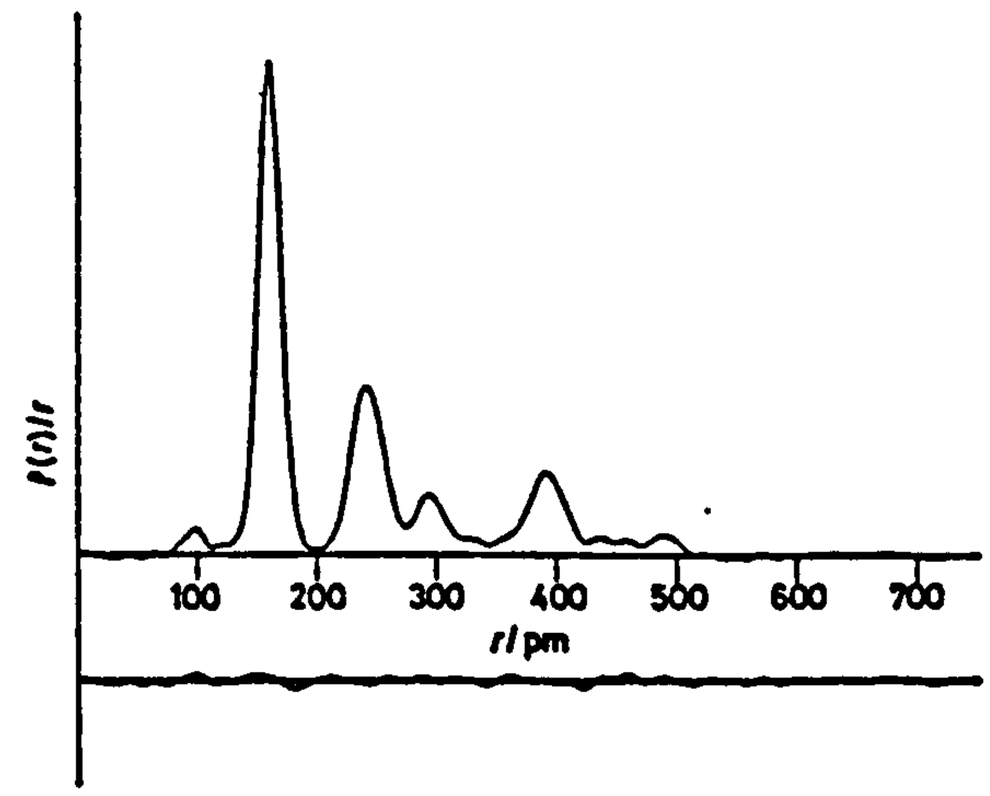

FIGURE 2 Observed and final difference radial distribution curves, $P(r)/r$, for $NH(PF_2)_2$, calculated with a damping factor of 0.000 015 nm^{-2}

solid. It seems highly likely that the gas-phase form has C_{2v} symmetry, and that the apparent 5° twist angles observed are shrinkage effects caused by torsional vibrations of the PF_2 groups. In this form there are four intramolecular F···H contacts of 263—270 pm, and these may provide the weak attractive forces that stabilise this arrangement. In the solid there are additional intermolecular F···H contacts: these do not appear to affect the structure of individual molecules, but only the packing arrangement.

The existence of two N–H stretching and two N–H in-plane deformation bands in the gas-phase i.r. spectrum

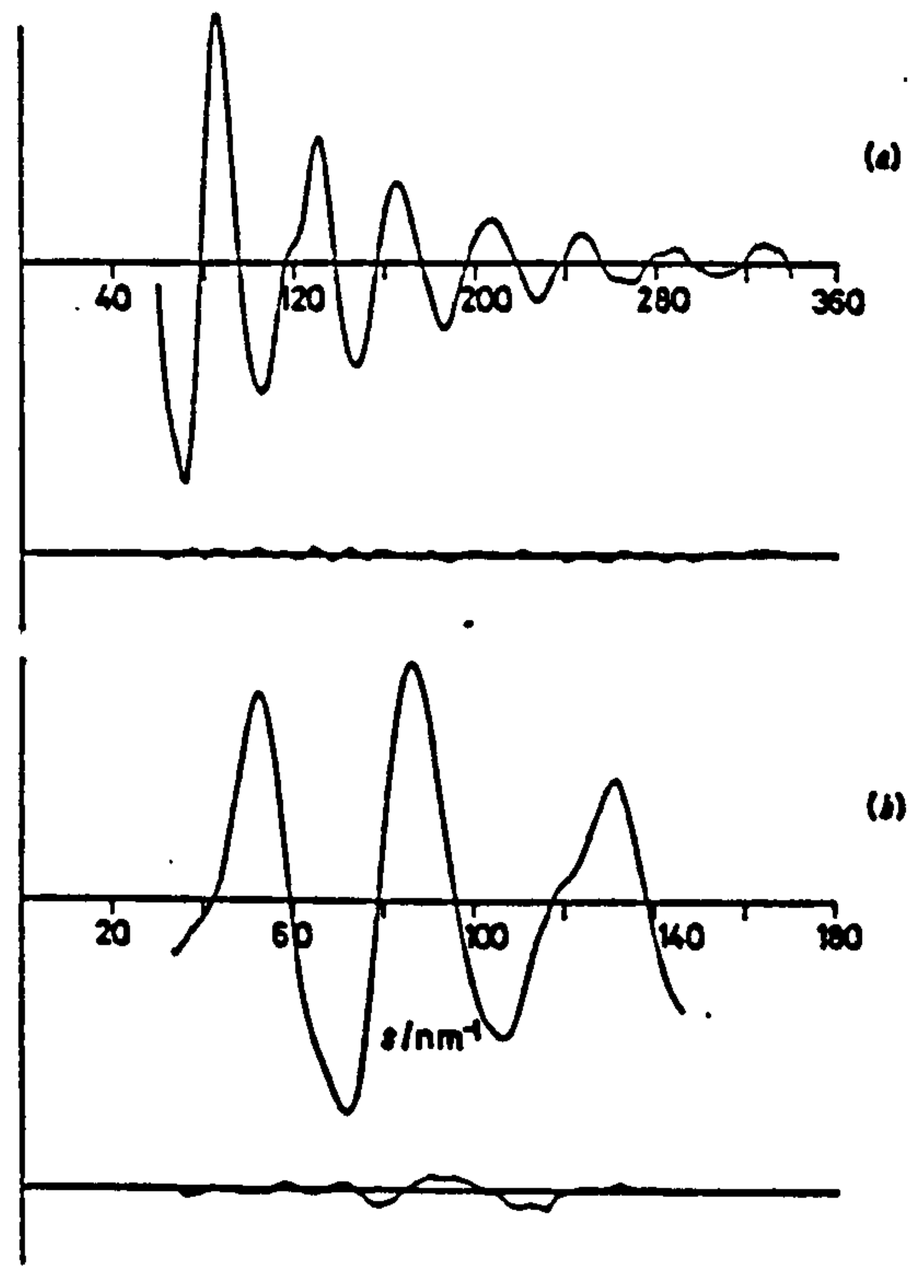

FIGURE 3 Observed and final weighted difference molecular-intensity curves, for nozzle-to-plate distances of (*a*) 128 and (*b*) 285 mm

of $NH(PF_2)_2$ [5] indicated that two conformers probably existed in the gas phase. This has now been confirmed by the structural study. In the less abundant form, one PF_2 group is twisted about 60° from the C_{2v} position. Why this particular structure should be favoured is not clear, but it should be noted that one F···H contact is

TABLE 3

Least-squares correlation matrix, multiplied by 100

	r_1	r_2	r_3	Angle 1	Angle 2	Angle 3	Angle 4	u_1	u_3	u_4	u_6	u_7	u_{11}	u_{12}	u_{17}	k_1	k_2	
r_1	100		−27			41		54										r_1
r_2		100		−23	54	−21	−47			−34	33	25			56			r_2
r_3			100															r_3
Angle 1				100	−47		−66	−24			−28		33	27	−35			1
Angle 2					100	−37				48	42				81	28		2
Angle 3						100		49							−23	−27		3
Angle 4							100			22			−49		−22			4
u_1								100								43		u_1
u_3									100									u_3
u_4										100					39	36	26	u_4
u_6											100				58			u_6
u_7												100	26			21		u_7
u_{11}													100					u_{11}
u_{12}														100				u_{12}
u_{17}															100			u_{17}
k_1																100	32	k_1
k_2																	100	k_2

Only correlations with absolute values greater than 0.2 are included.

TABLE 4

Structural parameters of some aminodifluorophosphines

Compound	Technique	Bond distance/pm		Angle/°			Ref.
		r(P–F)	r(P–N)	FPF	FPN	PNP	
$NH_2(PF_2)$	ED	158.1(3)	166.1(7)	95.3(11)	101.1(11)		1
	MW	158.7(4)	165.0(4)	94.6(2)	100.6(2)		2
$NMeH(PF_2)$	ED	159.3(4)	164.8(7)	94.1(8)	100.6(4)		11
$NH(PF_2)_2$	ED	158.4(3)	168.4(8)	95.6(10)	98.3(7)	122.1(7)	This work
$NH(PF_2)_2$	X	157.8(5)	166.7(10)	95.7(4)	99.4(4)	120.7(4)	6
$NMe(PF_2)_2$	ED	158.3(2)	168.0(6)	95.1(3)	99.6(3)	116.1(8)	4
$N(PF_2)_3$	ED	157.4(2)	171.2(4)	97.1(5)	99.0(4)	120.0	3

ED = Electron diffraction, gas phase; MW = microwave spectroscopy, gas phase; X = *X*-ray diffraction, crystalline phase.

now at 250 pm, which is slightly less than the sum of the van der Waals radii of fluorine and hydrogen.

It is not possible to draw conclusions about the conformation in solution of bis(difluorophosphino)amine from the present work, but it is interesting to note that the coupling constant $^3J(PP')$ is much smaller for this compound [5] than for substituted bis(difluorophosphino)-amines [12,13] and that large couplings have been associated with strong interactions between lone pairs of electrons on phosphorus atoms.[14] The existence of a conformer in which this interaction is reduced by the twisting of one PF_2 group away from the position giving maximum lone-pair interaction may provide a rationalisation of the observed n.m.r. coupling constants. We have studied the Raman spectrum of liquid $NH(PF_2)_2$ and have observed two N–H stretching bands at 3 315 and 3 355 cm^{-1}, with an intensity ratio of *ca.* 5 : 1. Thus it seems likely that in condensed fluid phases the conformational properties relate more closely to those in the vapour than to those in the crystal.

One of us (G. S. L.) thanks the S.R.C. for a research studentship.

REFERENCES

[1] G. C. Holywell, D. W. H. Rankin, B. Beagley, and J. M. Freeman, *J. Chem. Soc.* (*A*), 1971, 785.
[2] A. H. Brittain, J. E. Smith, P. L. Lee, K. Cohn, and R. H. Schwendeman, *J. Amer. Chem. Soc.*, 1971, **93**, 6772.
[3] D. E. J. Arnold, D. W. H. Rankin, M. R. Todd, and R. Seip, *J.C.S. Dalton*, 1979, 1290.
[4] E. Hedberg, L. Hedberg, and K. Hedberg, *J. Amer. Chem. Soc.*, 1974, **96**, 4417.
[5] D. E. J. Arnold and D. W. H. Rankin, *J.C.S. Dalton*, 1975, 889.
[6] M. J. Barrow, E. A. V. Ebsworth, M. M. Harding, and S. G. D. Henderson, *J.C.S. Dalton*, 1979, 1192.
[7] S. H. Bauer and K. Kimura, *J. Phys. Soc. Japan*, 1962, **17**, 300.
[8] R. L. Hilderbrandt and S. H. Bauer, *J. Mol. Structure*, 1969, **3**, 325.
[9] D. M. Bridges, G. C. Holywell, D. W. H. Rankin, and J. M. Freeman, *J. Organometallic Chem.*, 1971, **32**, 87.
[10] L. Schäfer, A. C. Yates, and R. A. Bonham, *J. Chem. Phys.*, 1971, **55**, 3055.
[11] G. S. Laurenson and D. W. H. Rankin, *J. Mol. Structure*, 1979, **54**, 111.
[12] E. A. V. Ebsworth, D. W. H. Rankin, and J. G. Wright, *J.C.S. Dalton*, 1977, 2348.
[13] E. A. V. Ebsworth, D. W. H. Rankin, and J. G. Wright, *J.C.S. Dalton*, 1979, 1065.
[14] D. E. J. Arnold, E. R. Cromie, and D. W. H. Rankin, *J.C.S. Dalton*, 1977, 1999.

[9/1272 *Received*, 9th *August*, 1979]

Journal of Molecular Structure, 71 (1981) 217—226
Elsevier Scientific Publishing Company, Amsterdam — Printed in The Netherlands

THE MOLECULAR STRUCTURE OF DIFLUOROPHOSPHINE SELENIDE, DETERMINED USING A COMBINATION OF GAS ELECTRON DIFFRACTION AND LIQUID-CRYSTAL NMR DATA

ALAN S. F. BOYD, GRAHAM S. LAURENSON and DAVID W. H. RANKIN*

Department of Chemistry, University of Edinburgh, West Mains Road, Edinburgh EH9 3JJ (Gt. Britain)

(Received 8 September 1980)

ABSTRACT

The molecular structure of difluorophosphine selenide has been determined by a combined analysis of gas-phase electron diffraction data and dipolar couplings obtained for a solution in a nematic phase. Geometrical parameters (r_a) are: r(P=Se) 202.6(4), r(P—F) 155.7(3), r(P—H) 142.2(7) pm, ∠SePF 116.8(3), ∠FPF 98.1(7), ∠SePH 118.6(7)°.

INTRODUCTION

In the study of molecular structures in fluid phases it is often found that the technique chosen does not provide sufficient information to enable a complete structure to be determined. Microwave spectroscopy can give only a very limited number of rotational constants, and there may be absolute or practical restrictions on the number of isotopic substitutions that may be made. In the case of NMR studies of solutes in liquid crystals, the amount of structural information is strictly limited by the availability of spinning nuclei and the symmetry of the molecule, and in no case has the complete shape and size been determined. In electron diffraction studies of gases, even relatively simple structures may be only partially determined if there are light and heavy atoms present together. Thus it is frequently necessary for additional information to be used, and normally one or more parameters are assigned reasonable fixed values. However, it is preferable to use additional experimental data, and there have been successful determinations of structures using a combination of rotational constant and electron diffraction data [1—3], and rotational constants have also been used to provide overall scaling factors in liquid-crystal NMR studies [4]. In this paper we present the results of a study of PF_2HSe using electron diffraction data combined with dipolar coupling constants.

22—2860/81/0000—0000/$02.50

EXPERIMENTAL

A sample of PF_2HSe was prepared by the reaction of bromodifluorophosphine with hydrogen selenide in the presence of mercury [5], and purified by fractional condensation in vacuo. The purity was checked spectroscopically.

Electron diffraction

Electron diffraction intensities were recorded photographically on Kodak Electron Image plates using the Cornell/Edinburgh diffraction apparatus [6, 7] operating at 42 kV. The sample was maintained at 250 K and the nozzle at room temperature (293 K) during exposures. Data were collected using two camera distances, 128 mm (3 plates) and 287 mm (3 plates), and were converted to digital form using a Jarrell—Ash double-beam microphotometer [8] with spinning plates. The electron wavelength, 5.822 ± 0.003 pm, was determined from the diffraction pattern of gaseous benzene.

Liquid-crystal NMR

Initial trials to find a suitable liquid-crystal solvent were performed using solutions of trifluorophosphine in a variety of materials with nematic phases. By far the best solvents found were "Liquid Crystal E1" and "Liquid Crystal E8" (both B.D.H.), which are mixtures of 4-alkyl or alkoxy-4'-cyanobiphenyls. These solvents were unreactive, had wide and low temperature ranges for their nematic phases, and also gave higher orientation parameters than any other solvents tried. In this work, samples were prepared containing 0.2 mmol of PF_2HSe in ca. 0.3 ml of "E8" in 5 mm tubes, and these solutions had a nematic phase between 235 and 325 K.

All NMR experiments were carried out using a Varian Associates XL100 spectrometer in the pulse and Fourier transform mode. Double resonance experiments were carried out using the instrument's built-in decoupler. Since the degree of orientation and hence the magnitude of the dipolar couplings change rapidly with temperature, it was essential to maintain temperature stability and also to ensure that temperatures could be reproduced exactly from experiment to experiment. The former was achieved by using small volumes of solution, and by allowing thermal equilibrium to be attained. This was considered to have occurred when two successive spectra gave the same line positions. Self-consistent sets of couplings were obtained by observing one nucleus at approximately the required temperature, and in subsequent experiments adjusting the temperature so that known splittings were reproduced exactly.

Values of indirect coupling constants were measured in the isotropic phase at 333 K. In order to check any temperature variation of the indirect couplings, attempts were made to record spectra at 353 K, but the solute was thermally unstable, and only poor-quality ^{19}F spectra could be obtained.

However, the PF and FH couplings showed no temperature variation, and the couplings observed at 333 K have been used in the derivation of all dipolar couplings.

The relative signs of the couplings observed in spectra of the nematic phase were determined by double resonance experiments, listed in Table 1. As J(PF) is known to be large and negative in all fluorophosphines, it was assumed that $J_{PF} + 2D_{PF}$ was negative, and other signs were related to this. The signs of indirect couplings were taken from ref. 9.

Refinement of electron diffraction structure

Calculations were performed on ICL 2970 and 2980 computers, using an established data reduction program [7], and the complex scattering factors of Schäfer et al. [10]. In all structural refinements it was assumed that the PF_2HSe molecule had C_s symmetry. The geometry was then defined by six parameters, chosen to be the P—Se, P—F and P—H bonded distances, and the angles SePF, FPF and SePH.

Combined electron diffraction/NMR analysis

For the combined structural analysis the usual least-squares refinement program [11] was modified so that any experimental data relating to geometrical parameters or amplitudes of vibration could be included. For each problem studied a specific routine must be provided, so that theoretical values equivalent to the experimental data may be calculated. The derivatives of these with respect to the refining parameters are then evaluated numerically. In the case of liquid-crystal NMR, the addition data are dipolar couplings, which may be calculated using eqn. (1):

TABLE 1

Double resonance experiments

Experiment	Couplings related	Relative signs
$^1H-\{^{31}P\}$	FH and PF	Opposite
	SeP and SeH	Equal
$^{19}F-\{^{31}P\}$	FH and PH	Equal
	SeF and SeP	Equal
	FF and PF	Opposite
$^{19}F-\{^{77}Se\}$	PF and SeP	Equal
	FH and SeH	Opposite
	FF and SeF	Opposite

$$D_{ij} = \frac{-\gamma_i \gamma_j h}{8\pi^2 r_{ij}^3} [S_{zz}(3\cos^2\theta_{ijz} - 1) + (S_{xx} - S_{yy})(\cos^2\theta_{ijx} - \cos^2\theta_{ijy}) + 2S_{xz}(\cos\theta_{ijx}\ \cos\theta_{ijz}) + 2S_{yz}(\cos\theta_{ijy}\ \cos\theta_{ijz}) + 2S_{xy}(\cos\theta_{ijx}\ \cos\theta_{ijy})] \quad (1)$$

where D_{ij} is the dipolar coupling between atoms i and j, with magnetogyric ratios γ_i and γ_j and separation r_{ij}: the angles of the i—j vector with respect to the molecular axes are θ_{ijx}, θ_{ijy} and θ_{ijz}, and the orientation parameters are S_{zz}, $S_{xx} - S_{yy}$, S_{xz}, S_{yz} and S_{xy}. In the present case the x-axis was defined as parallel to the Se—P bond, and the z-axis was perpendicular to the plane of symmetry. Thus S_{xz} and S_{yz} are zero, and the other three orientation parameters were included in the list of refineable parameters. When dipolar couplings recorded at two temperatures were used, three more orientation parameters were included, and the number of additional observations was doubled.

This modified refinement program may also take account of rotational constants [12], predicate observations [13, 14], or any other structural data, and will refine structures based solely on these data, without any need for electron diffraction data.

The weights given to the additional observations are important. For the electron diffraction data, an off-diagonal weight matrix is used, for which the elements are as follows:

$w_{ii} = (s_i - s_{\min})/(sw_1 - s_{\min})$	$s_{\min} \leqslant s_i \leqslant sw_1$
$w_{ii} = 1$	$sw_1 \leqslant s_i \leqslant sw_2$
$w_{ii} = (s_{\max} - s_i)/(s_{\max} - sw_2)$	$sw_2 \leqslant s_i \leqslant s_{\max}$
$w_{ij} = 0$	$i \neq j \pm 1$
$w_{ij} = -0.5(w_{ii} + w_{jj})(p/h)_k$	$i = j \pm 1$

where sw_1 and sw_2 are weighting points for the distance k, and are chosen by inspection, and p/h is the correlation parameter [15]. The values of the weighting functions used, correlation parameters and scale factors, are given in Table 2. For the additional observations, the weight matrix is extended with diagonal terms only, chosen so that weights are inversely proportional to the squared uncertainty of the observation and are scaled to the standard deviation of the fit of the electron diffraction data points.

Vibrational averaging

As molecules at about ambient temperature are involved in vibrational motions with periods (10^{-12}—10^{-14} s) much shorter than the NMR time scale (ca. 10^{-3} s), it is necessary to average all the quantities in eqn. (1) over vibrational motions. Provided the molecular reorientation rate in the solution is

TABLE 2

Weighting functions, correlation parameters and scale factors

Camera height (mm)	Δ_s (nm^{-1})	s_{min} (nm^{-1})	sw_1 (nm^{-1})	sw_2 (nm^{-1})	s_{max} (nm^{-1})	p/h	Scale factor
128.2	4	64	80	240	272	0.046	0.870(16)
287.4	2	32	50	110	136	0.483	0.874(36)

slow compared to the vibration rate, the two motions are uncorrelated, and the distance determined in the experiment is simply $\langle r_{ij}^{-3} \rangle^{-1/3}$, which is labelled r_d [16]. The electron diffraction experiment gives distances r_a, which are $\langle r_{ij}^{-1} \rangle^{-1}$. Using the relationship [17]

$$\langle r^k \rangle^{1/k} = r_e + 3au^2/2 + (k-1)u^2/2r_e \quad (2)$$

gives

$$r_d = r_a + u^2/2r_e \quad (3)$$

where u is the amplitude of vibration for the atom pair and a is the anharmonic constant. As the correction term is small, the differences between amplitudes of vibration of different isotopic species may be ignored, and r_a may be used instead of r_e. In all refinements an r_a structure has been considered.

RESULTS AND DISCUSSION

NMR spectra

Two self-consistent sets of NMR data were obtained by the method described above from ^1H, ^{19}F and ^{31}P spectra recorded at 253 and 293 K. The

TABLE 3

Couplings in PF_2HSe[a]

Nuclei	J 333 K	J 353 K	Δ[b] 253 K	Δ[b] 293 K	D 253 K	D 293 K
$^{31}P-^{19}F$	−1193.0(1)	−1193.0(1)	−1018.2(4)	−1173.8(5)	+87.4(3)	+9.6(4)
$^{31}P-^{1}H$	+720.2(1)	[c]	+2791.4(10)	+2506.3(20)	+1035.6(6)	+893.1(11)
$^{77}Se-^{31}P$	−1029.5(1)	[c]	−1207.3(10)	−1157.8(6)	−88.9(6)	−64.2(4)
$^{19}F-^{19}F$	—	—	+1314.7(30)	+781.0(7)	+438.2(10)	+260.3(2)
$^{19}F-^{1}H$	+91.3(1)	+91.3(1)	+1443.7(2)	+1110.0(4)	+676.2(3)	+509.4(2)
$^{77}Se-^{19}F$	−97.5(1)	[c]	−262.3(4)	−217.8(8)	−82.4(3)	−60.2(5)
$^{77}Se-^{1}H$	−13(1)[d]	[c]	−125.2(20)	−86.0(15)	−56.1(11)	−36.5(8)

[a] All couplings in Hz. Estimated standard deviations are given in parentheses. [b] $J + 2D$ or $3D$. [c] Not studied. [d] Taken from ref. 9.

splittings observed in the first-order spectra, indirect couplings measured from spectra of isotropic solutions and derived direct coupling constants are listed in Table 3.

Refinement of structure using electron diffraction data only

Using electron diffraction data only, it is a straightforward matter to refine the four geometrical parameters defining the heavy-atom structure, and four associated amplitudes of vibration, as there are four distinct peaks in the radial distribution curve (Fig. 1). Under normal circumstances, the parameters involving the hydrogen atom would not be refined, but on this occasion they were included in the final refinement, the results of which are listed as Refinement A in Table 4. The final R-factors were 0.10 (R_G) and 0.09 (R_D): the least-squares correlation matrix is given in Table 5, and the molecular scattering intensity data are shown in Fig. 2.

Combined structure analysis

The liquid-crystal NMR data provided seven additional observations at each temperature, and three parameters were required to define the molecular orientation at each temperature. It was soon apparent that the two sets of dipolar couplings gave essentially identical results, and in subsequent work all the couplings were considered simultaneously. Thus it is clear that there can be no significant change in structure with temperature over the range studied. The coupling constants were given weights dependent on their uncertainties (standard deviations of the measurements), with two exceptions. It proved to be impossible to obtain a value for J(SeH) in isotropic solution, as the compound was too unstable at 333 K for a long run, necessary to

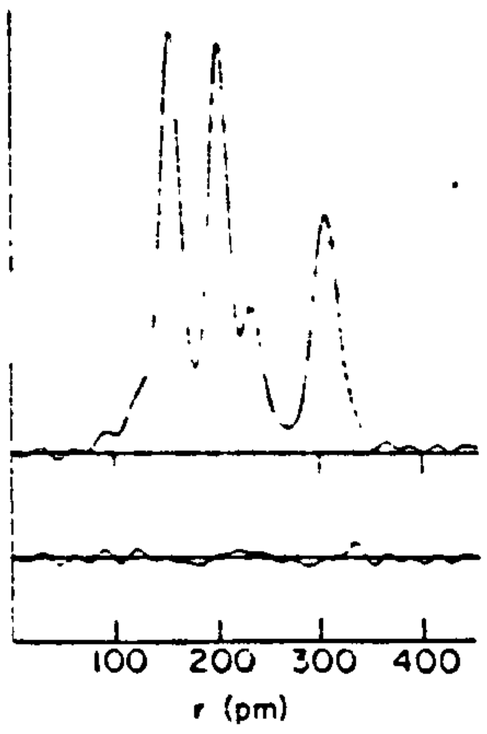

Fig. 1. Radial distribution curve, $P(r)/r$. Before Fourier inversion the data were multiplied by $s.\exp[(-0.00002s^2)(Z_{Se} - f_{Se})(Z_F - f_F)]$.

TABLE 4

Molecular parameters[a]

	Refinement A (ED only)		Refinement B (ED + NMR)	
	Distance (pm)	Amplitude (pm)	Distance (pm)	Amplitude (pm)
$r1$ P=Se	202.3(3)	4.9(5)	202.6(4)	4.8(6)
$r2$ P—F	155.8(2)	4.8(5)	155.7(3)	4.7(6)
$r3$ P—H	142.3(39)	8.5(fixed)	142.2(7)	8.5(fixed)
$r4$ Se · · · F	306.6(7)	8.3(6)	306.1(6)	8.4(7)
$r5$ F · · · F	234.6(8)	4.1(15)	235.2(10)	4.8(16)
$r6$ Se · · · H	313.1(110)	12.0(fixed)	298.0(8)	12.0(fixed)
$r7$ F · · · H	218.3(75)	13.0(fixed)	231.2(10)	13.0(fixed)
	Angle (°)		Angle (°)	
∠1 SePF	117.2(4)		116.8(3)	
∠2 FPF	97.7(5)		98.1(7)	
∠3 SePH	129.8(75)		118.6(7)	
			Orientation parameter	
$s1$ S_{zz}	(253 K)		−0.0535(5)	
$s2$ $S_{xx} - S_{yy}$	(253 K)		0.2173(23)	
$s3$ S_{xy}	(253 K)		0.0675(30)	
$s4$ S_{zz}	(293 K)		−0.0318(3)	
$s5$ $S_{xx} - S_{yy}$	(293 K)		0.1612(17)	
$s6$ S_{xy}	(293 K)		0.0581(21)	

[a]All distances are r_a. Quoted errors are estimated standard deviations determined in the least-squares analyses, increased to allow for systematic errors.

observe a ^{77}Se spectrum, and the weak selenium satellites could not be detected in a ^{1}H spectrum which was dominated by solvent resonances. It was therefore necessary to use a value measured for a solution in cyclohexane [9], and the uncertainty in D(SeH) was arbitrarily assumed to be 2 Hz. Secondly, it was found consistently that calculations did not reproduce the PSe coupling, the errors being 40—60 Hz. This was not entirely unexpected, as it is well known that for heavier elements there may be a sizeable anisotropic component of the indirect coupling [17], and there is no way that this can be estimated. The PSe couplings were assigned an uncertainty of 10 Hz in the refinements, which then converged to give the results listed as Refinement B in Table 4. The observed and calculated dipolar couplings and their uncertainties are listed in Table 6. The least-squares correlation matrix for refinement B is given in Table 7. It should be noted that the inclusion of the NMR data has greatly increased the correlations between geometrical parameters, and there are strong correlations between geometrical and

TABLE 5

Least-squares correlation matrix × 100, Refinement A[a]

$r1$	$r2$	$r3$	$\angle 1$	$\angle 2$	$\angle 3$	$u1$	$u2$	$u4$	$u5$	$k1$	$k2$	
100												$r1$
	100		−40	−40								$r2$
		100	−49		42							$r3$
			100		−70							$\angle 1$
				100								$\angle 2$
					100			−47	−53			$\angle 3$
						100	58		−43	72		$u1$
							100			70		$u2$
								100		47		$u4$
									100			$u5$
										100		$k1$
											100	$k2$

[a]Only elements with absolute values >40 are included.

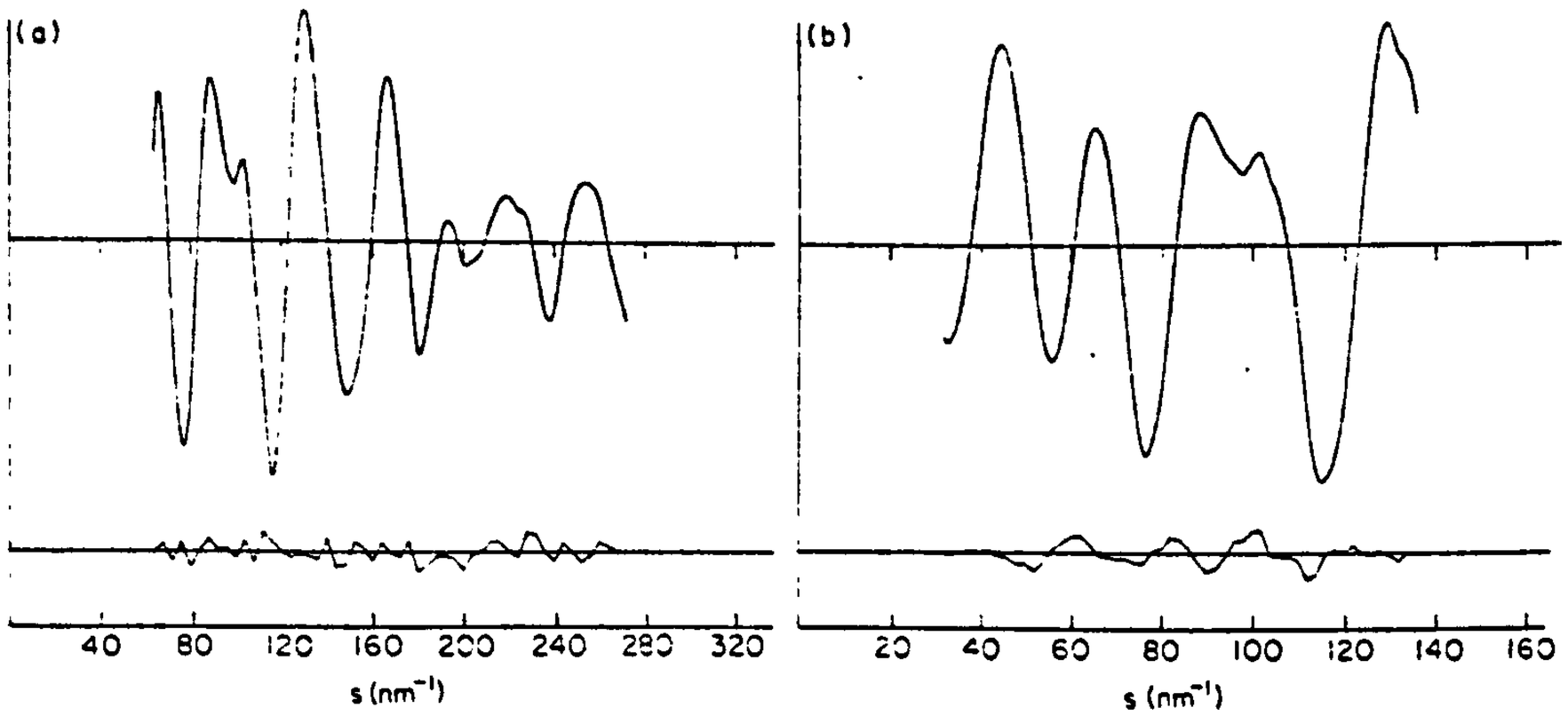

Fig. 2. Observed and final weighted difference molecular intensities for nozzle-to-plate distances of (a) 128 and (b) 287 mm.

orientation parameters, but amplitudes of vibration have not become correlated with other parameters.

The improvement in the precision of the geometrical parameters involving hydrogen in Refinement B is most striking. It is clear that the use of liquid-crystal NMR data may, in the right circumstances, be of very great value. However, care must be taken, for it is possible that there may be structural differences between gas and solution phases, and the problem of anisotropic components of indirect couplings is impossible to avoid. We are currently investigating other compounds in an attempt to assess the extent to which these uncertainties may be overcome.

TABLE 6

Dipolar couplings[a]

Nuclei	293 K			253 K		
	Observed	Calculated	Uncertainty	Observed	Calculated	Uncertainty
$^{31}P—^{19}F$	87.4	87.3	0.3	9.6	9.8	0.4
$^{31}P—^{1}H$	1035.6	1035.5	0.6	893.1	893.5	1.1
$^{77}Se—^{31}P$	−88.9	−151.7	10.0	−64.2	−108.1	10.0
$^{19}F—^{19}F$	438.2	438.4	1.0	260.3	260.3	0.2
$^{19}F—^{1}H$	676.2	676.2	0.3	509.4	509.4	0.2
$^{77}Se—^{19}F$	−82.4	−82.4	0.3	−60.2	−60.8	0.5
$^{77}Se—^{1}H$	−56.1	−62.2	2.0	−36.5	−40.1	2.0

[a] All couplings are in Hz.

TABLE 7

Least-squares correlation matrix × 100, Refinement B[a]

*r*1	*r*2	*r*3	∠1	∠2	∠3	*s*1	*s*2	*s*3	*s*4	*s*5	*s*6	*k*1	*k*2	
100														*r*1
	100													*r*2
		100	58		−75		92	−66		92	−60			*r*3
			100		−96		74	−94		77	−97			∠1
				100		−92	−59		−95	−55				∠2
					100		−84	94		−86	94			∠3
						100	57	−52	96	54				*s*1
							100	−84	55	99	−78			*s*2
								100	−50	−85	98			*s*3
100		52	−42											*s*4
		100	−81											*s*5
			100											*s*6
												100		*k*1
													100	*k*2

[a] Only elements with absolute values > 50 are included. There were no strong correlations between amplitudes of vibration and other refining parameters.

The geometrical parameters are in themselves unremarkable. The structure of the PF_2 unit is very similar to those in difluorophosphine sulphide [18] and difluorohalophosphine sulphides [19]. The P=Se distance, 202.6(4) pm, is substantially shorter than those in trialkyl- or aryl-phosphine selenides, which typically have bond lengths between 209 and 212 pm [20—22]; such shortening is commonly found when the phosphine has electronegative substituents. The P—H bond distance is slightly greater than that found by microwave spectroscopy for PF_2HS (139.2(5) pm) [19], but the SePH angle (118.6°) is very close to the SPH angle (119.2°) in PF_2HS.

ACKNOWLEDGEMENTS

We thank the Science Research Council for research grants, and a research studentship (to G. S. L.).

REFERENCES

1 K. Kuchitsu, T. Fukuyama and Y. Morino, J. Mol. Struct., 1 (1968) 463.
2 E. J. Jacob, H. B. Thompson and L. S. Bartell, J. Mol. Struct., 8 (1971) 383.
3 K. Kuchitsu, J. P. Guillory and L. S. Bartell, J. Chem. Phys., 49 (1968) 2488.
4 H. Spiesecke, Z. Naturforsch., Teil A, 25 (1970) 650.
5 L. Centofanti and R. W. Parry, Inorg. Chem., 9 (1970) 744.
6 S. H. Bauer and K. Kimura, J. Phys. Soc. Jpn., 17 (1962) 300.
7 C. M. Huntley, G. S. Laurenson and D. W. H. Rankin, J. Chem. Soc. Dalton Trans., (1980) 954.
8 R. L. Hilderbrandt and S. H. Bauer, J. Mol. Struct., 3 (1969) 325.
9 D. W. W. Anderson, E. A. V. Ebsworth, G. D. Meikle and D. W. H. Rankin, Mol. Phys., 25 (1973) 381.
10 L. Schäfer, A. C. Yates and R. A. Bonham, J. Chem. Phys., 55 (1971) 3055.
11 G. C. Holywell, D. W. H. Rankin, B. Beagley and J. M. Freeman, J. Chem. Soc. A, (1971) 785.
12 J. Dain, A. J. Downs, G. S. Laurenson and D. W. H. Rankin, J. Chem. Soc. Dalton Trans., in press.
13 L. S. Bartell, D. J. Romenesko and T. C. Wong, Molecular Structure by Diffraction Methods, Specialist Periodical Report, The Chemical Society, London, Vol. 3, 1977, p. 72.
14 G. S. Laurenson and D. W. H. Rankin, J. Chem. Soc. Dalton Trans., in press.
15 Y. Murata and Y. Morino, Acta Crystallogr., 20 (1966) 605.
16 P. Diehl and W. Niederberger, J. Magn. Reson., 9 (1973) 495.
17 J. Bulthuis and C. A. de Lange, J. Magn. Reson., 14 (1974) 13.
18 C. R. Nave and J. Sheridan, J. Mol. Struct., 15 (1973) 391.
19 L. Acha, E. R. Cromie and D. W. H. Rankin, J. Mol. Struct., in press.
20 P. J. Carroll and D. D. Titus, J. Chem. Soc. Dalton Trans., (1977) 824.
21 T. S. Cameron and B. Dahlen, J. Chem. Soc. Perkin Trans. 2, (1975) 1737.
22 Z. Galdecki, M. L. Glowka, J. Michalski, A. Okruszek and W. J. Stec, Acta Crystallogr., Sect. B, 33 (1977) 2322.

Gas-phase Molecular Structure of Difluoro(isoselenocyanato)phosphine determined by Electron Diffraction

By Stephen Cradock, Graham S. Laurenson, and David W. H. Rankin,* Department of Chemistry, University of Edinburgh, West Mains Road, Edinburgh EH9 3JJ

The molecular geometry of $PF_2(NCSe)$ has been investigated in the gas phase by electron diffraction. Mean amplitudes of vibration and perpendicular amplitude-correction coefficients have been derived from previously published spectroscopic data, and used to determine the average (r_a) structure. The principal parameters (r_α) for $PF_2(NCSe)$ are: r(P–F) 153.0(4), r(P–N) 164.9(12), r(N=C) 121.2(8), and r(C=Se) 168.1(10) pm; angle P–N–C 149.0(15), F–P–N 98.8(8), and F–P–F 97.9(14)°. The overall symmetry is C_s with the pseudohalide group lying *trans* to the F–P–F angle bisector.

ELECTRON-DIFFRACTION structure determinations have previously been carried out on $PF_2(NCO)$ and $PF_2(NCS)$.[1] These molecules show short P–N bonds and wide angles at nitrogen characteristic of aminodifluorophosphines.[2] These features have been explained in terms of some π bonding between the lone pair of electrons on nitrogen and vacant *d* orbitals on phosphorus. It is therefore of interest to see whether the structure of $PF_2(NCSe)$ follows the pattern set by the two difluorophosphine pseudohalides.

In the cases of $PF_2(NCO)$ and $PF_2(NCS)$, complications arose because both molecules exhibit a significant shrinkage effect in the electron-diffraction (r_a) structure determination due to low-frequency bending modes. Spectroscopic data were used in these cases to calculate perpendicular amplitude coefficients and linear shrinkage corrections which yielded average (r_a) structures when applied to the refined electron-diffraction (r_a) structure. The i.r. spectrum of $PF_2(NCSe)$ [3] similarly exhibits a low-frequency bending mode, at 55 cm^{-1}, and in this case the necessary corrections from spectroscopic data were applied to the refining structure, as the computer programs used offer the facility to refine either r_a or r_α structures. We report here the results of our structural studies of $PF_2(NCSe)$ and comment on the major differences between the r_a and r_α structures refined from the same data.

EXPERIMENTAL

A sample of $PF_2(NCSe)$ was prepared by condensing $PBrF_2$ onto the silver pseudohalide salt,[3] the product being subsequently purified *in vacuo* and the purity checked by i.r. spectroscopy.

Electron-diffraction scattering intensities were recorded photographically using the Cornell/Edinburgh diffraction apparatus.[3,4] With an accelerating potential of 43 kV and nozzle-to-plate distances of 128 and 285 mm, several sets of data were obtained for s in the range 34—268 nm^{-1}. The sample and the nozzle were held at room temperature (293 K). The background pressure was 4×10^{-7} Torr † and during a run this increased to 2×10^{-6} Torr. The ion gauge used for the above measurements was situated in the main chamber but removed somewhat from the nozzle.

† Throughout this paper: 1 Torr ≈ (101 325/760) Pa; 1 dyn = 10^{-5} N.

Photographic intensities were converted into digital form using a Jarrel–Ash double-beam microphotometer [5] with spinning plates. The electron wavelength was determined from the scattering pattern of gaseous benzene recorded immediately before the sample exposures. The weighting points used in the setting up of the off-diagonal weight matrix employed in the least-squares refinement program, together with correlation parameters and other experimental details, are shown in Table 1.

All calculations were done on the ICL 2970 computer at the Edinburgh Regional Computing Centre using established data-reduction [3] and least-squares refinement [6] programs.

TABLE 1

Weighting functions, correlation parameters, and scale factors

Camera height / mm	Δs	$s_{min.}$	sw_1	sw_2	$s_{max.}$		
			nm^{-1}			p/k†	Scale factor
128	4	60	80	200	268	0.014	0.919(31)
285	2	34	50	110	140	0.366	0.863(22)

† Correlation parameter, see ref. 6.

The scattering factors of Schäfer *et al.*[7] were used throughout.

Calculated Amplitudes of Vibration and K Values.—These were obtained using our program GTRIP, based on Schachtschneider's [8] GMAT routines for generating inverse kinetic energy matrices (G) for a molecular system or for each symmetry block. A versatile routine FGRUM calculates eigenvalues and allows an initial trial potential-energy matrix (F) to be modified interactively in one of three ways. (*a*) Specified F elements may be assigned new values. (*b*) Specified F elements may be included in a least-squares refinement based on the differences between observed and calculated frequencies and between observed and calculated isotope shifts; the required derivatives $\partial\nu/\partial F_{ij}$ are not calculated analytically but obtained numerically by altering F_{ij} to $F + \Delta F$ and rediagonalising to obtain eigenvalues $\lambda + \Delta\lambda$. (*c*) The entire F matrix may be altered in such a manner so as to fit the observed frequencies for one isotopic species by the so-called ' direct-fit ' procedure; this has the unfortunate property of leading to a solution with the same L vectors as the initial trial F matrix, so we have modified the procedure by eliminating any off-diagonal elements in the new F matrix below a specified threshold. The modified F matrix is then used as the starting point for a new ' direct-fit ' plus elimination cycle, and the process continues until convergence on the observed frequencies is achieved. It is

usually convenient to begin with a high threshold (1.0 or 0.5 mdyn Å^{-1}) and to reduce it progressively if convergence is slow: in this way most of the changes are forced into the diagonal F elements, and only a limited number of non-zero off-diagonal elements remain in the final F matrix, which now has L vectors that may differ substantially from those of the original trial.

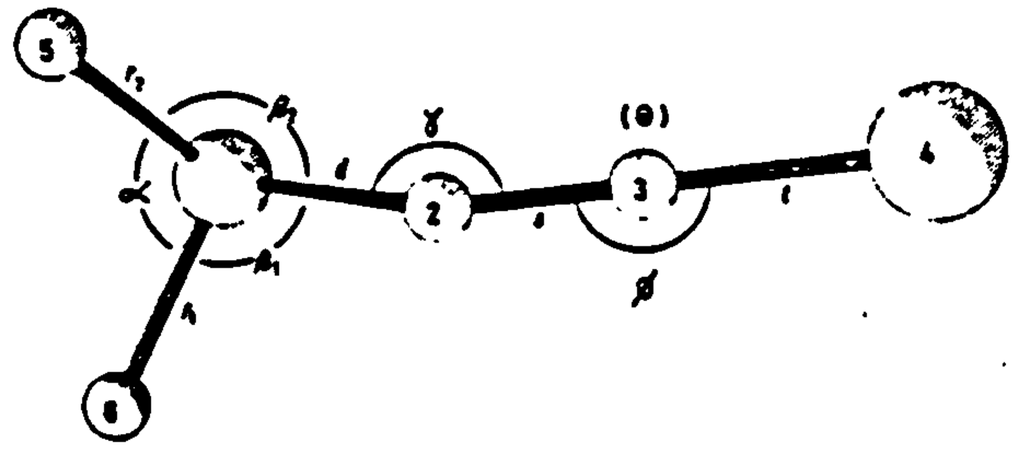

FIGURE 1 The *trans*-PF_2(NCSe) model with linear NCSe chain, symmetry C_s. Valence co-ordinates are indicated; ϕ is a linear bending in the symmetry plane, and θ is perpendicular to it. The twisting co-ordinate, τ, is generated by two torsions as $2^{-\frac{1}{2}}(\tau_{3214} + \tau_{3215})$

The L matrix corresponding to the final F matrix, chosen to reproduce observed frequencies and isotope shifts (where available), is then used to generate the mean-square Cartesian displacements for specified pairs of atoms. These are summed over all symmetry species and finally converted into u and K values by co-ordinate rotations appropriate to the atom pair. The amplitudes are calculated for 0 K and any specified higher temperature. GTRIP also includes facilities for calculation of Coriolis coupling terms and centrifugal distortion constants for symmetric top molecules.

Normal-co-ordinate Analysis.—The published values [3] for the fundamental vibration frequencies of PF_2(NCSe) were used in the normal-co-ordinate analysis. Figure 1 shows the applied molecular model and definition of valence co-ordinates. The normal modes of vibration are distributed

TABLE 2

Non-zero symmetry force constants ($\times 10^{-2}$, N m^{-1}) for PF_2(NCSe)

A'	1	5.72						
	2	1.10	13.50					
	3	−0.06		5.32				
	4	0.01			4.22			
	5					0.73		
	6				0.48		0.12	
	7				0.12			0.58
	8				−0.05			
A''	1	4.58						0.18
	2		0.64					
	3		−0.01	0.23				
	4				0.01			

into the symmetry species of the C_s symmetry group according to $\Gamma = 8A' + 4A''$. The set of symmetry co-ordinates S_1—S_{12} was constructed. Here R, D, S, and T

$S_1(A') = l$ $S_7(A') = (DS)^{\frac{1}{2}}\gamma$

$S_2(A') = s$ $S_8(A') = (ST)^{\frac{1}{2}}\phi$

$S_3(A') = d$ $S_9(A'') = 2^{-\frac{1}{2}}(r_1 - r_2)$

$S_4(A') = 2^{-\frac{1}{2}}(r_1 + r_2)$ $S_{10}(A'') = (RD/2)^{\frac{1}{2}}(\beta_1 - \beta_2)$

$S_5(A') = R\alpha$ $S_{11}(A'') = (ST)^{\frac{1}{2}}\theta$

$S_6(A') = (RD/2)^{\frac{1}{2}}(\beta_1 + \beta_2)$ $S_{12}(A'') = (RS)^{\frac{1}{2}}\tau$

designate the equilibrium distances of $R_{15} = R_{16}$, R_{12}, R_{23}, and R_{34} respectively (see Figure 1 for the atom numbering).

A harmonic force field for PF_2(NCSe) was developed which exactly fitted the observed vibrational frequencies. Table 2 shows the final results in terms of the symmetry F matrix. Table 3 gives the potential-energy distribution terms calculated from the developed force fields,[1] together with approximate descriptions of the normal modes of vibration, although mixing is so pronounced in some cases as to make simple assignments inadequate. Table 4 shows the calculated mean amplitudes of vibration for the normal modes of PF_2(NCSe) at 0 and 298 K, together with calculated K values at 298 K as used in the following r_α structure determination.

Refinement.—Molecular model. The molecule was assumed to have local C_s symmetry for the PF_2N group with the geometry being defined by the P–F, P–N, N=C, and C=Se distances, the angles F–P–F, F–P–N, P–N=C, and

TABLE 3

Frequency assignment, potential-energy distribution, and approximate description of normal modes for PF_2(NCSe)

Species	Frequency/cm^{-1}	Potential-energy distribution [a]	Approximate description
A'	1 972	90s	N=C str.
	920	23l + 29d + 42r	C=Se str.
	851	26l + 72d + 49r	P–F sym str.
	569	22l + 41d + 49β	P–N str.
	429	80α	NCSe bend
	396	21γ + 66ϕ	PF_2 bend
	262	15l + 20d + 49β	PF_2 def.
	77	74d + 156γ + 21ϕ	PNC bend
A''	851	95r	P–F asym str.
	490	39β + 52θ	NCSe bend
	347	54β + 41θ	PF_2 def.
	54	91τ	torsion

[a] For explanation of symbols see Figure 1 in ref. 1.

N=C=Se, and a torsion angle. The last was defined as zero when the F–P–F angle bisector was *trans* to the N=C bond.

Initial refinements of the r_a structure indicated that the N=C=Se angle could lie anywhere between 170 and 180°, and that it was strongly correlated with the P–N=C angle, which lay between 139 and 145°. This showed that there could be a large shrinkage arising from bending at nitrogen and carbon. The predominance of the P···Se peak in the radial-distribution curve (Figure 2) would ensure that this effect was pronounced. Therefore it was decided to concentrate on refinements of the r_α structure. This would also take account of the effects of the torsional vibration on any apparent distortion from C_s symmetry.

Average structure parameters (r_a) are related to those measured in the electron-diffraction experiment (r_a) by the expression (1) where u is the root-mean-square amplitude of

$$r_\alpha = r_a + (u^2/r_a) - K \qquad (1)$$

vibration and K is the perpendicular amplitude-correction coefficient. Thus, using r_a instead of r_e in the second term, and calculated values for u and K, we have been able to refine the r_α structure directly.

The final r_α parameters found for PF_2(NCSe), together with r_a values for all distances, are shown in Table 5. The P–N=C angle has widened from the r_a value (144°) to 149°. In the r_α structure the twist angle refined to zero and the symmetry now became exactly C_s with the N=C=Se chain exactly linear, and so only seven parameters were subsequently used to define the molecular geometry.

TABLE 4

Calculated amplitudes of vibration and K values at 0 and 298 K

	u/pm		K/pm	
	0 K	298 K	0 K	298 K
Distance				
P–F	4.10	4.18	0.37	1.78
P–N	4.59	5.39	0.45	2.31
N=C	3.67	3.69	0.54	1.18
C=Se	3.83	3.98	0.46	2.06
F···F	6.03	6.77	0.37	2.36
F···N	6.15	7.42	0.61	3.72
F···C	7.07	11.98	0.28	1.39
F···Se	7.79	17.30	0.02	0.04
P···C	5.14	6.80	0.20	0.62
P···Se	5.50	10.73	0.03	0.14
N···Se	3.91	4.15	0.38	2.35

In the final stages of the refinement, all independent geometrical parameters and amplitudes of vibration, with the exceptions of u(P–N) [= 1.2 u(C–Se)] and u(F···F) [= 1.0 u(F···N)], were free to refine.

Table 5 shows the final parameter set (r_a) for the PF_2(NCSe); the least-squares correlation matrix is given in Table 6, and the observed and difference molecular scattering curves are shown in Figure 3.

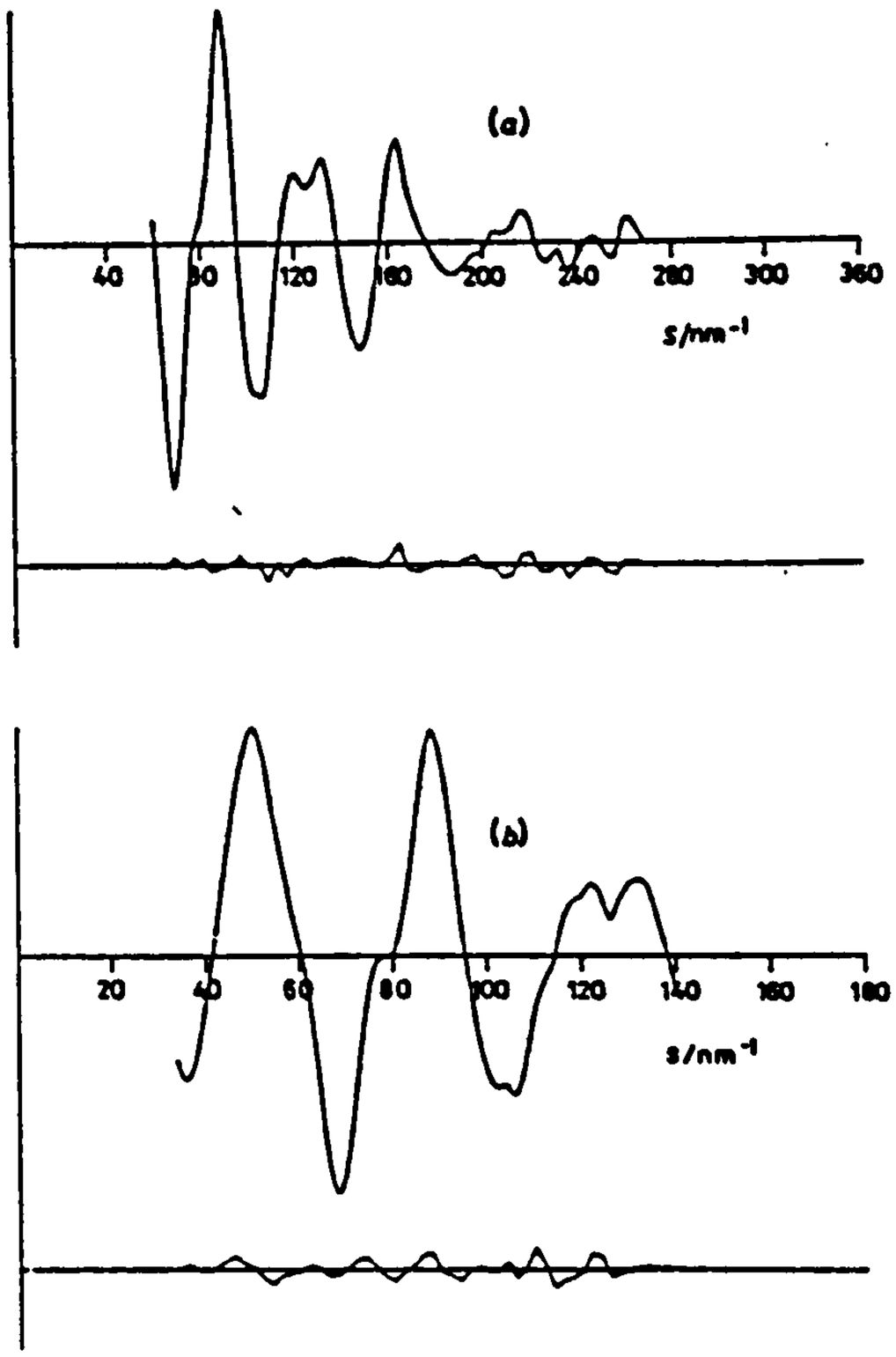

FIGURE 2 Observed and final weighted difference molecular scattering intensities for nozzle-to-plate distances of (a) 128 and (b) 285 mm

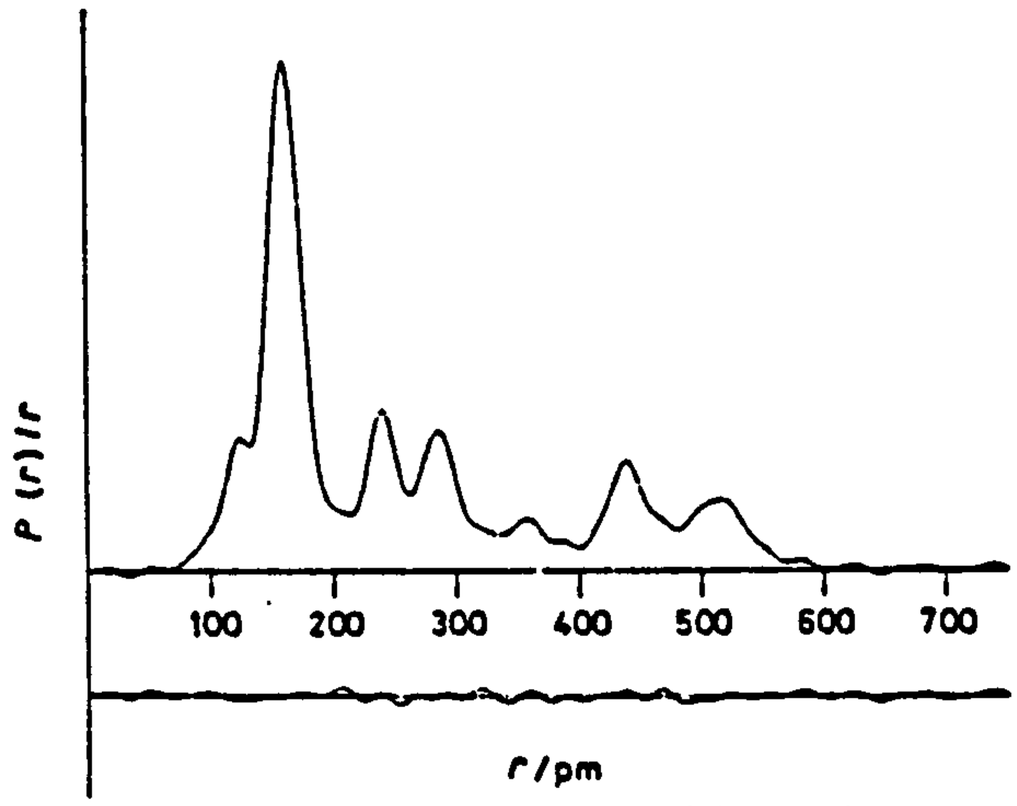

FIGURE 3 Observed and difference radial-distribution curves, $P(r)/r$, for PF_2(NCSe). Before Fourier inversion the data were multiplied by $s\{\exp[(-0.000\,02\ s^2)/(Z_{Se} - f_{Se})(Z_P - f_P)]\}$

DISCUSSION

In most structure determinations carried out on compounds containing the PF_2N group [1,2,8,10] the P–F and P–N distances are so close that refinement of all four parameters associated with these bonded distances is impossible, and u(P–F) and u(P–N) are usually constrained to refine together. In the case of PF_2(NCSe),

TABLE 5

Molecular parameters for PF_2(NCSe) *

Independent distances (pm)		Angles (°)	
r_a(P–F)	153.0(4)	F–P–F	97.9(14)
r_a(P–N)	164.9(12)	F–P–N	98.8(8)
r_a(N=C)	121.2(8)	P–N–C	149.0(15)
r_a(C=Se)	168.1(10)		

	u/pm		
	Electron diffraction		Vibrational spectroscopy
(a) Independent distances, r_a/pm			
r(P–F)	154.7(4)	4.7(11)	4.2
r(P–N)	167.0(12)	3.6(17)	5.4
r(C=N)	122.0(8)	5.9(12)	3.7
r(C=Se)	170.0(10)	3.0 (tied to u2)	4.0
(b) Dependent distances (pm)			
d(Se···N)	291.3(9)	6.7(17)	4.2
d(Se···P)	438.7(8)	12.8(8)	10.7
d(Se···F)	513.5(14)	21.4(13)	17.3
d(C···P)	276.4(11)	5.5(23)	6.8
d(C···F)	353.2(13)	17.3(23)	12.0
d(N···F)	245.0(11)	7.2(21)	7.4
d(F···F)	233.2(11)	7.2 (tied to u10)	6.8

* Estimated standard deviations derived from the least-squares analysis, increased to allow for systematic errors, are given in parentheses.

r(P–F) and r(P–N) are comparatively well resolved, whereas r(C=Se) overlaps with r(P–N) and the two amplitudes associated with these distances were refined as a single parameter. The relation between r(P–N) and r(C=Se) is clearly shown in the least-squares correlation matrix (Table 6). The correlation would have been more severe but for the fact that the sum of r(C=N) and

TABLE 6

Least-squares correlation matrix, multiplied by 100

				Angle													
r_1	r_2	r_3	r_4	1	2	3	u_1	u_2	u_3	u_4	u_5	u_6	u_7	u_8	u_9	u_{10}	k_1	k_2	
100								76											r_1
	100	53	−74		−62	−66													r_2
		100			−58	−67													r_3
			100							−70				−63					r_4
				100												89			1
					100											−56			2
						100	58												3
							100	84									74	65	u_1
								100									63	55	u_2
									100										u_3
										100				79					u_4
											100								u_5
												100							u_6
													100						u_7
														100					u_8
															100				u_9
																100			u_{10}
																	100	66	k_1
																		100	k_2

Only elements with absolute values greater than 0.5 are included.

TABLE 7

Comparison of geometric parameters of two-co-ordinate nitrogen compounds

	$PF_2(NCO)$ [a]	$PF_2(NCS)$ [a]	$PF_2(NCSe)$	$C(NPF_2)_2$ [b]	$SiH_3(NCSe)$ [c]
r_a(P–N)/pm	168.3(6)	168.6(6)	167.0(12)	168.0(6)	
r_a(P–F)/pm	156.3(3)	156.6(3)	154.7(4)	156.2(2)	
r_a(N=C)/pm	125.6(6)	122.1(6)	122.0(8)	124.0(5)	118.1(8)
r_a(C=Se)/pm			170.0(10)		175.9(7)
Angle MNC(r_a)/°	134.8(8)	144.0(7)	149.0(15)		180.0
Angle MNC(r_a)/°	130.6(8)	140.5(7)	143.9(13) [d]	132.8(5)	158.9(6)

[a] Ref. 1. [b] Ref. 12. [c] A. Fraser, G. S. Laurenson, and D. W. H. Rankin, unpublished work. [d] Linear N=C=Se assumed.

r(C=Se) is well defined by the N · · · Se distance in the linear pseudohalide moiety. Thus r(C=Se) is equal to d(Se · · · N) — r(C=N).

The angle found at nitrogen [149.0(15)°] is the widest yet reported for two-co-ordinate nitrogen bound to phosphorus,[11] but this value is not unexpected when compared to those for $PF_2(NCO)$, $PF_2(NCS)$, and $C(NPF_2)_2$.[12] In fact, all r_a structural parameters and r_a distances yield values consistent with those found for the two comparable pseudohalides. Parameters for $PF_2(NCSe)$, $PF_2(NCS)$, $PF_2(NCO)$, and $C(NPF_2)_2$, together with those for $SiH_3(NCSe)$, are compared in Table 7. Most amplitudes of vibration are found to be within experimental error of those calculated in the normal-co-ordinate analysis, despite the fact that this was undertaken prior to the gas-phase structure investigation and utilised slightly different parameters.

The final R_G and R_D factors [3] were 0.10 and 0.08 respectively. These are somewhat higher than usual for structures of small molecules undertaken at Edinburgh. This can be attributed to the rapid decay with increasing angle in the short-distance intensity data arising from destructive interference caused by the superposition of scattering from many differing interatomic distances of comparable scattering power, a feature illustrated by the form of the radial-distribution curve (Figure 3).

However, the R factors compare well with those obtained in the analyses of $PF_2(NCO)$ and $PF_2(NCS)$.

We thank the S.R.C. for a Research Studentship (to G. S. L.).

[0/1017 *Received*, 30*th June*, 1980]

REFERENCES

[1] D. W. H. Rankin and S. J. Cyvin, *J. Chem. Soc., Dalton Trans.*, 1972, 1277.
[2] C. M. Huntley, G. S. Laurenson, and D. W. H. Rankin, *J. Chem. Soc., Dalton Trans.*, 1980, 954.
[3] S. Cradock, E. A. V. Ebsworth, M. L. McConnell, D. W. H. Rankin, and M. R. Todd, *J. Chem. Soc., Dalton Trans.*, 1977, 1025.
[4] S. H. Bauer and K. Kimura, *J. Phys. Soc. Jpn.*, 1962, **17**, 300.
[5] R. L. Hilderbrandt and S. H. Bauer, *J. Mol. Struct.*, 1969, **3**, 325.
[6] D. M. Bridges, G. C. Holywell, D. W. H. Rankin, and J. M. Freeman, *J. Organomet. Chem.*, 1971, **32**, 87.
[7] L. Schäfer, A. C. Yates, and R. A. Bonham, *J. Chem. Phys.*, 1971, **55**, 3055.
[8] J. H. Schachtschneider and R. G. Snyder, *Spectrochim. Acta*, 1963, **19**, 117.
[9] G. S. Laurenson and D. W. H. Rankin, *J. Mol. Struct.*, 1979, **54**, 111.
[10] G. S. Laurenson and D. W. H. Rankin, *J. Chem. Soc., Dalton Trans.*, 1981, in the press.
[11] L. Vilkov and L. S. Khaikin, *Top. Curr. Chem.*, 1975, **53**, 38.
[12] D. W. H. Rankin, *J. Chem. Soc., Dalton Trans.*, 1972, 869.

The Molecular Structures of Difluorophosphino(disilyl)amine and Bis-(difluorophosphino)silylamine in the Gas Phase, determined by Electron Diffraction

By Graham S. Laurenson and David W. H. Rankin,* Department of Chemistry, University of Edinburgh, West Mains Road, Edinburgh EH9 3JJ

The molecular structures of difluorophosphino(disilyl)amine and bis(difluorophosphino)silylamine in the gas phase have been determined by electron diffraction. Both molecules have planar co-ordination at nitrogen, and Si–N bonds that are substantially longer than those in other silylamines. Principal bonds and angles (r_a) for $N(PF_2)(SiH_3)_2$ are r(P–F) 158.5(3), r(P–N) 168.0(4), r(Si–N) 175.5(4) pm: FPF 96.9(10), FPN 99.4(7), and SiNSi 119.3(17)°. For $N(PF_2)_2(SiH_3)$ principal parameters are r(P–F) 157.0(2), r(P–N) 169.1(4), r(Si–N) 176.7(7) pm: FPF 96.1(5), FPN 99.3(3), and PNP 117.6(7)°. In each compound the conformation adopted by the difluorophosphino-groups is such that the axes of the nitrogen and phosphorus lone-pair orbitals are approximately orthogonal.

THE molecular geometries of silicon- and phosphorus-substituted amines have been extensively studied. Trisilylamine [1,2] is the most widely known inorganic compound with planar co-ordination at nitrogen, and the wide SiNSi angle in disilylamine [3] suggests that the three bonds to nitrogen are coplanar. Similarly, the tertiary difluorophosphinoamine, $N(PF_2)_3$, has a planar NP_3 skeleton,[4] and the secondary amine has a wide PNP angle.[5,6] The planarity of the nitrogen in the primary amine, $NH_2(PF_2)$, is not so definitely established: a microwave study [7] suggests that the PNH_2 group is planar, whereas limited information from an electron-diffraction study favours a non-planar arrangement.[8] This apparent anomaly may arise from a low-frequency out-of-phase deformation, which would give a large shrinkage effect,[9] and similar low-frequency modes may account for the apparent non-planarity of the NC_2Si and NC_2P skeletons of $NMe_2(PF_2)$ [8] and $NMe_2(SiH_3)$.[10]

However, of the three amines containing both silyl and difluorophosphino-substituents, only one, $NH(PF_2)(SiH_3)$, has been the subject of a structural study.[11] It was therefore important to study the other two, $N(PF_2)_2(SiH_3)$ and $N(PF_2)(SiH_3)_2$, as these would be expected to have planar arrangements of the bonds to nitrogen. It was also of interest to see whether there was any evidence of competition between phosphorus and silicon for the nitrogen lone pair of electrons, leading to a shortening of one type of bond to nitrogen at the expense of the other type. Finally, the conformations adopted by the difluorophosphino-groups were of interest, as predictions about these had been made on the basis of n.m.r. coupling constants.[12]

EXPERIMENTAL

Samples of difluorophosphino(disilyl)amine and bis-(difluorophosphino)silylamine were prepared by literature methods [13] and purified by fractional condensation *in vacuo*: purities were checked spectroscopically.

Electron-diffraction scattering intensities were recorded using the Cornell–Edinburgh diffraction apparatus,[4,13] with nozzle-to-plate distances of 128 and 285 mm, and an accelerating voltage of *ca.* 43 kV. During exposure samples were maintained at 250 K, and the nozzle at room temperature, 293 K. Data were recorded on Kodak Electron Image plates, and obtained in digital form using a Jarrell–Ash double-beam microphotometer, with spinning plates.[14] The electron wavelengths were determined from the scattering patterns of gaseous benzene, recorded immediately before or after the sample plates.

All calculations were carried out on an ICL 2970 computer at the Edinburgh Regional Computing Centre, using established data reduction [4] and least-squares refinement programs.[15] Weighting points used in setting up the off-diagonal weight matrices are given, together with other experimental data, in Table 1. In all calculations the complex scattering factors of Schäfer *et al.*[16] were used.

Refinement.—Difluorophosphino(disilyl)amine. In refinements of the structure of $N(PF_2)(SiH_3)_2$ it was assumed that the $N(PF_2)$ group had local C_s symmetry, and that the two $N(SiH_3)$ groups had local C_{3v} symmetry. The $N(SiH_3)_2$ group was assumed to have C_s symmetry, with the two SiH_3 groups twisted away from the conformation in which one Si–H bond of each group was *trans* to the further N–Si bond. The $PNSi_2$ group was initially assumed to be planar, with C_{2v} symmetry, but distortions of the P–N bond, both in the plane and perpendicular to it, were subsequently permitted: in the final refinements the distortion in the plane was the only one allowed. Finally, the PF_2 group was

TABLE 1

Weighting functions, correlation parameters, and scale factors

Compound	Camera height/mm	Wavelength/pm	Δs/nm^{-1}	$s_{min.}$/nm^{-1}	sw_1/nm^{-1}	sw_2/nm^{-1}	$s_{max.}$/nm^{-1}	p/h	Scale factor
$N(PF_2)(SiH_3)_2$	128.5	5.799	4	60	80	230	260	0.146	0.806(14)
	284.3	5.799	2	26	40	120	144	0.469	0.727(13)
$N(PF_2)_2(SiH_3)$	128.4	5.854	4	64	80	240	316	0.348	0.960(18)
	285.6	5.854	2	26	30	120	142	0.446	0.900(13)

allowed to twist, about the P–N bond, with zero twist angle defined for the conformation in which the FPF angle bisector lay in the NSi_2 plane.

With these assumptions, the structure was defined by 11 geometrical parameters. Although there were strong correlations between parameters (Table 2) caused by overlap of peaks in the radial distribution curve (Figure 1), it was soon clear that the $PNSi_2$ skeleton was planar, and that the three angles at nitrogen were equal, within experimental error. Most of the other heavy-atom parameters refined easily, but the three bonded distances P–F, P–N, and Si–N were strongly correlated, and occasionally the relative positions of the P–F and P–N distances would reverse. On the basis of known bond lengths in other difluorophosphinoamines [4,8,11,17] the ratio r(P–N) : r(P–F) was assumed to be 1.060 ± 0.002 : 1, and this 'predicate observation' [18] was used as an additional experimental datum in subsequent refinements. Similarly, the ratio F–P–N : F–P–F was taken to be 1.035 ± 0.015 : 1, and this mild constraint was sufficient to stabilise the refinements.

TABLE 2

Least-squares correlation matrix (×100) for $N(PF_2)(SiH_3)_2$ *

	r_1	r_2	r_3	Angle 1	Angle 2	Angle 4	Angle 5	Angle 7	u_3	u_5	u_6	u_{11}	u_{14}	u_{20}	k_1	k_2
r_1	100	42							56							
r_2		100							69							
r_3			100					−53							51	
1				100	−45	−40				67						
2					100					−62		−55				
4						100	−57					−79		−45		
5							100									
7								100			43			46	−42	−43
u_3									100							
u_5										100						
u_6											100			46		
u_{11}												100	−44			
u_{14}													100			
u_{20}														100		
k_1															100	
k_2																100

* Only elements with absolute values ≥ 40 are included.

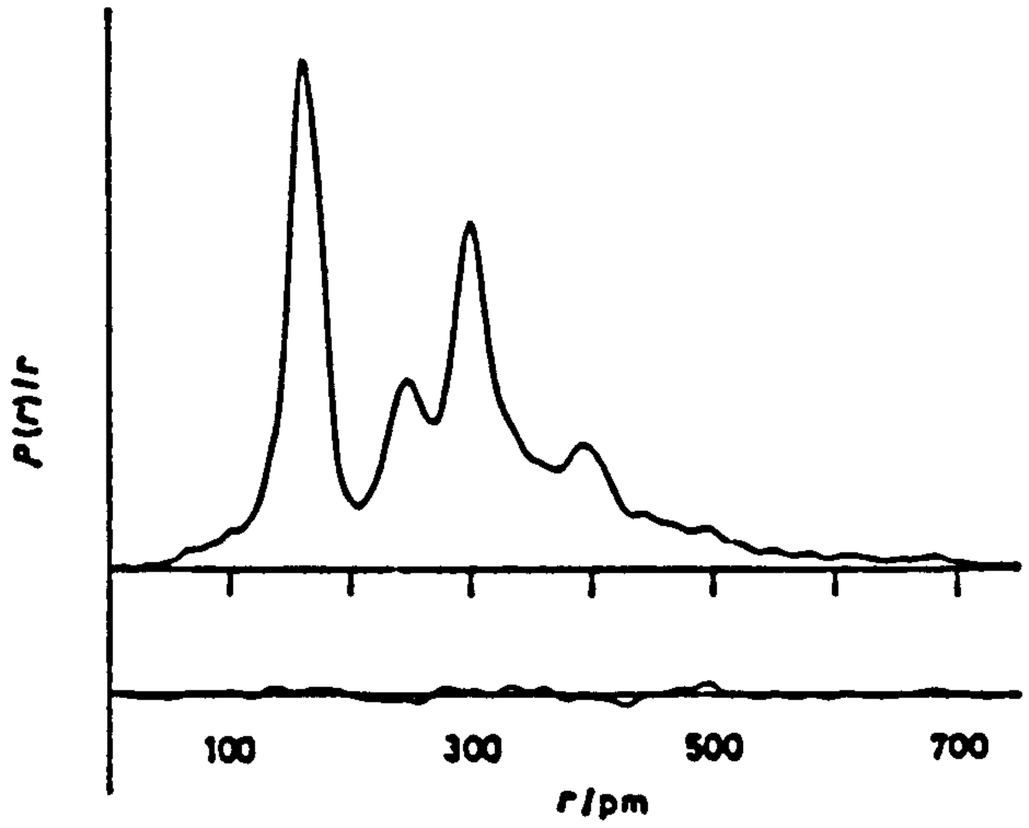

FIGURE 1 Observed and difference radial distribution curves. $P(r)/r$, for $N(PF_2)(SiH_3)_2$. Before Fourier inversion the data were multiplied by $s \cdot \exp[-0.000\,015\, s^2/(Z_P - f_P)(Z_F - f_F)]$

The conformation adopted by the $-PF_2$ group was found by fixing the twist angle at various values, and comparing the R factors obtained. By coincidence, the radial distribution curves for twist angles of 10 and 80° are extremely similar but the 10° form gives a significantly lower R factor, and other parameters refine to more reasonable values with the larger twist angle. The silyl twist angle was also found by a similar process, but other parameters associated with hydrogen-atom positions could not be refined, and were fixed at reasonable values.

TABLE 3

Molecular parameters for $N(PF_2)(SiH_3)_2$ *

	Distance/pm	Amplitude/pm
(*a*) Independent distances		
r_1 (P–F)	158.5(3)	4.7 (fixed)
r_2 (P–N)	168.0(4)	5.3(5)
r_3 (Si–N)	175.5(4)	5.3 (tied to u_3)
r_4 (Si–H)	149.0 (fixed)	8.8 (fixed)
(*b*) Dependent distances		
d_3 (F · · · N)	249.1(12)	10.8(11)
d_4 (F · · · Si)	407.3(15)	11.3(12)
d_7 (F · · · Si)	385.4(21)	11.3 (tied to u_6)
d_8 (F · · · Si)	295.7(22)	11.3 (tied to u_6)
d_9 (F · · · Si)	324.0(19)	11.3 (tied to u_6)
d_{10} (F · · · F)	237.3(18)	10.8 (tied to u_5)
d_{11} (Si · · · Si)	304.0(25)	10.1(6)
d_{12} (Si · · · P)	296.7(13)	10.1 (tied to u_{11})
d_{13} (Si · · · P)	298.1(23)	10.1 (tied to u_{11})
d_{16-22} (F · · · H)	255.5—514.7	11.1(39)
d_{20-26} (P · · · H)	309.9—402.2	11.9(39)
d_{20} (N · · · H)	266.2(15)	12.0 (fixed)
d_{20-23} (Si · · · H)	339.5—428.4	11.9 (tied to u_{20})
d_{23} (H · · · H)	242.5 (fixed)	12.0 (fixed)
d_{24-26} (H · · · H)	296.7—530.8	20.0 (fixed)
(*c*) Independent angles/°		
Angle 1 (F–P–F)	96.9(10)	
Angle 2 (F–P–N)	99.4(7)	
Angle 3 (N–Si–H)	110 (fixed)	
Angle 4 (Si–N–Si)	120.0(15)	
Angle 5 (P–N in plane def.)	0.5(9)	
Angle 6 (SiH_3 twist)	8 (fixed)	
Angle 7 (PF_2 twist)	14.0 (12)	

* All distances are r_a.

The results of the final refinement, for which R_G was 0.08 and R_D was 0.06, are given in Table 3. Errors quoted are

estimated standard deviations obtained in the least-squares analysis, increased to allow for systematic errors. The observed and final weighted difference molecular scattering intensities are shown in Figure 2. The structure of the molecule is shown in Figure 3(*a*).

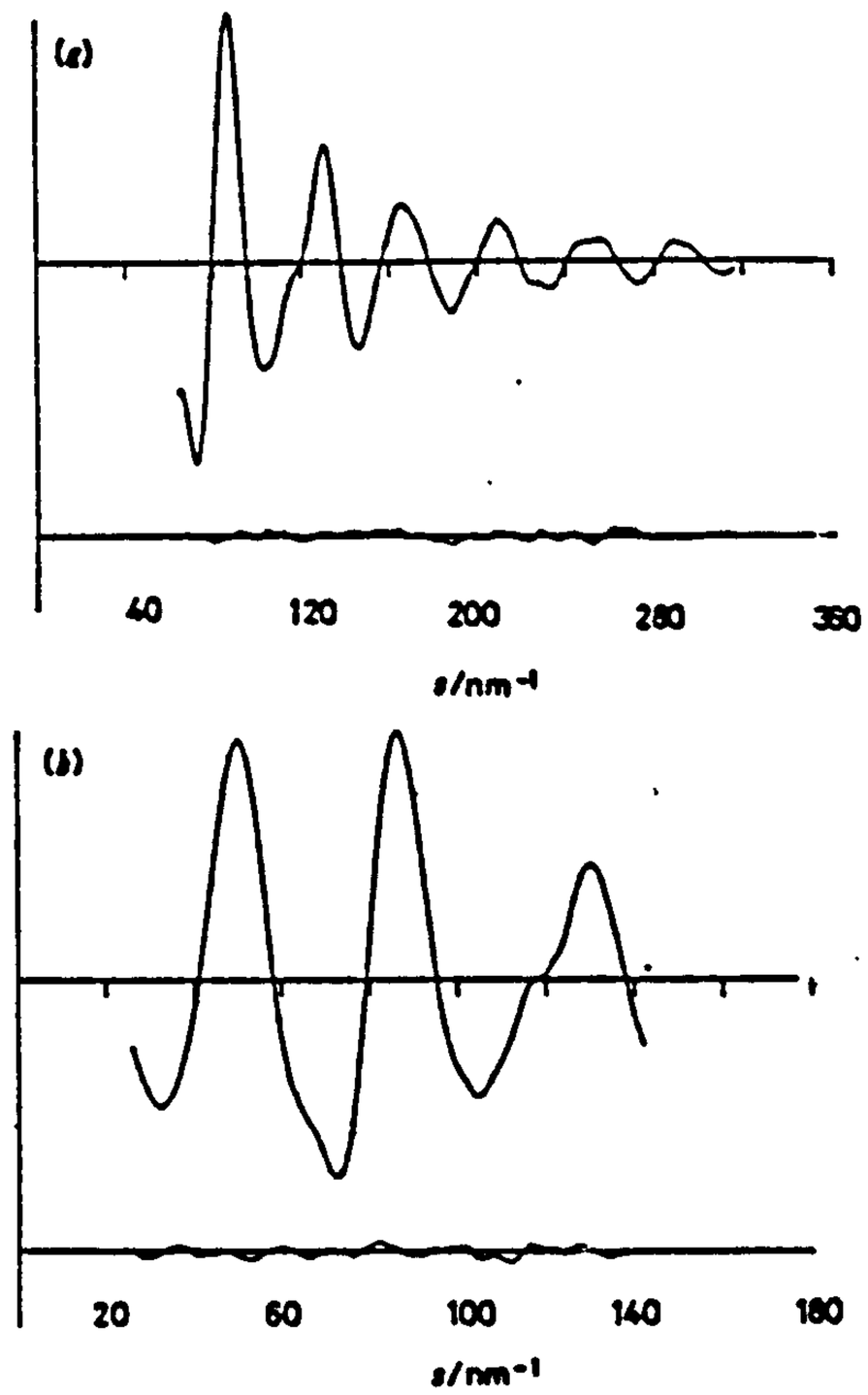

FIGURE 2 Observed and final weighted difference molecular scattering intensities for $N(PF_2)(SiH_3)_2$ at nozzle-to-plate distances of (*a*) 128 and (*b*) 284 nm

Bis(difluorophosphino)silylamine.—In the molecular model used for the refinements of this structure, it was assumed that the two $N(PF_2)$ groups were identical, and had C_s symmetry, that the $N(SiH_3)$ group had C_{3v} local

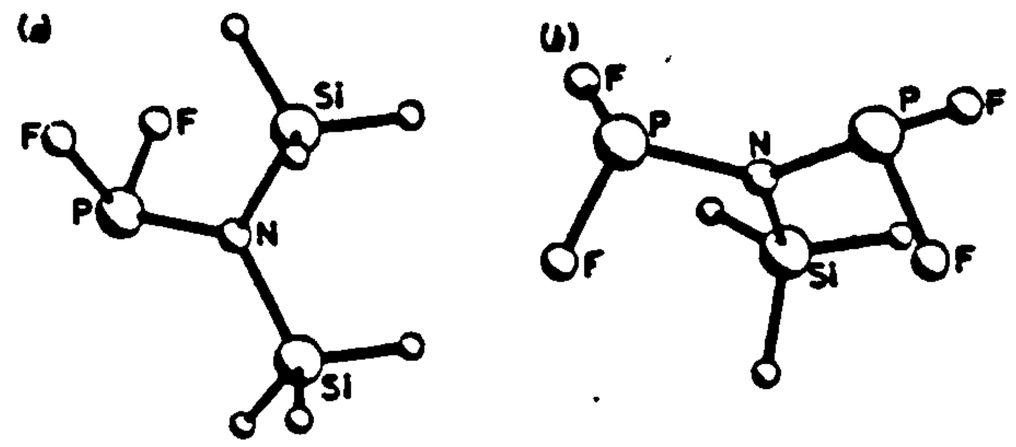

FIGURE 3 Molecular structures of (*a*) $N(PF_2)(SiH_3)_2$ and (*b*) $N(PF_2)_2(SiH_3)$

symmetry, and that the P_2NSi skeleton had C_s symmetry. It was soon apparent that the bonds to nitrogen were co-planar, and in the later refinements this was assumed, with a single angle (PNP) describing the co-ordination at nitrogen.

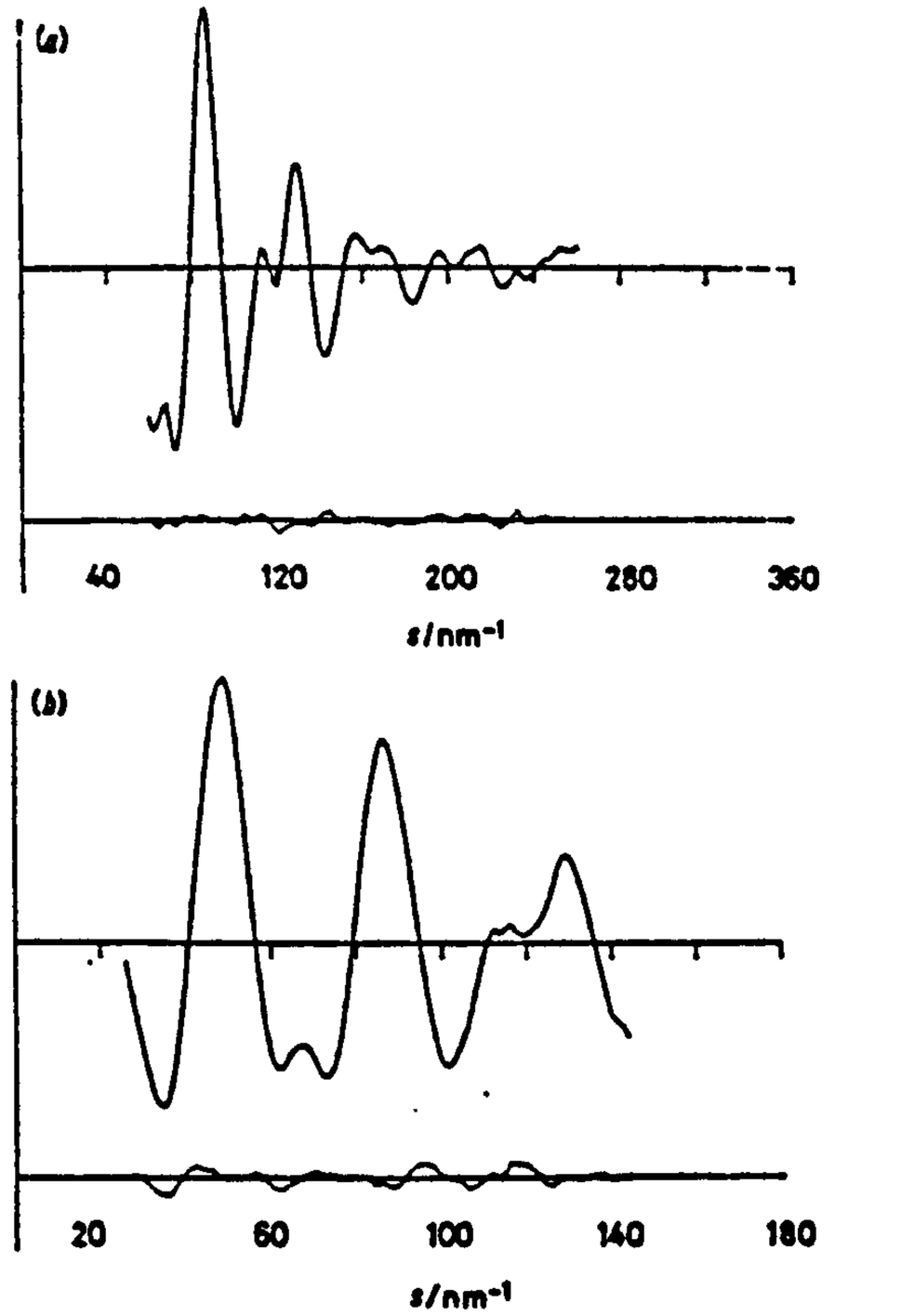

FIGURE 4 Observed and final weighted difference molecular scattering intensities for $N(PF_2)_2(SiH_3)$ at nozzle-to-plate distances of (*a*) 128 and (*b*) 285 nm

The conformation was described by three angles. The SiH_3 twist angle was taken to be zero when one Si–H bond lay in the skeletal plane. The two PF_2 twist angles were defined to be zero when the FPF angle bisectors lay *cis*

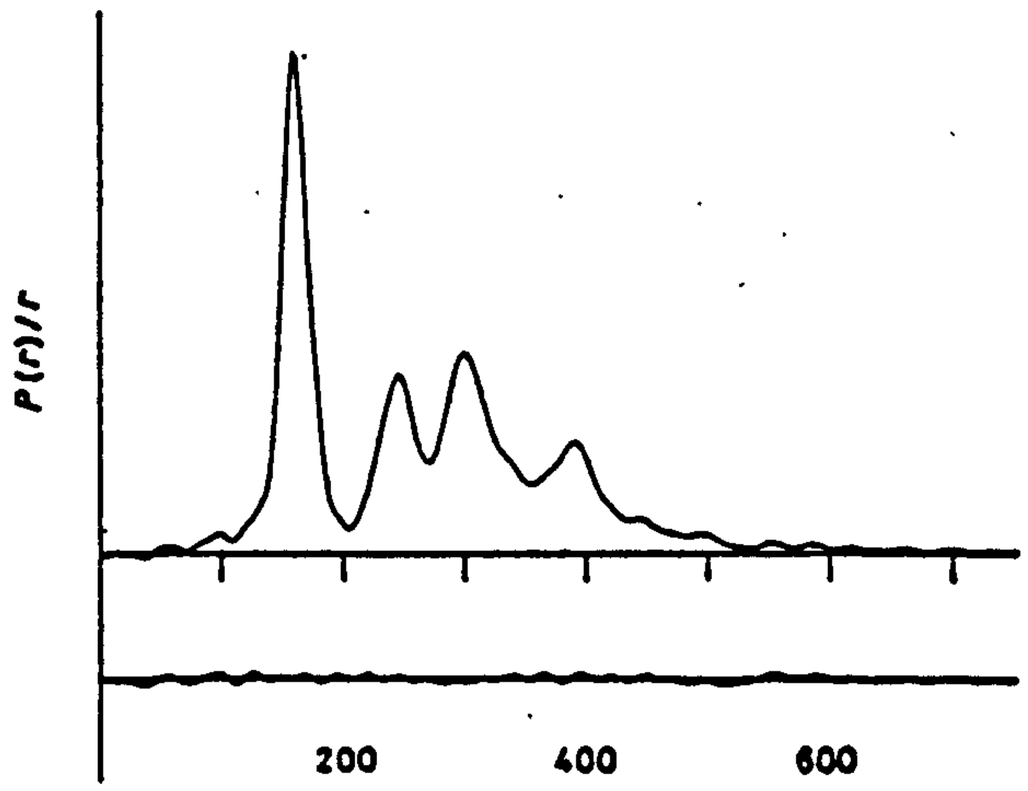

FIGURE 5 Observed and difference radial distribution curves, $P(r)/r$, for $N(PF_2)_2(SiH_3)$. Before Fourier inversion the data were multiplied by $s \cdot \exp[-0.000\,015\,s^2/(Z_P - f_P)(Z_P - f_P)]$

to the N–Si bond. These two angles could be constrained to be equal, or equal and opposite, giving C_s or C_s symmetry to the $N(PF_2)_2Si$ unit, or they could be varied independently.

TABLE 4

Molecular parameters for $N(PF_2)_2(SiH_3)$ *

		Distance/pm	Amplitude/pm
(*a*)	**Independent distances**		
	r_1 (P–F)	157.0(2)	4.7(3)
	r_2 (P–N)	169.1(4)	5.2 (tied to u_1)
	r_3 (Si–N)	176.7(7)	5.2 (tied to u_1)
	r_4 (Si–H)	143.8(30)	8.8 (fixed)
(*b*)	**Dependent distances**		
	d_5 (N ··· F)	248.7(5)	8.1(8)
	d_6 (F ··· F)	233.5(8)	8.1 (tied to u_5)
	d_7 (F ··· F)	496.5(8)	21.2(25)
	d_8 (F ··· F)	431.2(7)	21.2 (tied to u_7)
	d_9 (F ··· F)	445.2(7)	21.2(tied to u_7)
	d_{10} (F ··· Si)	316.2(31)	25.6(25)
	d_{11} (F ··· Si)	309.6(30)	25.6 (tied to u_{10})
	d_{12} (P ··· Si)	301.2(6)	11.5(7)
	d_{13} (P ··· F)	386.5(24)	14.0(7)
	d_{14} (P ··· F)	391.8(21)	14.0 (tied to u_{13})
	d_{15} (P ··· P)	289.3(11)	11.5 (tied to u_{13})
	d_{16-27} (F ··· H)	260.5—455.8	22 (fixed)
	d_{28} (H ··· H)	237.3(50)	18 (fixed)
	d_{29-31} (P ··· H)	328.6—419.0	18 (fixed)
	d_{32} (N ··· H)	264.7(21)	15 (fixed)
(*c*)	**Independent angles/°**		
	Angle 1 (F–P–F)		96.1(5)
	Angle 2 (F–P–N)		99.3(3)
	Angle 3 (P–N–P)		117.6(7)
	Angle 4 (N–Si–H)		110 (fixed)
	Angle 5 (PF_2 twist)		−3.3(27)
	Angle 6 (SiH_3 twist)		50 (fixed)

* All distances are r_a.

Of the 11 geometrical parameters, only the NSiH and the SiH_3 twist angles could not be refined. The latter was fixed at 50°, the value giving the lowest R factor in a series of test refinements. The PF_2 twist angles were varied over a wide range, but the lowest R factors were obtained when both angles were close to zero; a small C_s distortion was preferred to a C_2 distortion.

The results of the final refinement, for which R_G was 0.06 and R_D was 0.04, are listed in Table 4, and the least-squares correlation matrix is given in Table 5. The intensity data are shown in Figure 4, and the radial distribution curve in Figure 5. The molecular structure is shown in Figure 3(*b*).

DISCUSSION

The gas-phase structures of $N(PF_2)(SiH_3)_2$ and $N(PF_2)_2(SiH_3)$ in both cases reveal an entirely planar arrangement of ligands around nitrogen. The absence of any apparent shrinkage due to out-of-plane deformations of the NR_3 group may be attributed to the fact that the atoms bound to nitrogen in all cases contact each other at distances approximating to the sums of their Bartell hard-sphere radii,[19] precluding closer approach.

The angles at nitrogen are 120° within experimental error in the case of $N(PF_2)(SiH_3)_2$. A slight narrowing of the PNP angle in $N(PF_2)_2(SiH_3)$ from 120° [118.2(10)°] may be due to the absence of steric crowding between neighbouring PF_2 groups, since the fluorines tend to point away from each other in the preferred conformation.

In both molecules r(Si–H) was fixed at a reasonable value and r(P–F) refined to a value consistent with those expected for the F_2PN moiety, as shown in Table 6. Since some π character can be assigned to the R–N bonds, which are in all cases shorter than those expected for a corresponding single bond, some interest lay in investigating the effect of PF_2 and silyl groups competing for the lone pair on nitrogen. It was found that while the P–N bond lengths for the mono and bis PF_2 species, being 168.0(4) pm and 169.1(4) pm respectively, were substantially shorter than those found in $N(PF_2)_3$ [171.1(4) pm],[4] the Si–N bond lengths in both cases were some 2—3 pm longer than that measured in trisilylamine (Table 6). This clearly demonstrates that the PF_2 group has a greater propensity for accepting electron density from the p orbital on nitrogen than the silyl group, and this is almost certainly due to the electron-withdrawing effect of the fluorines bonded to phosphorus. It has been shown that replacing hydrogens with fluorines on silyl groups bound to nitrogen shortens the Si–N bond,

TABLE 5

Least-squares correlation matrix (×100) for $N(PF_2)_2(SiH_3)$ *

				Angle												
r_1	r_2	r_3	r_4	1	2	3	5	u_1	u_5	u_7	u_{10}	u_{12}	u_{13}	k_1	k_2	
100		51						40								r_1
	100	−43			−57											r_2
		100				46		40			46					r_3
			100											−40	−47	r_4
				100					66							1
					100				−35		−43					2
						100						63				3
							100			48	48		60			5
								100						47		u_1
									100							u_5
										100			48			u_7
											100			48	48	u_{10}
												100				u_{12}
													100			u_{13}
														100	64	k_1
															100	k_2

Angle

* Only elements with absolute values ≥40 are included.

from 171.5 pm in $NMe_2(SiH_3)$ [10] to 165 pm in $NMe_2(SiF_3)$.[20] We hope soon to undertake a gas-phase study of the molecular $NH(PMe_2)_2$ which may therefore be expected to have P–N bonds substantially longer than those found for $NH(PF_2)_2$.

The angles at phosphorus require no special comment: FPF and FPN in both cases give expected values for the F_2PN group (Table 6). Typical values for these parameters range from 95—97° and 98—100° respectively. In the case of $NH(PF_2)(SiH_3)$ it may be that these strongly correlated angles have been reversed in the refinements.

The conformation of the PF_2 groups in PF_2 amines is generally of some interest, since they can be directed by two factors: lone-pair repulsions between P and P or P and N; and attractive interactions between F and H, the latter being important for all NR_3 compounds (R = PF_2, SiH_3, CH_3, or H) containing PF_2 groups, except $N(PF_2)_3$. In general fluorine–hydrogen interactions predominate over lone-pair repulsions, as is evident in the cases of $NMe(PF_2)_2$ [21] and $NH(PF_2)_2$ [5] where attractive H···F interactions force the phosphorus lone pairs, although orthogonal to that on nitrogen, to lie *cis* to each other in the major conformer for each molecule. For $N(PF_2)_2(SiH_3)$ and $N(PF_2)_2(SiH_3)$ n.m.r. studies had already been used to predict the likely orientations of the PF_2 groups.[12] It has been suggested [22,23] that some two- or three-bond couplings to three-co-ordinate phosphorus are sensitive to conformation, with large couplings resulting from atoms lying *cis* to the lone pair on phosphorus. In $N(PF_2)_2(SiH_3)$ both $^3J(^{31}P^1H)$ and $^2J(^{31}P^{29}Si)$ are small (3.5 and 7 Hz respectively), indicating that the FPF bisectors lie *cis* to the silyl group. In $N(PF_2)(SiH_3)_2$ n.m.r. couplings have been explained in terms of the average of one *cis* and one *trans* J(PX) (X = ^{29}Si or ^{1}H), indicating fast rotation of the PF_2 group on the n.m.r. time scale. These predictions have been verified by the present study.

In $N(PF_2)_2(SiH_3)$ the PF_2 torsions refined as a single parameter, with the best fit being for a conformation where the $N(PF_2)_2$ group adopts a local C_s symmetry with the FPF angle bisectors lying 3° away from being *cis* to the Si–N bond. This result is identical in principle to those found for $NH(PF_2)_2$ and $NMe(PF_2)_2$, and a similar situation has been predicted for $N(GeH_3)(PF_2)_2$.[22] We are at present undertaking a gas-phase structural determining the conformations of the PF_2 groups. $N(PF_2)(SiH_3)_2$ contains H···F contacts from 255.5 pm and $N(PF_2)_2(SiH_3)$ similar contacts from 260.5 pm. The lower values in both cases correspond to the sum of the van der Waals radii for fluorine and hydrogen, and represent the optimum distance for maximum H···F interaction.

TABLE 6

Geometric parameters for some difluorophosphino- and silyl-amines

Compound	Distances/pm			Angles/°	
	r(P–F)	r(P–N)	r(Si–N)	FPF	FPN
$N(PF_2)_3$ [a]	157.4(2)	171.1(4)		96.9(3)	99.2(3)
$N(PF_2)_2(SiH_3)$ [b]	157.0(2)	169.1(4)	176.7(7)	96.1(5)	99.3(3)
$N(PF_2)(SiH_3)_2$ [b]	158.7(3)	168.0(4)	175.5(4)	96.9(10)	99.4(7)
$N(SiH_3)_3$ [c]			173.4(2)		
$NH(PF_2)_2$ [d]	158.4(3)	168.4(8)		95.6(10)	98.3(7)
$NH(PF_2)(SiH_3)$ [e]	157.5(3)	165.4(6)	172.4(7)	101.6(12) [f]	95.2 [f]
$NH(SiH_3)_2$ [g]			172.5(3)		

[a] Ref. 4. [b] This work. [c] Ref. 2. [d] Ref. 5. [e] Ref. 11. [f] See text. [g] Ref. 3.

We thank the S.R.C. for research grants and a Research Studentship (to G. S. L.).

[0/1093 *Received*, 10th *July*, 1980]

REFERENCES

[1] K. Hedberg, *J. Amer. Chem. Soc.*, 1955, **77**, 6491.
[2] B. Beagley and A. R. Conrad, *Trans. Faraday Soc.*, 1970, **66**, 2740.
[3] D. W. H. Rankin, A. G. Robiette, G. M. Sheldrick, W. S. Sheldrick, B. J. Aylett, I. A. Ellis, and J. J. Monaghan, *J. Chem. Soc.* (*A*), 1969, 1224.
[4] D. E. J. Arnold, D. W. H. Rankin, M. R. Todd, and R. Seip, *J.C.S. Dalton*, 1979, 1290.
[5] C. M. Huntley, G. S. Laurenson, and D. W. H. Rankin, *J.C.S. Dalton*, 1980, 954.
[6] M. J. Barrow, E. A. V. Ebsworth, M. M. Harding, and S. G. D. Henderson, *J.C.S. Dalton*, 1979, 1192.
[7] A. H. Brittain, J. E. Smith, P. L. Lee, K. Cohn, and R. H. Schwendeman, *J. Amer. Chem. Soc.*, 1971, **93**, 6772.
[8] G. C. Holywell, D. W. H. Rankin, B. Beagley, and J. M. Freeman, *J. Chem. Soc.* (*A*), 1971, 785.
[9] W. B. Jennings, personal communication.
[10] C. Glidewell, D. W. H. Rankin, A. G. Robiette, and G. M. Sheldrick, *J. Mol. Structure*, 1970, **6**, 231.
[11] D. E. J. Arnold, E. A. V. Ebsworth, H. F. Jessep, and D. W. H. Rankin, *J.C.S. Dalton*, 1972, 1681.
[12] E. A. V. Ebsworth, D. W. H. Rankin, and J. G. Wright, *J.C.S. Dalton*, 1979, 1065.
[13] S. H. Bauer and K. Kimura, *J. Phys. Soc. Japan*, 1962, **17**, 300.
[14] R. L. Hilderbrandt and S. H. Bauer, *J. Mol. Structure*, 1969, **3**, 325.
[15] D. M. Bridges, G. C. Holywell, D. W. H. Rankin, and J. M. Freeman, *J. Organometallic Chem.*, 1971, **32**, 87.
[16] L. Schäfer, A. C. Yates, and R. A. Bonham, *J. Chem. Phys.*, 1971, **55**, 3055.
[17] G. S. Laurenson and D. W. H. Rankin, *J. Mol. Structure*, 1979, **54**, 111.
[18] L. S. Bartell, D. J. Romenesko, and T. C. Wong, 'Molecular Structure by Diffraction Methods,' *Specialist Periodical Reports*, The Chemical Society, London, 1977, vol. 3, p. 72.
[19] L. S. Bartell, *J. Chem. Phys.*, 1960, **32**, 827.
[20] D. E. J. Arnold, E. A. V. Ebsworth, H. F. Jessep, and D. W. H. Rankin, *J.C.S. Dalton*, 1972, 1681.
[21] E. Hedberg, L. Hedberg, and K. Hedberg, *J. Amer. Chem. Soc.*, 1974, **96**, 4417.
[22] E. A. V. Ebsworth, D. W. H. Rankin, and J. G. Wright, *J.C.S. Dalton*, 1977, 2348.
[23] A. H. Cowley, M. J. S. Dewar, W. R. Jackson, and W. B. Jennings, *J. Amer. Chem. Soc.*, 1970, **92**, 1085.

Molecular Structure of Bis(difluorophosphino)germylamine in the Gas Phase, determined by Electron Diffraction

By Graham S. Laurenson and David W. H. Rankin,* Department of Chemistry, University of Edinburgh, West Mains Road, Edinburgh EH9 3JJ

The molecular structure of $N(GeH_3)(PF_2)_2$ in the gas phase has been determined by electron diffraction. The $NGeP_2$ skeleton is planar, and the Ge–N bond is substantially longer than those found in $N(GeH_3)_3$. Principal geometric parameters (r_a) are: r(P–F) 159.2(5), r(P–N) 169.8(8), and r(Ge–N) 188.9(13) pm; angle FPF 96.5(11), FPN 99.6(5), and PNP 114.0(8)°. The conformation adopted by the PF_2 groups is one in which the axes of the nitrogen and phosphorus lone pairs are almost orthogonal, while those of the two phosphorus atoms lie approximately *cis* to each other in the skeletal plane.

A COMPREHENSIVE study has recently been completed on amines containing difluorophosphino- and/or silyl groups bound to nitrogen.[1-9] However, of the five amines with germyl groups bound to nitrogen so far reported[10,11] only one, the very unstable trigermylamine, has been the subject of a gas-phase structure investigation.[12] We have therefore undertaken an electron-diffraction structural study of the molecule $N(GeH_3)(PF_2)_2$, the stability of which relative to trigermylamine appears to be increased by the presence of the two difluorophosphino-groups.

Certain geometrical features likely to be exhibited by this molecule could be predicted from previously determined structures of other amines. First, in all NR_3 compounds (R = PF_2, SiH_3, or GeH_3) so far studied the skeletal group was found to be planar, arguably due to delocalisation of the lone pair from the p orbital on nitrogen, and the short M–N bonds found in these compounds have been attributed to some increase in bond order due to $p \rightarrow d$ π bonding from the donor p orbital on nitrogen to vacant d orbitals on the ligands. Furthermore, it has recently been shown that, where PF_2 and SiH_3 groups are bound to the same central nitrogen atom, the electronegative PF_2 groups cause the bonds from nitrogen to silicon to lengthen.[9] Thus we would expect the Ge–N bond to be substantially longer here than in trigermylamine.[12]

Predictions of the likely conformation of the difluorophosphine groups have been made on the basis of the very low $^3J(^{31}P^1H)$ coupling constant (2 Hz) found in the initial study of this molecule.[11] It was suggested that a maximum coupling constant would be obtained when the lone pair on phosphorus lay *cis* to a germyl proton. Therefore it was concluded that it is the fluorine atoms which must lie *cis* to the germyl group. The value for $^3J(^{31}P^{31}P)$ of 405 Hz at room temperature lends further support to this theory, since the two phosphorus lone pairs lying *cis* to each other would generate a large coupling. A similar effect is observed in $NMe(PF_2)_2$[13] and in other bis(difluorophosphino)-compounds.

The conformation suggested by the above evidence would be exactly analogous to that found for $N(PF_2)_2(SiH_3)$,[9] and therefore seems entirely reasonable.

EXPERIMENTAL

A sample of bis(difluorophosphino)germylamine was prepared by the liquid-phase reaction (1) between bis(difluorophosphino)amine and germyl iodide, in the presence of trimethylamine.[11] The product was purified by repeated

$$NH(PF_2)_2 + GeH_3I + NMe_3 \longrightarrow N(GeH_3)(PF_2)_2 + [NMe_3H]I \quad (1)$$

fractional condensation on a vacuum line, and the purity was checked spectroscopically.

Electron-diffraction scattering intensities were recorded using the Cornell/Edinburgh diffraction apparatus,[14,15] with nozzle-to-plate distances of 128 and 288 mm and an accelerating voltage of *ca.* 44 kV. During exposures, samples were maintained at 283 K and the nozzle at room temperature (298 K). Data were recorded on Kodak Electron Image plates, and obtained in digital form using a Jarrell–Ash double-beam microphotometer, with spinning plates.[16] The electron wavelengths were determined from the scattering patterns of gaseous benzene, recorded immediately before or after the sample plates.

Calculations were carried out on ICL 2970 and 2980 computers at the Edinburgh Regional Computing Centre, using established data-reduction and least-squares refinement programs.[16] Weighting points used in setting up the off-diagonal weight matrices are given, together with other experimental data, in Table 1. In all calculations the complex scattering factors of Schäfer *et al.*[17] were used.

TABLE 1

Weighting functions, correlation parameters, and scale factors for $N(GeH_3)(PF_2)_2$

Camera height / mm	Wavelength / pm	Δs	$s_{min.}$	sw_1	sw_2	$s_{max.}$	p/h	Scale factor
				nm^{-1}				
128.16	5.811	4	68	100	240	320	0.363	0.750(35)
288.31	5.811	2	34	44	120	140	0.442	0.724(24)

Refinement.—In refinements of the structure of $N(GeH_3)(PF_2)_2$ the $NGeP_2$ skeleton was initially assumed to be planar, although an out-of-plane distortion of the germyl group was subsequently permitted. Local C_s and C_{3v} symmetries were assumed for the NPF_2 and $NGeH_3$ groups respectively. Furthermore, the torsion angles of the two PF_2 groups, defined as zero when the FPF bisectors lay *cis* to the germyl group, were constrained so as to maintain either C_s or C_2 local symmetry for the $N(PF_2)_2$ moiety. The germyl torsion angle was defined as zero when one Ge–H

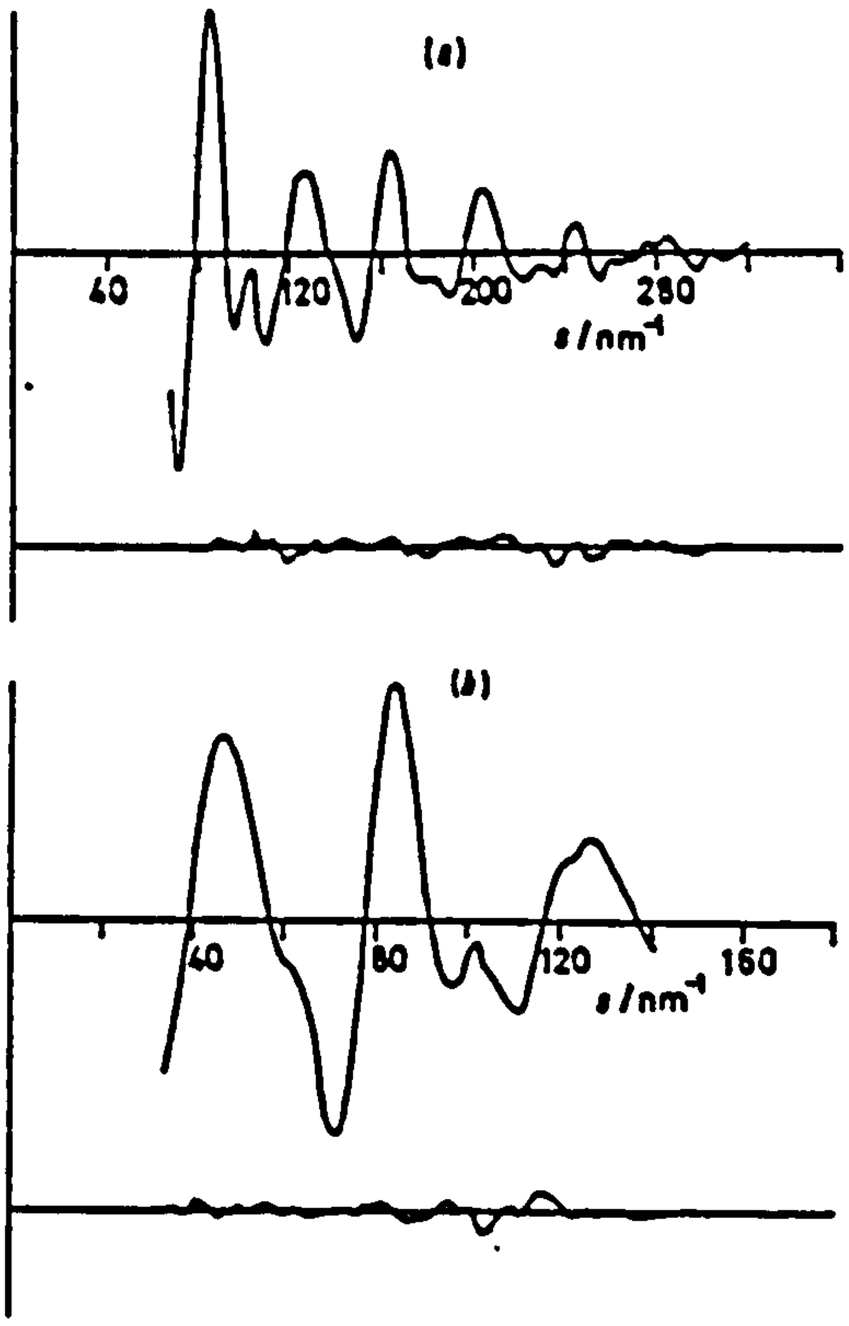

FIGURE 1 Observed and final weighted difference molecular-scattering intensities at nozzle-to-plate distances of (*a*) 128 and (*b*) 288 mm

bond lay in the skeletal plane, and in all cases positive torsion angles corresponded to clockwise rotations about the M–N bonds viewed from M to N. With the adoption of these assumptions, the structure could be defined by 11 geometrical parameters.

The conformation of the germyl group was found by varying the torsion angle and observing the *R* factors obtained. Of the other parameters involving hydrogen, NGeH was fixed at the tetrahedral angle of 110° and *r*(Ge–H) refined to a reasonable value, albeit with a large estimated standard deviation. All other parameters refined satisfactorily, and it was subsequently found that a somewhat lower *R* factor was obtained when the $N(PF_2)_2$ fragment was constrained to C_s symmetry than when it had C_2 symmetry.

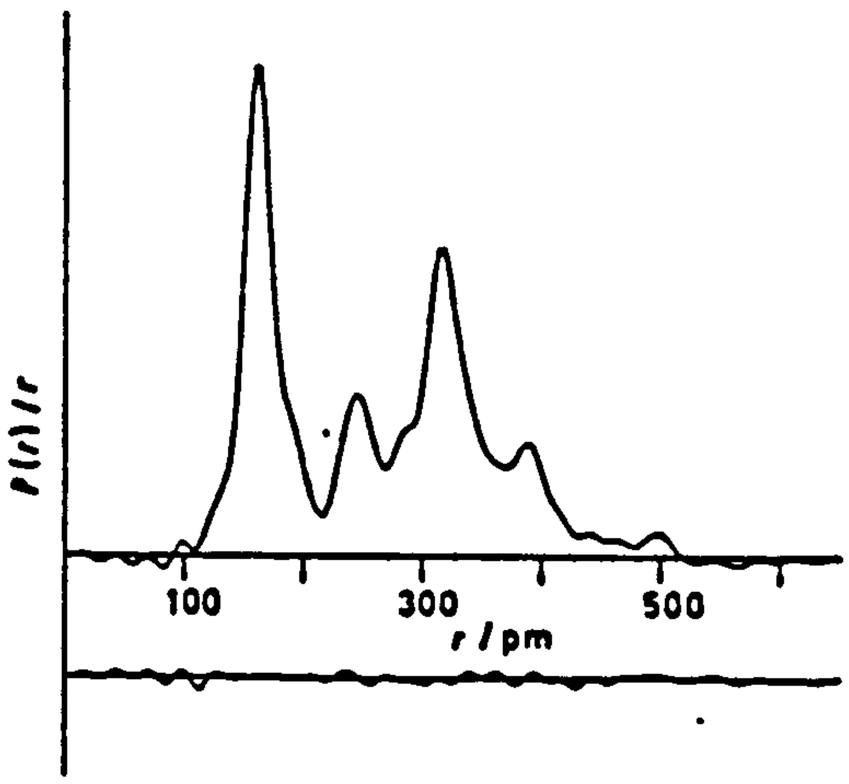

FIGURE 2 Observed and difference radial-distribution curves, $P(r)/r$. Before Fourier inversion the data were multiplied by $s \cdot \exp[-0.000\,015\,s^2/(Z_{Ge} - f_{Ge})(Z_P - f_P)]$

TABLE 2

Molecular parameters for $N(GeH_3)(PF_2)_2$ *

	Distance/pm	Amplitude/pm
(*a*) Independent distances		
r_1 (P–F)	159.2(5)	4.9(11)
r_2 (P–N)	169.3(8)	3.4(28)
r_3 (N–Ge)	188.9(13)	6.2(15)
r_4 (Ge–H)	153.6(43)	8.8 (fixed)
(*b*) Dependent distances		
d_5 (N ··· F)	251.3(6)	7.4(15)
d_6 (P ··· F)	237.6(16)	7.4 (tied to u_5)
d_7 (F ··· F)	499.6(11)	10.2(15)
d_8 (F ··· F)	458.4(23)	10.2 (tied to u_7)
d_9 (F ··· F)	421.4(28)	10.2 (tied to u_7)
d_{10} (F ··· Ge)	318.8(11)	17.7(17)
d_{11} (F ··· Ge)	335.3(12)	17.7 (tied to u_{10})
d_{12} (P ··· Ge)	315.3(6)	8.4(6)
d_{13} (P ··· F)	394.8(9)	10.3(13)
d_{14} (P ··· F)	381.2(12)	10.3 (tied to u_{13})
d_{15} (P ··· P)	284.7(10)	7.0(12)
d_{16-27} (F ··· H)	296—467	22.0 (fixed)
d_{28} (H ··· H)	250(7)	18.0 (fixed)
d_{29-31} (P ··· H)	343—435	18.0 (fixed)
d_{32} (N ··· H)	281(4)	15.0 (fixed)
(*c*) Independent angles/°		
1 (FPF)		96.5(11)
2 (FPN)		99.6(5)
3 (PNP)		114.0(8)
4 (Ge–N, out-of-plane def.)		0 (see text)
5 (NGeH)		110 (fixed)
6 (PF_2, twist)		8.2(10)
7 (GeH_3, twist)		28.0 (see text)

* All distances are r_a values.

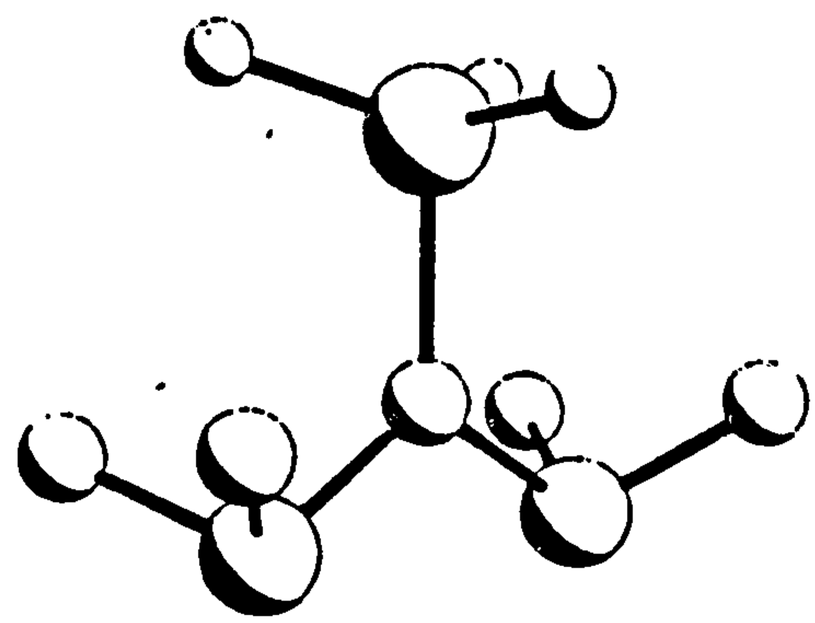

FIGURE 3 Molecular structure of $N(GeH_3)(PF_2)_2$

Results of the final refinement, for which R_G was 0.12 and R_D was 0.08, are given in Table 2. Errors quoted are estimated standard deviations derived from the least-squares analysis, increased to allow for systematic errors of 0.1%. The observed and final weighted difference molecular-scattering intensity curves are shown in Figure 1.

The radial-distribution curve is shown in Figure 2 and the molecule is depicted in Figure 3. Finally, the correlation matrix derived from the final least-squares analysis is given in Table 3.

RESULTS AND DISCUSSION

The $NGeP_2$ skeletal group was found to be entirely planar with no apparent shrinkage, a result also found for $N(PF_2)_2(SiH_3)$.[9] Any deviation from planarity resulted in a large increase in R factor.

This has been attributed to the electronegative PF_2 group having greater π-acceptor capability than the silyl group.[9] Since the difference is greater in the germyl than the silyl case, it could be argued that the former is a weaker π acceptor than the latter.

The PNP angle of 114.0(8)° is somewhat small, and the P···P non-bonded contact (285 pm) is at the small end of a range of values found for other bis(difluorophosphino)amines [Table 4(*a*)]. Using the formula $a(P\cdots Ge) = \frac{1}{2}[d(Ge\cdots Ge) + d(P\cdots P)]$, and assuming values for $d(Ge\cdots Ge)$ [12,13] and $d(P\cdots P)$ of 316 and 290 pm respectively, the expected value for the germanium–phosphorus distance would be 303 pm. The observed value of 315 pm suggests that the narrow PNP angle found is not a result of steric crowding due to the germyl group. By comparing the results tabulated for all bis(difluorophosphino)amines it can be seen that $d(P\cdots P)$ here is similar to that found in the methyl case, and less than 5 pm smaller than that found for $N(PF_2)_2(SiH_3)$. In the silyl case, it may be that the PNP angle is marginally wider because the fluorine

TABLE 3

Least-squares correlation matrix (×100) for $N(GeH_3)(PF_2)_2$

	r_1	r_2	r_3	r_4	Angle 1	Angle 2	Angle 3	Angle 6	u_1	u_2	u_3	u_6	u_7	u_{10}	u_{12}	u_{13}	u_{15}	k_1	k_2	
r_1	100	−60	−64						74	85								51	60	r_1
r_2		100	−79	−50		−59	−72		−85	−79										r_2
r_3			100				82		81	78										r_3
r_4				100			50													r_4
Angle 1					100							68								1
Angle 2						100														2
Angle 3							100		66	61										3
Angle 6								100							−70					6
u_1									100	92								57	61	u_1
u_2										100	57							50	58	u_2
u_3											100									u_3
u_6												100								u_6
u_7													100							u_7
u_{10}														100					54	u_{10}
u_{12}															100			59		u_{12}
u_{13}																100				u_{13}
u_{15}																	100			u_{15}
k_1																		100	71	k_1
k_2																			100	k_2

Only elements with absolute values equal to or greater than 50 are included.

TABLE 4

Important geometrical parameters [a]

(*a*) For some bis(difluorophosphino)amines $NR(PF_2)_2$

R	r(P–F)	r(P–N)	Angle FPF	Angle FPN	Angle PNP	d(P···P)	Shortest d(F···H)	Ref.
H	158.4(3)	168.4(8)	95.6(10)	98.3(7)	122.1(7)	294.8(14)	250	2
CH_3	158.4(2)	168.1(7)	95.2(5)	99.8(4)	115.9(10)	285.1(11)	(not given)	*b*
SiH_3	157.0(2)	169.1(4)	96.1(5)	99.3(3)	117.6(7)	289.3(11)	260(4)	9
GeH_3	159.2(5)	169.8(8)	96.5(11)	99.6(5)	114.0(8)	284.7(10)	297(3)	*c*
PF_2	157.4(2)	171.1(4)	96.9(3)	99.2(3)	120 (fixed)	296.4(6)		1

(*b*) For some germyl- and silyl-amines (M = Si or Ge)

Compound	r(M–N)	Ref.
$N(GeH_3)_3$	183.6(5)	12
$N(SiH_3)_3$	173.4(2)	4, 5
$N(GeH_3)(PF_2)_2$	188.9(13)	*c*
$N(SiH_3)(PF_2)_2$	176.7(7)	9

[a] All distances in pm, all angles in degrees. [b] E. Hedberg, L. Hedberg, and K. Hedberg, *J. Am. Chem. Soc.*, 1974, **96**, 4417. [c] This work.

The geometrical parameters of the NPF_2 groups [r(P–N), r(P–F), angles FPN and FPF] all refined to expected values, commensurate with those found in other bis(difluorophosphino)amines [Table 4(*a*)]. The value found for r(P–N) of 169.8(8) pm is close to that found in $N(PF_2)_2(SiH_3)$ [169.1(4) pm], indicating that steric crowding due to the bulkier germyl group is not severe.

The Ge–N bond length in this study deserves special comment: compared to trigermylamine this parameter is over 5 pm longer. A similar difference has been observed for the analogous silylamines [Table 4(*b*)].

atoms are attracted to the silyl protons, whereas in $N(CH_3)(PF_2)_2$ optimum H···F contact would be possible with a narrower PNP angle. In the germyl case the shortest H···F distance is too long (297 pm) for any strong interaction to take place, as the optimum distance for this lies in the region 250—265 pm,[2,3,4,8,10] and it appears here that the PNP angle relaxes back to a smaller value.

The conformation of the PF_2 groups can be deduced directly from the form of the radial-distribution curve, since only a configuration in which the FPF angle bisectors lay *trans* to each other would give rise to F···F distances up to 500 pm. The apparent distortion of *ca.* 8° away from C_{2v} symmetry for the $N(PF_2)_2$ moiety probably represents torsional shrinkage away from the higher symmetry. The result is in accordance with the expectations discussed above.

We thank the S.R.C. for research grants and a research studentship (to G. S. L.).

[0/1364 *Received*, 2*nd September*, 1980]

REFERENCES

[1] D. E. J. Arnold, D. W. H. Rankin, M. R. Todd, and R. Seip, *J. Chem. Soc., Dalton Trans.*, 1979, 1290.
[2] C. M. Huntley, G. S. Laurenson, and D. W. H. Rankin, *J. Chem. Soc., Dalton Trans.*, 1980, 954.
[3] G. C. Holywell, D. W. H. Rankin, B. Beagley, and J. M. Freeman, *J. Chem. Soc. A*, 1971, 785.
[4] K. Hedberg, *J. Am. Chem. Soc.*, 1955, **77**, 6491.
[5] B. Beagley and A. R. Conrad, *Trans. Faraday Soc.*, 1970, **66**, 2740.
[6] D. W. H. Rankin, A. G. Robiette, G. M. Sheldrick, W. S. Sheldrick, B. J. Aylett, I. A. Ellis, and J. J. Monaghan, *J. Chem. Soc. A*, 1969, 1224.
[7] G. C. Glidewell, D. W. H. Rankin, A. G. Robiette, and G. M. Sheldrick, *J. Mol. Struct.*, 1970, **6**, 231.
[8] D. E. J. Arnold, E. A. V. Ebsworth, H. F. Jessep, and D. W. H. Rankin, *J. Chem. Soc., Dalton Trans.*, 1972, 1681.
[9] G. S. Laurenson and D. W. H. Rankin, *J. Chem. Soc., Dalton Trans.*, 1981, 425.
[10] D. W. H. Rankin, *J. Chem. Soc. A*, 1969, 1926.
[11] E. A. V. Ebsworth, D. W. H. Rankin, and J. G. Wright, *J. Chem. Soc., Dalton Trans.*, 1977, 2348.
[12] C. Glidewell, D. W. H. Rankin, and A. G. Robiette, *J. Chem. Soc. A*, 1970, 2935.
[13] J. F. Nixon, *J. Chem. Soc. A*, 1969, 1087.
[14] S. H. Bauer and K. Kimura, *J. Phys. Soc. Jpn.*, 1962, **17**, 300.
[15] R. L. Hilderbrandt and S. H. Bauer, *J. Mol. Struct.*, 1969, **3**, 325.
[16] D. M. Bridges, G. C. Holywell, D. W. H. Rankin, and J. M. Freeman, *J. Organomet. Chem.*, 1971, **32**, 87.
[17] L. Schäfer, A. C. Yates, and R. A. Bonham, *J. Chem. Phys.*, 1971, **55**, 3055.
[18] C. Glidewell, D. W. H. Rankin, A. G. Robiette, and G. M. Sheldrick, *J. Chem. Soc. A*, 1970, 315.
[19] G. S. Laurenson and D. W. H. Rankin, *J. Mol. Struct.*, 1979, **54**, 111.

The Molecular Structure of Tetraborane(10) in the Gas Phase as determined by a Joint Analysis of Electron-diffraction and Microwave Data

By C. John Dain and Anthony J. Downs,* Department of Inorganic Chemistry, University of Oxford, South Parks Road, Oxford OX1 3QR
Graham S. Laurenson and David W. H. Rankin,* Department of Chemistry, University of Edinburgh, West Mains Road, Edinburgh EH9 3JJ

The structure of the gaseous tetraborane(10) molecule, B_4H_{10}, has been redetermined by electron diffraction. The new analysis confirms not only that the structure comprises a folded diamond of boron atoms bridged by four hydrogen atoms, but also (*i*) that the B–H–B bridges are unsymmetrical, the $H_2B–H_b$ distance being 17 pm longer than the $HB–H_b$ distance, and (*ii*) that the bridging hydrogen atoms are situated 5.6 pm above the plane defined by the three boron atoms of each $H_2B(HB)_2$ moiety to fall within the fold of the tetraboron framework. Other salient parameters are (distances correspond to r_a; figures in parentheses are the estimated standard deviations of the last digits): r[B(1)–B(2)] 185.6(0.4), r[B(1)–B(3)] 170.5(1.2), r[B(1)–H_t] 122.1(1.4), r[B(2)–H_t] 119.4(0.7), r[B(1)–H_b] 131.5(0.9), r[B(2)–H_b] 148.4(0.9) pm; H_t–B(2)–H_t' 122.7(3.5), H_t''–B(1)–B(3) 111.2(3.5), and the dihedral angle between the two planes B(1)B(2)B(3) and B(1)B(3)B(4) 117.1(0.7)° (t = terminal, b = bridging).

SINCE its discovery in 1912 by Stock and Massenez,[1] tetraborane(10) has attracted much attention; indeed its isolation and characterization marked the beginning of systematic studies of the boron hydrides. To date, however, there has been no accurate determination of the structure of the gaseous molecule. The results of *X*-ray diffraction studies on single crystals at low temperature [2] and of electron-diffraction studies on the vapour,[3] published simultaneously, have shown that the skeleton of the B_4H_{10} molecule consists of a folded diamond of boron atoms linked by four hydrogen bridges. The structure of the molecule in the crystalline state has been further refined [4,5] but, in common with other structure determinations using *X*-ray methods, the analysis gives unrealistic results, particularly for the distances between the boron and terminal hydrogen atoms.[6] The electron-diffraction investigation [3] failed to locate accurately the positions of the bridging hydrogen atoms which are a primary feature of the structure. Many theoretical calculations involving the B_4H_{10} molecule have been ventured; these have been based mainly on the molecular dimensions deduced from the crystal structure, with appropriate corrections to the positions of the hydrogen atoms.[7]

We have reinvestigated the structure of the gaseous tetraborane(10) molecule by electron diffraction. In this we have had two principal aims: (*i*) the accurate definition of the positions of as many atoms as possible, (*ii*) the exploration of the relationship between the structure of the B_4H_{10} molecule and molecules like $MMe_2(B_3H_8)$ (M = Al or Ga) [8] formally derived from tetraborane(10). During our investigations, we were acquainted with the results of a microwave study of the gaseous B_4H_{10} molecule;[9] in this study the r_s structure of the boron skeleton had been determined with fair precision, but the hydrogen atoms had not been located. We found that the results agreed well with the parameters deduced from our early calculations based on the electron-scattering pattern of the B_4H_{10} molecule; we have made use of the rotational constants calculated from the microwave spectrum as additional data for our final refinement calculations.

EXPERIMENTAL

The synthesis and manipulation of tetraborane(10) were achieved using a conventional high-vacuum line having stopcocks and ground-glass joints lubricated with Apiezon L grease. The reaction between polyphosphoric acid (B.D.H.) and tetramethylammonium octahydridotriborate (Strem Chemicals Inc.) gave a yield of *ca.* 40% of tetraborane(10) [10] which could be separated from the other higher boranes produced by fractional distillation *in vacuo*. The purity of the resulting tetraborane(10) was checked by measuring the vapour pressure of the liquid at 0 °C [11] and the i.r. spectrum of the vapour.[12]

Electron-scattering patterns were recorded photographically on Kodak Electron Image plates using the Edinburgh/Cornell gas diffraction apparatus.[13,14] The sample was held at 209 K (corresponding to an equilibrium vapour pressure of *ca.* 10 mmHg †) in an ampoule closed by a greased stopcock and gained access to the nozzle of the diffraction apparatus *via* a greased glass taper joint and a stainless steel needle valve. Six plates were exposed at a nozzle-to-plate distance of 128 mm and three at a nozzle-to-plate distance of 285 mm. With an electron wavelength of *ca.* 5.12 pm determined from the scattering pattern given by benzene vapour, these distances gave a range of 28—356 nm^{-1} in the scattering variable *s*. The intensity measurements were recorded digitally using a modified Jarrell–Ash microdensitometer: [15] this gave for its output *ca.* 800 data points spaced at equal intervals across the diameter of a plate which was rotated continuously about its centre.

Calculations were performed on an ICL 2970 computer at the Edinburgh Regional Computing Centre with the aid of the programs for data reduction [14] and least-squares refinement [16] previously described. The complex scattering factors listed by Schäfer *et al.*[17] were used throughout. The weighting functions applied to setting up the off-diagonal weight matrix are given in Table 1 together with the appropriate scale factors, correlation parameters, and electron wavelengths. Each of the data sets (two corre-

† Throughout this paper: 1 mmHg ≈ 13.6 × 9.8 Pa.

sponding to three plates each of the six exposed at a nozzle-to-plate distance of 128 mm and one corresponding to three plates exposed at a distance of 285 mm) was assigned an appropriate scale factor which was itself separately refined. been refined on this basis by full-matrix least-squares analysis. We have not been in a position to apply shrinkage corrections in any of our refinements although the analysis points to some relatively large amplitudes of vibration.

TABLE 1

Nozzle-to-plate distances, weighting functions, correlation parameters, scale factors, and electron wavelengths

Nozzle-to-plate distance/ mm	Δs/ nm^{-1}	$s_{min.}$/ nm^{-1}	sw_1/ nm^{-1}	sw_2/ nm^{-1}	$s_{max.}$/ nm^{-1}	Correlation, p/h	Scale factor, k *	Electron wavelength/ pm
128.5	4	60	80	300	356	0.1361	1.003(30)	5.120
128.4	4	60	80	300	356	0.3644	0.945(30)	5.134
284.6	2	28	44	134	164	0.4871	0.913(27)	5.120

* Figures in parentheses are the estimated standard deviations of the last digits.

STRUCTURE ANALYSIS

Previous studies based on the crystal structure at low temperature and on the electron-diffraction pattern of the vapour imply that the tetraborane(10) molecule conforms to C_{2v} symmetry. On this basis an attempt has been made to interpret the vibrational spectra of the species $^{10}B_4H_{10}$, $^{11}B_4H_{10}$, $^{10}B_4D_{10}$, and $^{11}B_4D_{10}$.[12] In our analysis we have adopted a structural model consistent with this symmetry and admitted a total of ten independent geometrical parameters. With reference to the numbering scheme of Figure 1, these parameters are the two distances B(1)–B(2) and B(1)–B(3), an average B–H distance, the difference Δ_1 between the average B–H_b and B–H_t distances, the difference Δ_2 between the middle B(1)–H_t'' and the apical B(2)–H_t distances, the difference Δ_3 between the inner B(1)–H_b and the outer B(2)–H_b distances, the two angles H_t–B(2)–H_t' and H_t''–B(1)–B(3), the dihedral angle α between the two planes B(1)B(2)B(3) and B(1)B(3)B(4), and an angle β describing the orientation of the plane B(1)H_bB(2) with respect to the plane B(1)B(2)B(3) (t = terminal, b = bridging). The inclusion of this last parameter has enabled us to explore the departure from planarity of the five-membered ring B(1)H_bB(2)H_b'B(3) discernible in

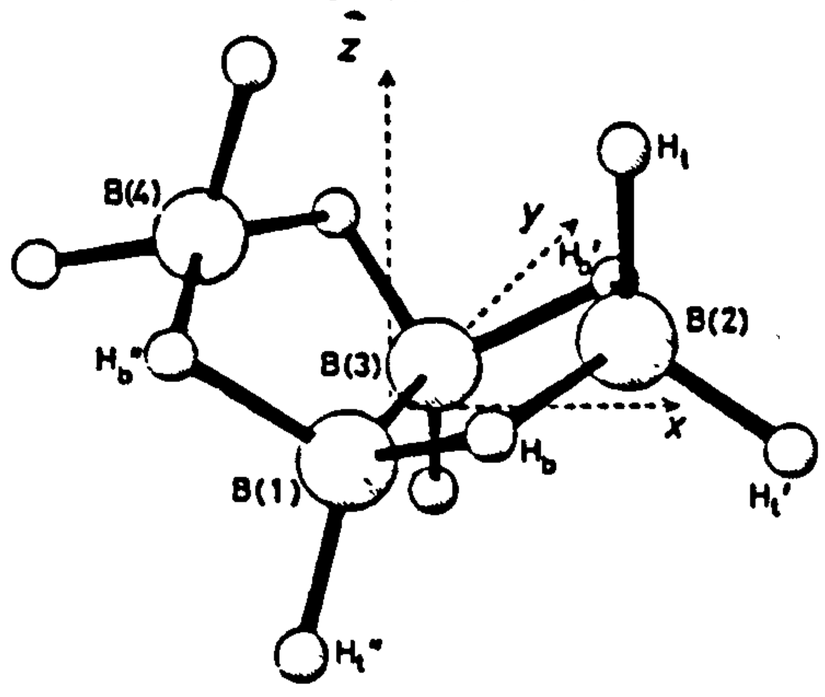

FIGURE 1 Perspective view of the tetraborane(10) molecule

the crystal structures of tetraborane(10) [4] and the related compound beryllium bis(octahydridotriborate), $Be(B_3H_8)_2$.[18] It was not practicable to use a model where the mutual orientation of the planes B(1)B(3)$H_b$$H_b$' and B(2)$H_b$$H_b$' is defined by an independent parameter but this angle γ has been calculated as a dependent parameter in our refinements.

Molecular-scattering intensities have been calculated by established procedures [19] and the molecular structure has

Unfortunately the vibrational spectra ascribed to the different isotopic versions of the tetraborane(10) molecule [12] do not lend themselves to detailed vibrational analysis: thus product-rule calculations reveal inconsistencies in the assignments which militate against any calculations designed

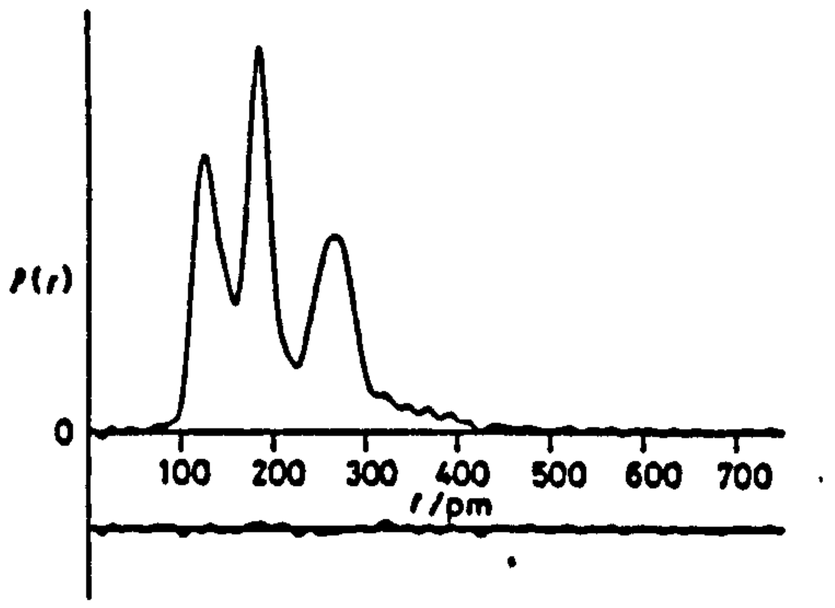

FIGURE 2 Observed and difference radial-distribution curves, $P(r)$ *versus* r, for tetraborane(10). Before Fourier inversion the data were multiplied by $s.\exp[(-0.000\,015\,s^2)/(s_B-f_B)(s_M-f_M)]$

to elicit even a crude force field. In the absence of more definitive information about the vibrational properties of the molecule, there is little prospect of gaining a clearer picture of the amplitudes of vibration. We infer, however, that any effects of shrinkage will be within the limits of error defined by the estimated standard deviations.. Such deviations as quoted take into account the effects of correlation between molecular parameters and have been augmented to allow for systematic errors in the electron wavelength, nozzle-to-plate distance, *etc.*

Combination of the scaled experimental data sets yields, after Fourier inversion, the radial-distribution curve $P(r)/r$ shown in Figure 2. The three prominent peaks correspond to scattering from various groups of atom pairs: that at *ca.* 120 pm originates in all the B–H_b and B–H_t distances, that at *ca.* 180 pm in the B(1)–B(2) and B(1)–B(3) distances, and that at *ca.* 270 pm in the B(2) · · · B(4) and six non-bonded B · · · H distances. The weak features at distances in excess of 300 pm result from long B · · · H and H · · · H distances.

In the analysis of the electron-diffraction data, strong correlations were found, particularly between parameters defining the various B–H (bonded) distances and between B–B–H angles, and it became clear that the limited information available from the data was insufficient to define the structure fully. Analysis of the microwave spectrum of tetraborane(10) by Simmons *et al.*[9] gives an r_s structure for

the B_4 skeleton of the molecule in close agreement with our r_a structure. However, these authors have made no attempt to fit the overall rotational constants and it seemed profitable therefore for us to use the rotational constants for $^{11}B_4{}^1H_{10}$ as additional data in our refinements.

Each extra observation was given a weight inversely proportional to the square of the estimated uncertainty of the observation and scaled to the standard deviation of the electron-diffraction observations. As no force field was available, it was not possible to correct observed rotational constants B_0 to B_z, nor could r_z[9] parameters be derived from the diffraction data. However, the combined analysis was not being used to give extreme precision in the refined parameters but to resolve parameters that would otherwise be unacceptably strongly correlated, and so no vibrational corrections were applied. The close agreement of the microwave r_s and electron-diffraction r_a structures for the B_4 skeleton suggests that no major errors are introduced by this technique. The procedure provided a dramatic resolution of some of the problems posed by correlation of molecular parameters.

In our least-squares analysis of the electron scattering with the additional constraints imposed by the rotational constants, we have been able to refine simultaneously all ten of the geometrical parameters used to specify the tetraborane(10) molecule, as well as six amplitudes of vibration. The vibrational parameters relate to the atom pairs B(1)–B(2), B(1)–B(3), B(2) · · · B(4) and three groups of distances each refined as a single parameter comprising (*i*) the bonds involving the bridging hydrogen atoms B(1)–H_b and B(2)–H_b, (*ii*) the bonds to the terminal hydrogen atoms B(1)–H_t and B(2)–H_t, and (*iii*) six non-bonded B · · · H atom pairs with separations in the neighbourhood of 260 pm. The convergence of the structural refinement was relatively well defined and inspection of the final least-squares correlation matrix (given in Table 2) shows strong correlation between the angles α (the dihedral angle), β [defining displacement of the bridging hydrogen atoms with respect to the plane B(1)B(2)B(3)], H_t–B(2)–H_t', and H_t–B(1)–B(3), and the distances B(1)–B(2), B(1)–B(3), and B–H (average).

The closeness of the fit may be gauged by the difference (*i*) between the experimental radial-distribution curve and that derived from the optimum refinement (Figure 2) and (*ii*) between the experimental and calculated intensities of molecular scattering (the results appropriate to both nozzle-to-plate distances being combined to yield a single intensity curve in Figure 3). Table 3 lists the values of the geometric and vibrational parameters associated with the optimum refinement (for which $R_G = 0.098$ and $R_D = 0.079$), together with the estimated standard deviations. It includes (*i*) the magnitudes of the rotational constants calculated on the basis of the $^{11}B_4H_{10}$ molecule (to be compared with the corresponding parameters deduced from the microwave spectrum) and (*ii*) co-ordinates of the non-equivalent components B(1), B(2) and the four different species of hydrogen atom which make up the B_4H_{10} molecule.

TABLE 2

Least-squares correlation matrix (× 100) * for the molecule tetraborane(10)

Distances										Angles				Vibrational amplitudes			Scale factors			
P_1	P_2	P_3	P_4	P_5	P_6	P_7	P_8	P_9	P_{10}	u_1	u_2	u_3	u_4	u_5	u_6	k_1	k_2	k_3	
100	72	77	−24	47	−48	95	92	−96	75	13	24	70	8	−71	−79	−2	−2	8	P_1
	100	57	7	18	−47	68	83	−72	59	−37	−11	48	5	−52	−68	−3	−3	7	P_2
		100	−20	74	−33	92	88	−88	74	9	30	60	−14	−54	−78	28	26	23	P_3
			100	−54	35	−26	−4	10	−8	−30	5	−33	−25	38	24	48	45	38	P_4
				100	−22	63	46	−54	46	9	14	21	−33	−51	−60	0	0	−3	P_5
					100	−49	−46	46	−32	3	0	−22	−48	50	34	12	12	5	P_6
						100	95	−96	78	14	29	70	2	−68	−82	11	10	15	P_7
							100	−97	78	−1	22	68	1	−62	−81	17	15	21	P_8
								100	−79	−8	−30	−64	1	66	81	−15	−14	−20	P_9
									100	−6	5	51	−13	−63	−63	0	−1	0	P_{10}
										100	72	40	34	11	13	28	27	28	u_1
											100	31	24	15	5	70	68	62	u_2
												100	37	−38	−51	6	6	13	u_3
													100	4	21	7	7	12	u_4
														100	66	36	35	36	u_5
															100	15	16	11	u_6
																100	86	72	k_1
																	100	70	k_2
																		100	k_3

* Numbers in bold type indicate marked correlation.

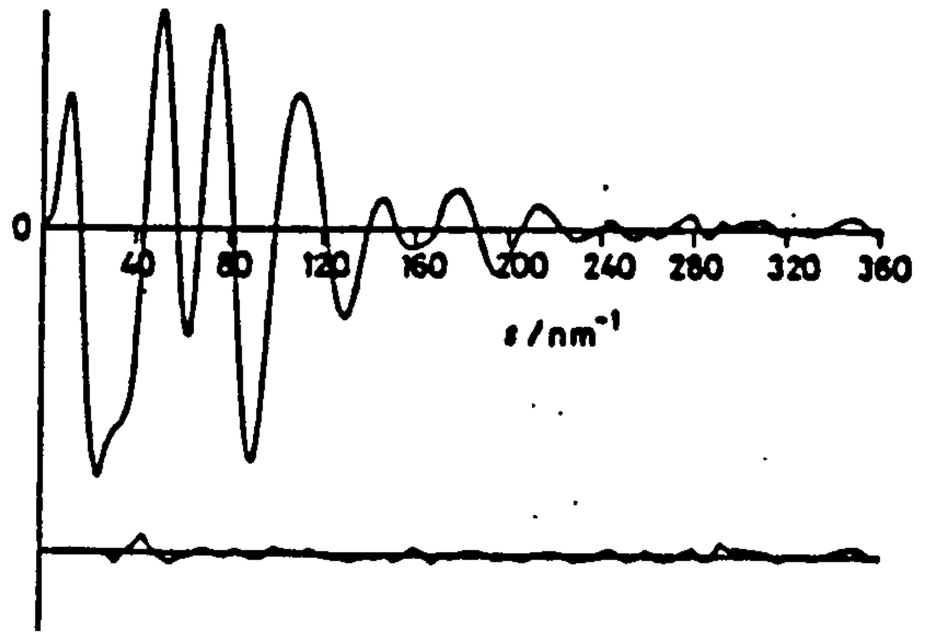

FIGURE 3 Experimental and final difference molecular-scattering intensities (combined) for tetraborane(10)

DISCUSSION

The results of our structural analysis of the gaseous tetraborane(10) molecule, based on its electron-diffraction pattern, are not radically different from those deduced

for the molecule in the crystalline solid at low temperature by X-ray diffraction;[4,5] the principal innovation is the more realistic location of the hydrogen atoms. Table 4 affords a detailed comparison of the dimensions of B_4H_{10} as determined not only by different physical methods[3,4,9] but also on the basis of FSGO (floating

TABLE 3

Molecular parameters [a] for tetraborane(10)

(*a*) Independent geometrical parameters

P_1	r[B(1)–B(3)]/pm	170.5(1.2)
P_2	r[B(1)–B(2)]/pm	185.6(0.4)
P_3	r(B–H) (average)/pm	129.2(0.8)
P_4	Δ_1/pm, r(B–H_b) (average) − r(B–H_t) (average)	18.7(1.0)
P_5	Δ_2/pm, r[B(1)–H_t''] − r[B(2)–H_t]	2.8(1.9)
P_6	Δ_3/pm, r[B(1)–H_b] − r[B(2)–H_b]	−16.9(0.9)
P_7	Dihedral angle, α/°	117.1(0.7)
P_8	Angle H_t–B(2)–H_t'/°	122.7(3.5)
P_9	Angle B(3)–B(1)–H_t''/°	111.2(3.5)
P_{10}	Dip angle, β/° [b]	3.1(0.6)

(*b*) Final distances and vibrational amplitudes

	Distance/pm	Amplitude/pm
d_1[B(1)–B(3)]	170.5(1.2)	7.6(0.9)
d_2[B(1)–B(2)]	185.6(0.4)	8.4(0.3)
d_3[B(1)–H_b]	131.5(0.9)	8.0(1.3)
d_4[B(2)–H_b]	148.4(0.9)	8.0 (tied to u_3)
d_5[B(1)–H_t'']	122.1(1.4)	8.1(0.6)
d_6[B(2)–H_t]	119.4(0.7)	8.1 (tied to u_5)
d_7[B(2) ··· B(4)]	281.3(1.0)	24.5(6.0)
d_8[B(3) ··· H_t'']	242.9(2.9)	11.2 (tied to u_9)
d_9[B(2) ··· H_t'']	276.6(1.1)	11.2(1.2)
d_{10}[B(2) ··· H_b'']	278.3(1.9)	11.2 (tied to u_9)
d_{11}[B(1) ··· H_t]	267.6(2.4)	11.2 (tied to u_9)
d_{12}[B(4) ··· H_t]	394.0(1.3)	39.2 (fixed)
d_{13}[B(4) ··· H_t]	286.2(1.5)	49.8 (fixed)
d_{14}[B(1) ··· H_b]	255.7(1.7)	11.2 (tied to u_9)
d_{15}[B(1) ··· H_t]	251.4(1.5)	11.2 (tied to u_9)

(*c*) Dependent angles/°

Angle between planes B(1)B(3)$H_b$$H_b'$ and B(2)$H_b$$H_b'$, γ	170.3(1.6)
B(3)B(1)H_b	115.1(1.8)
B(1)H_bB(2)	82.8(0.7)
H_bB(2)H_b'	143.7(3.5)
H_bB(1)H_t''	108.7(3.3)
H_bB(1)H_b''	97.0(1.9)
B(1)B(2)B(3)	54.7(0.6)
B(2)B(1)B(3)	62.7(0.6)

(*d*) Co-ordinates/pm [c]

Atom	*x*	*y*	*z*
B(1)	0.0	−85.2	0.0
B(2)	140.6	0.0	86.1
H_b	98.5	−141.0	66.9
H_t	120.3	0.0	203.7
H_t'	250.6	0.0	39.6
H_t''	0.0	−129.3	−113.9

(*e*) Rotational constants/MHz

Constant	Observed value [d]	Calculated value	Difference
B_x	5 592.817(21)	5 594.171	−1.354
B_y	6 198.643(23)	6 200.627	−1.984
B_z	11 013.388(19)	11 015.213	−1.825

[a] Figures in parentheses are the estimated standard deviations of the last digits. [b] The dip angle, β, represents the movement of H_b out of the plane B(1)B(2)B(3) and around the axis B(1)–B(2), a positive sign indicating movement towards the concave side of the molecule. [c] The origin is at the midpoint of B(1)–B(3). [d] Ref. 9.

spherical Gaussian orbital) calculations.[20] The table also includes the dimensions of the molecule $Be(B_3H_8)_2$ whose structure, as determined by crystallographic methods,[18] is likely to be closely related to that of B_4H_{10}.

The gaseous B_4H_{10} molecule can be described in terms of a skeleton comprising a folded diamond of boron atoms with a dihedral angle of 117° between the two planes B(1)B(2)B(3) and B(1)B(3)B(4) with bridging hydrogen atoms spanning the edges of the diamond. These hydrogen atoms do not coincide with the planes B(1)B(2)B(3) and B(1)B(3)B(4) but are located 5.6(5.0) pm above them so as to fall within the fold of the tetraboron skeleton; this compares with a displacement of 16 pm found for the B_4H_{10} molecule in crystalline tetraborane(10).[4]

The unsymmetrical nature of the B–H–B bridges is also evident in that the bridging hydrogen atom forms a bond to the apical BH_2 group which is 17 pm longer than that to the middle BH group. Again this is in keeping not only with the molecular structure established by X-ray diffraction in which the two bonds differ in length by 16 pm,[4] but also with the ^{11}B–^1H coupling constants in the n.m.r. spectra of tetraborane(10) in the liquid phase.[21] The rather different result found by Simmons *et al.*[9] may arise from the fact that in determining the r_a structure no allowance has been made for the probable change in B–H distances on replacement of hydrogen by deuterium. Such unsymmetrical B–H–B bridges appear to be a feature of the higher boranes as witnessed for example by the structures of the molecules B_5H_7CO,[22] $B_6H_{10}(PPh_3)_2$,[23] and $B_{10}H_{14}$.[24,25] For the purposes of our calculations, we have assumed that the hydrogen atoms surrounding the apical boron atoms B(2) and B(4) conform locally to C_{3v} symmetry. On this basis, the puckering of the two five-membered rings B(1)(μ-H)-B(2)(μ-H)B(3) and B(1)(μ-H)B(4)(μ-H)B(3) can be interpreted as relieving the potential non-bonded $H_t \cdots H_t$ contact between the two opposing BH_2 fragments. The assumption that the B_4H_{10} molecule as a whole belongs to the C_{3v} symmetry group does not require that the immediate environments of the B(2) and B(4) atoms belong to the same symmetry group and it would be possible in principle to explore the capacity of the electron-diffraction pattern to accommodate departures from this local symmetry. In practice, however, the problems of correlation mentioned in the preceding section limit the definition of the parameters associated with the BH_2 groups which are subject as a result to comparatively large standard deviations. These circumstances make it unrealistic to seek a more precise definition of the apical $H_2B(\mu\text{-}H)_2$ fragments but we estimate that any changes in the parameters occasioned by relaxation of the local C_{3v} symmetry are within the limits of the standard deviations quoted in Table 3.

There is one notable difference between the dimensions deduced for the B_4H_{10} molecule in the gas phase and the crystalline solid. This concerns the length of what is commonly termed the 'direct' B–B bond between the atoms B(1) and B(3). The tetrahedral covalent radius of 88 pm assigned to boron[26] implies a B(1)–B(3) distance close to that reported for the B_4H_{10} molecule in crystalline tetraborane(10), namely 175 pm.[4] On the basis of both the microwave and electron diffraction measurements, the B(1)–B(3) distance in the gaseous molecule is about 171 pm, close to the distance between

TABLE 4

A comparison of the molecular parameters of tetraborane(10) as determined by various methods with those determined for beryllium bis(octahydridotriborate) [a]

Parameter	B_4H_{10} Electron diffraction [b]	B_4H_{10} X-ray [c]	B_4H_{10} Microwave [d]	B_4H_{10} Electron diffraction [e]	B_4H_{10} FSGO calculation [f]	$Be(B_3H_8)_2$ X-ray [g]
(a) Distances/pm						
B(1)–B(3)	176	175.0	171.8(0.2)	170.5(1.2)	231	176.6(0.3)
B(1)–B(2)	185	184.5	185.4(0.2)	185.6(0.4)	193	183.4(0.4)
B(2) · · · B(4)	288	278.6	280.6(0.1)	281.3(1.0)	245	
B(1)–H_b	143	121	142.8(2.0)	131.5(0.9)	134	106—119(2)
B(2)–H_b	133	137	142.5(2.0)	148.4(0.9)	178	131—138(2)
B(2)–H_t	119	111		119.4(0.7)	124, 130	105—110(2)
B(1)–H_t''	119	111		122.1(1.4)	127	106—114(2)
(b) Angles between pairs of planes/°						
B(1)B(3)B(2) and B(1)B(3)B(4)	124.5	118.1	117.4(0.3)	117.1(0.7)	104.4	115.0
B(1)B(3)$H_b$$H_b'$ and B(2)$H_b$$H_b'$		154		170.3(1.6)		
B(1)B(3)B(2) and B(1)H_bB(2)		170		176.9(0.6)		
(c) Displacement of H_b from the B(1)B(2)B(3) plane/pm		16		5.6(5.0)	23.6	0—6
(d) Angles/°						
H_bB(2)H_t'	125.8	126		122.7(3.5)		122.2 (1.6)
B(3)B(1)H_t''	118.3	118		111.2(3.5)		114.5, 115.3 (1.1)
B(3)B(1)H_b				115.1(1.8)		109.3, 106.5 (1.2)
B(1)H_bB(2)		91.8		82.8(0.7)		94.5, 96.9 (1.4)
H_bB(2)H_b'		134.7		143.7(3.5)		133.7, 131.5 (1.3)
H_bB(1)H_t''		95.6		108.7(3.3)		109.2, 113.5 (1.5)
H_bB(1)H_b''		95.6		97.0(1.9)		98.1, 100.6 (1.4)
B(1)B(2)B(3)		56.6		54.7(0.6)	73.5	57.5 (0.1)
B(2)B(1)B(3)		61.7		62.7(0.6)	53.2	61.2 (0.1)

[a] Estimated standard deviations are given in parentheses where values are available. [b] Ref. 3. [c] Ref. 4. [d] Ref. 9. [e] This work. [f] Ref. 20. [g] Ref. 18.

the apical and basal boron atoms in the gaseous B_5H_9 molecule [27] and some related compounds.[28]

It may be remarked that the eclipsing of the terminal B–H bonds of the adjacent B–H and BH_2 units in the tetraborane(10) molecule can be relaxed by a combination of the vibrational fundamentals ν_{17} and ν_{18} (see ref. 12). It is possible therefore for the molecule to assume C_2 rather than C_{2v} symmetry in its equilibrium conformation without any marked distortion of the B(1)B(2)B(3)B(4) skeleton. With a more complete characterization of the vibrational properties of the B_4H_{10} molecule, it is possible that the vibrational amplitudes calculated on the basis of a suitable force field will improve upon the analysis of the electron-diffraction results. Hence it may be possible to assess the effects of shrinkage and of the assumption by the molecule of an equilibrium configuration with less than C_{2v} symmetry. There is no reason to suppose, however, on the evidence of the analysis reported here, that the molecular model we have adopted is in need of significant improvement.

In conclusion, therefore, we feel that our analysis affords the most realistic determination of the molecular structure of tetraborane(10) to be achieved to date, with all the atoms relatively well located.

We thank Dr. N. P. C. Simmons for his courtesy in showing us, prior to publication, the results of the microwave study of tetraborane(10). We also thank Mr. M. T. Barlow and Miss H. E. Reynolds for practical assistance with the electron-diffraction measurements and the S.R.C. for research grants and the award of research studentships (to C. J. D. and G. S. L.).

[0/1234 *Received*, 4th *August*, 1980]

REFERENCES

[1] A. Stock and C. Massenez, *Chem. Ber.*, 1912, **45**, 3539.
[2] C. E. Nordman and W. N. Lipscomb, *J. Am. Chem. Soc.*, 1953, **75**, 4116.
[3] M. E. Jones, K. Hedberg, and V. Schomaker, *J. Am. Chem. Soc.*, 1953, **75**, 4116.
[4] C. E. Nordman and W. N. Lipscomb, *J. Chem. Phys.*, 1953, **21**, 1856.
[5] G. S. Pawley, *Acta Crystallogr.*, 1966, **20**, 631.
[6] D. S. Jones and W. N. Lipscomb, *Acta Crystallogr.*, 1970, **A26**, 196.
[7] E. Switkes, I. R. Epstein, J. A. Tossell, R. M. Stevens, and W. N. Lipscomb, *J. Am. Chem. Soc.*, 1970, **92**, 3837.
[8] J. J. Borlin and D. F. Gaines, *J. Am. Chem. Soc.*, 1972, **94**, 1367.
[9] N. P. C. Simmons, A. B. Burg, and R. A. Beaudet, to be published.
[10] D. F. Gaines and R. Schaeffer, *Inorg. Chem.*, 1964, **3**, 438.
[11] R. W. Parry and M. K. Walter, *Prep. Inorg. React.*, 1968, **5**, 45.
[12] A. J. Dahl and R. C. Taylor, *Inorg. Chem.*, 1971, **10**, 2508.
[13] S. H. Bauer and K. Kimura, *J. Phys. Soc. Jpn.*, 1962, **17** (Supplement B–II), 300.
[14] C. M. Huntley, G. S. Laurenson, and D. W. H. Rankin, *J. Chem. Soc., Dalton Trans.*, 1980, 954.
[15] R. L. Hilderbrandt and S. H. Bauer, *J. Mol. Struct.*, 1969, **3**, 325.
[16] D. M. Bridges, G. C. Holywell, D. W. H. Rankin, and J. M. Freeman, *J. Organomet. Chem.*, 1971, **32**, 87.
[17] L. Schäfer, A. C. Yates, and R. A. Bonham, *J. Chem. Phys.*, 1971, **55**, 3055.
[18] J. C. Calabrese, D. F. Gaines, S. J. Hildebrandt, and J. H. Morris, *J. Am. Chem. Soc.*, 1976, **98**, 5489.
[19] See for example H. M. Seip, 'Molecular Structure by Diffraction Methods,' *Specialist Periodical Reports*, The Chemical Society, London, 1973, vol. 1, p. 7.
[20] J. Bicerano and A. A. Frost, *Theor. Chim. Acta*, 1974, **36**, 81.
[21] J. B. Leach, T. Onak, J. Spielman, R. R. Rietz, R. Schaeffer, and L. G. Sneddon, *Inorg. Chem.*, 1970, **9**, 2170.
[22] J. D. Glore, J. W. Rathke, and R. Schaeffer, *Inorg. Chem.*, 1973, **12**, 2175.
[23] M. M. Mangion, J. R. Long, W. R. Clayton, and S. G. Shore, *Cryst. Struct. Commun.*, 1975, **4**, 501.
[24] A. Tippe and W. C. Hamilton, *Inorg. Chem.*, 1969, **8**, 464.
[25] V. S. Mastryukov, O. V. Dorofeeva, and L. V. Vilkov, *J. Struct. Chem. (Engl. Transl.)*, 1975, **16**, 110.
[26] L. Pauling, 'The Nature of the Chemical Bond,' 3rd edn., Cornell University Press, Ithaca, 1960, p. 246.
[27] D. Schwoch, A. B. Burg, and R. A. Beaudet, *Inorg. Chem.*, 1977, **16**, 3219.
[28] J. D. Wieser, D. C. Moody, J. C. Huffman, R. L. Hilderbrandt, and R. Schaeffer, *J. Am. Chem. Soc.*, 1975, **97**, 1074.

Group 3 Tetrahydroborates. Part 4.[1] The Molecular Structure of Hydridogallium Bis(tetrahydroborate) in the Gas Phase as determined by Electron Diffraction

By Michael T. Barlow, C. John Dain, and Anthony J. Downs,* Department of Inorganic Chemistry, University of Oxford, South Parks Road, Oxford OX1 3QR
Graham S. Laurenson and David W. H. Rankin,* Department of Chemistry, University of Edinburgh, West Mains Road, Edinburgh EH9 3JJ

Gaseous $Ga(BH_4)_2H$, as studied by electron diffraction, appears to consist of monomeric $HGa[(\mu\text{-}H)_2BH_2]_2$ molecules with five-fold co-ordination of the gallium atom, a single terminal (t) Ga–H bond, and two doubly bridged (b) tetrahydroborate groups. The primary features of the structure involve the dimensions: r(Ga–B) 217.2(0.5), r(Ga–H) (average) 177.4(1.7), and r(B–H) (average) 127.7(1.4) pm; B–Ga–B 112.2(1.5)° (distances correspond to r_a; figures in parentheses are the estimated standard deviations of the last digits). Results are given for refinements based on a structural model with C_2, symmetry imposed, but a significantly better fit to the experimental data is achieved if this constraint is relaxed so that the $Ga(\mu\text{-}H)_2B$ moieties assume an unsymmetrical form with r(Ga–H_b) 176.2(1.5) and 189.1(2.5) pm and r(B–H_b) 125.0(8.1) and 145.6(3.3) pm. The five hydrogen atoms directly bound to the gallium atom form a slightly distorted rectangularly based pyramid. The features of the structure are collated with those of other hydridogallium and tetrahydroborate derivatives.

In our investigations of molecular species in which the tetrahydroborate group competes with ligands like H, CH_3, or NH_2 for co-ordination of an aluminium or gallium centre [2,3] we have determined the structures of the tetrahydroborates $M(BH_4)Me_2$ (M = Al or Ga) [4] and $Al(BH_4)_2Me$ [1] by analysing the electron-scattering patterns of the gaseous molecules. We now report the results of applying a similar analysis to the novel species hydridogallium bis(tetrahydroborate) whose synthesis and characterization have been the focus of recent studies.[2,5]

To judge by its vapour density, hydridogallium bis(tetrahydroborate) vaporizes as monomeric molecules. The two most plausible structures involve either (*i*) a five-co-ordinate gallium atom with a single terminal Ga–H bond and two doubly bridged tetrahydroborate groups (1) or (*ii*) a cyclic skeleton with a four-co-ordinate gallium atom derived from the topologically favoured form [6] of the hypothetical borane B_3H_9 (2). The

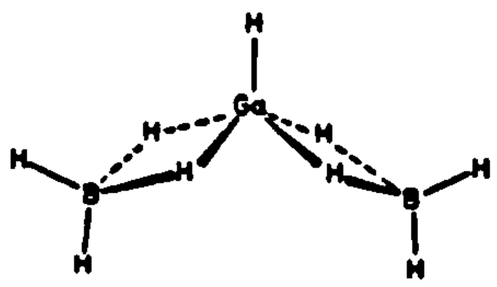

(1)

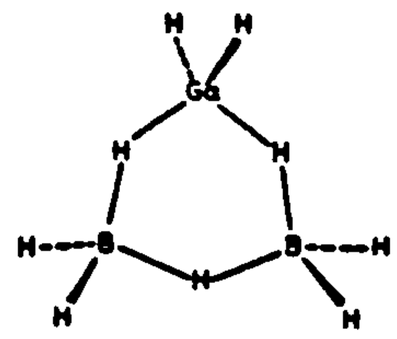

(2)

presence in the i.r. spectrum of features characteristic of a single Ga–H and dihydrogen-bridged $Ga(\mu\text{-}H)_2BH_2$ units,[2,5,7] taken with the absence of the sort of spectral pattern normally associated with the $-BH_2-H-BH_2-$ unit,[2,8] argues strongly in favour of structure (1). There is then a range of possible models for the framework of the molecule depending upon the configuration of the five hydrogen atoms directly co-ordinated to the gallium atom. At one extreme, the unique terminal hydrogen atom occupies the apex and the bridging hydrogen atoms make up the rectangular base of a pyramid (corresponding to C_{2v} symmetry); at the other, the arrangement approximates to a trigonal bipyramid with the terminal hydrogen atom in an equatorial site (corresponding to C_s symmetry). The partially resolved rotational structure of the i.r. band associated with an H_t–GaB_2 deformation mode points to, but does not establish, principal moments of inertia which are consistent with C_s more than C_{2v} symmetry for the gaseous molecule.[2] The results of the electron-diffraction studies reported here are analysed to resolve these uncertainties and to determine the dimensions and amplitudes of vibration of the molecule.

EXPERIMENTAL

Gallium(III) chloride was produced by the direct reaction of the elements and purified by repeated vacuum sublimation; lithium tetrahydroborate supplied by B.D.H. was recrystallized from diethyl ether immediately before use. Hydridogallium bis(tetrahydroborate) was prepared, as reported previously,[2,5] by the interaction of the powdered solids at *ca.* 228 K in the absence of a solvent, the product being removed from the solid mixture under continuous pumping. Fractionation *in vacuo* gave samples of $Ga(BH_4)_2H$ which were judged to be pure on the evidence of the melting point (*ca.* 203 K), the vapour pressure at 228 K (*ca.* 10 mmHg †), and the i.r. spectrum of the vapour.[2,5] Our experience is that decomposition of the liquid tends to set in at temperatures much above 228 K whereas the vapour at a pressure of *ca.* 10 mmHg has a half-life typically in the order of 10 min at room temperature with the formation of gallium metal, hydrogen, and diborane in accordance with equation (1).[5] In common with related compounds,

$$Ga(BH_4)_2H \longrightarrow Ga + \tfrac{3}{2}H_2 + B_2H_6 \qquad (1)$$

$Ga(BH_4)_2H$ is also sensitive to attack by traces of oxygen or moisture and apparatus intended to contain it was

† Throughout this paper: 1 mmHg ≈ 13.6 × 9.8 Pa.

conditioned accordingly.[3,4] Purified samples of the compound were stored at 77 K.

The first attempts to measure electron-scattering patterns involved a Balzers KD.G2 gas-diffraction apparatus but yielded photographic plates of relatively poor quality. Subsequent measurements were made using Kodak Electron Image plates and the Edinburgh/Cornell gas-diffraction apparatus.[9,10] Before each series of exposures, the glass ampoule containing the sample was re-evacuated while the contents were held first at 77 and then at 178 K to remove any hydrogen or diborane resulting from decomposition. With the sample held at 228 K and the nozzle close to 298 K, the scattering pattern of the vapour was then measured at nozzle-to-plate distances of 128.5 and 284.9 mm. The electron wavelength was 5.126 pm, as determined by reference to the scattering pattern of benzene vapour, and the nozzle-to-plate distances corresponded in these circumstances to a range of 10—360 nm^{-1} in the scattering variable s. The intensities of the patterns recorded on each of the six plates judged to be satisfactory were measured using a modified Jarrell-Ash microdensitometer.[11]

Some problems were experienced as a result of a reaction between the photographic emulsion and the vapour of $Ga(BH_4)_2H$. This reaction caused a significant deterioration of the signal-to-noise ratio, particularly at low scattering intensities on the plates exposed at the shorter nozzle-to-plate distance. It was found that the effects could be minimized by leaving the plates in air for 24 h before developing.

Calculations were performed on an ICL 2970 computer at the Edinburgh Regional Computing Centre using the programs for data reduction [10] and least-squares refinement [12] described previously and with the complex scattering factors listed by Schäfer *et al.*[13] The weighting functions used to set up the off-diagonal weight matrix are given in Table 1 together with the correlation parameters and final scale factors.

TABLE 1

Nozzle-to-plate distances, weighting functions, correlation parameters, and scale factors

Nozzle-to-plate distance/mm	Δs	$s_{min.}$	sw_1	sw_2	$s_{max.}$	Correlation, p/k	Scale factor, k *
			nm^{-1}				
128.5	4	84	100	216	248	−0.0763	0.996(63)
284.9	2	32	56	120	160	0.2872	0.912(42)

* Values refer to refinement A (see Table 2). Figures in parentheses are the estimated standard deviations of the last digits.

STRUCTURE ANALYSIS

The vibrational spectra of $Ga(BH_4)_2H$ in the gaseous and solid phases [4,5] favour the adoption of structure (1), with two bidentate tetrahydroborate groups. The radial-distribution curve, $P(r)/r$ *vs.* r, derived from the experimental data sets after scaling, combination, and Fourier transformation, is depicted in Figure 1. Of the prominent peaks, that at *ca.* 120 pm is identified with scattering from all the directly bonded B–H atom pairs. The broad feature at 150—190 pm is similarly due to all the directly bonded Ga–H atom pairs. Most conspicuous is the peak near 215 pm which must be associated with the Ga–B pairs and the location of which leaves little doubt that the molecule contains dihydrogen-bridged $Ga(\mu\text{-}H)_2BH_2$ units, as in structure (1), rather than the monohydrogen-bridged $Ga(\mu\text{-}H)BH_3$ units implied by structure (2). This conclusion receives strong support from the Ga–B distance of *ca.* 234 pm determined by electron diffraction of the molecule $Me_2GaB_3H_8$ wherein the gallium atom is linked *via* a *single* hydrogen bridge to each of two boron atoms of the B_3H_8 fragment.[14] The weaker, relatively broad features of the radial-distribution curve near 300 and 360 pm are associated mainly with scattering from the non-bonded atom pairs $Ga \cdots H_t$ and $B \cdots B$ respectively. Other weak features can be ascribed to distal $B \cdots H$ and $H \cdots H$ non-bonded atom pairs.

The electron-scattering pattern of the vapour was analysed first in terms of a structural model possessing C_{2v} symmetry with the five hydrogen atoms directly linked to the gallium located at the vertices of a rectangular-based

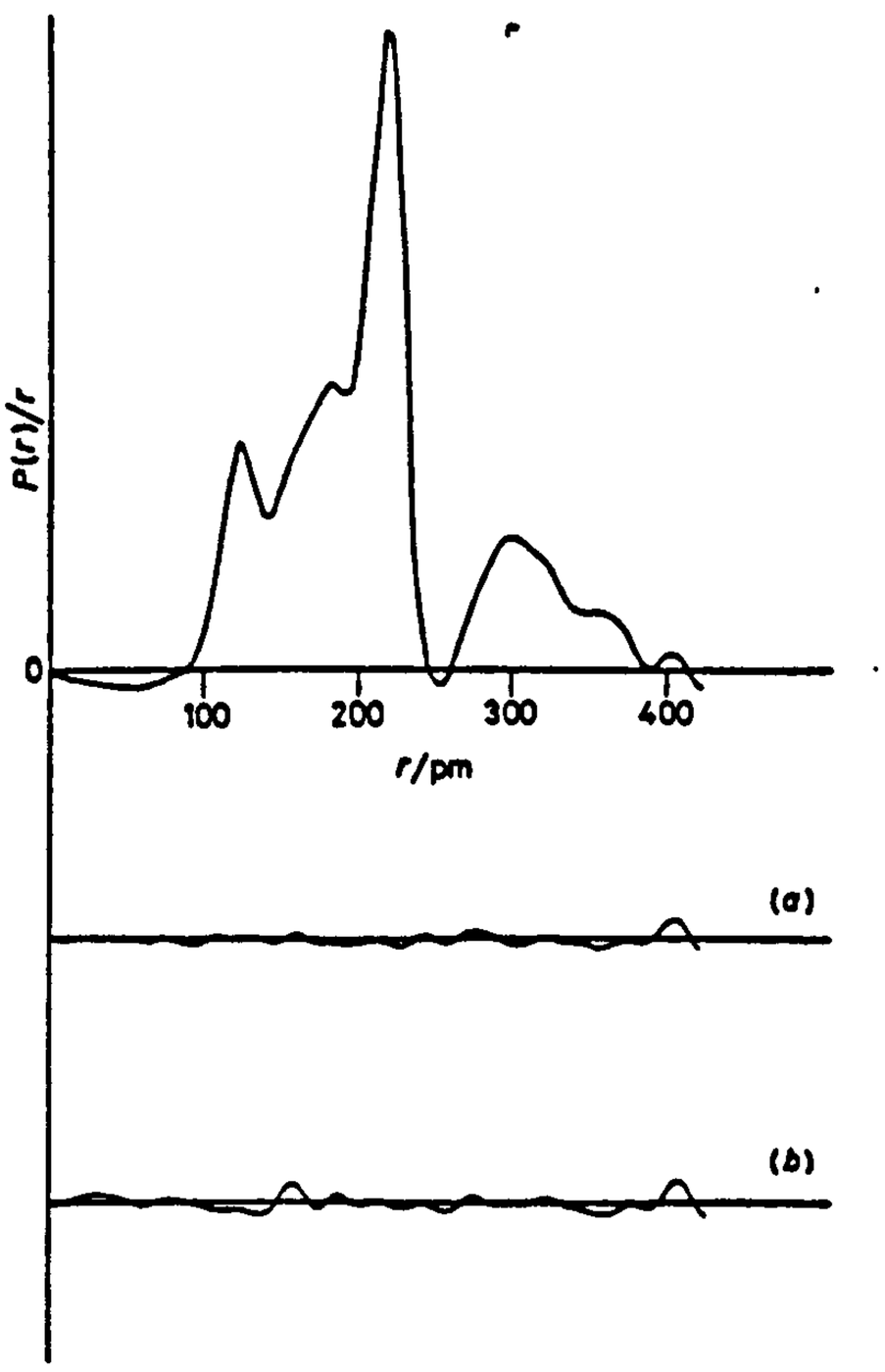

FIGURE 1 Observed radial-distribution curve, $P(r)/r$ against r, for $Ga(BH_4)_2H$. Before Fourier inversion the data were multiplied by $s \cdot \exp[(-0.000\,020\,s^2)/(z_{Ga} - f_{Ga})(z_B - f_B)]$. Final difference curves are shown (*a*) for refinement A involving a model with C_s symmetry and unsymmetrical $Ga(\mu\text{-}H)_2B$ bridges and (*b*) for refinement B involving a model with C_{2v} symmetry and symmetrical $Ga(\mu\text{-}H)_2B$ bridges

pyramid. The calculations failed, however, to give a reasonable account of the measured scattering. The principal flaw could be traced to the peak in the experimental radial-distribution curve arising from the directly bound Ga–H atom pairs. The shape of this feature could not be reproduced by the scattering intensity derived from a unique Ga–H_t and four equivalent Ga–H_b bonds and any reasonable values for the corresponding amplitudes of vibration. Hence we were led to modify the model to admit the possibility of non-equivalent Ga–H_b distances within each of the $Ga(\mu\text{-}H)_2BH_2$ moieties. To enable the bond order of each of the Ga–H_b–B bridges to be conserved, non-equivalence of the two B–H_b distances was also allowed. Another modification included the facility to permit the simultaneous rotation of the $Ga(\mu\text{-}H)_2BH_2$ units about the Ga–B axes. This twisting was defined by an angle θ such that the condition $\theta = 0$ corresponds to a molecular conformation in which the planes of the two $Ga(\mu\text{-}H)_2B$ groupings are normal to the $HGaB_2$ skeleton whereas $\theta = 45°$ produces an $H_tGa(H_b)_4$ polyhedron approximating to a trigonal bipyramid with the terminal hydrogen atom occupying an equatorial site. Such a model conforms overall to C_s symmetry. We have assumed moreover that the B–H_t bond lengths in each tetrahydroborate group are equal and that the plane containing the $B(H_t)_2$ fragment not only bisects the H_bBH_b angle but is normal to the $Ga(H_b)_2B$ plane.

The final model used to describe the hydridogallium bis(tetrahydroborate) molecule employed the ten independent parameters specified in Table 2(*a*). The optimum solution found for the structure constrained to preserve C_s symmetry (for which R_G exceeded 0.2) was used to initiate refinement calculations designed to investigate the effects first of conceding non-equivalence of the Ga–H_b and B–H_b distances and then of twisting the BH_4 groups about the Ga–B axes. A markedly better account of the experimental scattering pattern was thus achieved although the effects of correlation made it impossible to refine independently the amplitudes of vibration associated with the Ga–H distances. A wide range of values was tried for these amplitudes; the values listed as refinement A in Table 2 correspond to the best solution judged in terms of the R factor, R_G, but do not lend themselves to refinement.

The amplitudes thus determined are admittedly rather smaller than might be expected by comparison with the metal–hydrogen distances of some related compounds [*e.g.* $Al(BH_4)_2Me$ 10 pm,[1] $Al(BH_4)_3$ 12.5 pm,[18] and $Ga(BH_4)Me_2$ 10 pm [4]] but are well within the range of values found for the Ge–H bonds of typical hydridogermanium compounds (5—13 pm).[19] A more exact evaluation of the amplitudes of vibration of the $Ga(BH_4)_2H$ molecule could be realised only *via* a detailed normal co-ordinate analysis, whereas it has been possible to date to offer no more than a partial assignment of the vibrational spectra in terms of the appropriate group vibrations.[3] The lack of information about the vibrational properties of the molecule had the additional consequence of precluding any assessment of shrinkage effects. A possible explanation of the C_s structure apparently favoured by the molecule might, it is true, be founded on a model intrinsically retaining C_{2v} symmetry while subject to a large amplitude of rocking of the BH_4 groups about their rest positions. Such a vibration would,

TABLE 2

Molecular parameters [a] for $Ga(BH_4)_2H$

(*a*) Independent geometrical parameters

	Parameter	Distance/pm or angle/°: Refinement A, C_s model	Refinement B, C_{2v} model
P_1	r(Ga–B)	217.2(0.5)	217.4(0.4)
P_2	r(Ga–H) (average)	177.4(1.7)	174.4(1.9)
P_3	r(B–H) (average)	127.7(1.4)	122.2(1.1)
P_4	Δ_1, r(Ga–H_b) (average) − r(Ga–H_t)	26.1(1.7)	27.7(2.5)
P_5	Δ_2, r(Ga–H_b') − r(Ga–H_b)	12.9(2.6)	0 [b]
P_6	Δ_3, r(B–H_b) (average) − r(B–H_t)	15.1(7.4)	4.2(5.5)
P_7	Δ_4, r(B–H_b') − r(B–H_b)	−20.5(7.9)	0 [b]
P_8	Angle H_t–B–H_t	125.0(5.0) [c]	125.0(5.0) [c]
P_9	Angle B–Ga–B	112.2(1.5)	111.4(1.4)
P_{10}	θ, $Ga(\mu\text{-}H)_2B$ twist	4.1(6.0)	0 [b]

(*b*) Molecular distances, interbond angles, and amplitudes of vibration

Parameter	Refinement A, C_s model: Distance/pm or angle/°	Amplitude/pm	Refinement B, C_{2v} model: Distance/pm or angle/°	Amplitude/pm
r(Ga–H_t)	156.5(2.4)	6.0 [b]	152.3(3.5)	9.5(1.2)
r(Ga–H_b)	176.2(1.5)	9.5 [b]	180.0(1.6)	13.6 [d]
r(Ga–H_b')	189.1(2.5)	9.5 [b]		
r(B–H_t)	120.2(3.1)	6.5 [c]	120.1(2.3)	8.3 [f]
r(B–H_b')	125.0(8.1)	7.1 [c]	124.3(3.6)	9.9(1.4)
r(B–H_b)	145.6(3.3)	7.9(3.1) (κ_{12})		
r(Ga–B)	217.2(0.5)	7.3(0.7) (κ_1)	217.4(0.4)	6.9(0.7)
r(Ga ··· H_t)	292.7(2.2)	18.4(3.0) (κ_{12})	292.9(2.0)	16.6(2.0)
r(B ··· B)	360.6(2.5)	9.4(3.6) (κ_{12})	359.1(2.8)	9.2(3.9)
Angle H_b–Ga–H_b'	76.8(4.2)	—	69.7(3.3)	—
R_G	0.159		0.190	

[a] Figures in parentheses are the estimated standard deviations of the last digits; the unsymmetrically bridging hydrogens are designated H_b and H_b'. [b] Fixed. [c] See text. [d] Tied to the Ga–H_t amplitude. [e] Tied to the B–H_b amplitude κ_{12} in the ratios 1 : 1.1 and 1 : 1.2. [f] Tied to the B–H_b amplitude.

TABLE 3

Least-squares correlation matrix (×100) * corresponding to refinement A for the molecule $Ga(BH_4)_2H$

Distances							Angles		Vibrational amplitudes				Scale factors		
P_1	P_2	P_3	P_4	P_5	P_6	P_7	P_9	P_{10}	u_1	u_{11}	u_{12}	u_{13}	k_1	k_2	
100	72	13	−23	**63**	53	56	−24	58	−57	−37	35	2	−22	−26	P_1
	100	40	−28	52	54	41	−15	65	−50	−45	34	0	−25	−37	P_2
		100	−36	−27	65	22	0	18	−40	4	29	0	10	25	P_3
			100	−3	−61	−63	3	−12	58	7	−26	−1	5	−18	P_4
				100	13	35	−18	60	−29	−27	25	2	−20	−40	P_5
					100	85	−16	57	−88	−2	61	3	7	27	P_6
						100	−20	59	−87	−2	58	4	8	22	P_7
							100	−26	21	11	−25	−16	11	10	P_9
								100	−58	−12	70	4	−6	−7	P_{10}
									100	18	−53	−3	10	−9	u_1
										100	19	3	85	76	u_{11}
											100	−1	18	36	u_{12}
												100	2	0	u_{13}
													100	65	k_1
														100	k_2

* Numbers in bold type indicate marked correlation.

however, imply a change in Ga–H bond length of at least 20 pm in the course of its motion. Our experience of other molecules containing dihydrogen-bridged tetrahydroborate groups, *e.g.* $M(BH_4)Me_2$ (M = Al or Ga) [4] and $Al(BH_4)_2Me$,[1] gives no grounds for invoking a motion of this kind or indeed for anticipating that the results of our calculations would be radically altered by due allowance for shrinkage effects. The estimated standard deviations (e.s.d.s) which we associate with the molecular parameters calculated here are likely to be at least comparable in magnitude with the effects of shrinkage; such deviations take into account not only the effects of correlation but also any systematic errors in the electron wavelength, nozzle-to-plate distance, *etc.*

With the aid of a molecular model possessing C_s symmetry we have been able in our least-squares analysis of the molecular-scattering intensities to compass the simultaneous refinement of the 13 independent parameters listed under refinement A in Table 2 as well as the scale factors for the two data sets. The convergence of the structural refinement proceeded satisfactorily on the whole. As revealed by the final least-squares correlation matrix reproduced in Table 3, pronounced correlation occurs between Δ_1, Δ_2, Δ_3, and Δ_4 and between the Ga–B and average Ga–H distances; there are as a result relatively large e.s.d.s associated with the final values taken by some of the structural parameters.

The angle H_t–B–H_t does not yield to refinement. After refining the rest of the parameters to optimum values, therefore, we have carried out calculations to explore the dependence of R_G on this angle. It appears that R_G is at a minimum for an angle of 125°, but our attempts at refinement on the basis of this value have been frustrated by very strong correlation between the H_t–B–H_t angle and the other parameters implicating the terminal hydrogen atoms of the tetrahydroborate groups. In the circumstances we we have had little option but to assign to this angle a value of 125° with a probable e.s.d. on the evidence of our calculations in the order of 5°.

The success of the calculations may be judged by the difference (*i*) between the experimental radial-distribution curve and that simulated for the best model (Figure 1), and (*ii*) between the experimental and calculated intensities of molecular scattering (Figure 2). A perspective view of the $Ga(BH_4)_2H$ molecule in the ultimate form consistent with this model is shown in Figure 3.

After optimizing the refinement on the basis of a molecular model with C_s symmetry, we have carried out further calculations in which the structural parameters deduced

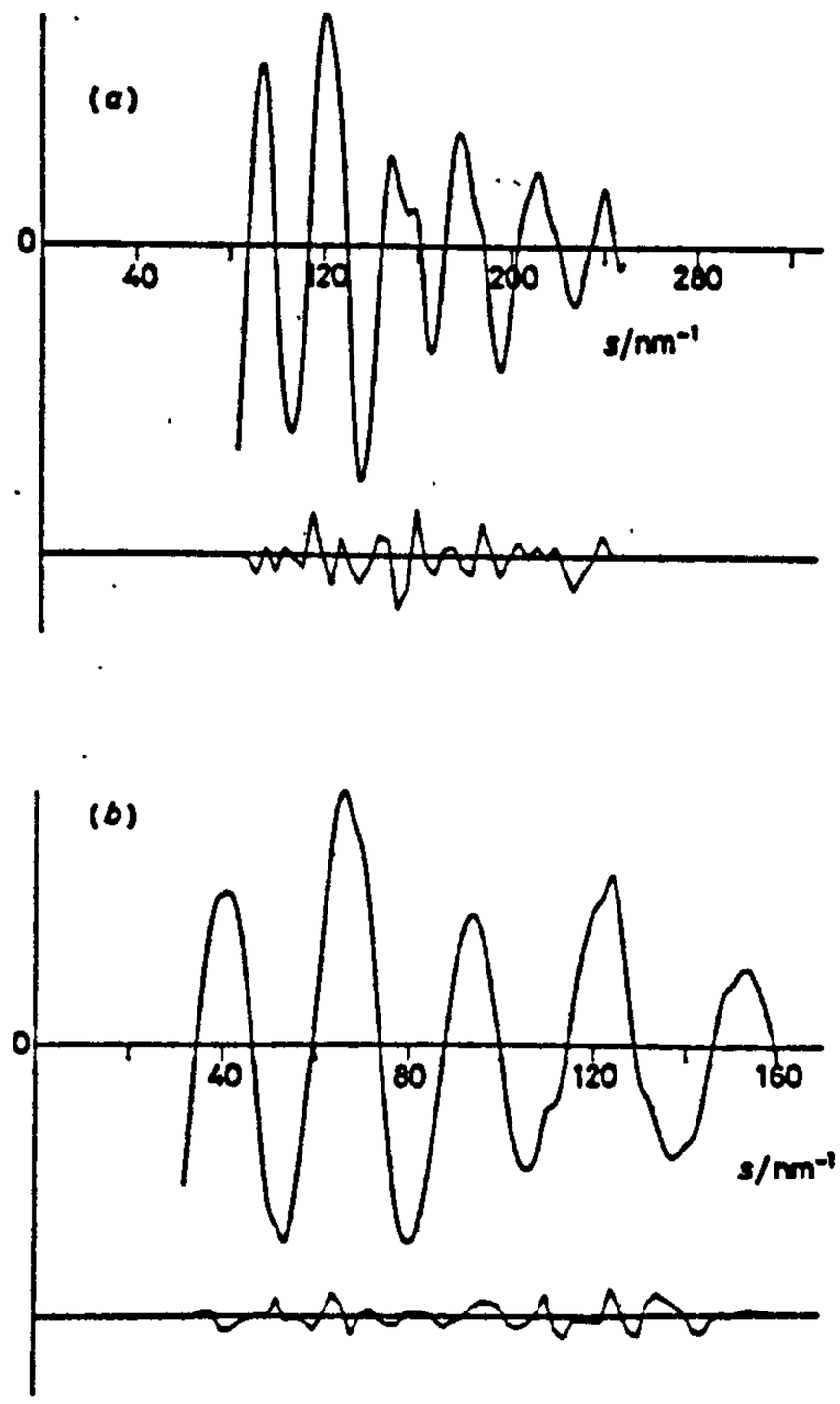

FIGURE 2 Experimental and final difference molecular-scattering intensities based on refinement A for $Ga(BH_4)_2H$; nozzle-to-plate distances (*a*) 128.5 and (*b*) 284.9 mm

for the skeleton of the $Ga(BH_4)_2H$ molecule have again been constrained to preserve C_{2v} symmetry. Hence we have sought to check whether the unsymmetrical form apparently assumed by the $Ga(\mu\text{-}H)_2B$ moieties gives the best account of the experimental data. The calculations reveal two significant features. First, the *R* factor, R_G, increases from 0.159 for the C_s model to 0.190 for the optimum solution

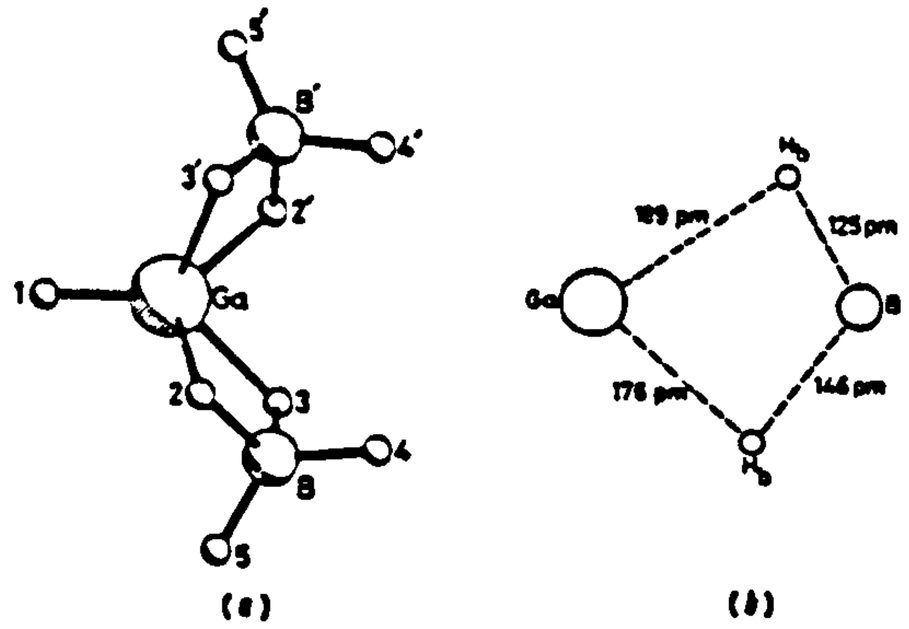

FIGURE 3 (*a*) Perspective view of the molecule $Ga(BH_4)_2H$ and (*b*) geometry of the bridging $Ga(\mu\text{-}H)_2B$ groupings corresponding to refinement A

afforded by the C_{2v} model (see also Figure 1). Secondly, there is an increase in the amplitudes of vibration of the directly bound Ga–H atom pairs now amenable to refinement as a single parameter. There is otherwise little change in the values deduced for the remaining molecular parameters (see refinement B in Table 2). The C_s structure with its unsymmetrical $Ga(\mu\text{-}H)_2B$ units seems therefore to represent the more likely equilibrium geometry for the $Ga(BH_4)_2H$ molecule.

DISCUSSION

The most unusual feature about the structure of hydridogallium bis(tetrahydroborate) which complies best with the measured electron-scattering pattern is the unsymmetrical nature of the dihydrogen bridges linking the BH_4 groups to the metal centre. None of the molecular structures involving bidentate or tridentate tetrahydroborate groups investigated hitherto shows any clear sign of non-equivalent hydrogen bridges and certainly nothing transcending either the effects of crystal packing or the limited accuracy with which such hydrogen atoms can be located by *X*-ray diffraction. To judge by its electron-diffraction pattern, however, the $Ga(BH_4)_2H$ molecule adopts in the optimum refinement a conformation in which each of the four-membered $Ga(H_b)_2B$ rings possesses Ga–H_b distances of 176 and 189 pm and B–H_b distances of 125 and 146 pm (see Figure 3). This dissymmetry tends towards the formulation $Ga(H_t)$–$B(H_t)$ with a direct gallium–boron bond and the adoption of a semi-terminal role by the bridging hydrogen atoms. Some supporting evidence for the non-equivalence of the bridging hydrogen atoms is to be found in the vibrational spectra of $Ga(BH_4)_2H$ which contain not one but two features attributable to Ga–H_b stretching modes, at *ca.* 1 300 and at *ca.* 1 400 cm^{-1},[3] whereas the corresponding modes of dimethylgallium tetrahydroborate have been assigned frequencies close to 1 400 cm^{-1}.[17]

In the absence of independent information about the vibrational properties of the molecule, there is no cause to attach undue weight to the relatively small spans ascribed by the optimum solution to the vibrational amplitudes of directly bonded Ga–H_b and B–H_b distances. It is true that the values are significantly smaller than those associated with the molecular model retaining C_{2v} symmetry, albeit at the overall expense of an inferior account of the experimental results. Other sources of independent information must also be tapped before it is possible realistically to investigate any subtle effects on the terminal $B(H_t)_2$ fragments evoked by the apparent dissymmetry of the $Ga(H_b)_2B$ units.

At 217 pm, the Ga–B distance in $Ga(BH_4)_2H$ differs but little from that in $Ga(BH_4)Me_2$ (216 pm) [4] approximating to the sum of the tetrahedral covalent radii of the gallium and boron atoms (214 pm). This lends support to the assignment of a major role to direct metal–boron bonding, a feature also inferred from the Raman [2,17,18] and u.v. photoelectron [2,19] spectra exhibited by these and other tetrahydroborate molecules.

Structural characterization has been extended previously to only a handful of compounds containing terminal Ga–H bonds. Nevertheless, at 156.5 pm, the Ga–H_t bond length in $Ga(BH_4)_2H$ is consistent with the relatively wide range of 138—173 pm spanned by corresponding bond lengths in crystalline cyclic or cage-like complexes containing four- or five-co-ordinate gallium atoms linked to oxygen, nitrogen, and at least one terminal hydrogen atom.[20] It is also consistent with the appreciably narrower range of 150—156 pm spanned by the Ge–H bonds of typical hydridogermanium compounds.[16]

The magnitude of the B–Ga–B angle (112°) might be taken to imply that Ga–H_t is a sterically demanding group, perhaps with its relatively localized bonding electrons occupying more space in the valence shell of the gallium atom than the delocalized electrons associated with the 'electron deficient' $Ga(\mu\text{-}H)_2B$ units. With reference to the numbering scheme of Figure 3, however, closer inspection reveals that the angles subtended by the different Ga–H bonds are as follows: H(1)GaH(2) 117, H(1)GaH(3) 119, H(2)GaH(2') 126, and H(3)GaH(3') 121°. Hence it appears that the five hydrogen atoms are distributed more or less uniformly about the gallium atom to which they are directly linked. The apparent peculiarities of the structure then seem to stem less from the influence of the Ga–H_t group than from the co-ordination number of the metal atom and the mode of ligation of the BH_4 groups. Co-ordination numbers in excess of four are still far from common in gallium compounds [21] and it is relevant perhaps to note how the reaction of lithium tetrahydroborate with gallium(III) chloride affords not the six-fold co-ordination of the tris(tetrahydroborato)-derivative $Ga(BH_4)_3$ [to

be expected by analogy with the corresponding reaction between $LiBH_4$ and aluminium(III) chloride] [15,22] but the uneasy five-fold co-ordination of the bis(tetrahydroborato)-derivative $Ga(BH_4)_2H$. The constraints of co-ordination number and ligating properties may likewise account for the formation of the four-co-ordinate compound $Ga(BH_4)(Me)H$ in place of the expected five-co-ordinate species $Ga(BH_4)_2Me$ when $LiBH_4$ reacts with methylgallium dichloride.[3]

Investigations of the effect of varying the $Ga(\mu\text{-}H)_2B$ twist angle θ have shown that the R factor passes through a minimum when $\theta = 4°$ although this value is subject to an e.s.d. of about 6°. Such a twisting is barely significant, particularly as we note that it is described exactly by the in-phase torsional mode of the two BH_4 groups. Nevertheless the distortion is in such a direction as to place the longer $Ga{-}H_b$ bonds along the axis of a trigonal bipyramid while also increasing rather than decreasing the interaction between the terminal hydrogen atoms H(4) and H(4') otherwise held apart by the unsymmetrical geometry of the $Ga(\mu\text{-}H)_2B$ groups. Within the limits of our calculations, the $Ga(BH_4)_2H$ molecule resembles $Al(BH_4)_2Me$ [1] in that the five atoms directly co-ordinated to the metal centre complete what approximates to a rectangular pyramid rather than a trigonal bipyramid. In the circumstances, the demands of the tetrahydroborate group as a bidentate ligand with an unusually small 'bite' may well regulate the geometry of the co-ordination polyhedron centred on the metal atom; certainly the conjunction of two such ligands with a monodentate ligand is expected to give a rectangular pyramid on the basis of calculations designed to minimize the total repulsion energy in the co-ordination sphere of the central atom.[23]

The i.r. spectrum of gaseous hydridogallium bis(tetrahydroborate) includes near 730 cm^{-1} an absorption characterized by partially resolved P, Q, and R branches of roughly equal intensity.[3] This is believed to arise from the in-plane deformation mode of the $H_t{-}GaB_2$ skeleton. The atomic co-ordinates in the optimum refinement of the electron-scattering pattern have been used to calculate the principal moments of inertia of the $Ga(BH_4)_2H$ molecule which emerges as an asymmetric rotor possessing C_2 symmetry. Hence it is possible to identify the contour of the band near 730 cm^{-1} with that of an 'AC hybrid'.[24] At 19.9 cm^{-1}, the P–R separation thus calculated is in reasonable agreement with the measured separation of 23 ± 1 cm^{-1}, particularly in view of the approximations which the calculations must entail.

We acknowledge with thanks the contributions made by Dr. P. D. P. Thomas who attempted the first measurements and refinements of the electron-diffraction pattern of $Ga(BH_4)_2H$, Professor D. W. J. Cruickshank for provision of experimental facilities, and Mrs. V. Ulbrecht for practical assistance with these measurements carried out at U.M.I.S.T. We thank the S.R.C. for research grants and the award of research studentships (to M. T. B., C. J. D., and G. S. L.).

[0/1747 *Received*, 12*th November*, 1980]

REFERENCES

[1] Part 3, M. T. Barlow, C. J. Dain, A. J. Downs, P. D. P. Thomas, and D. W. H. Rankin, *J. Chem. Soc., Dalton Trans.*, 1980, 1374.
[2] P. D. P. Thomas, D.Phil. Thesis, University of Oxford, 1977; A. J. Downs and P. D. P. Thomas, unpublished work.
[3] M. T. Barlow, D.Phil. Thesis, University of Oxford, 1981; M. T. Barlow and A. J. Downs, unpublished work.
[4] M. T. Barlow, A. J. Downs, P. D. P. Thomas, and D. W. H. Rankin, *J. Chem. Soc., Dalton Trans.*, 1979, 1793.
[5] A. J. Downs and P. D. P. Thomas, *J. Chem. Soc., Chem. Commun.*, 1976, 825.
[6] W. N. Lipscomb, 'Boron Hydrides,' Benjamin, New York, 1963, p. 53.
[7] T. J. Marks, W. J. Kennelly, J. R. Kolb, and L. A. Shimp, *Inorg. Chem.*, 1972, 11, 2540.
[8] See, for example, R. T. Paine and R. W. Parry, *Inorg. Chem.*, 1972, 11, 268; R. K. Hertz, H. D. Johnson, II, and S. G. Shore, *ibid.*, 1973, 12, 1875; P. C. Keller, *J. Am. Chem. Soc.*, 1974, 96, 3078; D. J. Saturnino, M. Yamauchi, W. R. Clayton, R. W. Nelson, and S. G. Shore, *ibid.*, 1975, 97, 6063.
[9] S. H. Bauer and K. Kimura, *J. Phys. Soc. Jpn.*, 1962, 17 (Suppl. B-II), 300.
[10] C. M. Huntley, G. S. Laurenson, and D. W. H. Rankin, *J. Chem. Soc., Dalton Trans.*, 1980, 954.
[11] R. L. Hilderbrandt and S. H. Bauer, *J. Mol. Struct.*, 1969, 3, 325.
[12] A. S. F. Boyd, G. S. Laurenson, and D. W. H. Rankin, *J. Mol. Struct.*, 1981, 71, 217.
[13] L. Schäfer, A. C. Yates, and R. A. Bonham, *J. Chem. Phys.*, 1971, 55, 3055.
[14] C. J. Dain, A. J. Downs, and D. W. H. Rankin, *J. Chem. Soc., Dalton Trans.*, 1981, 2465.
[15] A. Almenningen, G. Gundersen, and A. Haaland, *Acta Chem. Scand.*, 1968, 22, 328.
[16] D. W. H. Rankin, A. G. Robiette, G. M. Sheldrick, B. Beagley, and T. G. Hewitt, *J. Inorg. Nucl. Chem.*, 1969, 31, 2351; C. Glidewell, D. W. H. Rankin, A. G. Robiette, G. M. Sheldrick, B. Beagley, and S. Cradock, *J. Chem. Soc. A*, 1970, 315; C. Glidewell, D. W. H. Rankin, and A. G. Robiette, *ibid.*, p. 2935; J. D. Murdoch, D. W. H. Rankin, and C. Glidewell, *J. Mol. Struct.*, 1971, 9, 17; J. D. Murdoch, D. W. H. Rankin, and B. Beagley, *ibid.*, 1976, 31, 291; B. Beagley and A. R. Medwid, *ibid.*, 1977, 38, 239.
[17] A. J. Downs and P. D. P. Thomas, *J. Chem. Soc., Dalton Trans.*, 1978, 809.
[18] T. A. Keiderling, W. T. Wozniak, R. S. Gay, D. Jurkowitz, E. R. Bernstein, S. J. Lippard, and T. G. Spiro, *Inorg. Chem.*, 1975, 14, 576; B. E. Smith, H. F. Shurvell, and B. D. James, *J. Chem. Soc., Dalton Trans.*, 1978, 710.
[19] A. J. Downs, R. G. Egdell, A. F. Orchard, and P. D. P. Thomas, *J. Chem. Soc., Dalton Trans.*, 1978, 1755.
[20] S. J. Rettig, A. Storr, and J. Trotter, *Can. J. Chem.*, 1974, 52, 2206; 1975, 53, 58, 753.
[21] K. Wade and A. J. Banister, 'The Chemistry of Aluminium, Gallium, Indium, and Thallium,' Pergamon, Oxford, 1975; A. Pidcock, *M.T.P. Int. Rev. Sci., Inorg. Chem., Ser. 2*, 1975, 1, 300.
[22] H. I. Schlesinger, H. C. Brown, and E. K. Hyde, *J. Am. Chem. Soc.*, 1953, 75, 209.
[23] M. C. Favas and D. L. Kepert, *Prog. Inorg. Chem.*, 1980, 27, 417.
[24] W. A. Seth Paul, *J. Mol. Struct.*, 1969, 3, 403.

List of Courses Attended

Molecular Structure and Spectra	(15)	Drs. S. Cradock and D.W.H. Rankin
Cage and Cluster Compounds	(5)	Dr. T.A. Stephenson
Neutrons in Chemistry	(5)	Several
Multiple Resonance Spectroscopy	(5)	W. MacFarlane
Departmental Seminars	(3 years)	
Departmental Evening Seminars	(3 years)	